Physical-chemistry of cobalta-bis-(dicarbollides) nano-ions in interaction with (biological) interfaces

Tania Merhi

THÈSE

Pour obtenir le grade de

Docteur

Délivré par l'**Ecole Nationale Supérieure de Chimie de Montpellier**

Préparée au sein de l'école doctorale Chimie Balard (ED 459)
Et de l'Institut de Chimie Séparative de Marcoule (UMR 5257)

Spécialité : **Chimie Séparative, Matériaux et Procédés**

Présentée par **Tania MERHI**

Physical chemistry of cobalta-bis-(dicarbollides) nano-ions in interaction with (biological) interfaces

Soutenue le 05/10/2020 devant le jury composé de

Mme Reiko Oda, Directeur de recherche, IEC Bordeaux	Rapporteur
Mr Niki Baccile, Chargé de recherche, LCMC Paris	Rapporteur
Mme Christine Ebel, Directeur de recherche, IBS Grenoble	Examinateur
Mme Benedicte Prelot, Directeur de Recherche, ICG Montpellier	Examinateur
Mr Frédéric Taran, Directeur de recherche, JOLIOT/SCBM CEA Saclay	Examinateur
Mme Christine Almunia, Dr, JOLIOT/LI2D CEA Marcoule	Invitée
Mr Pierre Bauduin, Dr, ICSM CEA Marcoule	Directeur thèse
Mr Olivier Diat, Directeur de Recherche, ICSM CEA Marcoule	Co-directeur

Acknowledgements

The work presented in this manuscript took place at the ICSM institute in the laboratory of ions with active interfaces directed by Olivier who I would like to thank for welcoming me to his team.

I would like to express my deepest gratitude to my supervisor, Dr. Pierre Bauduin, and to my co-supervisor Olivier Diat, for their extraordinary understanding, scientific and personal support and also patience.

I would like also to thank Dr. Jean Armengaud for welcoming me for more than one year at the Li2D laboratory at Cea-Marcoule and for his scientific advices. Special thanks to Dr. Christine Almunia for her kindness, guidance and friendly and perpetual advice during our collaboration. Thanks to her for all the support, the patience and also, for the good moments that I spent with her. I would like also to thank all the Li2D members for their kindness and help.

I also want to thank Prof. Emanuel Schneck for welcoming me for ten days at the Max Planck Institute in Potsdam and for our collaboration at the DESY synchrotron in Hamburg. My thanks to Prof. Dr. Gerald Brezesinski for his patience and his explanations during my experiments at the DESY synchrotron. I also thank the members of the Max Planck institute for their welcome during my stay in Potsdam.

I am thankful to Prof. Clara Vinas and Prof. Francesc Teixidor for welcoming me warmly during one week at the Ciència de Materials de Barcelona (ICMAB-CSIC). I also thank all the members of ICMAB for their welcome during my stay in Barcelona.

I would like to thank all the members of the jury especially Dr. Reiko Oda and Dr. Niki Baccile for having accepted to be the reporters of this work and for their remarks and suggestions which were useful in improving the quality of this manuscript.

A big thank to all ICSM members. My thanks to Dr. Luc Girard and to Alban Jonchère for their support. I am heartily thankful to all my colleagues and great friends especially Ioanna and Chen for their continued support and the best memories of my thesis. To Zijie, the future Doctor and my love, no words to thank you, your incredible calm character and faithful support during all the stages of my PhD, thank you for everything…

This thesis is dedicated to my beloved family that always supported me even from a long distance. Although the very difficult situation in my country Lebanon, they never stopped encouraging me. Thank you mom and dad, thank you Marvin for bringing happiness to our life. My deepest gratitude for you, I love you…

Contents

Abstract

Metalla-bis-(dicarbollides), such as the COSAN anion $[Co(C_2B_9H_{11})_2]^-$, have attracted much attention in biology but a deep understanding of their interactions with cell-components is still missing. For this PhD work, we first studied the interactions of COSAN with glucose moiety, a neutral chemical function that is ubiquitous at biological interfaces. Octyl-glucopyranoside surfactant (C8G1) was chosen as a model as it self-assembles in water into micelles and creates a hydrated glucose-covered interface. Using complementary scattering and spectroscopic techniques, we have deduced from experiments that at low COSAN content and below the critical micellar concentration (CMC) of C8G1, COSAN binds to C8G1 monomers through the hydrophobic effect. Above the CMC of C8G1, COSAN adsorbs onto C8G1 micelles through the superchaotropic effect. At high COSAN concentrations, COSAN disrupts C8G1 micelles and the assemblies become similar to COSAN micelles but with small amount of solubilized C8G1. Therefore, COSAN binds in a versatile way to C8G1 upon either the hydrophobic or the superchoatropic effect depending on their relative concentrations. Then we extended this study to another type of interface, a compressed Langmuir monolayer containing glycolipids over a subphase containing various concentration of COSAN and also other types of nano-ions such as polyoxometalates. Varying the headgroup chemistry (one or two galactoside functions) and the alkyl chain saturation we observed different behaviour of nano-ion in interaction with the subsurface of the glycolipids and this as a function of the surface pressure. Using synchrotron techniques, we found superchaotrope nano-ions interact preferentially with species in gas or in the liquid expended phases than with the solid phase whose crystalline structure is not affected. Lower the charge density of the nano-ions and weaker the interaction between the sugar head groups, stronger is the interaction between the nano-ions and the glycolipids. Finally, in a last part, more complex interfaces were considered and investigated such as proteins. Using electrophoretic methods, we observed some preferential interaction of COSAN with proteins characterized by various secondary structures, a research opening that will be explored for another PhD subject.

Les (métalla-bis-dicarbollides), tels que l'anion COSAN $[Co(C_2B_9H_{11})_2]^-$, intéressent beaucoup les biologistes, mais il manque encore une compréhension approfondie de leurs interactions avec les composants cellulaires. Pour ce travail de thèse, nous avons d'abord étudié les interactions de COSAN avec une fonction sucre neutre type glucose qui est omniprésente aux interfaces biologiques. Le tensioactif octyl-glucopyranoside (C8G1) a été choisi comme molécule modèle car il s'auto-assemble sous la forme de micelle directe dans l'eau et crée une interface recouverte de glucose hydraté. En utilisant des techniques complémentaires de diffusion et de spectroscopie, nous avons déduit des expériences qu'à une faible teneur en COSAN et en dessous de la concentration micellaire critique (CMC) du C8G1, l'anion COSAN se lie aux monomères C8G1 par l'effet hydrophobe. Au-dessus de la CMC de C8G1, le COSAN s'adsorbe sur les micelles de C8G1 par effet superchaotropique. À des concentrations élevées de COSAN, l'anion COSAN impacte les micelles C8G1 pour former des assemblages plus petits, similaires aux micelles de COSAN et solubilisant une partie du C8G1. Par conséquent, COSAN se lie de manière polyvalente à C8G1 par un effet hydrophobe ou superchotropique selon leurs concentrations relatives. Nous avons ensuite étendu cette étude à un autre type d'interface, une monocouche de Langmuir contenant des glycolipides et plus ou moins comprimée avec en sous-phase aqueuse différentes concentrations de COSAN mais également d'autres types de nano-ions tels que les polyoxométalates. En variant la chimie du groupe de tête (une ou deux fonctions galactosides) et la saturation de la chaîne alkyle, nous

avons observé un comportement différent du nano-ion en interaction avec les têtes polaires glycolipidiques et ce en fonction de la pression de surface. En utilisant les techniques X de synchrotron, nous avons constaté que les nano-ions superchaotropes interagissent préférentiellement avec les espèces dans les phases gazeuses ou dans les phases liquides expansées plutôt qu'avec les phases solides dont la structure cristalline n'est pas affectée par la présence des nano-ions. Plus la densité de charge des nano-ions est faible et plus l'interaction entre les groupes de tête de sucre en surface est faible, plus l'interaction entre les nano-ions et les glycolipides est forte. Enfin, dans une dernière partie, des interfaces plus complexes ont été étudiées, comme celle des protéines. En utilisant des méthodes électrophorétiques, nous avons observé une interaction préférentielle du COSAN avec des protéines caractérisées par diverses structures secondaires, une ouverture de recherche qui sera explorée dans un autre sujet de doctorat.

General introduction

Ions are everywhere whatever the surrounding medium, solid, liquid or gas and because they are charged, every ion is surrounding by an ionic atmosphere that screens its charge and that is characterized by a dielectric constant. This is why the matter is globally neutral. Their interactions with their surrounding environment are characterized by electrostatic interactions that can be repulsive or attractive and also by dipolar attractive interaction due to the fluctuation of the electric field produced by the ionic atmosphere. One of the main features of ion is their propensity to migrate if the surrounding medium enable it, hence the Greek origin of the “ion” term that means “to go, to move”. This is the case of water, a familiar liquid and so specific due to its dynamical H-bond network that it is considered as the source of life for human. However, this source of life is in part related to ion migrations through the extracellular domains, inside the cells (in the cytoplasm) and between them where they achieve essential roles. Here some example: the co-transportation of other molecules that are essential for the cells through the cell membranes, a key role in signal transduction for sodium ions. The salt balance in the human body which plays a key role for the membrane potential via the difference in charges inside and outside the cells (sodium, potassium and calcium ions) is very important for some functions (contract of the muscles, pump the heart…), the oxygen transport with Fe^{2+} or Fe^{3+} as well as being main components like the phosphates ions for the nucleic acids (DNA and RNA) and for the cell membranes (phospholipids).[Ussing, 2013]

Over the years, it was demonstrated that the hydration state of the ions and more globally the activity of the ions and the solvent has to be taken into account in numerous properties or physico-chemical characteristics and has to be considered as specific of the ion nature.

Ions have indeed specific effects that seem to be beyond the electrostatic interactions. Specific ion effects (SIE) have been described in the literature since 1880s for the first time by Franz Hofmeister who classified the ions according to their water withdrawing capability.[Hofmeister, 1888; Kunz, 2004] In general, interactions based on specific ion effects with other compounds are mediated by water molecules.[Kunz, 2010]

Later on, ions were classified into two classes, chaotropes and kosmotropes. Chaotropes are weakly hydrated ions that can increase the solubility of the proteins in aqueous solutions (salting-in). Whereas kosmotropes are strongly hydrated ions that can decrease the solubility of the proteins (salting-out).[Collins, 1997; Collins, 2004]

Much more recently, specific ion effects were also investigated with ions of nanometric size i.e. larger than classical ions. Nanometer-sized ions comprise different varieties of molecules,

such as the boron and the metal-oxygen clusters. For large ions, characterized by a low charge density, their “salting-in” effects are found to be much more pronounced than for classical ions.[Assaf, 2018] Indeed, it has been shown that some of polyoxometalates anions and boron clusters adsorb on neutral hydrated surfaces or molecules [Naskar, 2015; Buchecker, 2017; Buchecker, 2018; Hohenschutz, 2020] or bind to the hydrophobic pockets of macrocycle molecules such as cyclodextrin at low concentrations, in the millimolar range.[Assaf, 2015; Warneke, 2016; Assaf, 2018]

In this thesis project, we wanted to investigate more these phenomena, to characterize more deeply the strength and the thermodynamical conditions of these specific properties. We have focused our research on boron clusters and more especially on metalla-bis-(dicarbollide)s compounds type. Why these compounds? Because they are chemically and thermally very stable whatever the medium.[Gabel, 2015; Grimes, 2016] Moreover, in term of objectives and strong motivation in my research, boron cluster compounds (including metalla-bis-(dicarbollide)s) have several interests in the medical and the pharmaceutical fields as will be described in the following chapter. Therefore, the ion specific interactions of boron clusters with biological interfaces have to be understood more deeply in order to develop their applications in this field. We have made the choice to investigate their interactions with carbohydrates systems and proteins.

Carbohydrates or carbohydrate molecules or chains and often-called sugar (saccharide) or polymer sugars are the most abundant biomolecules on earth and have many different functions in the living systems. For example, ABO blood types corresponding to a classification of human blood are determined by sugars on blood cells.[Sharon, 1993] Carbohydrates are a constituent of the backbone of nucleic acids.[Gabius, 2017] Cells and other cellular structures (nucleus, mitochondria) are delimited by biological membranes that are responsible of molecular translocation into and out of the cells as well as intercellular communications and many different important functions.[Sharon, 1993] Lipid bilayer is the common structure for all these biological membranes. However, cells carry also a sugar-based parts that consist of glycoproteins and glycolipids, two types of complex carbohydrates in which sugars groups are linked to lipids and membrane proteins.[Sharon, 1993] Carbohydrates have complex structure, for example, two monosaccharides can form 11 different disaccharides, and four monosaccharides can form 35 560 tetrasaccharides. Therefore, monosaccharides represent the letters that make words (signals) in our system with high coding capacity making the carbohydrates the primary markers for cell recognition.[Sharon, 1993; Gabius, 2017] Noting that the array of carbohydrates on cancer cells is strikingly different from that on normal ones.[Sharon, 1993]

The importance and the abundance of carbohydrates (including glycolipids) in human body were the reason why in this project we had chosen to investigate their interactions with the cobalt-bis-(dicarbollide) (or COSAN) nano-ion. For that, the interactions of the COSAN with glucoside molecules in monomeric or aggregated forms and glycolipid monolayers were investigated and will be detailed in the second and the third chapter of this thesis manuscript respectively.

In the former part, a neutral classical surfactant with sugar head, n-octyl-β-d-glucopyranoside (C8G1) was chosen as it provides a hydrated glucose covered surface by forming direct micelles in water, above its critical micellar concentration (CMC = 19 - 25.8 mM) (page 66 in the reference [Ruiz, 2008]). In addition, the interactions of cobalt-bis-(dicarbollide) with classical, dimer and oligomer sugars were investigated in order to gain better understanding on the interactions with C8G1 aggregates. COSAN is an anion that exhibits surfactant properties in aqueous solution and form aggregates. Therefore, mixtures of C8G1 and of COSAN result in the investigation of two surface active and aggregate forming molecules: a classical (aliphatic tail-polar head) amphiphilic surfactant and a non-conventional surfactant respectively. Different techniques were used in order to investigate these interactions on the molecular (UV-vis spectroscopy, NMR) and supramolecular scales (light, X-ray and neutron scattering) as well as the surface tension measurements as complementary technique.

In the second part we extended the study of the former part by investigating the interactions of the COSAN anion (and polyoxometalate, another type of nanometer-sized anion) with a monolayer of saturated mono- and di-galactosyldiacylglycerol (MGDG-sat and DGDG-sat) at various state of 2D-compression. MGDG-sat and DGDG-sat are amphiphilic molecules with sugar polar heads and long hydrophobic alkyl chains. In addition of being carbohydrates, glycolipid monolayers can be considered as simple model for biological membranes. In aqueous phase, they adsorb at the air/water interface, and when in Langmuir trough, compression of the surface increases the glycolipids concentration and lead the formation of monolayer. These interactions were investigated using synchrotron techniques at the DESY-synchrotron in Hamburg. Adsorbed nano-ions on the glycolipid monolayer were quantified using the total X-ray fluorescence measurements (TXRF). The effects of nano-ions on the ordering of glycolipid molecules were investigated using grazing incidence X-ray diffraction technique (GIXD). Grazing incidence X-ray off specular (GIXOS) technique was applied also to determine the electron density profile of the monolayer at the interface.

In the last chapter of this project, we studied the interactions of COSAN with proteins. Proteins are large biomolecules or macromolecules composed of one or more chains of amino acids

residues. Proteins are one of the main constituents in biological systems where they are an essential part of organisms and participate in every process within the cells. Therefore, the study of the interactions of COSAN with proteins is mandatory. In addition, as will be described with more details in the last chapter, interesting effects of the cobalt-bis-(dicarbollides) on some proteins (like HIV protease) are found in the literature. The main objective of this work was to go further in the understanding and specificity of the COSAN interactions mode with proteins. For that, the interactions of COSAN with the proteins of HeLa cells, i.e. human cancer cells, were investigated using the isoelectric focusing gel (IEF) technique coupled to a mass spectrometry analysis. IEF was used as a technique to separate proteins basing on their isoelectric points (the pH at which the global charge of a protein is neutral). When COSAN anions interact with a protein, the total charge of the protein will be modified, and so its isoelectric point. In addition, we investigated the interactions of cobalt-bis-(dicarbollide) with a set of nine standard proteins used usually as IEF marker (reference for pH). Further investigations of the identified standard proteins that interacted with the cobalt-bis-(dicarbollide) were performed in order to characterize further their interactions using the UV-visible spectroscopy, the dynamic light scattering (DLS) and the zeta potential measurements.

Chapter 1

State of the art

It is difficult to write an exhaustive review on ions and their specific effect at the risk of sounding too basic and naïve whereas it exists very detailed reviews or books on the subject and I will certainly forget to cite many important works on the subject. However, the studies of some famous professor's names in this field such as Hofmeister, Collins, Ninham, Cremer, Lo Nostro, Kunz, Jungwirth, Leontidis, Parsegian, Horinek have to be read and I hope that the main information that come up will be highlighted in this chapter. What I can write is that specific effects of ions in solutions and in interaction with surfaces/interfaces are related to forces beyond their electrostatic interactions that result from their electrical charges considered as point.

I. Ions and their specific effects

I-1. Water withdrawing capability

Franz Hofmeister, a professor of pharmacology at the University of Prague, was the first in to investigate ion specific effects (ISE) and to classify salts (and not isolated ions) according to their water withdrawing capability.[Hofmeister, 1888; Kunz, 2004] The investigation of ions effect on protein precipitation – salting-out of globulins such as albumins from serum blood or white-eggs - were the starter experiments, carried out by one of his student, S. Lewith.[Kunz, 2004] According to Hofmeister and Lewith experiments, the effects of laxative and less diffusible salts (magnesium, citrate, tartrate or sulfates) is stronger than the effects of mobile and diuretic salts (chloride and nitrates). Then, systematic and extended studies from his collaborators have led to decline similar ion specific effects to many different colloidal systems. They generalized these concepts based on the propensity of salts to associate with water and their power to desorb water from another substance, two closely related aspects used for a general classification of ion specificity. However, the rules were rather empiric and the classification that required a full understanding of the ions hydration is much more complex. This is the case when the salt concentrations are above 0.1 M, when mixtures of salts are present in solution or even when pH or temperature are varying. It is nevertheless important to notice that these first investigations were carried out to the profit of pharmacology and biology and on the impact of electrolytes on protein's solubility in water, a property on which we come back regularly during this thesis.

The terms of mobility and laxative versus diuretic for the salts were mentioned and they imply the notions of viscosity and water activity that were investigated as a function of salt concentration and temperature. Indeed, beyond the electrostatic contribution, the (relative) water viscosity varies linearly with the concentration of electrolyte. This contribution can be either positive or negative. Ions having high charge density clusterize around them a large amount of water molecule. In other words, the H-bond network around these ions is less dynamics, so the water molecules being less free are less mobile.[Adamson, 2012] The contribution of the ion specificity to the viscosity of the electrolyte solution is in that case, positive. These types of ions are qualified of kosmotropes or water-structure making. At the opposite, for ions with much weaker interaction with water, the contribution of the ion specificity to the viscosity of the electrolyte solution is negative (see Fig. 1). These types of ions are qualified of chaotropes or water-structure breaking.

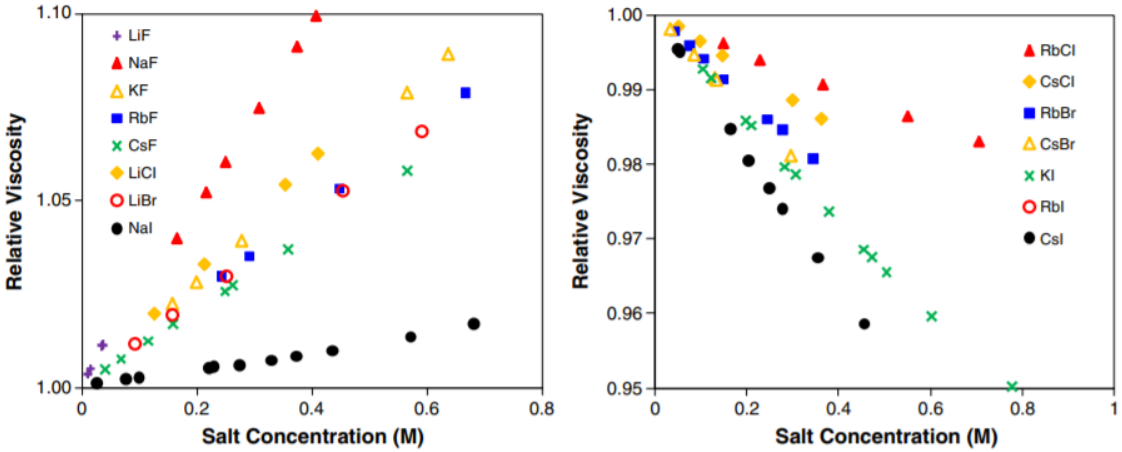

Figure 1. left- Fig 6 of ref Ozdemir 2011: Measured viscosity (relative to water) of aqueous solutions of kosmotropic (left) and chaotropic (right) salts at 25 °C.[Ozdemir, 2011] (Adapted from Desnoyers JE, Perron G. J Solution Chem 1972;1:199–212.[Desnoyers, 1972])

As mentioned just above, the variation of the activity coefficient of the electrolyte solutions as a function of concentration presents also an effect strongly correlated with the ion/counter-ion hydration.[Stokes, 1948] Some contributions out of the validity range of the Debye-Huckel electrostatic theory take into account some ion's hydration shell that are specific of the ions and even more important for the couple anion/cation. For example, for a given concentration, >0.5 M, the mean activity coefficient of a Li^+Br^- in water is much higher than those of a K^+Br^-.[Stokes, 1948]

I-2. Matching water affinities

The water withdrawing capability proposed by Prof. F. Hofmeister was revisited about 100 years later by Kim D. Collins in a more sophisticated model of matching water affinities.[Collins, 1997] These new rules enable to explain and quantify more widely the thermodynamical properties of electrolyte solutions such as activities but also the heating or cooling effect of electrolyte solutions upon varying salt concentration. These rules are based on ion pairing energies in competition with ion hydration and summarized in the very well-known "volcano" graphs,[Morris, 1968] inspired from the Morris data (see Fig. 2-a): The enthalpy of solution of chaotrope-chaotrope and kosmotrope-kosmotrope salts is positive (takes up heat) such for Cs^+I^- or Li^+F^-, whereas the enthalpy of solution of chaotrope-kosmotrope and kosmotrope-chaotrope salts is negative (gives off heat) such for Li^+Cl^- or Cs^+F^- and as it is mentioned in figure 5 caption in ref Collins 97 (see Fig. 2-b).[Collins, 1997] Another representation of this competition between ion pairing and hydration is shown under the graph Fig. 2-c extracted from ref Collins 2004.[Collins, 2004]

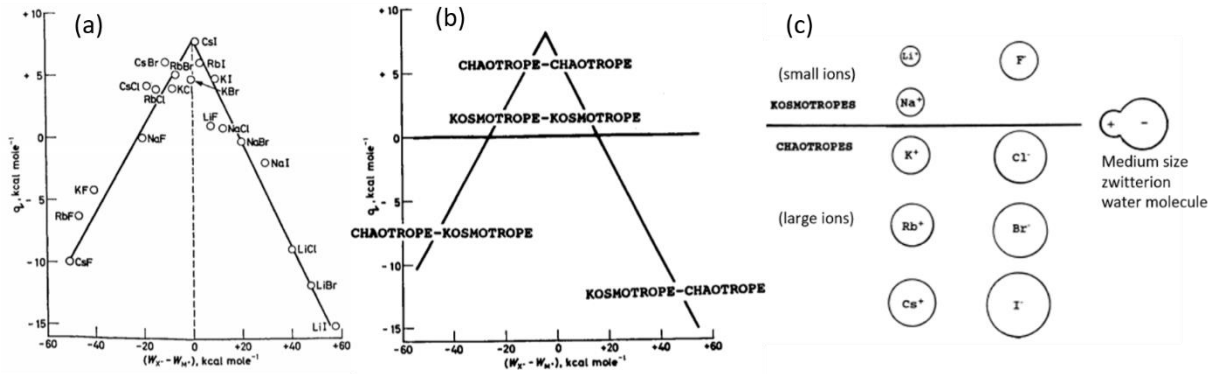

Figure 2. (a) Fig 8 of ref Morris 69: relationship between the standard heat of solution of a crystalline alkali halide (ordinate axis) and the difference between the absolute heats of hydration of the corresponding gaseous anion and cation.[Morris, 1968] (b) Fig 5B from Collins 97: Identification of ions as chaotropes (weakly hydrated) or kosmotropes (strongly hydrated). The enthalpy of solution of chaotrope-chaotrope and kosmotrope-kosmotrope salts is positive (takes up heat), whereas the enthalpy of solution of chaotrope-kosmotrope and kosmotrope-chaotrope salts is negative (gives off heat).[Collins, 1997] (c) Fig. 6 from Collins 2004: The horizontal line represents the strength of water-water interactions.[Collins, 2004]

As shown in Fig. 2-c, small ions (kosmotropes), will not form inner sphere ion pairs with large ions (chaotropes), the point of charge in the center of the small ion being closer to the medium size of the oppositely charged part of water molecule than to the point of charge of the large chaotropic ion. So oppositely charged ions will form together inner sphere ion pairs when they have a comparable water affinities.[Collins, 2004] Chloride anion and sodium cation are considered as neutral ions i.e. are on the limit between chaotropes and kosmotropes.[Leontidis, 2016] This explains perhaps why common salt effect to check ionic screening effect in soft-matter systems is usually brine. This enable to exclude ion specific effect when only electrostatic phenomenon has to be probed.

This rule of ion pairing is often summarized under the expression “like seeks like” and works well for the alkali-halide couples. More generally, what is subjacent to this rule is that we have to include a molecular-scale structure model of the ion and its solvent shell to the classical mean-field theories of ions distribution, especially when the ion concentration is beyond 0.1M. Therefore, another facet to understand ion specific effect is to consider an excluded volume mechanism above a certain concentration for kosmotropic salts that can induce a salting-out of soluble molecules. The ion size that determine its charge density and thus its effective size with its hydration shell is important and explains also why the ion specific effect are more significant for anions than for cations.

Kosmotropic or chaotropic ions are also qualified of hard and soft respectively following the concept of hard and soft acid/base (HSAB theory) introduced by Pr. R. Pearson in the sixties. This concept is related to the charge localization or delocalization within the atomic or molecular species and that determines strongly their mutual interaction, more or less ionic, more or less “covalent”.[Pearson, 1963]

I-3. Ion specific effects versus surface/interface

In soft matter and colloidal science, charged interfaces are ubiquitous and the ion specific effect has also an impact on the electrostatic repulsion between dispersed objects. Indeed, ion-pairing effect between an ionic function at a surface or interface and its counterion in the bulk solution follows the same rule as in the bulk: “like seeks like”. However, the interfacial features more or less polar, more or less hydrophobic, with non-uniformly charge covering can affect the order of the ion specificity classification. Various works of simulation in the 2000 years have help to understand some subtle effect of ion partitioning between the surface and the bulk, related to the ion polarizability strongly associated to the ion size but also to the surface charge density. That was the case of the P. Jungwirth and D. J. Tobias work in 2000 for alkali halide salts at water/air interface [Jungwirth, 2000] and consolidated by some experimental work such as from P. Koelsch and H. Motschmann via ellipsometry measurement [Koelsch, 2004] or of course in agreement with old data of surface tension from N.L. Jarvis et M.A. Scheiman in 1968 [Jarvis, 1968] (and concatenated with other data in ref L. Pegram et al in 2007 [Pegram, 2007]). Ions distribution at liquid/liquid interfaces were also the subject of numerous experimental and theoretical studies and we can cite for example the paper of G. Luo 2006 [Luo, 2006] for evaluating the right mean potential versus the distance to the interface to analyze X-ray reflectivity data.

Once these interfaces are covered with surfactant molecules then the surface tension can be strongly modified as a function of the association “ionic polar head/ counterion” used. It is known for a long time that within the alkali series, the cation are more or less bound to the sulfate head group of anionic SDS micelles and with a sort of selectivity that follows $Cs^+ > Rb^+ > K^+ > Na^+ > Li^+$ for monovalent cations and $Ba^{2+} > Sr^{2+} > Ca^{2+} > Mg^{2+}$ for divalents.[Schulz, 1998] The concept of partial dehydration due the ion pairing between chaotropic species or between kosmotropic species – the sulfate group of the SDS being rather soft or chaotrope [Vlachy, 2009] as well as the Cs cation in the precedent example – enables to explain these selectivities. One important consequence of the ion binding or pairing is the variation of the surface interaction between the polar heads of the surfactant that can be translated into a modification of the packing parameter and thus a variation of the surfactant film curvature.[Israelachvili, 2011] Impact on critical micellar concentration [Mukerjee, 1967; Pegram, 2008; Moreira, 2010], phase transition [Gustavsson, 1975; Renoncourt, 2006; Vlachy, 2008] and even solubility on double chains cationic surfactant varying the counter-anions were observed and analyzed always in line with Collins’ concept.[Ninham, 1983; Brady, 1986; Regev, 1994]

However, reversed Hofmeister series were underlined [Boström, 2005] and observed with some biological systems. As for example, it can be the case when proteins are out of its isolectric point (pI), at higher or lower pH, or when electrostatic and ion specific effects superimposed as a function of their concentration through double layer formation.[López-León, 2008; Dishon, 2009; Zhang, 2009; Flores, 2012] So direct and reversed series were summarized through the well-known phase diagram established by N. Schwierz, D. Horinek and R. R. Netz in their Langmuir article in 2010 [Schwierz, 2010], simulating the potential of mean force potential of alkali halide salts in interaction with surfaces of different polarities and surface charges (see Fig. 3).

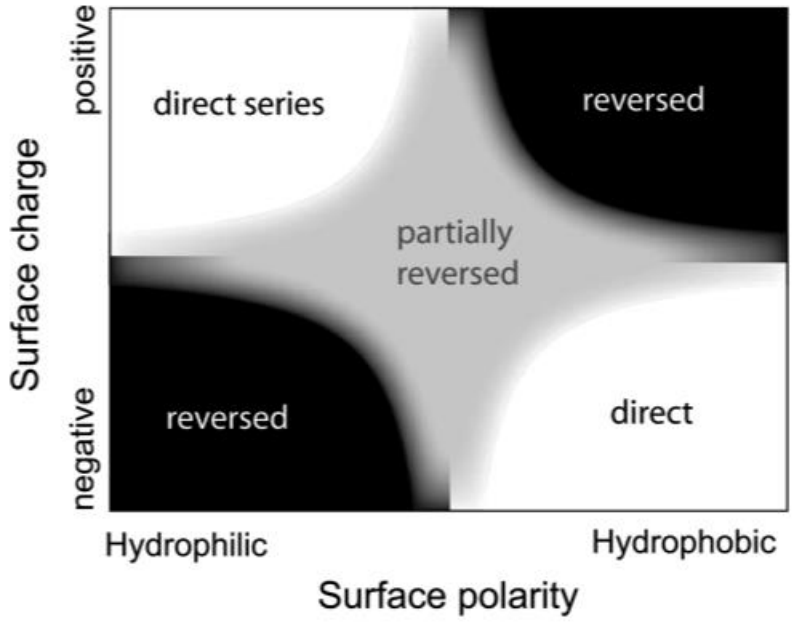

Figure 3. Schematic Hofmeister phase diagram as a function of surface charge and polarity, featuring direct and reversed series as well as partial reversion.[Schwierz, 2010]

From these studies, the ISE and the Hofmeister series appear to be clear for the extreme cases. For neutral and heterogeneous surfaces or interfaces, more subtle considerations have to be taken into account because of the local charge densities carried by the chemical end groups (see Fig. 4).

An interesting example of ISE on neutral macromolecules is those from Cremer group investigating the variation of the lower critical solution temperature (LCST) of well-known thermoresponsive PNIPAM macromolecules (poly-Nisopropylacrylamide). Indeed, PNIPAM becomes insoluble in water above around 30°C via a de-hydration mechanism of the most hydrophilic functions of the molecules, the amide groups. Salt in water can either re-inforce or reduce this effect depending if using kosmotropic or chaotropic ions.

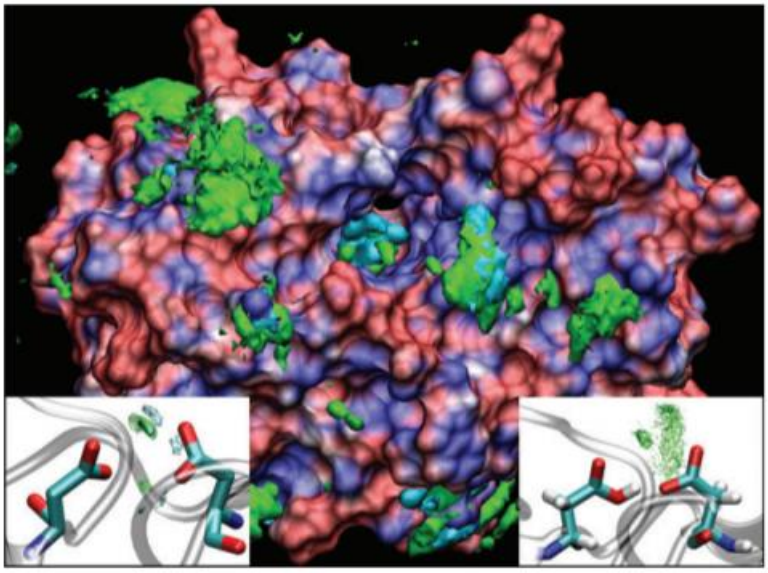

Figure 4. Caption of figure 2 from J. Heyda et al work.[Heyda, 2009] Distribution of sodium (green) and potassium (cyan) ions at the surface of HIV-1 PR averaged over a simulation in the mixed NaCl/KCl solution (0.25M each salt). The color coding of the surface reflects the electrostatics (red – positive and blue – negative). Insets show detailed distributions of Na+ and K+ in the vicinity of the deprotonated (left) and singly protonated (right) Asp pair at the active site.

The former ones act again as a water carriers and polarize water molecules that were directly hydrogen bonded with the hydrophilic moieties of the macromolecules (the de-hydration effect) whereas it is demonstrated that for the latter ones a binding effect directly with some of the functions such as amide has to be considered. This binding effect can be analyzed as a sorption mechanism that can achieve a saturation state. It brings some charges onto the macromolecules that finally increase its solubility and increase its LCST. This work on PNIPAM is interesting and the solubilization effect directly related to the presence of kosmotropic and chaotropic ions can be correlated to the cloud temperature shifts (ΔT) for nonionic surfactants such as polyethylene types was used for a long time to classify all the ions series via their lyotropic number, a non-linear function of ΔT (see Fig. 5).[Schott, 1984] It is important to notice that the temperature variation effects observed on cloud points or LCST (or UCST) variation as a function of salt concentration are much more pronounced for kosmotropic than chaotropic anions and we will come back on this point later in this chapter.

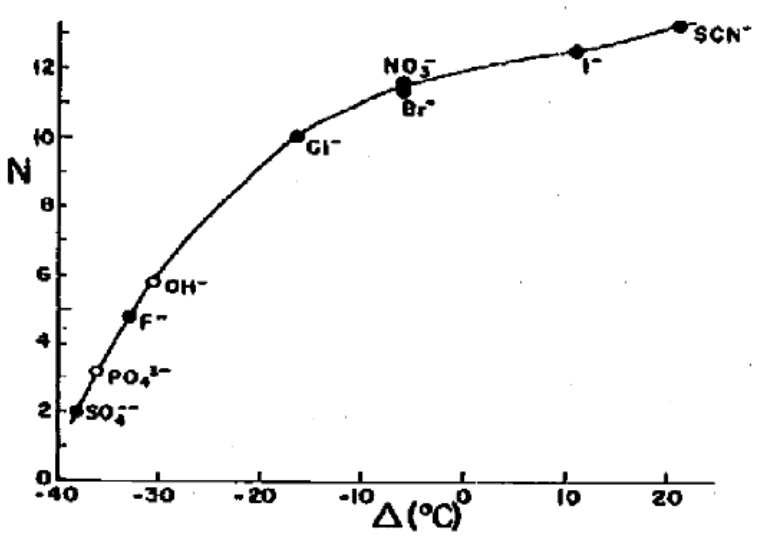

Figure 5. A caption of the Fig. 1 from the paper of Schott 1984.[Schott, 1984] This figure represents the lyotropic number of some kosmotropic and chaotropic anions as a function of the octoxynol 9 (triton X-100) non-ionic surfactant cloud point shift values of their sodium salts.

I-4. ISE and Langmuir isotherm

As written previously, the local charge density carried by the chemical end groups at a surface or along macromolecules is important to be taken into account to quantify ISE and the hydration via the interaction of the water molecules through dipolar interaction or H-bonds is determinant. One way to tune this density is to vary the surface pressure, as it can be applied using a Langmuir trough. When molecules are insoluble, they can be spread at water/air interface and compressed while the surface tension is recorded. Then the surface pressure can be determined at a given temperature as a function of surface per molecule in order to determine their lateral interaction through a lateral equation of state and that can be modulated via ISE when salts are solubilized in the subphase.[Aroti, 2007]

ISE on amphiphilic lipid's and phospholipid's layers as models of cellular membrane interfaces were investigated by numerous groups. The big advantage for these types of systems is that the variability of the chemistry at the level of the polar heads (neutral, cationic, anionic or zwitterionic, monomeric or oligomeric) or at the level of the aliphatic chains (single, double, short, long, saturated or not) enable to probe an infinity of surface packing, homogeneous or heterogeneous, ordered or non-ordered.

As an example, let's focalize on studies about the effect of sodium salts of monovalent anions (NaCl, NaBr, $NaNO_3$, NaI, $NaBF_4$, $NaClO_4$, and NaSCN) in concentrations range between 0.5 and 1.5 M and at two different temperatures on Langmuir monolayers of zwitterionic lipid 1,2-dipalmitoyl-sn-glycero-3-phosphocholine (DPPC).[Aroti, 2004; Christoforou, 2012] The

monolayer at 12°C on pure water is characterized by a first order transition between a gaseous phase and an ordered phase (see Fig. 6).[Christoforou, 2012] Whereas the monolayer at 20°C is characterized by a first order transition from liquid expanded (LE) phase to a liquid condensed phase (LC) upon compression before to achieve the ordered phase at higher compression (see Fig. 7).[Aroti, 2004] As shown in Fig. 6 at 12°C, the addition of more chaotropic salt or increasing the concentration for one of the chaotropic salt, increases the surface pressure at fixed molecular area and a biphasic domain is observed between LE and LC phase as observed at higher temperature without salt. Moreover, the LE phase is formed at higher surface per molecule.

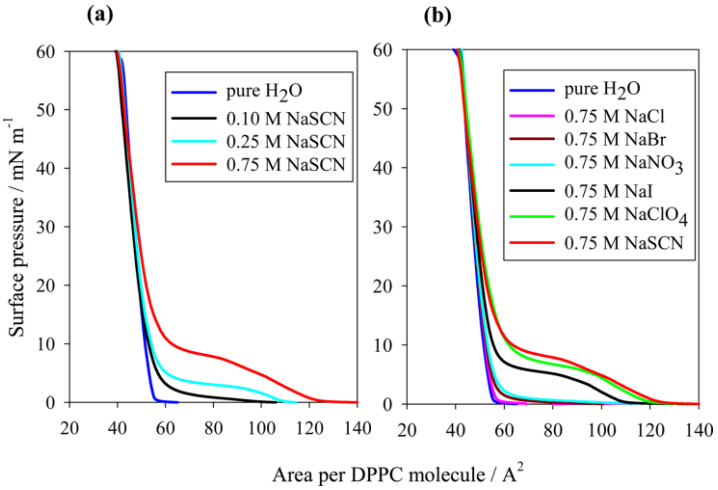

Figure 6. Pressure−area isotherms of DPPC monolayers at 12 °C on (a) NaSCN solutions of various concentrations, and (b) 0.75 M solutions.[Christoforou, 2012]

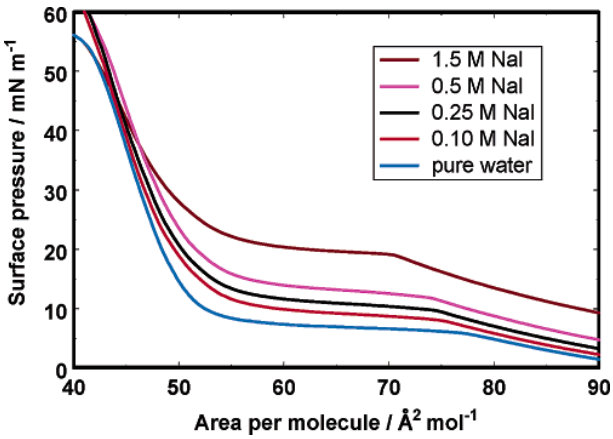

Figure 7. Pressure−area isotherms of DPPC monolayers at 20°C in the presence of sodium iodide salt at different concentrations Extracted from Aroti et al 2004. [Aroti, 2004]

At 20°C and upon addition of chaotropic salts, the transition from liquid expanded phase (LE) to the condensed phase (LC) is shifted to the lower molecular areas, the LE phase is stabilized.

This argument is in agreement with additional informations from IRRAS[1] about chains conformation.[Dluhy, 1988; Mitchell, 1988; Hunt, 1989] It was also demonstrated from GIXOS method, that the tilt angle in LC phase in presence of electrolytes increases, which may be due to the expansion of the monolayer at fixed surface pressure. Untilted DPPC phase can be observed in two cases: if the area requirement of the head group can be changed by dehydration or reorientation from parallel to vertical alignment, and if alkanes are inserted into the hydrophobic part of the monolayer (mixed monolayers). Such effect is shown at very low concentrations (5×10^{-5} M) of the strongly chaotropic and surface active tetraphenyl borate anion (TPB).[Christoforou, 2012]

Brewster-angle microscope (BAM) was used to study the morphology (size and shape) of the DPPC monolayer domains at 20°C and 56 $A^{\circ 2}$ per molecule, and in the presence of 1 M of salt solutions (see Fig. 8), 0.5 M, anions having no significant effects on the size and shape of the LC monolayers.[Aroti, 2004]

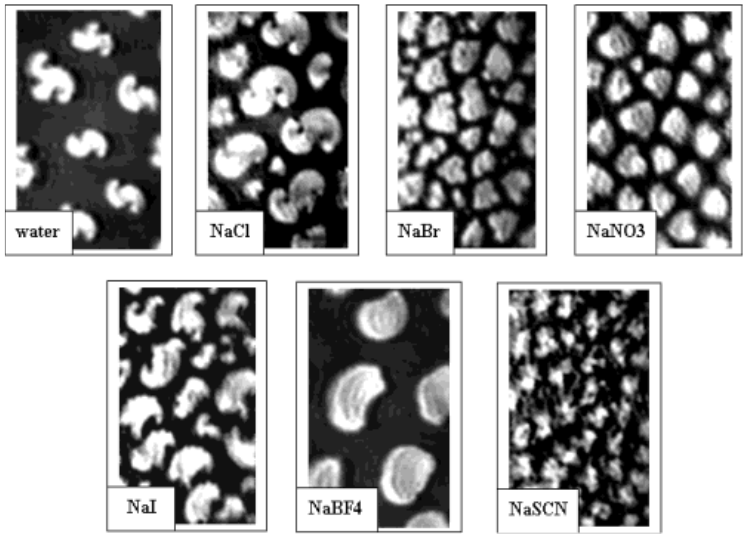

Figure 8. A caption of Fig. 4 in the paper of Aroti et al. 2004 [Aroti, 2004]: BAM images of LC phase domains of DPPC for a surface area of ca. (56 ($\pm$1) $Å^2$ per molecule in the presence of 1 M solutions of NaCl, NaBr, $NaNO_3$, NaI, $NaBF_4$, and NaSCN. A picture of DPPC monolayers on pure water at 56 $Å^2$ per molecule is also included for comparison.

In general, Cl^- has no significant effect, while Br^-, NO_3^-, and I^- make the shape of the LC domains rounded rather than triskelion. BF_4^- has a stronger effect, and SCN^-, which is considered as the most chaotropic anion, reduces the size of the domains. The shape of 2D LC domains is influenced by a competition between the line tension (which favor rounded shape) and the electrostatic interactions (which favor elongated domains). In this case, it was

[1] Spectroscopic technique to evaluate local chain conformation from a variation of the chemical function vibration signature.

assumed that the adsorption of anions onto the monolayer screens its dipole potentials, therefore, the electrostatic forces are reduced and make the shape of the LC domains more rounded.[Aroti, 2004]

Phenomenological continuum models were used to analyze the surface pressure versus salt concentration isotherms of the lipidic monolayer in its LE phase. The Fig. 9 describes qualitatively three modes of interaction between chaotropic ions and the lipidic interface (see Fig. 9) [Leontidis, 2009]: The first is the “local binding” model characterized by a binding constant. The second is the model of “ionic partitioning” in a diffuse lipid layer considering the polar head region as a second phase adjacent and different to the bulk. In that case, the model requires two parameters characterizing the anion partitioning coefficient and a parameter of interaction between the anions and the lipids. Within the third model of “dispersion forces” only the polarization parameter of the most polarizable ion was taken into account. The second and the third models are suitable and highlight the collective character of the interaction description with appears relevant to describe the pressure isotherms. However as mentioned in this article this does not necessarily prove that no anion-lipid binding occurs at the interfaces, but if there is, it is not the dominant mode of interaction in this system (with some exceptions).[Leontidis, 2009]

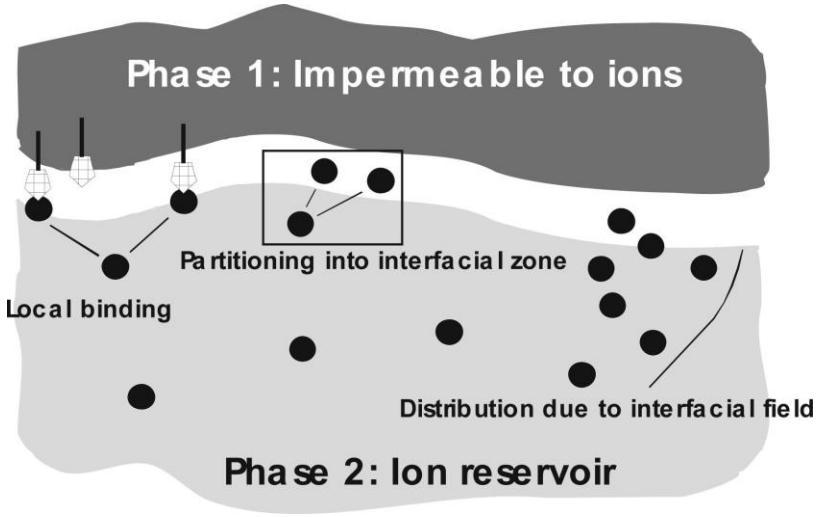

Figure 9. Three modes of specific ion interaction at a boundary between two phases.[Leontidis, 2009]

It was found also that it exists an excellent correlation of the partitioning chemical potentials as a function of the ionic radius, suggesting that specific anion effects on this lipid model system are mostly a matter of ionic size.[Leontidis, 2009] Therefore, the ionic size may be the reason behind the stronger effect observed with SCN^- in most studies of interactions of anions with lipid layers, knowing that SCN^- is a linear molecule and this can make it easier to enter within

the lipid bilayer than spherical anions like I^-. It was also suggested that the binding of cation (i.e. the sodium) on the lipid head groups can lead to lipid clustering which leads also to a density inhomogeneities of the LE phase and therefore anions can use these comfortable and less dense pockets at the interface as solubilization sites for penetrating within the lipidic layer.[Aroti, 2007; Leontidis, 2009; Leontidis, 2009]

It was observed that anions swell also phospholipidic bilayers, an effect linked to an increase of the area per lipid headgroup. This was again attributed to lateral electrostatic interactions arising from charging through the adsorption of the anions. The chaotropic anions I^- and SCN^- have the strongest effect on the DPPC headgroup area. [Rydall, 1992] This effect increased with the decreasing of the anion surface charge density where the largest effect was with ClO_4^- with the highest association constant about 115 M^-. In this study, the authors assumed that the factor determining whether an anion will interact with the lipid bilayer is the ease with which that anion loses its hydration shell. [Vácha, 2010; Leontidis, 2017] Thus, the free energy increases, and the cost of cavity creation to accommodate ions is reduced. This contribution is sufficient to drive the anions to the lipid interfaces. Molecular dynamic simulations have provided fundamental atomic-level description that can explain the experimental results and explain the interactions of anions with bilayers: large anions penetrate more deeply into the bilayer than small anions such as Cl^-. Large anions are energetically more stable in a hydrophobic environment than the Cl^-.[Sachs, 2003]

I-5. IES and protein stability

Proteins are large biomolecules or macromolecules with molecular weight between 10 000 and 100 000 Daltons, where Dalton is the weight of one hydrogen atom. They are composed of amino acids associated in a specific order via peptide bounds through reactions of condensation for making residues, determined by the base sequence of nucleotides in the DNA coding for the protein. Twenty amino acids take place naturally and commonly found in proteins but since they can undergo some chemical reactions such as phosphorylation, hydroxylation, methylation, acylation or glycosylation, the inventory is even wider. There are three types of natural amino-acids depending on the properties of their side chains: (i) charged side chains (positive or negative), (ii) polar uncharged side chains and (iii) aromatic and aliphatic hydrophobic side chains.[Arefian, 2017] The glycine (polar) and the alanine (apolar) are the simplest amino-acids (see Annex IV-1 for the structure and the properties of the twenty standard amino acids). A linear sequence of amino acid residues is called a polypeptide. The conformation of proteins depends on the repulsive and attractive interactions between polar

and non-polar groups in the side chains of amino acids. The protein can be linear or coiled and folded like globular proteins. There are four levels of protein structures :

(i) The primary structure, on which the final protein structure depends ultimately, corresponds to the sequence of amino acids in a specific order,

(ii) The secondary structure corresponding to the favored combination of angles between N and C atoms within the polymeric backbone and that assign the most stable configuration and stabilized via hydrogen bonds between closed residues. α-helix and β-pleated structures are the most known secondary structures,

(iii) The tertiary structure corresponds to the 3D conformation of the polypeptides in its native state that means folded. Polar functions are oriented toward the outside whereas the apolar functions are oriented towards the core of the structure. The specificity of the 3D conformations is crucial for their activity by a dynamical and suitable orientation of some sites to interact with other molecules.

(iv) The quaternary structure is how the subunits of a protein (when they exist) are arranged and oriented respect to each other.

Proteins are essential parts of organisms and participate in every process within the cells. Each protein has unique functions. Some proteins have structural or mechanical functions, other proteins are important in cell signaling, immune responses, cell adhesion, and the cell cycle. Examples of proteins include whole classes of important molecules, among them enzymes, hormones, and antibodies.

Proteins have acidic and basic groups. There are two acidic side chains amino acids: aspartic acid (Asp) and glutamic acid (Glu) that have carboxylic groups with pKa low enough to lose protons and then become negatively charged (COO^-). On the other hand, the basic groups are the amino acids with basic side chains: lysine, arginine and histidine, this latter is weaker than lysine and arginine (pKa = 10.67, 12.10 and 9.09 for the side chains respectively). Proteins can be positively or negatively charged or even neutral depending on the pH. The pH at which the protein is neutral is called the isoelectric point (pI):

(i) For pH lower than pI: the carboxyl group COO^- combine with H^+ and become COOH (uncharged).

(ii) For pH higher than pI: For example, primary ammonium (NH_3^+) groups lose a proton H^+ and become uncharged (NH_2).

(iii) At intermediate pH: the protein possesses positive and negative charges at the same time i.e., zwitterions.[Whitford, 2013]

Proteins hydration represent about 10 or 20 percent of their molecular weight. Considering a surface of protein, the hydration shell around a protein is not homogeneous and depends on each segment of the protein, therefore, the specific ion effects will be influenced.[Kunz, 2010] Very qualitatively, water layers at a protein surface can be divided into three layers: [Collins, 2004] the first one close to the protein surface or the solvation layer (), the second layer or transition layer, and the third layer or the bulk surface layer (see Fig. 10).

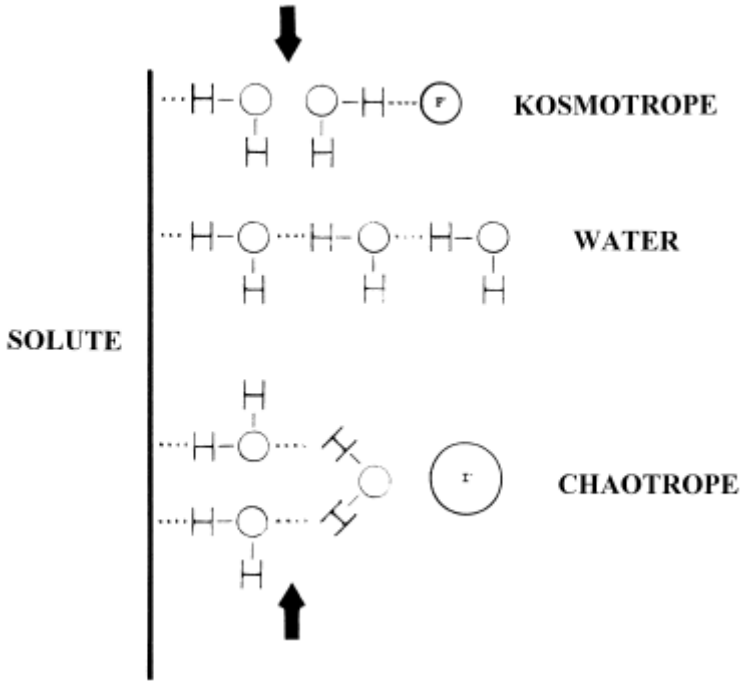

Figure 10. Fig 9 in the paper of Collins 2004. Interfacial water near the polar surface of a test solute (protein molecule).[Collins, 2004]

If a kosmotropic ion is inserted into the third layer, water molecules in the second layer will solvate this strongly hydrated ion, and cannot participate to the protein hydration: in that case the protein forms crystals contacts. In the opposite case, when a chaotropic ion is inserted into the third layer, the second layer of water is released and can “help out” the first layer to hydrate more the protein and lead to the unfolding of it by increasing the solvent exposed surface area.[Collins, 2004] The positive charges of the protein are weakly hydrated (ammonium, guanidinium and imidazolium ions). For proteins with an excess of weakly hydrated positive charges, weakly hydrated anions interact with these positive sites and neutralize the protein, which then crystallizes. Hofmeister effect is reversed [Ries-Kautt, 1997; Retailleau, 1997]. In contrast, for proteins with an excess of strongly hydrated negative charges (carboxylates RCOO-), highly hydrated cations interact with and dehydrate the excess of strongly hydrated sites (normal Hofmeister effect).

Coming back on the protein solubility and stability, it appears evident that this type of macromolecules represents perhaps the most complex colloidal structure in term of surface polarity and charge with patchy surface distribution. Moreover, protein in solution are often prepared in buffer that enable to stabilize an optimal polymeric conformation, a structural and dynamical equilibrium between the internal hydrophobic, H-bonding and electrostatic interactions. So, the quantification of salt effect for the salting-in or out although qualitatively predictive remains and will remain a challenge. A work of molecular dynamic simulation from Jungwirth et al is a good example to illustrate this complexity.[Vrbka, 2006] They focused on "the distribution of sodium, choline, sulfate, and chloride ions around two proteins, horseradish peroxidase (HRP) and bovine pancreatic trypsin inhibitor (BPTI) with the aim to elucidate ion adsorption at the protein surface. Although the two proteins under investigation are very different from each other, the ion distributions around them are remarkably similar. Sulfate is always strongly attached to the proteins, choline shows a significant, but unspecific, propensity for the protein surfaces, and sodium ions have a weak surface affinity, while chloride has virtually no preference for the protein surface. In mixtures of all four ion-species in protein solutions, the resulting distributions are almost a superposition of the distributions of sodium sulfate and choline chloride, except that sodium partially replaces choline close to the proteins. The present simulations support a picture of ions interacting with individual ionic and polar amino acid groups rather than with an averaged protein surface. The results thus show how subtle the so-called Hofmeister and electroselectivity effects are in salt solution of proteins, making all simplified interaction models questionable.[Vrbka, 2006] All is summarized in this article's abstract and this leaves a lot of place for experimental studies in order to find some possible correlation between ion sorption or binding onto proteins with either the 3D structure of the protein or its surface topology and ionic potential.

Nevertheless, it seems to be clear from many studies that the balance between salting out nonpolar groups and salting in the peptide groups defines both classes of stabilizing salts and denaturant salts.[Baldwin, 1996]

As a conclusion, ions in aqueous solutions exhibit specific effects that are beyond their electrostatic interactions. Their specific effects depend on their size, polarizability and charge density. Weakly hydrated ions (chaotropic ions) are large with low charge density and high polarizability. The water molecules in their surrounding hydration shell is less structured that the water molecules in the bulk. Consequently, the hydration shell around these ions can be easily loosed so that the ions can adsorb to interfaces or other substances in the solution. The chaotropic effect is the tendency of chaotropic ions to interact with hydrophobic and neutral polar surfaces.[Chandler, 2005; Biedermann, 2014] This effect is orthogonal to the hydrophobic effect.[Assaf, 2018] The binding of hydrophobic species and chaotropic anions is

related to de-solvation. Indeed, water molecules of the solvation shell around hydrophobic species are highly structured, contrary to the water molecules around chaotropic anions. Therefore, the desolvation of hydrophobic species is entropically favored, while it has a negative enthalpic component for chaotropes [Assaf, 2018] and a positive water structural entropy for ionic hydration, indicating a loss of hydrogen bonds between water molecules within the hydration shell.[Marcus, 2009] Therefore, the de-solvation of the chaotropic anion leads to the recovery of hydrogen bonds between water molecules.[Assaf, 2015] Chaotropic anions with higher polarizability and higher capacity of dehydration have more tendency to adsorb into surfaces. In addition, the solution viscosity decreases in the presence of chaotropes. On the other hand, strongly hydrated ions are relatively small with high charge density and low polarizability. The water molecules in their surrounding hydration shell is more structured that the water molecules in the bulk. Consequently, the solution viscosity increases in the presence of these ions called the kosmotropic ions. Therefore, ions are classified as kosmotropes, chaotropes or neutral (neither kosmotropes nor chaotropes) under the Hofmeister or lyotropic series that are represented in Fig. 11. In general, the effects of anions are stronger than cations. Anions can affect the intermolecular interactions of water molecules more than cations, this effect is associated to the larger size of anions that are more polarizable. Therefore, anions have more propensity to change the interfaces properties than cations.[Bastos-González, 2016] The understanding of the specific effects of salts is very important. Specific interactions between ions and molecules modify their chemical, physical and biological properties. The Hofmeister classification of ions help to predict the effect of ions on biological molecules (proteins, lipid membranes…) and therefore, help to know the molecular mechanisms of biological processes.[Kobayashi, 2017]

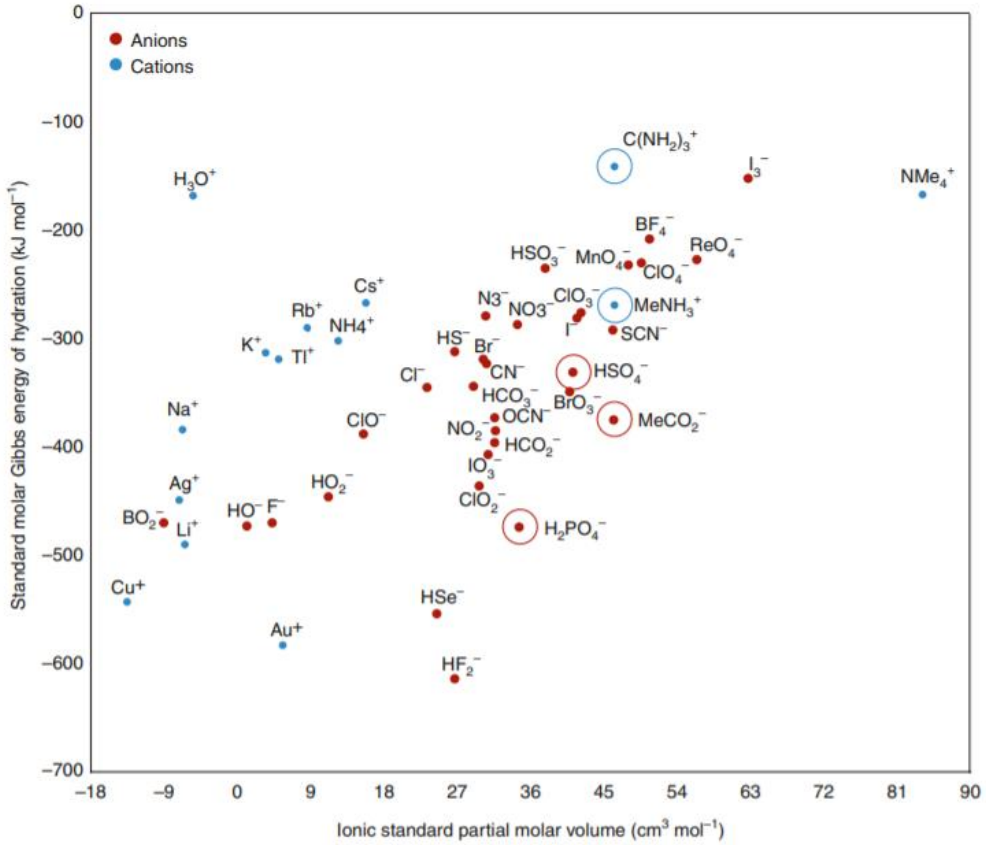

Figure 11. Hofmeister series. Caption of Fig. 1 from the paper of Gibb 2019: Plot of the ionic standard partial molar volume of monovalent ions against their standard molar Gibbs free energy of hydration. Ions near the top of the graph are weakly solvated and, therefore, in these cases, water can be viewed as more easily pushed aside so that the ion can form alternative non-covalent interactions with other solutes. In contrast, strongly solvated ions near the foot of the graph can be viewed as difficult to interact with.[Gibb, 2019]

Recently, Pr. Leontidis have extended the lyotropic series in comparison to chaotropes (see Fig. 12). Cl^- is a neutral ion separating kosmotropes from chaotropes.[Leontidis, 2016] Considering the Hofmeister series and comparing the hydrophobic anions to ClO_4^- and SCN^- chaotropic anions, hydrophobic anions that disrupt soft matters and lead to a phase transition can be placed at the right side of these chaotropes.[Leontidis, 2016] PF_6^- is demonstrated to be at the limit between simple chaotropes and structure-disrupting ions[Leontidis, 2016] and can be qualified as superchaotropic anions (see section superchaotropes below). Beyond the hydrophobic ions on the right side are placed the hydrotropes and surfactants. No clear line is between hydrophobes and hydrotropes as their effect is quite similar,[Leontidis, 2016] where hydrotropes are ionic organic compounds that have an amphiphilic structure, like surfactants, but their hydrophobic part is too short to make self-assemblies. Hydrotropes increase the solubility of weakly soluble organic molecules and hydrophobic molecules above a concentration around 0.5 M.[Neuberg, 1916; Dhapte, 2015]

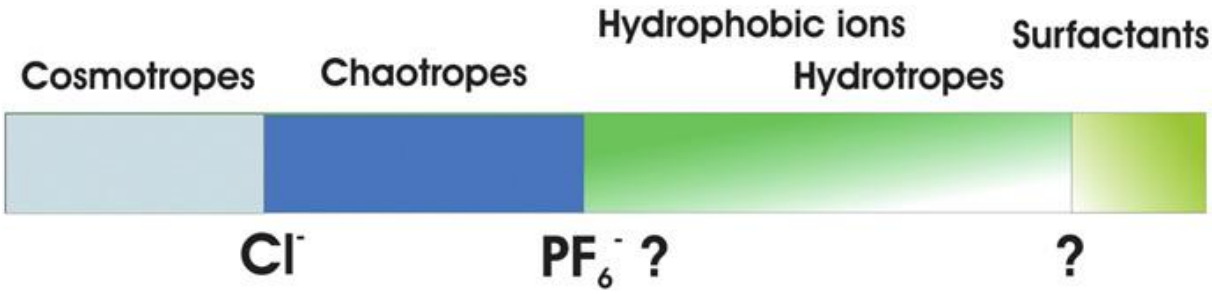

Figure 12. Merging of the lyotropic line with the surfactant domain through the action of hydrophobic and hydrotropic anions.[Leontidis, 2016]

II. Specific effects of nanometer-sized ions

The extension of the classical Hofmeister series to larger ions up to nanometer-size i.e. much larger than classical ions (~0.2-0.3 nm), with so a decreased of the charged density and thus a much weaker hydration, enabled to observe exalted chaotropic properties.[Assaf, 2015; Naskar, 2015; Leontidis, 2016; Assaf, 2018] This effect was qualified as a superchaotropic behavior related to a strong water-mediated interaction between the ion and a solute or an interface. This binding is entropically favored by the release of water molecules from a part of the hydration shell of the nano-ions as well as a part of the surface or of the solute hydration shell.[Buchecker, 2018] Nano-ions of different chemical structures have been investigated and referred to as superchaotropic ions.

II-1. Antagonistic salts: Bulky organic ions

The Hofmeister series were often extended with organic hydrophobic ions, such as the tetraphenyl borate anion Ph_4B^-, the tetraphenyl arsonium cation Ph_4As^+ and the tetraphenyl phosphonium chloride PPh_4Cl that interact strongly with hydrophobic interfaces as superchaotropic ions (see Fig. 13).[Bastos-González, 2016] Tetraphenyl borate salt is considered as antagonist due to the fact that the anion is hydrophobic (large anion so that the hydrogen bonds are deformed and the hydration shell is destroyed) and the counter-cation is hydrophilic.[Sadakane, 2018] Thus, in mixture of polar and apolar solvents (water/oil), the ion and the counter-ion interact asymmetrically with the solvents where the hydrophobic ion preferably dissolves in the oil phase and the hydrophilic counter-ion preferably dissolves in water. Therefore, these superchaotropic organic compounds show surface activity in aqueous solutions [Winkler, 2017] as well as at a water/oil interface. As a consequence, the presence of such antagonistic salts leads to the decrease of the interfacial tension that increases the solubilization of hydrophobic species in water [Winkler, 2017] and lead to the formation of mesophases and ordered structures such as membranes.[Sadakane, 2009; Sadakane, 2013;

Onuki, 2016; Sadakane, 2018] Noting that Michler et al. consider the tetraphenyl borate as a surfactant rather than antagonist basing on their definition of an antagonistic salt as a substance that decrease the interfacial tension after redistribution of the ion and counter-ion between the water and oil phases which cannot be the case at a surface (water/air).[Michler, 2015]

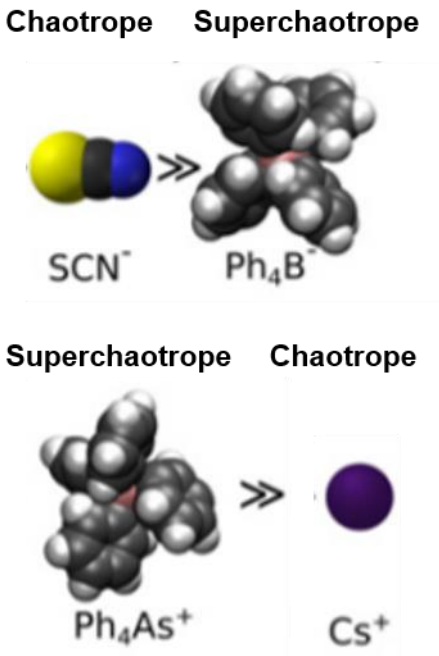

Figure 13. Extended Hofmeister series from Bastos-Gonzalez et al. review.[Bastos-González, 2016]

II-2. Polyoxometalates (POMs) anions

Polyoxometalates are metal-oxide nanometer sized anion clusters belonging to inorganic compounds. POMs are consisting of early transition metals (V, Ta, Nb, Cr, Mo, W) at a high oxidation state, where the largest number of examples are consisting mainly of V, W and Mo.[Borrás-Almenar, 2003] It has been shown that the classical Keggin and Dawson POMs, adsorb at the non-ionic polar surface of tetraethylene glycol monooctyl ether (C_8EO_4) and n-octyl-β-d-glucopyranoside (C8G1) micelles, where the adsorption has a physicochemical nature (not covalent binding).[Naskar, 2015; Buchecker, 2018] POMs adsorb on the surface of C8G1 micelles whereas they penetrate into the polyethoxylated headgroups of C_8EO_4 micelles. It was suggested that this different behavior is due to the difference in hydration around the polar groups the polyethoxylated groups (PEG) or the glucose moieties.[Naskar, 2015] The self-assembly of systems containing polyethoxylated group being very sensitive to the hydration, cloud point measurements of C_8EO_4 neutral surfactant above its CMC were performed in the presence of POMs (HPW, HSiW) and classical ions from the Hofmeister series.[Naskar, 2015; Buchecker, 2018] The cloud point (CP) of a surfactant corresponds to the temperature at which a phase transition or liquid/liquid phase separation is observed in the

solution upon heating.[Heskins, 1968; Naskar, 2015; Buchecker, 2018] This phenomenon can be explained by the loss of hydrogen bonds between the surfactant headgroups and water molecules and therefore a change in the packing parameter that leads to the elongation of micelles at higher temperature.[Glatter, 2000] In the presence of chaotropic ions, the CP of C_8EO_4 is shifted to higher temperature (few degrees for high concentration of salt) due to a growth of intermicellar repulsion forces referred to as a salting-in effect. However, in the presence of POMs, the CP of C_8EO_4 is shifted to much higher temperatures and at low concentration of salt (mmol) compared to the classical ions such as I^- and SCN^-. The observed effect of POMs on the C_8EO_4 CP is due to POMs anions adsorption onto C_8EO_4 micellar surface via the solvent-mediated phenomenon (chaotropic effect) increasing the intermicellar repulsions that prevent the phase separation. Therefore, it was suggested that the Hofmeister series can be extended to the chaotropic side using superchaotropic anions such as the polyoxometalates anions.[Naskar, 2015; Buchecker, 2018] In addition, it has been demonstrated that the charge density of the POM anion determine its chaotropic behavior, where POMs with lower charge densities exhibit stronger super-chaotropic behavior.[Buchecker, 2018] POMs with lower charge densities are less hydrated, which means that their dehydration upon adsorption to surfaces presents a lower energy cost.[Buchecker, 2018]

POMs can also form new self-assemblies with non-ionic and soluble molecules. As an example it was observed and investigated that water soluble polymers such as the thermoresponsive short chain poly (N-isopropylacrylamide) (PNIPAM) [Buchecker, 2019] and the polyethylene glycol oligomers (PEG) [Buchecker, 2017] can form large micrometric sheets with molecular thickness, mixed globules and nano-assemblies and that can be modulated via electrostatic screening.

Indeed, an interesting point behind the ion adsorption mechanism is first the “saturation” of the process. Lateral electrostatic repulsion onto the surface or the interface will limit the concentration of the superchaotropic anions at the surface. So, increasing the concentration of superchaotropic ion in the solution will lead above the saturation to a “self”-screening effect. However, a large difference exists with more classical ionic systems: since the ion adsorption mechanism is associated to a partial de-hydration of the polar surface, once the electrostatic repulsion is screened the system will precipitate. This subtle balance was used to form POM-PEO crystals as an example.[Buchecker, 2017]

II-3. The boron-based ionic clusters

It was shown that the boron-based anionic clusters, dodecaborate and the cobalt-bis-(dicarbollide) anions can be also considered as superchaotropic anions. Classical cloud point measurements of adenine and riboflavin in the presence of dodecaborates showed a pronounced increasing of their solubility compared to classical chaotropic anions.[Assaf, 2015] In addition, it was shown that the hydrophilic dodecaborate inorganic anions ($B_{12}X_{12}^{2-}$, X = H, Cl, Br, I) and cobalt-bis-(dicarbollide) derivatives exhibit strong binding affinity with γ-cyclodextrin forming inclusion complexes, with the weaker binding affinity observed with $B_{12}H_{12}^{2-}$.[Assaf, 2015; Assaf, 2019] Cyclodextrins (CDs) are a family of water-soluble macrocyclic oligosaccharides consisting of glucose units.[Szejtli, 1998] α-, β-, and γ -CD with 6, 7, and 8 units respectively, have a cone shape with a hydrophobic cavity mimicker of biological binding sites and can encapsulate organic guest molecules,[Assaf, 2016] they are known for their usage as drug delivery.[Challa, 2005] In general, hydrophobic effect is the driving force for the binding of a guest with a macrocycle host with a positive entropic contribution upon the release of structured water molecules that solvate the hydrophobic guest.[Assaf, 2018] Dodecaborates anions are highly soluble in water[Karki, 2012] where the hydrophobic effect cannot be considered as the driving force for their high binding affinity. It was demonstrated that the driving force of the binding between dodecaborates and γ-cyclodextrin is the chaotropic effect with a negative entropic component due to the formation of structured complexes.[Assaf, 2015] It was assumed that the low association constant of $B_{12}H_{12}^{2-}$ is due the non-matching size between this compound and the cyclodextrin cavity,[Assaf, 2015] and the high hydrophilicity (high charge density) of this compound compared to the halogenated one.[Hohenschutz, 2020] It has been shown that the binding affinity of COSANs is stronger than dodecaborates.[Assaf, 2019] Indeed, COSANs anions are larger than dodecaborates with lower charge density, meaning that they are more superchaotropic than dodecaborates. The formation of host-guest complexes of POMs with macrocycles was also shown to originate from the superchaotropic effect of POMs enabling the elaboration of complex multiscale hybrid materials.[Wu, 2015; Moussawi, 2017; Moussawi, 2017]

III. Boron chemistry and compounds- Metallacarboranes

Boron is an element belonging to the group 13 in the periodic table with three valence electrons, its chemical properties are similar to carbon and silicon with electronegativity 2.05 lower than the electronegativity of carbon (2.55). The abundance of boron in the earth's crust is around 10 ppm which means that it is the 38th most abundant element. Boron element can

be found in water, rocks and soils where minerals borax $Na_2[B_4O_5(OH)_4].8H_2O$ and kernite $Na_2[B_4O_6(OH)_2].3H_2O$ are the most important source.[DeFrancesco, 2016] Between natural products containing boron, Boromycin was the first product isolated containing boron which (showed an anti-HIV activity.[Kohno, 1996] Organoboron compounds contain at least one bond of carbon-boron, they have interests in several applications for more than 60 years including pharmaceutical uses, boron neutron capture therapy (BNCT), materials science and others.[DeFrancesco, 2016] Polyhedral boron hybrids or boron cluster compounds are an important class of boron compounds such as the metallacarboranes that belong to carboranes family. Metallacarboranes (MCs) are inorganic molecular clusters made of boron and carbon atoms, among which the metalla-bis-(dicarbollide) anions synthesized first by Hawthorne in 1965[Hawthorne, 1965] are one of the most studied carboranes compounds in the last decades.[Dash, 2017] These $[M(III)(C_2B_9H_{11})_2]^-$ anions are composed of two bulky dicarbollide semicages, each of them bearing two negative charges that "sandwich" a metal cation ($M=Co^{III}$, Ni^{III}, Fe^{III}) through different rotamers (cisoid, gauche and transoid) depending on their environment. The remaining negative charge is delocalized over the entire structure[Hawthorne, 1965] and is counterbalanced by a counterion, which is typically a proton or an alkali cation. MCs can be also closed polyhedral and named with the prefix "*closo*", or fragments of deltahedra when at least one vertices is absent. "*Arachno"* and "*nido"* metallacarboranes is when one and two vertices are absent respectively.[Grimes, 2000] The metalla-bis-(dicarbollide) nano-ion investigated in this project is a cobalt-bis-(dicarbollide) $[Co(C_2B_9H_{11})_2]^-$.

III-1. Cobalt-bis-(dicarbollide) anion

The cobalt-bis-(dicarbollide) $[Co\ (C_2B_9H_{11})_2]^-$ is a nanometric-size theta shape (represented by the Greek letter θ) anion with dihedral angle about 3.7°(see Fig. 14).[Sivaev, 1999] Cobalt-bis-(dicarbollide) is composed of two bulky carborane cages made of boron and carbon atoms, each of them bearing two negatively charges and sandwiching a cobalt metal ion in its +III oxidation state, hence it is named COSAN (Co=cobalt; SAN=sandwich). The remaining single negatively charge is delocalized over the entire volume (0.45 nm^3) giving rise to a low charge density (2.2 charge per nm^3). The two carboranes cages of COSAN are in mutual rotation with an angle about 37° and the cobalt metal ion is equidistant from the 2 cages even though the distance Co-C is barely shorter than the distance Co-B.[Sivaev, 1999] Cesium-COSAN (CsCOSAN) is the commercial form of COSAN purchased from Katchem for our studies and has limited solubility in water (0.975 mM at 23°C).[Kohno, 1996] Since in this project we are interested by the study of the interactions of COSAN with biological molecules and interfaces, Sodium-COSAN (NaCOSAN) is the most recommended form as Na^+ is an important and

abundant cation in our body. Therefore, a cation-exchange procedure was performed to exchange CsCOSAN by NaCOSAN that have high solubility in water (see Annex IV-3).

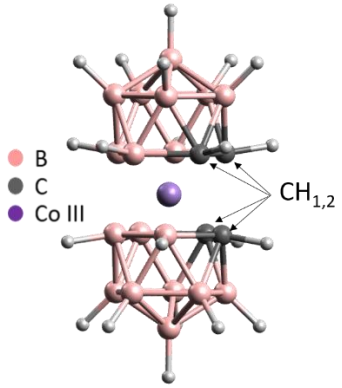

Figure 14. Cis-COSAN structure $[Co\ (C_2B_9H_{11})_2]^-$.

COSAN is characterized by a surfactant behavior in aqueous solution. COSAN adsorb to the water/air interface decreasing the surface tension.[Bauduin, 2011; Gassin, 2015] As classical surfactants, when increasing the concentration, COSAN starts to self-assemble in the bulk phase making large aggregates above a critical concentration around 0.01 mM with a radius of 20 nm for HCOSAN (basing on SANS and SLS analysis) referred to as monolayer vesicles of COSAN. COSAN vesicles have a high aggregation number about 12 500∓100 where COSAN molecules are perpendicular to the shell surface.[Bauduin, 2011] Further increase of COSAN concentration, above a critical aggregation concentration (CAC) about 10 mM, small aggregates (radius about 1.16 nm) start to form and they are comparable to surfactant micelles. Noting that, COSAN small aggregates have a few aggregation number around 14 and doesn't have a core shell structure due to the lack of a clear amphiphilic structure (hydrophilic heads and hydrophobic tails).[Bauduin, 2011] COSAN vesicles coexist with micelles above the CAC.[Bauduin, 2011] Halogenated COSAN or I_2COSAN can form lyotropic lamellar phases in water when increasing the concentration above 100 mM.[Brusselle, 2013]

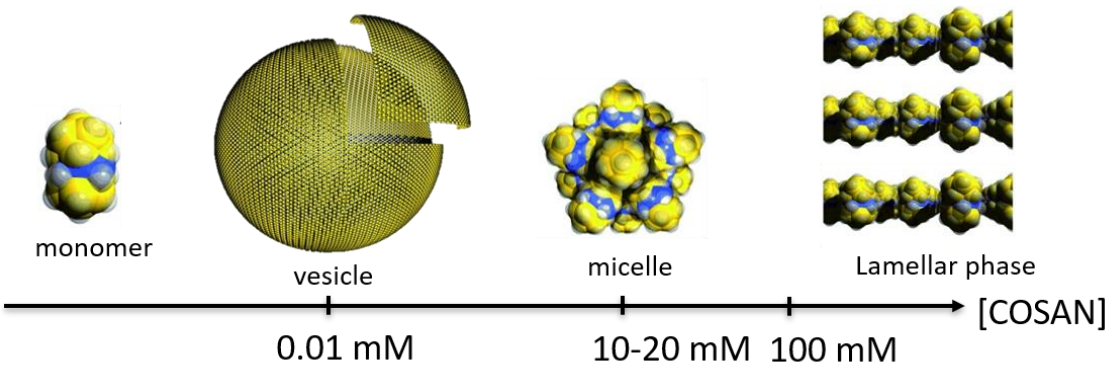

Figure 15. COSAN self-assembling representation in aqueous solution.

Interactions between COSAN anions in solution results from a balance between long range repulsive forces, due to their ionic nature, and short range attractive forces such as dispersion, hydrophobic forces and formation of unconventional di-hydrogen bounds between CH and BH vertices of opposite polarity. Carbon atom is slightly more electronegative than boron atom (B-$H^{\delta-}$ ⋯ $^{\delta+}$H-C).[Brusselle, 2013] It was suggested that the equatorial part of COSAN around the cobalt atom is the most hydrophilic.[Farràs, 2013] More recently, implicit solvent DFT calculations [Malaspina, 2020] has proposed that the cis-COSAN rotamer of COSAN, the most stable rotamer in water, presents an amphiphilic character responsible for its surfactant properties in water. In the cis-rotamer, a small hydrophobic part is delimited by the four carbon atoms and the hydrophilic part with the boron atoms.[Malaspina, 2020]

III-2. Interests for metallacarboranes

Transition metal metallacarboranes have different domains of applications concerning antitumor agents, catalysis and recovery of metals from radioactive waste.[Grimes, 2016] Metallacarboranes are characterized by the presence of one or more metal in their structure that are bound covalently into a carborane cage and by their robustness and their versatility which make them interesting as catalysts that can be created for specific purposes in addition of replacing conventional catalysts and the possibility of being recycled.[Grimes, 2016] The most interesting applications of carboranes and metallacarboranes concern the medical field. This is due to some specific properties that they possess. They are thermally and chemically stable in biological systems where they resist to degradation and they have low toxicity. In general, they are lipophilic (hydrophobic) that is advantageous for biomedical applications.[Grimes, 2016] In addition, they have the possibility to be functionalized [Dash, 2017] and produce a large variety of different compounds that have specific roles in therapy. Therefore, their biological activity and their potentials make them very interesting and promising for medical and pharmaceutical applications.

III-2-i. Metallacarboranes as HIV protease inhibitors

HIV is a retrovirus consisting of a single stranded RNA with a reverse transcriptase enzyme that creates DNA strand which is then inserted into the genome of the host cell. This virus attacks and destroys T CD4+ lymphocytes which are responsible for the coordination of the immune response. This is called immunodeficiency. HIV protease has an essential role for the HIV replication, therefore, antiviral drugs (pseudopeptide compounds) were designed for the

inhibition of the activity of HIV. The development of resistant strains of the protease that can mutate is a major problem for the current protease inhibitors.[Prejdová, 2004; Yin, 2006]

It was demonstrated by Cigler et al. in 2005 the capacity of icosahedral metallacarboranes, as nonpeptidic compounds, to inhibit the HIV protease where it is suggested that this binding blocks the flap closure of the protease protein.[Cígler, 2005] The most active compound was a cobalt-bis-(dicarbollide) derivative, especially the one with pairs of ether-linked cobalt-bis-(dicarbollide), with an inhibition constant (k_i) in the nM scale.[Cígler, 2005; Řezáčová, 2009] In addition, this compound showed no toxicity up to 50 μM. A study of the parent compound, the cobalt-bis-(dicarbollide) with HIV protease showed that the cobalt-bis-(dicarbollide) make a complex with HIV protease by binding 2 molecules of this compound in the hydrophobic pocket formed by side chains of the protease with possible hydrophobic interactions and unconventional hydrogen bonds.[Cígler, 2005; Kožíšek, 2008] Later on, it was demonstrated that the cobalt-bis-(dicarbollide) keep the flaps of the HIV protease semi-open where the two cobalt-bis-(dicarbollide) anions bond asymmetrically into the active site of the HIV protease (see Fig. 16).

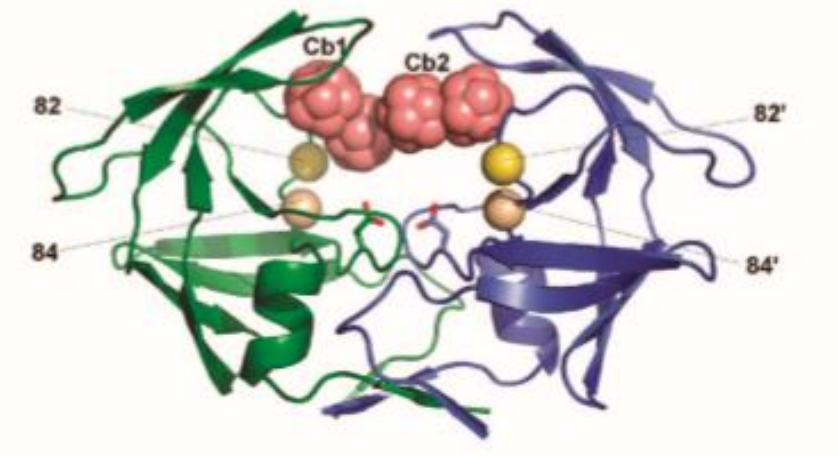

Figure 16. Cis cobalt-bis-(dicarbollide) binding to the hydrophobic pocket of HIV protease.[Kožíšek, 2008]

III-2-ii. Carboranes (or metallacarboranes) in BNCT

Boron neutron capture therapy (BNCT) is a technique for the treatment of cancer cells based on the absorption of low energy neutrons by the tumor cells containing nonradioactive ^{10}B isotopes. Boron containing carrier compound (^{10}B) that should accumulate preferentially in tumor cells to avoid the damage of surrounding normal tissue has to be injected within the patient. The boron isotope ^{10}B is stable, when absorbing a neutron, it becomes ^{11}B that is an unstable isotope. ^{11}B disintegrate and produce high energy transfer lithium-7 and energetic α-particles (^{4}He), this would be highly lethal to the tumor cells.[Hawthorne, 1998; Barth, 1999;

Coderre, 2003] For high efficiency, 20-40 µg of boron atom should be incorporated into one gram of tumor and localized preferably near the nucleus[Gabel, 1987] and respect the criteria of low toxicity. Carboranes have high boron content which make them interesting for boron neutron capture therapy where they can deliver ^{10}B isotope.[Leśnikowski, 2005] Researches are initiated in order to find biochemically active carboranes where metallacarboranes clusters, more specifically the cholesterol-metallacarborane conjugates incorporated into liposomes membranes [Białek-Pietras, 2013] and the cobalt-bis-(dicarbollide) derivatives,[Leśnikowski, 2005; Volovetsky, 2017] are found to be good candidates that showed also low toxicity (in a specific limit of concentrations).[Grimes, 2016; Fuentes, 2018] In addition, their high lipophilicity is advantageous and help the transfer of the carrier molecules across the blood brain barrier as well as lipid bilayer which could enhance the cellular uptake.[Endo, 2001; Grimes, 2016]

Other biological activities of metallacarboranes are observed,[Grimes, 2016] they can be used as anticoagulant as they have inhibition effect on the α-human thrombin which is an agent responsible for blood coagulation.

III-2-iii. Cobalt-bis-(dicarbollide) or COSAN

COSAN and I_2COSAN can pass through cell and synthetic lipid membranes.[Verdiá-Báguena, 2014; Tarrés, 2015; Rokitskaya, 2017] Cell membranes are composed of lipid molecules that are amphiphilic and form bilayers that control the translocation of ions, biomolecules and metabolites between the outside and the inside of the cell. As B-H bonds are not present in cells, RAMAN spectroscopy is a good technique that can be used in order to follow the uptake of COSAN by cells.[Tarrés, 2014] B-H stretching band is at a frequency of 2570 cm^{-1}, this band is detectable only when the concentration of COSAN is above 10 mM.[Tarrés, 2014] It was demonstrated by Marius Tarrés et al. that COSAN and I_2COSAN when added to the medium culture of human embryonic kidney living cells (HEK293), accumulate highly inside the cells for at least four hours (see Fig. 17).[Tarrés, 2014]

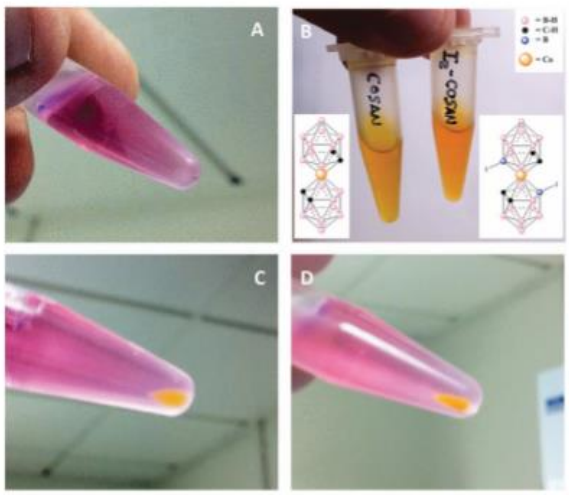

Figure 17. Visual inspection of the orange color coming from COSAN and I_2COSAN concentrated within the HEK293 cells.[Tarrés, 2014]

When COSAN is up taken by living cells, their effect on the viability of the cells is indirect.[Tarrés, 2015] COSAN change the cell morphology (cell rounding) and stop their proliferation and growth with an effective dose ED_{50} between 99 and 157 µM that corresponds to the concentration of COSAN that produces a biological effect (stop of the proliferation) for 50% of the cells. In some cases, for exposure time ≥ 8 hours, apoptosis of cells can be occurred. Cell washing and removing of COSAN (after maximum 5 hours of exposure), allow the recovery of the cells that start again to proliferate and grow.[Tarrés, 2015] The effect of I_2COSAN on cells is stronger than COSAN. I_2COSAN concentration inside the cell is found to be 3-4 times more than COSAN, therefore, the cells washed exposed to I_2COSAN took longer time to recover after washing than COSAN.[Tarrés, 2015] Noting that I_2COSAN is more lipophilic than COSAN, its partition coefficient between octanol-water is higher than COSAN. It has been shown that the effect of the counter cation (H^+, Na^+ and Li^+ were tested) is negligible.[Tarrés, 2015]

Interestingly, it was also demonstrated that after the uptake of COSAN by cancer and normal cells, COSAN accumulate mainly in the membranes and nucleus (30% in the nucleus) with no cytotoxicity even after long incubation time[Fuentes, 2018] which make them interesting for BNCT that requires accumulation of boron near or in the nucleus to increase its efficiency.[Gabel, 1987] The nucleus contains the genetic materials i.e. DNA (anionic polyelectrolytes), therefore, the interactions between the DNA and COSAN were investigated. It was demonstrated that COSAN interact strongly with DNA and form nanohybrid nanomaterials. The mode of interactions was shown to be by intercalation of COSAN to double stranded helix but only in the presence of NaCl salt that screen the phosphate groups of DNA.[Fuentes, 2018]

On the other hand, it was demonstrated for the first time by Verdia-Baguena et al. that COSAN and I_2COSAN pass through synthetic lipid membranes without driving force (voltage) and without altering the membrane (the membrane electrical capacitance was intact) with translocation rate of I_2COSAN lower than COSAN.[Verdiá-Báguena, 2014] Translocation of CsCOSAN and its derivatives through lipid bilayer membranes represented by liposomes vesicles was also investigated by Assaf et al.[Assaf, 2019] A solution of liposomes loaded with host/dye (cyclodextrin/dapoxyl sodium sulfonate) reporter pair was prepared. The addition of COSAN to the solution decreased the dye fluorescence indicating that COSAN entered the endo-liposomal space and displace the dye from the host cavity (see Fig. 18). This was the case for all COSAN derivatives but with different translocation kinetics where the kinetic of translocation of halogenated COSANs is faster than unhalogenated ones in contrast to what was found by Verdia-Baguena et al.

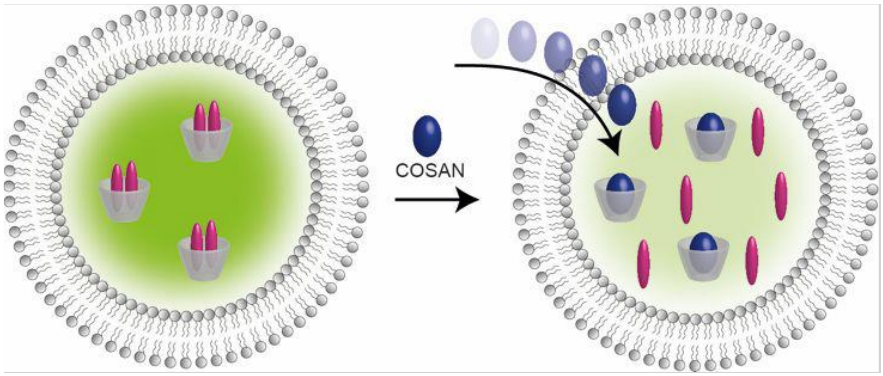

Figure 18. COSAN translocation through a vesicular lipid bilayer loaded with host/dye reporter pair.[Assaf, 2019]

Interestingly, COSAN can be functionalized to produce a large variety of COSAN derivatives for specific applications.[Grimes, 2016; Dash, 2017]

IV. Annex of chapter 1

IV-1. The twenty common amino acids

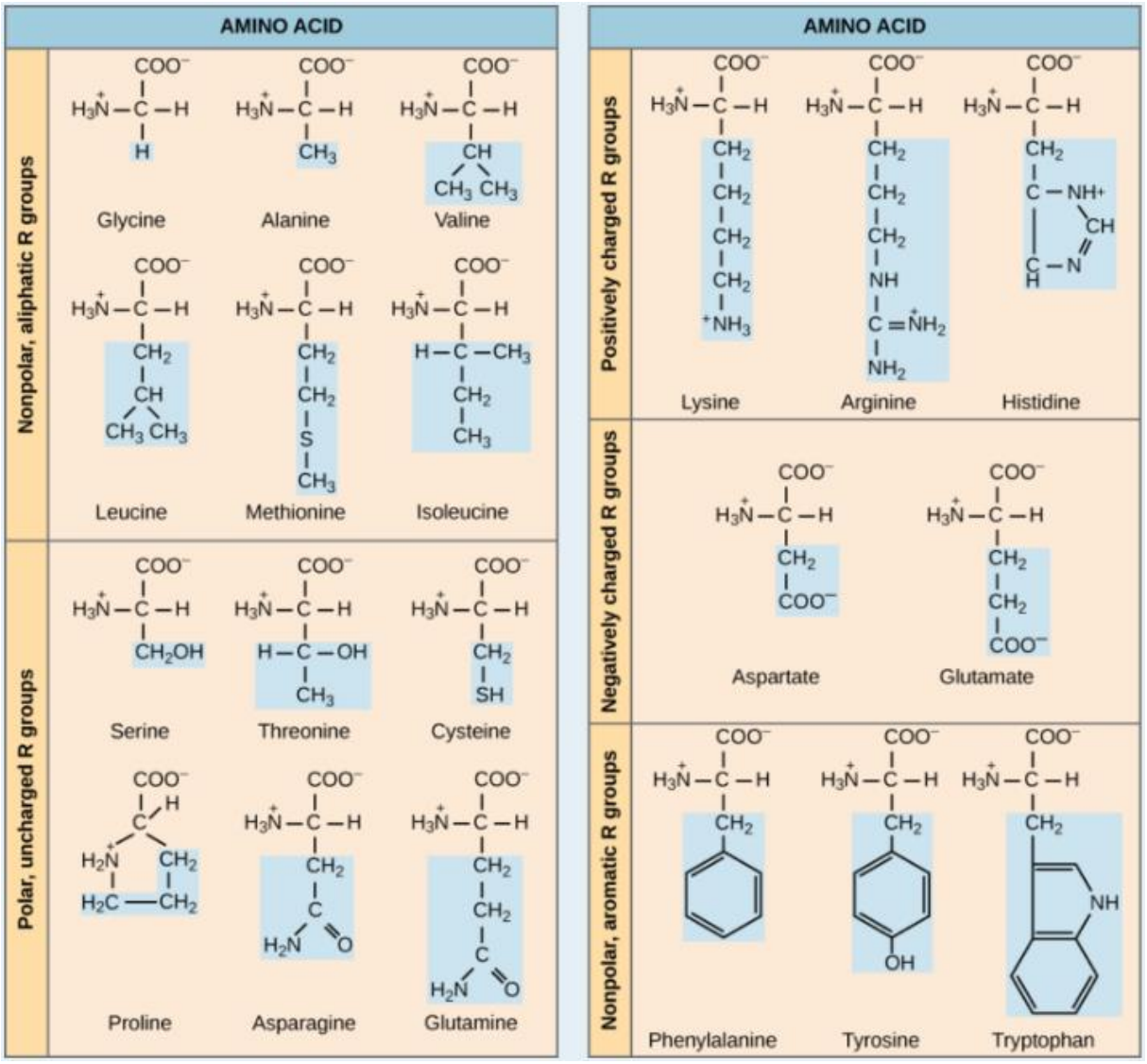

Figure 19. Structures and properties of the twenty amino acids commonly found in proteins. In general, the non-polar amino acids are inside the protein core.

IV-2. Surfactant system

Surfactants are surface active molecules i.e. in aqueous solution, they adsorb on the air/water interface where they decrease the surface tension. They are characterized by their amphiphilic structure. Amphiphiles are molecules that have hydrophilic charged (cationic or anionic) or uncharged (nonionic) headgroup and hydrophobic tail in their structure. In general, surfactants have moderate size hydrophobic tail.

In aqueous solution, surfactants monomers are in equilibrium between soluble monomers in the bulk phase and adsorbed monomers at the air/water interface below certain concentration called the critical micellar concentration (CMC). When the air/water interface is saturated by surfactants molecules forming a monolayer or bilayers i.e. the concentration of surfactants is

above the critical micellar concentration, the surface tension becomes constant (see Fig. 20). At a constant surface tension, the surfactants start to form self-assemblies in the bulk phase, resulting in globular, wormlike or threadlike aggregates.

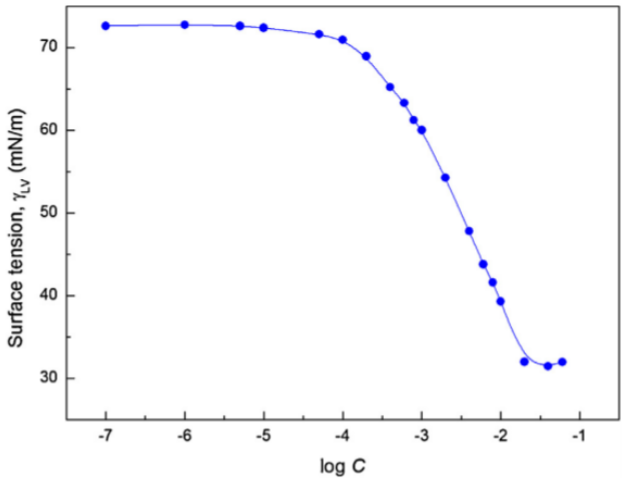

Figure 20. Example of the surface tension measurements of the octyl glucopyranoside surfactant from extracted from the paper of Manko et al. 2014.[Mańko, 2014] The surface tension is plot as a function of the surfactant concentration in logarithmic scale.

Self-assembly of surfactants is driven by the hydrophobic effect that is the tendency of oil (hydrophobic tails) to avoid mixing with water molecules because of the high energy cost associated to the disruption of the hydrogen bond network of water by the surfactant alkyl chain. Therefore, the hydrophobic tails are pointing inside the aggregates whereas the hydrophilic headgroups are pointing toward the aqueous phase.[Kronberg, 2003] This hydrophobic effect is equilibrated with the entropy of the system. Aggregates formation decreases the entropy of the system (increase of order) that is therefore, entropically unfavorable. When the surfactant concentration increases, this unfavorable contribution of entropy decreases, and when the chemical potential of free monomers become almost equal to the chemical potential of surfactants in the aggregates, aggregates start to form (at the CMC).[Bergström, 2000]

In a thermodynamic point of view, the free energy of micellization per surfactant molecule denoted as $\Delta\mu_{mic}$, depends on the following factors: (i) two factors related to the hydrophobic tails i.e. the hydrophobic effect and the chain conformational entropy and (ii) two other factors related to the hydrophilic headgroups i.e. the electrostatic and the excluded volume repulsive interactions between headgroups. The total free energy of the self-assembly process can be expressed as follows:

$$\Delta G_{tot} = N\Delta\mu_{mic} + \Delta G_{agg} = 0$$

$\Delta G_{agg} = -T\Delta S$ is the unfavorable free entropy of the self-assembly, where T is the temperature. N is the number of surfactant molecules. As the aggregation process decreases the order of the system, ΔS is negative and then ΔG_{agg} is positive. Therefore, $\Delta \mu_{mic}$ (where the hydrophobic effect contributes mainly) should be negative in order to overcome the unfavorable entropy.

Amphiphiles can be surfactants or lipids. Lipids are biomolecules and they are the main components of cell membranes. They have larger hydrophobic tails than surfactants and form bilayers structures in water, their headgroups can be zwitterionic i.e. having positive and negative charges at the same time.

IV-2-i. Packing parameter

Surfactant aggregates can have different geometries that are thermodynamically favored over others. Therefore, it is interesting to define the packing parameter of the surfactant that can predict the aggregate geometry. In general, spherical micelles are the most favorable thermodynamically. For a spherical micelle, the packing parameter is as follows:

$$R = \frac{3v}{a_0}$$

R is the spherical micelle radius, v is the volume of the hydrophobic chain, a_0 is the surface area per amphiphile at the hydrocarbon-water interface. The radius of a spherical micelle cannot be above the length of the fully extended hydrocarbon chain (l_c), therefore, if:

$\frac{v}{a_0.l_c} > \frac{1}{3}$ spherical micelles cannot be formed.

$\frac{1}{3} < \frac{v}{a_0.l_c} < \frac{1}{2}$ elliptical, rod or cylindrical micelles can be formed.

$\frac{1}{2} < \frac{v}{a_0.l_c} < 1$ bilayers (lamellar phase, vesicles or liposomes) can be formed.

$\frac{v}{a_0.l_c} > 1$ reverse aggregates can be formed.[Israelachvili, 1976]

IV-3. Cation exchange CsCOSAN-NaCOSAN

NaCOSAN was obtained from CsCOSAN salt via an ion-exchange process. The CsCOSAN was first dissolved in a brine medium (500 mg CsCOSAN in 500 ml NaCl 1 M) to exchange cations (Cs^+–Na^+). In a second step, the extraction of the NaCOSAN was carried out via a liquid/liquid extraction process using 500 ml of diethyl ether solvent. After vigorous stirring followed by washing three times with 500 ml of 1 M NaCl, NaCOSAN were extracted from

diethyl ether into water. NaCOSAN powder was recovered by evaporation of water under vacuum and lyophilization. NaCOSAN powder was characterized by thermogravimetric analysis (ATG) to quantify the amount of water molecules. It was determined of about 15% by weight or about 3.5 water molecules per NaCOSAN molecule.

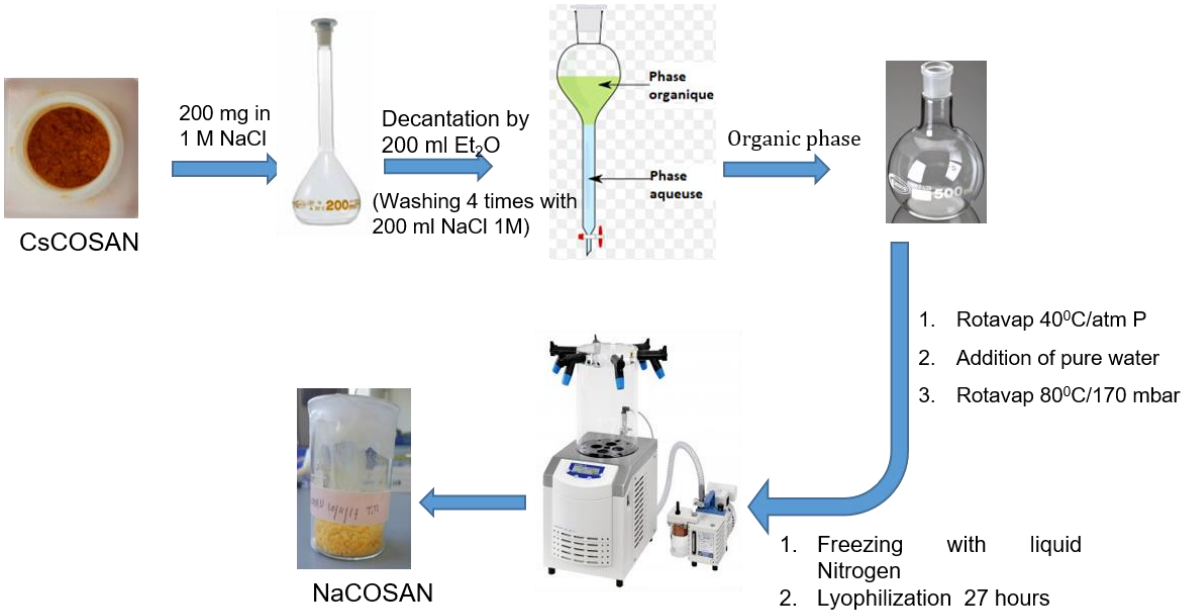

Figure 21. Cation exchange procedure CsCOSAN-NaCOSAN.

Chapter 2

Interactions between COSAN anion and sugar moieties in water

I-Introduction

As described in the first chapter, COSAN and its derivatives exhibit peculiar activities on biological systems. The previously highlighted surfactant properties of COSAN derivatives, which are unique for inorganic species without amphiphilic structure, are most likely responsible for their biological activities.

In this chapter, we have investigated the surfactant behavior of COSAN in combination with a non-ionic sugar-based surfactant. Indeed, sugars or carbohydrates that are often-called sugar (saccharide) or polymer sugars are the most abundant biomolecules on earth, are ubiquitous in the vegetal and animal world, and have many different functions in the living systems with for example a key role at cell's surface involved in cell recognition and signaling pathways.[Sharon, 1993]. For example, ABO blood types corresponding to a classification of human blood are determined by sugars on blood cells.[Sharon, 1993] Carbohydrates are a constituent of the backbone of nucleic acids.[Gabius, 2017] Cells and other cellular structures (nucleus, mitochondria) are delimited by biological membranes that are responsible of molecular translocation into and out of cells as well as intercellular communications and many different important functions.[Sharon, 1993] Lipid bilayer is the common structure for all these biological membranes. However, cells carry also a sugar-based parts that consist of glycoproteins and glycolipids, two types of complex carbohydrates in which sugars groups are linked to lipids and membrane proteins.[Sharon, 1993] Carbohydrates have complex structure, for example, two monosaccharides can form 11 different disaccharides, and four monosaccharides can form 35 560 tetrasaccharides. Therefore, monosaccharides represent the letters that make words (signals) in our system with high coding capacity making the carbohydrates the primary markers for cell recognition.[Sharon, 1993; Gabius, 2017] Noting that the array of carbohydrates on cancer cells is strikingly different from that on normal ones.[Sharon, 1993]

We focused here on the interaction of COSAN with sugars moieties, mostly glucose. Therefore, the main goal of this chapter is thus to investigate the interactions between COSAN and glucoside surfactants in monomeric (isolated) form in bulk solution or in aggregated forms, i.e. interactions between COSAN and sugars at surfaces. A neutral classical surfactant with sugar head, n-octyl-β-d-glucopyranoside (C8G1) (see Scheme 1) was chosen as it provides a glucose covered surface by forming direct micelles in water, above its critical micellar concentration (CMC = 19 - 28 mM) (page 66 in the book review [Ruiz, 2008]). In addition, C8G1 is non-toxic and biodegradable substance.[Ruiz, 2008]

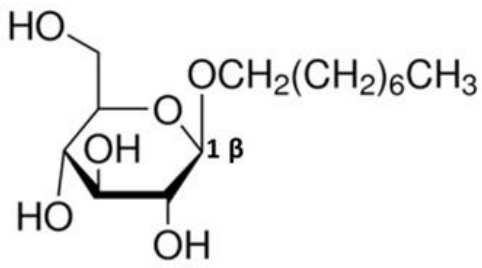

Scheme 4. Molecular structure of octyl-glucopyranoside (C8G1).

Since COSAN is also known to be surface active and to form vesicles in water below 10 mM and micellar type aggregates above a critical aggregation concentration (CAC) around 10 mM (with a first order transition), COSAN/C8G1 mixtures were investigated in a wide range of concentration from around 0.1 mM to 150 mM.

Mixtures of two classical surfactants are known to form mixed micelles driven mostly by high mixing entropy[Abe, 2004] and showing some synergetic effect, i.e. a significant decrease in the CMC of the surfactant mixtures compared to the pure compounds.[Bergström, 2000; Abe, 2004; Lainez, 2004; Zhang, 2004; Jańczuk, 2019] COSAN and classical surfactants have highly different chemical structures but they share properties: surface activity, micelle/vesicle formation, formation of lyotropic lamellar phases and foaming behavior. However, the origin of these properties is different for classical surfactants and COSAN. On one hand, the surfactant property of classical surfactants relies on (i) the hydrophobic effect arising from the contact of the surfactant (flexible) alkyl chain with water and (ii) their amphiphilic structure (hydrophilic-hydrophobic sequence). On the other hand, COSAN is a bulky rigid nanometric size anion without a clear hydrophilic-hydrophobic sequence and it is generally admitted that its self-assembly in water is due to a combination of the hydrophobic effect, intermolecular di-H bonds and van der Waals forces. Therefore, mixtures of COSAN and C8G1 differs from classical mixed surfactant systems but its investigation is of fundamental interest to deeper understand the intermolecular forces of COSAN with organic molecules in water. This work has therefore two main objectives, expressed here as questions: 1) How does COSAN interact with a classical organic and non-ionic surfactant? and 2) How does COSAN interact with the glucose moiety in bulk at interfaces?

II. Mixed surfactant systems

Mixed surfactant systems of ionic and non-ionic surfactants in aqueous solutions are well described in the literature.[Rosen, 1982; Holland, 1992; Bergström, 2000; Zhang, 2004; Jańczuk, 2019] The CMC value of their mixtures were estimated, as well as the composition of mixed micelles.

Since the hydrophobic effect that is the driving force for surfactants self-assembly is not related to the headgroups, mixed surfactants can be formed. This is the case of the ideal mixing in the aggregates, especially for surfactants with the same headgroups.[Holland, 1992] For ideal surfactant mixtures, the CMC of mixed aggregated depends linearly to the micelles composition.[Bergström, 2000; Jańczuk, 2019]

$$\frac{1}{CMC} = \frac{\alpha_1}{CMC_1} + \frac{1-\alpha_1}{CMC_2} \; Eq.1$$

Where α_1 is the mole fraction of surfactant 1 in mixture with surfactant 2 in the bulk phase, CMC_1 and CMC_2 are the CMCs for pure surfactants 1 and 2 respectively.

When mixing surfactants of different types, electrostatic interactions between headgroups should be considered. This is the case of the non-ideal mixing in the aggregates.[Holland, 1992] In the latter case, surfactant mixtures of different surfactant types exhibit synergistic effect on the system properties. Therefore, mixed surfactant systems are interesting for different applications such as detergency [Jost, 1988] and improvement of the oil recovery.[Shah, 2012] It was demonstrate that the synergistic effect is not only due to the interactions between surfactants headgroups, but mostly to the contribution of entropy to the free energy of aggregation process.[Bergström, 2000] In addition, synergistic effects increase with increasing asymmetry between the surfactants in mixture.[Holland, 1992; Bergström, 2000] For nonideal surfactant mixtures, the CMC of mixed aggregates deviates from the *Eq. 1*. and can be expressed as follow [Bergström, 2000]:

$$CMC(x_1) = f_1(x_1)x_1CMC_1 + f_2(x_1)(1-x_1)CMC_2 \;\; Eq.2$$

Where $f_1(x_1)$ and $f_2(x_1)$ are the activity factor functions that depend on the interaction parameter β:

$$f_1(x_1) = \exp[(1-x_1)^2\beta] \;\; Eq.3$$

$$f_2(x_1) = \exp[{x_1}^2\beta] \;\; Eq.4$$

Where $\beta = 0$ for ideal mixing, deviation of β from zero indicates interactions between surfactants headgroups. If β<0 the deviation of CMC from linear behavior is <0. If β>0 the deviation of CMC from linear behavior is >0. For mixtures of monovalent ionic and nonionic surfactants, like the case of COSAN/C8G1 mixtures, the interaction parameter β is between -5 and -1 i.e. the CMC of mixed aggregates decreases compared to the pure surfactant systems.[Holland, 1992] It was shown for mixtures of sugar-based surfactant with ionic surfactant that the synergistic effect is originated from ion-dipole interactions.[Zhang, 2004] Ion-dipole interactions is when an ion approaches a polar molecule, this molecule is oriented so that its charges of opposite sign to the ion interact with this latter.

We will see in the § III-5 that the CMC variation does not follow the behavior of an ideal mixing. This means that a specific interaction exists between COSAN and C8G1 and this is why we decided to probe the system under a different angle of investigation.

III. COSAN with C8G1 surfactant and with classical sugars/oligosaccharides

III-1. Interactions between COSAN and C8G1 at the supramolecular scale at low COSAN content

As mentioned in the introduction, metallacarboranes in water form charged vesicles in equilibrium with non-aggregated COSAN in solution below a critical aggregation concentration (CAC) of about 10 mM. Light scattering is a suitable and sensitive technique to characterize large aggregates or colloids in solution and was already used to characterize COSAN vesicles (see Annex V-1).[Matějíček, 2006; Uchman, 2010; Bauduin, 2011] The static scattered intensity was recorded, at a fixed scattering angle of 100°, as a function of the C8G1 concentration for given COSAN concentrations between 1 and 10 mM (see Fig. 1).

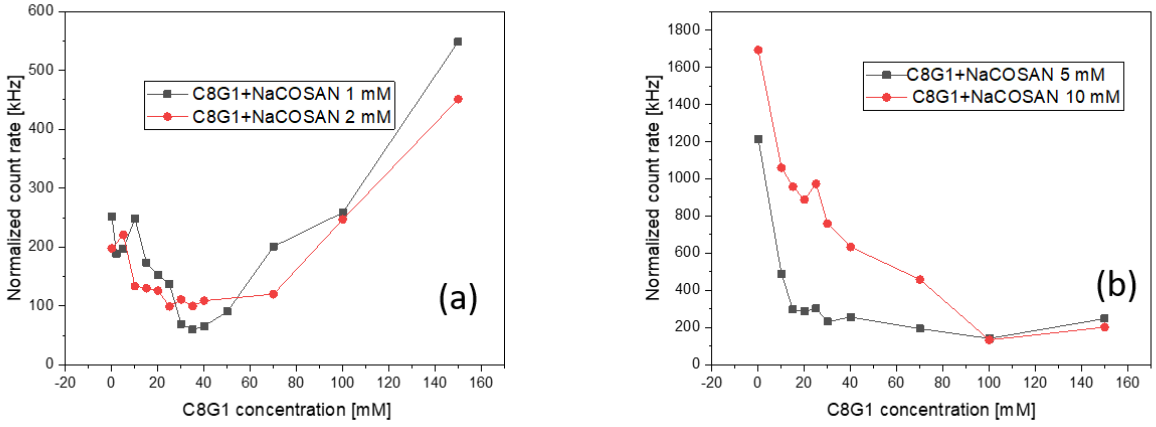

Figure 1. Light scattered intensity at a fixed scattering angle of 100° as a function of C8G1 concentration [mM] and at (a) [NaCOSAN] = 1 and 2 mM (b) [NaCOSAN] = 5 and 10 mM. NaCOSAN forms vesicles in equilibrium with monomers in this concentration range.

For [NaCOSAN] = 1 and 2 mM (Fig. 1-a), a significant decrease in the scattered intensity is observed at low C8G1 concentrations (< 30 mM and 25 mM for NaCOSAN 1 and 2 mM respectively). For higher C8G1 concentrations, a gradual increase beyond 40-50 mM and > 70

mM of C8G1 for NaCOSAN 1 and 2 mM respectively. So, three regimes seem to emerge from this first measurement.

For [NaCOSAN] = 5 and 10 mM (Fig. 1-b), a significant decrease in the scattered intensity is also observed at low C8G1 concentrations, without increase of the signal in the C8G1 concentration range (0-150 mM). Then, the auto-correlation functions of the scattering signal were recorded and analyzed. A typical series of time correlation functions $g_2(\tau) - 1$ are shown in lin-log plot in Fig. 2 for [COSAN] = 1, 2, 5 and 10 mM and for different C8G1 concentrations.

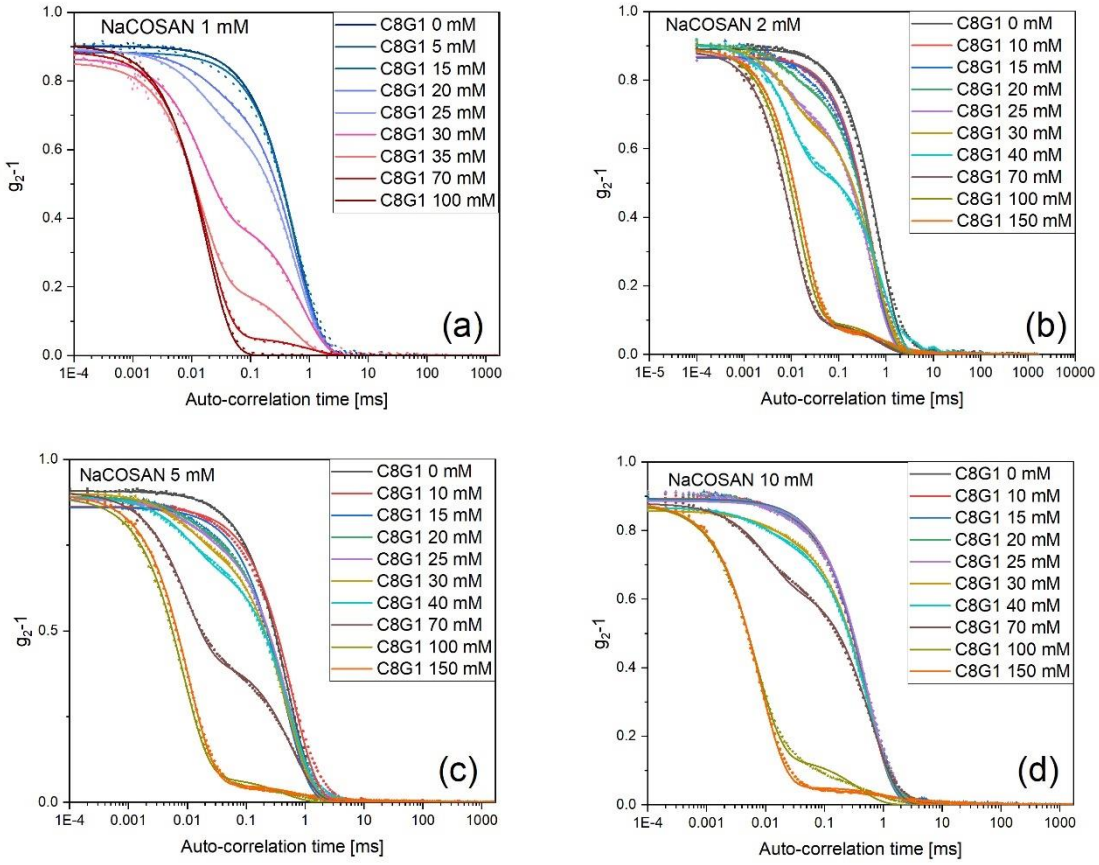

Figure 2. Auto-correlation functions obtained by dynamic light scattering and plotted for a scattering angle of 100°. [NaCOSAN] = 1, 2, 5 and 10 mM and [C8G1] from 0 to 150 mM. Dots are the experimental data; solid lines represent the adjustment using a mono or a bi-exponential decay function.

We can clearly observe three sets of auto-correlograms can be identified depending on the concentration of C8G1 and for all COSAN concentrations. At low C8G1 concentrations ([C8G1] < 15-30 mM depending on COSAN concentration), the auto-correlation function $(g_2(\tau) - 1)$ is characterized by a decay at long correlation times (τ) in the ms range and can be fitted using a single mode exponential function:

$$g_2 - 1 = \beta_1 \exp(-2\Gamma_1 \tau) \quad \text{Eq. 5}$$

with β_1 a coherence factor constant that depends on the detector area, optical alignment, and particles scattering properties, Γ_1 a decay constant related to the behavior of particles.

At high C8G1 concentrations (> 70 mM) and for [NaCOSAN] = 1 mM, the correlation function is characterized by a decay at much shorter correlation times of some hundredths of ms and can be also fitted using a single mode exponential function, with β_2 and Γ_2 as fitting parameters. At intermediate C8G1 concentrations, for all COSAN concentrations, the auto-correlation functions were fitted with a biexponential model by combining both the slow and fast modes and adjusting their relative amplitudes. The slow and fast modes correspond to the contributions of large and small scattering objects respectively.

A deeper analysis of characteristic frequencies $\Gamma_{1\ or\ 2}$ determined at different scattering angles θ and expressed as a wave vector $q = 2\pi n\ /\lambda \sin(\theta/2)$, where n the refractive index and λ is the laser wavelength, reveals nearly a q^2-dependence indicating an isotropic diffusive motion of the aggregates present in solutions. Hydrodynamic radius R_H of the aggregates were estimated by using the Stokes-Einstein relation:

$$D = \frac{kT}{6\pi\eta R_H} \quad Eq.6$$

Where D is the diffusion coefficient obtained from the slopes of the $\Gamma_{1\ or\ 2}$ vs. q^2 plots, see Annex V-2, T is the sample temperature, k is the Boltzmann constant and η is the solvent viscosity. R_H is plotted as a function of C8G1 concentration in Fig. 3 and 4.

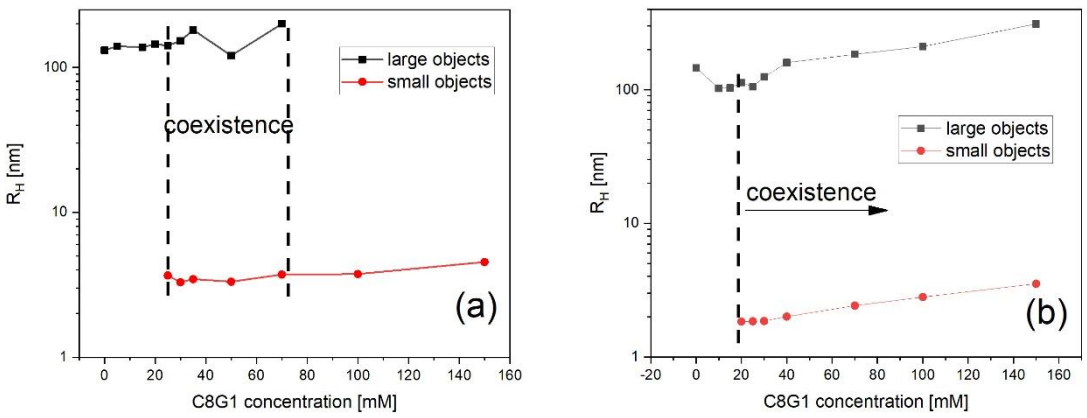

Figure 3. Hydrodynamic radius [nm] calculated from Stokes-Einstein equation as a function of C8G1 concentration for (a) [NaCOSAN] = 1 mM and (b) [NaCOSAN] = 2 mM. Black dots refer to large objects (NaCOSAN vesicles) and red dots refer to small objects (C8G1 micelles or mixed aggregates). Coexistence region is observed (framed between the dashed lines).

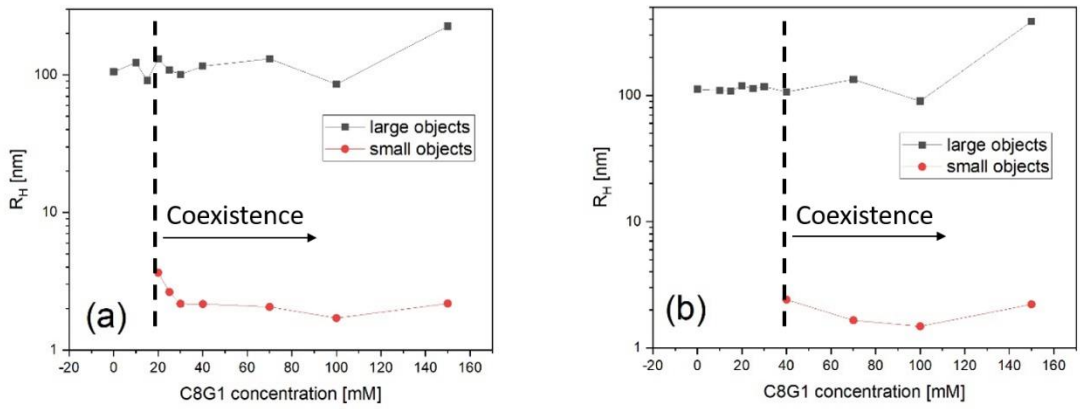

Figure 4. Hydrodynamic radius [nm] calculated from Stokes-Einstein equation as a function of C8G1 concentration for (a) [NaCOSAN] = 5 mM and (b) [NaCOSAN] = 10 mM. Black dots refer to large objects (NaCOSAN vesicles) and red dots refer to small objects (C8G1 micelles or mixed aggregates). Coexistence region is observed.

For [NaCOSAN] = 1 mM, the three C8G1 concentration regimes appear clearly: first, for [C8G1] < 20 mM, we determined a R_H value of around 120 nm which corresponds to the size of NaCOSAN vesicles, in agreement with data from literature.[Matějíček, 2006] Second, for 20 < [C8G1] ≤ 70 mM, two values of R_H around 3.5 nm and around 120 nm were obtained corresponding respectively to the size of C8G1 micelles ($R_H \approx 2.8$ nm, Fig. 5) and the size of COSAN vesicles which both coexists. Third, at higher C8G1 concentrations (> 70 mM), a single value of R_H is determined and corresponds to about the hydrodynamic radius of pure C8G1 micelles.

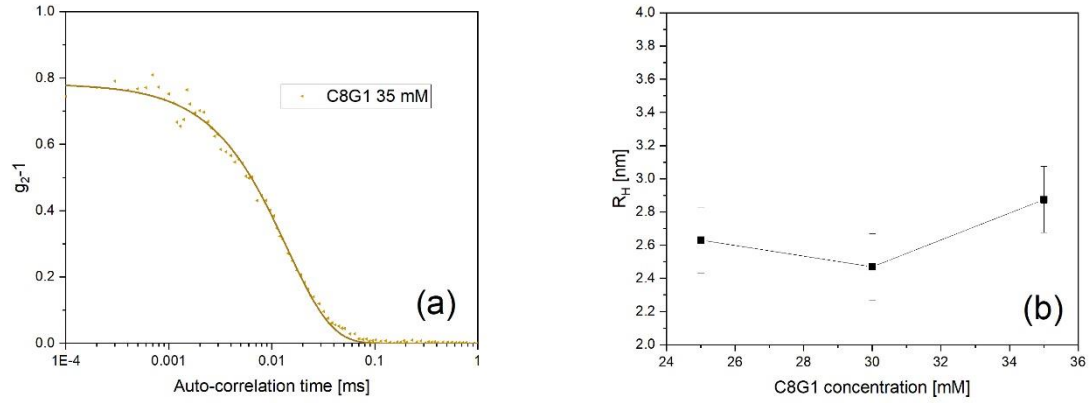

Figure 5. (a) Auto-correlation functions obtained by dynamic light scattering and plotted for a scattering angle of 100° for [C8G1]>25 mM in pure water. Dots are the experimental data; solid lines represent the adjustment using a mono exponential decay function. (b) Hydrodynamic radius [nm] calculated from Stokes-Einstein equation as a function of C8G1 concentration at different angles.

For [NaCOSAN] = 2, 5 and 10 mM (see Fig. 2 and 4), two C8G1 concentration regimes appear clearly: first, for [C8G1] < 20-40 mM, R_H of around 120 nm are obtained which corresponds to the size of NaCOSAN vesicles. Second, for 20-40 < [C8G1] < 150 mM, two values of R_H (3.5 nm and 120 nm) are obtained corresponding respectively to the size of C8G1 micelles and COSAN vesicles which coexist. By increasing COSAN concentration, a broadening of the coexistence region by increasing COSAN concentration was observed (Fig. 4). Therefore, more C8G1 is required to destabilize the COSAN vesicles when COSAN concentration is increased. This suggests the presence of equilibrated aggregates with short COSAN-C8G1 distances, which was specifically investigated by UV-vis and NMR spectroscopy.

As a summary, the increase in C8G1 concentration leads first to the decrease in the concentration of vesicles without any impact on their size. A possible explanation is a shift of the equilibrium between COSAN in vesicle state and COSAN in its monomeric state upon C8G1 addition. This equilibrium is due to a competition between the COSAN-COSAN and COSAN-H2O interactions. Binding between C8G1 (monomer) and COSAN monomer could explain the shift in the monomer-vesicle equilibrium of COSAN towards the COSAN monomer, leading a decrease in the vesicle concentration. By further increase in the C8G1 concentration above its CMC in pure water, small aggregates, with a size comparable to the bare C8G1 micelles, appear and are in coexistence with remaining COSAN vesicles. For NaCOSAN 1 mM, at higher C8G1 concentrations (> 70 mM), the vesicles are not detectable and the scattered signal is then only due to small aggregates with a size close to bare C8G1 micelles. The increase in the scattered intensity is thus attributed to the increase of the small aggregates concentration.

Remark: in our system it is difficult to conclude about the saturation where the plateau is reached, maybe the saturation that we observe is due to the non-sufficient amount of COSAN molecules in the solution, in plus, in our experiment the concentration of C8G1 was not fixed i.e. the amount of surface in the solution, instead, the adsorbate concentration (COSAN) was fixed and we change the surface concentration (C8G1).

III-3. Interactions between COSAN and C8G1 at the molecular scale and at low COSAN content

The orange color of COSAN aqueous solution comes from the maximum absorption in the visible region at λ_{max} = 445 nm (ε = 440 $L.mol^{-1}.cm^{-1}$).[Hawthorne, 1968; Mátel, 1982; Bühl, 2005] It corresponds to the transition from 80 to 83 according to Kohn-Sham MO numbers and is very weak compared to the maximum absorption in the UV region at 293 nm (ε = 30980

L.mol^{-1}.cm^{-1}) which corresponds to the transition from 81 to 84.[Hawthorne, 1968; Mátel, 1982; Bühl, 2005] UV-visible spectroscopy (see Annex V-3) was measured on NaCOSAN solutions and comparable ε and λ_{max} values, ε = 368.4/20136 L.mol^{-1}.cm^{-1} and λ_{max} = 446/280 nm for the UV-visible absorptions, with the ones obtained for CsCOSAN in methanol in a previous investigation).[Hawthorne, 1968; Mátel, 1982; Bühl, 2005] As C8G1 does not absorb in the range of wavelengths investigated here (190-600 nm), UV-visible measurements were carried out to study the evolution in the local environment of COSAN, for example induced by a change in its hydration/solvation or by its binding to a solute, upon addition of C8G1. The UV-vis spectra of NaCOSAN 1, 2, 5 and 10 mM solutions were collected with increasing C8G1 concentration from zero up to 150 mM (see Fig. 6).

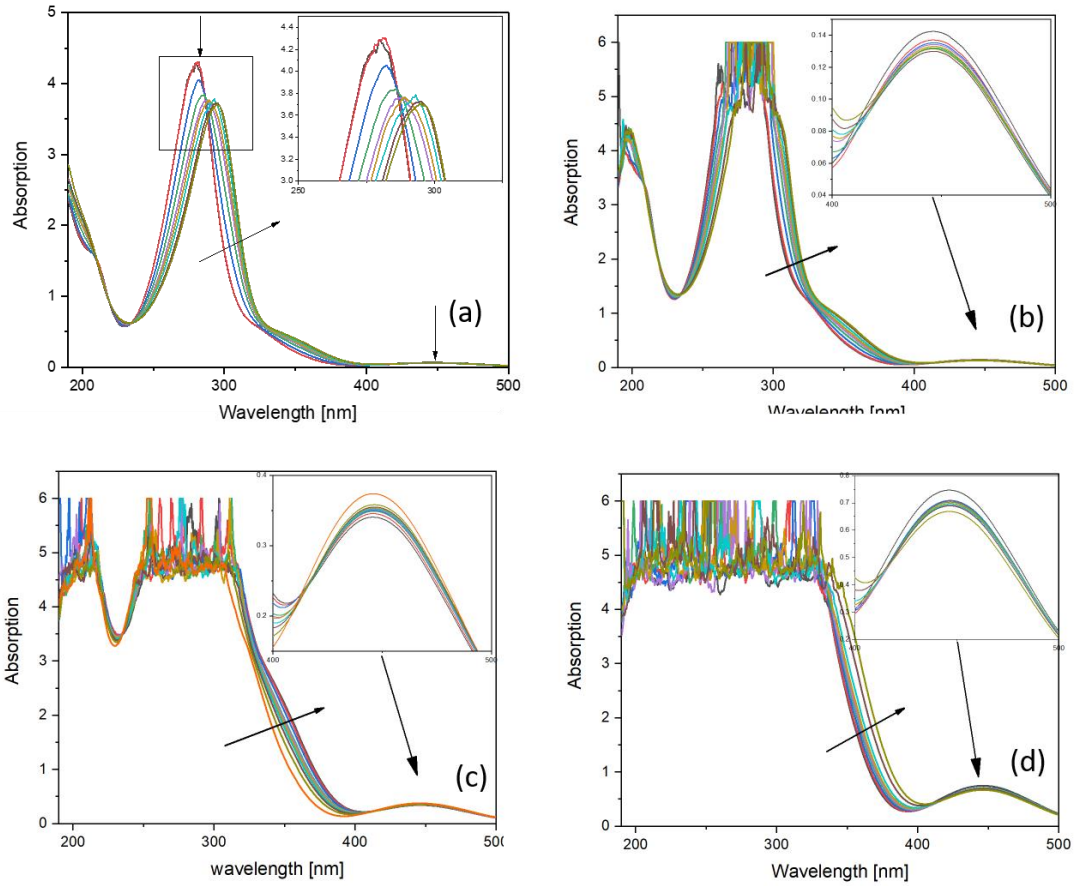

Figure 6. UV-visible absorption of (a) [NaCOSAN] = 1 mM, (b) [NaCOSAN] = 2 mM, (c) [NaCOSAN] = 5 mM and (d) [NaCOSAN] = 10 mM at different concentrations of C8G1 ranging from 0 to 150 mM as a function of wavelength range from 190 to 600 nm. The oblique arrow represents the increase of the C8G1 concentration. For NaCOSAN 1 mM, the peak in the UV range shows a shift of the absorption wavelength upon adding C8G1, a zoom of the UV peak around 280 nm. For NaCOSAN concentrations above 1 mM, the spectra are saturated in the UV range.

For NaCOSAN 1 mM, the presence of C8G1 affects significantly the UV absorption signal by decreasing the maximum absorption (hypochromic effect) and shifting continuously the peak position toward the higher wavelengths (bathochromic effect) (Fig. 6). These significant effects indicate a strong change in the electronic environment of COSAN presumably due the building of close contact COSAN/C8G1 aggregates. The visible peak is much less affected in the presence of C8G1, showing only a variation of its intensity within the first 20 mM of C8G1 and no noticeable shift of the absorption band position (see Fig. 7).

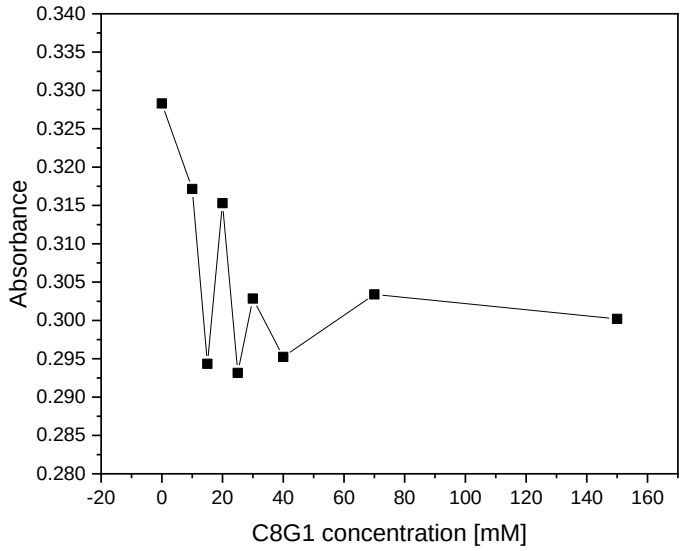

Figure 7. Absorption of COSAN at 446 nm for [NaCOSAN] = 1 mM as a function of C8G1 concentration.

By plotting λ_{max} and the normalized peak intensity as a function of C8G1 concentration in the presence of NaCOSAN 1 mM (Fig. 8-a), it is clearly noticeable that the signal changes abruptly at around 10 mM C8G1, well below the CMC of C8G1 in pure water (CMC_0^{C8G1}= 19-25.8 mM).[Ruiz, 2008] This result may be explained by a strong interaction between COSAN with C8G1 monomers and/or by a decrease in the CMC of C8G1 induced by the COSAN i.e. by the adsorption of COSAN anion onto C8G1 micelles reducing therefore its chemical potential as previously observed with polyoxometalate nano-ions.[Girard, 2019] In order to solve this question, the CMC of C8G1 will be investigated in a following section by surface tension measurement and ^{1}H-NMR. In Fig. 8-a, it can be observed that the absorbance and λ_{max} are strongly affected for 10 < [C8G1] < 50 mM, and then reach a plateau for [C8G1] > 50 mM. By considering that the changes in the absorbance and λ_{max} are attributed to the C8G1-COSAN binding, it can be assumed that the plateau region corresponds to a concentration range where

the COSAN is completely bound to C8G1, presumably onto C8G1 micelles considering that this range is well above its CMC.

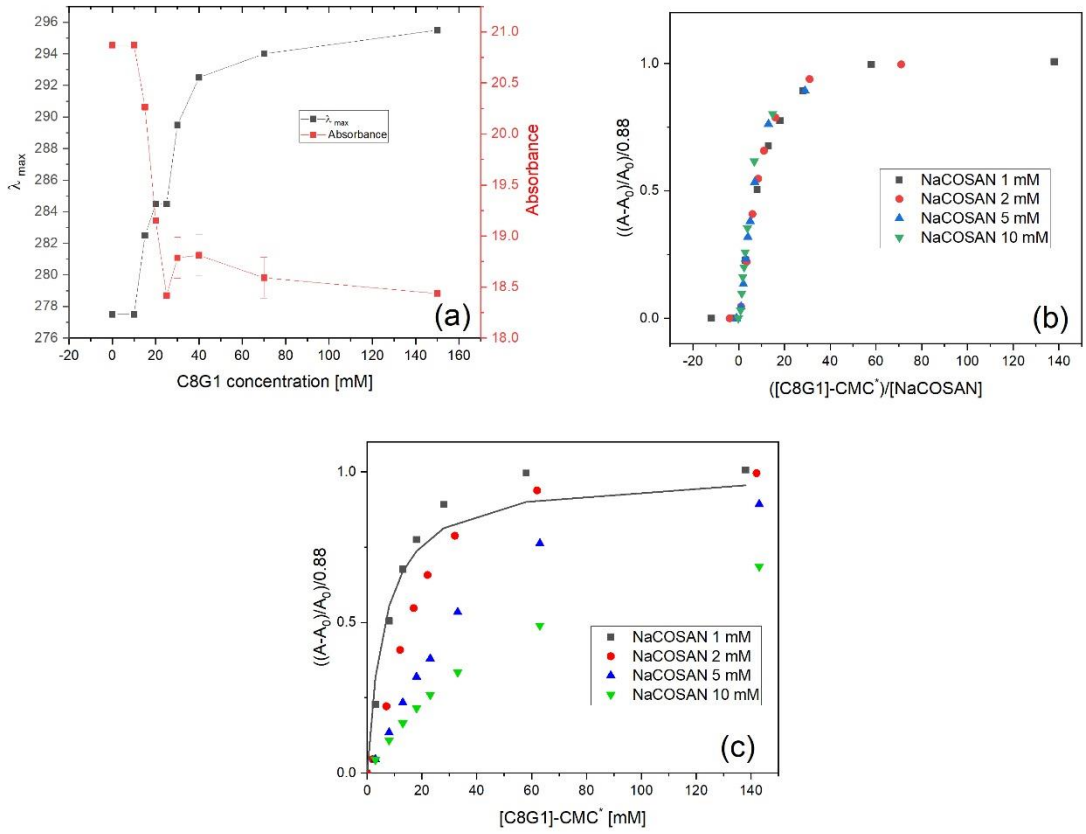

Figure 8. (a) Wavelength at the maximum of absorption (λ_{max}) [nm] (in black) and the absorption of COSAN at λ_{max} for [NaCOSAN] = 1 mM as a function of C8G1 concentration (in red). (b) Master curve of the normalized absorption of COSAN at 350 nm divided by the limit value (0.88), obtained at saturation of the normalized absorption for [NaCOSAN] = 1 and 2 mM (see Fig. 4c), as a function of a concentration ratio where CMC* is an offset parameter. (c) Normalized absorption of COSAN at 350 nm divided by the limit value (0.88) as a function of reduced C8G1 concentration. Full line is the result of a fitting procedure using a Langmuir model as in Eq. 7.

Table 1. CMC* parameter to get the master curve in Fig. 8-b for the normalized UV-absorption variation as a function of C8G1 concentration.

[NaCOSAN]/ mM	CMC*/ mM
1	12
2	8
5	7
10	7

For COSAN concentrations 2, 5 and 10 mM, and in order to compare the results both with for COSAN 1 mM, we recorded the absorbance values at 350 nm, and not at λ_{max}, because UV

absorption at around 280 nm is outside the validity range of the Beer-Lambert law for COSAN concentrations above 1 mM (Fig. 6-b-c-d). First, *A* the absorbance of NaCOSAN in the presence of C8G1 was normalized as $\frac{(A-A_0)}{A_0}$, where A_0 is the absorbance of NaCOSAN in pure water at 350 nm. The normalized absorbance, $\frac{(A-A_0)}{A_0}$, reaches a plateau at high C8G1 concentrations for 1 and 2 mM of NaCOSAN but not for 5 and 10 mM. The plateau value of the normalized absorbance is around 0.88, i.e. $\lim_{[C8G1]\to\infty}(\frac{A-A_0}{A_0}) \approx 0.88$, and appears to be independent of NaCOSAN concentration, at least here for 1 and 2 mM. In order to rationalize further the results for the different COSAN concentrations, the normalized absorbance was divided by this latter limit value and plotted as a function of a reduced concentration term, $\frac{[C8G1]-CMC^*}{[COSAN]}$, in order to get a master curve (see Fig. 8-b) where CMC* is an offset parameter (see table 1). This parameter represents the critical micellar concentration of C8G1 in the presence of NaCOSAN, i.e. the concentration above which COSAN starts to interact with C8G1. This value decreases from around 20 without COSAN down to (at least) 7 mM in the presence of 10 mM of COSAN. A decrease in the CMC of C8G1 corresponds to a stabilization of the micellar state by increasing COSAN concentration, as it was observed previously with POMs and C8G1.[Girard, 2019] A master curve indicates here that the pertinent variable is the ratio between the amount of micelles and the COSAN anions. The shape of the master curve recalls the shape of a Langmuir adsorption isotherm model. Therefore, Langmuir association constant *K* could be estimated by adjusting the normalized UV-adsorption using the following expression (see Fig. 8-c):

$$\frac{\frac{(A-A_0)}{A_0}}{0.88} = \frac{K \times ([C8G1]-CMC^*)}{1+K\,([C8G1]-CMC^*)} \quad Eq.7$$

A *K* value of ≈ 0.16 mM^{-1} was determined. However, the Langmuir model does not enable to fit perfectly the experimental results. Indeed, the Langmuir model reproduces well the experimental at low [C8G1]-CMC* values, where the slope is the highest, but fails in reproducing the saturation level, which appears at much higher concentrations in the model compared to the experimental results. This discrepancy between the model and the experimental results is likely to arise from the non-linear local interactions between COSANs once adsorbed, an effect which is not taken into account in the very simplistic Langmuir model. Nevertheless, it is important to notice that the *K* value is rather high for an ion interacting with nonionic micelles. Taking into account the shape of the master curve with a plateau above a concentration ratio of about 50, around the aggregation number of C8G1 micelles, suggests that COSAN interact with the surface developed by the micelles.

III-4. Interactions between COSAN and classical sugars/oligosaccharides: Low COSAN content.

To gain a better understanding on the interactions between COSAN and C8G1 self-assemblies (and sugars), UV-visible measurements were performed at a fixed concentration of COSAN 1 mM and in the presence of 100 mM of classical sugars (D-(+)-glucose and D-(+)-galactose), sugar dimers (D-(+)-sucrose, D-(+)-cellobiose), and sugar oligomers (maltodextrin with 6-7 glucose units) with concentrations ranging from 0.1 to 100 mM. As shown in Fig. 9-a, no evolution of the UV-visible spectrum was observed in the presence of classical and dimer sugars. On the other hand, increasing maltodextrin concentration induced hypochromic and bathochromic effects (Fig. 9-b), as observed with C8G1.

This indicates strong interactions between COSAN and maltodextrin, suggesting that there is a collective effect of the glucose moieties, meaning that many close glucose units are required to bind to COSAN. Such a collective interaction is also expected at the surface of C8G1 micelles covered with glucose moieties if we consider an adsorption mechanism of the COSAN molecules onto C8G1 micelles. It was recently shown that COSANs binds strongly in the cavity of γ-cyclodextrin,[Assaf, 2019] a cyclic oligomer of glucose with 8 glucose units. Interestingly the results here suggest that a cavity is not required to observe the binding to COSAN anion.

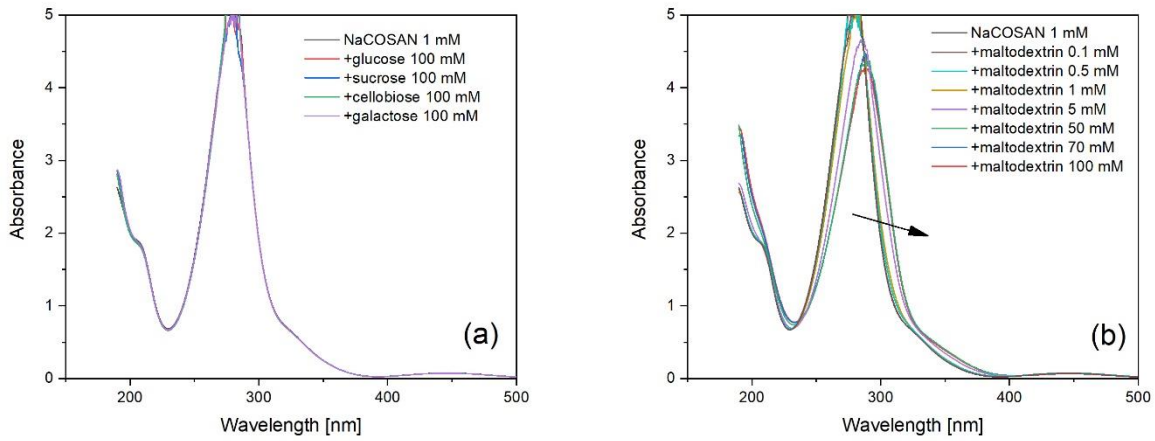

Figure 9. UV-visible absorption of [NaCOSAN] = 1 mM in the presence of different sugars as a function of wavelength range from 190 to 600 nm.

The plot of λ_{max} as a function of maltodextrin concentration (Fig. 10) shows an evolution in the UV signal above around 1 mM maltodextrin and a plateau at about 10 to 20 mM.

By plotting the normalized UV λ_{max} as a function of maltodextrin concentration (Fig. 11), the plateau is achieved at about 10 to 20 mM of maltodextrin. Making the assumption that this

variation can be assimilated to COSAN molecules adsorption onto maltodextrin oligomers, we can estimate of about 0.1 to 0.05 COSAN per maltodextrin molecule (degree of polymerization around 7). COSAN adsorption number is low compared to that found for C8G1 micelles, which found to be 5 to 10 COSAN molecules per micelle, which mean around 0.7 COSAN molecule per 7 C8G1 molecules.

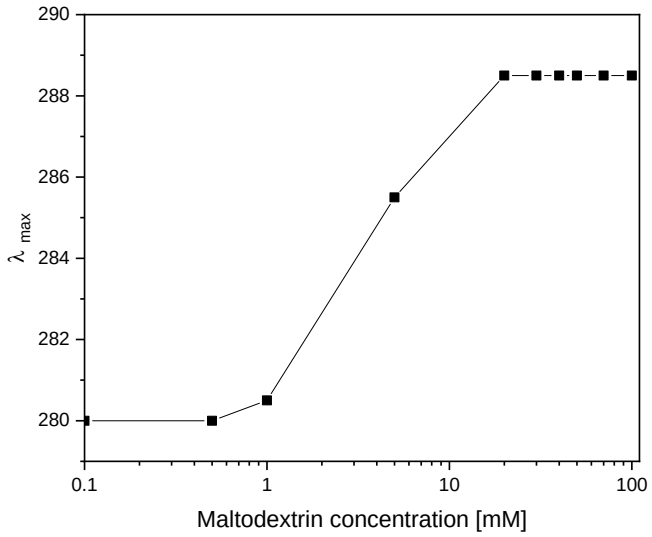

Figure 10. Wavelength at the maximum of absorption (λ_{max}) [nm] for [NaCOSAN] = 1 mM as a function of maltodextrin concentration [mM].

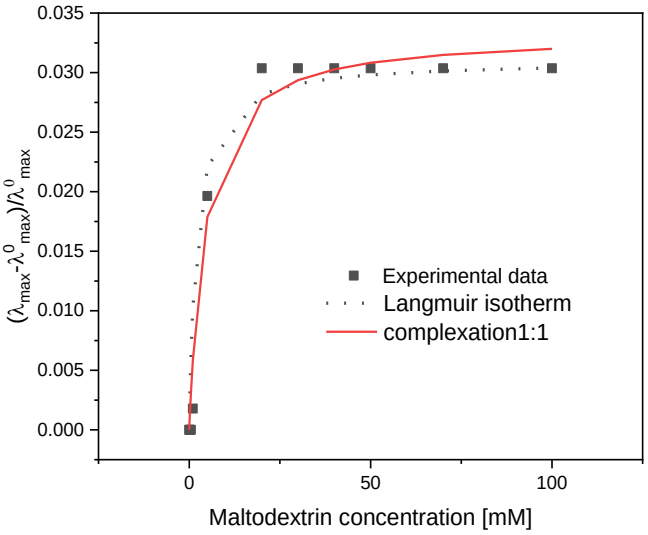

Figure 11. Normalized UV λ_{max} for [NaCOSAN] = 1 mM as a function of maltodextrin concentration [mM]. dotted line is the fit data using Eq. 3 and solid line is the fit data using 1:1 binding model as described below.

The 1:1 binding model which can be expressed as:

Two species A and B form AB species, where: [A], [B] and [AB] corresponds respectively to the concentrations of free maltodextrin, free NaCOSAN and NaCOSAN/maltodextrin complex. The equilibrium of the complex formation can be described by an association constant:

$$k = \frac{[AB]}{[A] \times [B]} \; Eq.8$$

$$[A]_0 = [A] + [AB] \quad Eq.\ 9$$

$$[B]_0 = [B] + [AB] \quad Eq.\ 10$$

$$k\ ([AB])^2 - [k\ ([A]_0 + [B]_0) + 1]\ [AB] + k\ [A]_0\ [B]_0 = 0 \quad Eq.\ 11$$

The COSAN-maltodextrin adsorption constant was evaluated as previously by fitting the evolution of λ_{max} with a standard Langmuir isotherm model, see the fitting in Fig. 11. Considering that this Langmuir model does not fit very well the experimental data, a 1:1 (COSAN:maltodextrin) stochiometric binding model [Thordarson, 2011] was also applied. Both models do not enable to fit properly the experimental data but gives a rough estimate, i.e. the order of magnitude, of the binding/adsorption, which is around 0.4 mM^{-1}. However, this mean value of K is in the same order of magnitude that the adsorption constant of 0.16 mM^{-1} obtained for COSAN onto C8G1 micelles.

III-5. Effect of COSAN on the micellization of C8G1

In order to confirm the COSAN-C8G1 interactions at concentration below CMC_0^{C8G1}, complementary ^1H NMR with ^{11}B decoupling experiments were carried out at fixed COSAN concentrations by varying C8G1 concentration. The evolution of the difference in the chemical shift, $\delta - \delta_{C8G1}^{1mM}$, of the proton on the anomeric carbon of C8G1 ($H_{1\beta}$), (see Scheme.1), is shown in Fig.12.

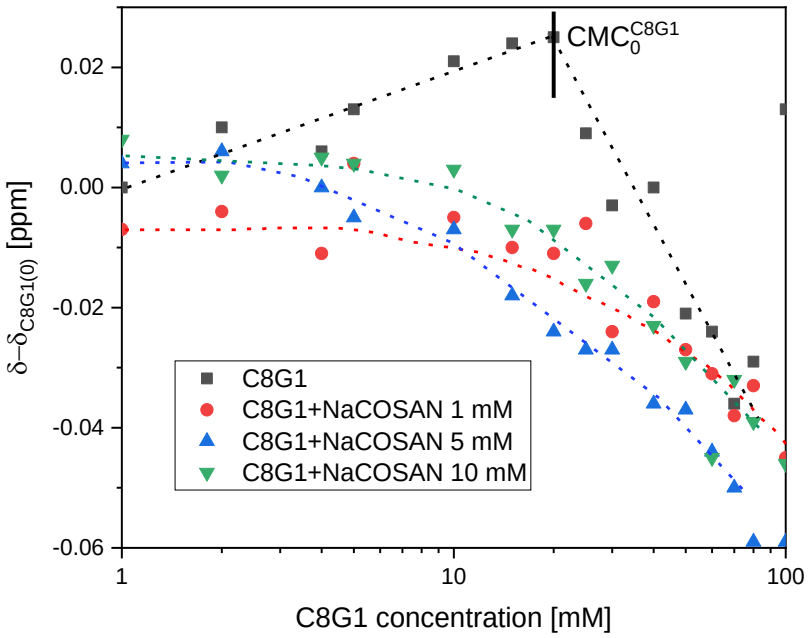

Figure 12. Evolution of the difference in the chemical shift, $\delta - \delta_{C8G1}^{1mM}$,(where δ_{C8G1}^{1mM} is the chemical shift of C8G1 monomers at 1 mM), of the hydrogen 1β of C8G1 as a function of [C8G1] in the presence of [NaCOSAN] = 1, 2, 5 and 10 mM. Doted lines are drawn manually in order to guide the reader's eyes.

For the pure C8G1 system, the evolution in the chemical shift difference shows a maximum, through successive shielding and deshielding behaviors, at around 20 mM, which is around CMC_0^{C8G1}. In the presence of NaCOSAN, the evolution in the chemical shift difference is highly affected even at very low C8G1 concentrations (1 mM). Moreover, at higher C8G1 concentrations, a smooth break in the evolution of the signal is observed in the presence of NaCOSAN 1, 2, 5 and 10 mM and can be attributed to micellization of C8G1. This break, appears below CMC_0^{C8G1} which suggests that COSAN leads to a decrease in the CMC of C8G1, i.e. C8G1 micelles are stabilized by COSAN.

In order to investigate further how the C8G1 aggregation process is affected in the presence of COSAN, surface tension measurements of C8G1 solutions in pure water and with COSAN at given concentrations were performed. COSAN shows surface activity by decreasing the surface tension of water, independently of the nature of the counterion, from 72 mN.m^{-1} to about less than 60 mN.m^{-1}. [Uchman, 2015; Gassin, 2015; Zaulet, 2018] The precise determination of surface tension is difficult using the pendant droplet method, or with other techniques, because of very long equilibrium times, which is likely due to the complex aggregation equilibrium between monomers and vesicles in the pre-micellar concentration region.[Fernandez-Alvarez, 2017]

Nevertheless, Fig. 13 shows the surface tension of C8G1 solutions with and without COSAN. Without COSAN, the surface tension by addition of C8G1 shows the classical evolution obtained for surfactants: a strong decrease followed by a plateau at concentration above the CMC. For C8G1, the break is clearly observed here at a value of 22 mM, which is well in agreement with literature data, CMC_0^{C8G1} = 19 - 25.8 mM.[Ruiz, 2008] In the presence of 1 mM COSAN (Fig.8a), the break in the surface tension is significantly shifted to lower C8G1 concentrations to around 15 mM, even if it is not so sharp. By increasing COSAN concentration to 2 mM, the surface tension curve is much affected showing an overall increase in the surface tension over the all C8G1 concentration range. This makes the break in the surface tension curve much smoother and hardly detectable, at lower C8G1 concentrations around 10 mM. For higher COSAN concentrations 5, 8 and 10 mM, the surface tension shows a much smoother evolution as a function of C8G1 concentrations and the break is not anymore detectable, except maybe at 10 mM COSAN at around 50 mM C8G1. However it is difficult here, by only discussing surface tension measurements, to associate this smooth break to a micellization process. Note here that at low C8G1 concentrations the surface tension is low and does not reach the value of water because of the surface activity of COSAN itself, which in pure water starts to be measurable for concentrations above 1 – 2 mM.[Uchman, 2015; Gassin, 2015; Zaulet, 2018] Considering the long equilibrium time associated with the measurement of surface tension with COSAN, the surface tension results here at high COSAN contents, or high COSAN/C8G1 ratios, will not be further discussed. However, the decrease in the CMC of C8G1 at low COSAN content is consistent with UV results (see the previous section) and suggests that C8G1 micelles are stabilized by COSAN.

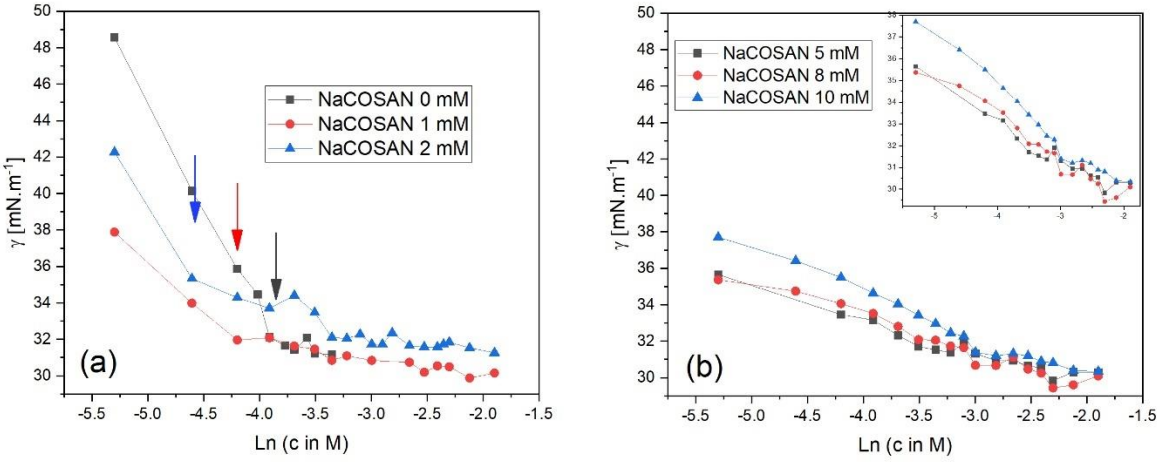

Figure 13. Surface tension (γ) [mN.m^{-1}] of C8G1 solutions in the presence of [NaCOSAN] = 0, 1, and 2 mM (a) and at 5, 8 and 10 mM (b), as a function of C8G1 concentration. Arrows indicate where the break of curve is considered.

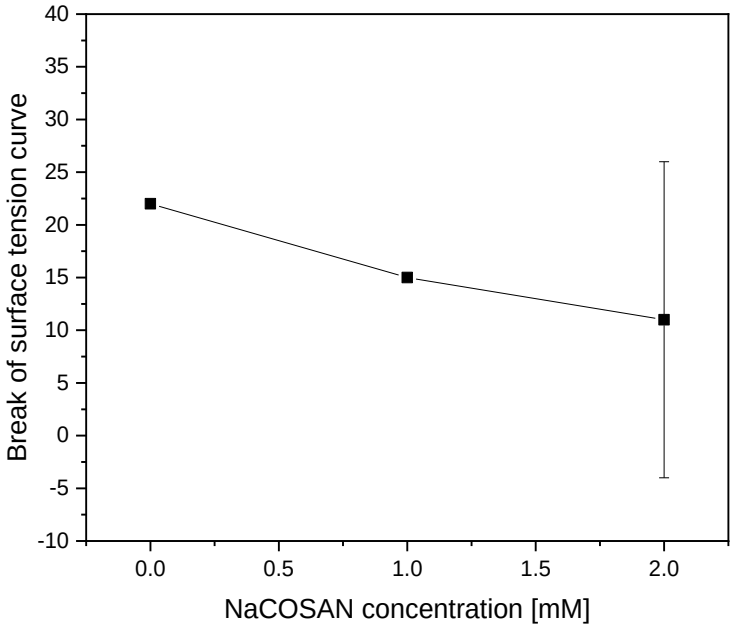

Figure 14. Plot of C8G1 concentration at the break of the curve obtained from figure 8 as a function of NaCOSAN concentration [mM].

Mixing classical surfactants lead, for most systems, to a significant decrease in their CMCs which originates mainly from high mixing entropy.[Hua, 1982; Bergström, 2000; Patel, 2009] Many examples showing decreased CMC values for C8G1 by addition of anionic or cationic surfactants can be found in literature.[Lainez, 2004; Jańczuk, 2019] In surfactant systems, the formation of micelles is stimulated by the hydrophobic effect because of the high energy cost associated to the disruption of the hydrogen bond network of water by the surfactant alkyl chain. In mixed surfactant micelles, alkyl chains (and polar heads) are therefore all equally mixed.

If we return to the analysis described in §II of this chapter, the mole fraction of each surfactant in the bulk is the same for each surfactant in the mixed micelles for an ideal surfactant mixture. [Jańczuk, 2019]

Here, a model for ideal surfactant mixture was applied (see Fig. 15) using the equation 1 in §II:

$$\frac{1}{CMC} = \frac{\alpha_1}{CMC_1} + \frac{1-\alpha_1}{CMC_2} \qquad (1)$$

If α_1 is the mole fraction of C8G1 in the mixture in the bulk phase (I have only two values of α_1, 0.85 and 0.94), CMC_1 is the CMC of C8G1 in pure water and CMC_2 is the CMC of NaCOSAN in pure water, the CMC of binary mixture can be calculated from the equation 1.

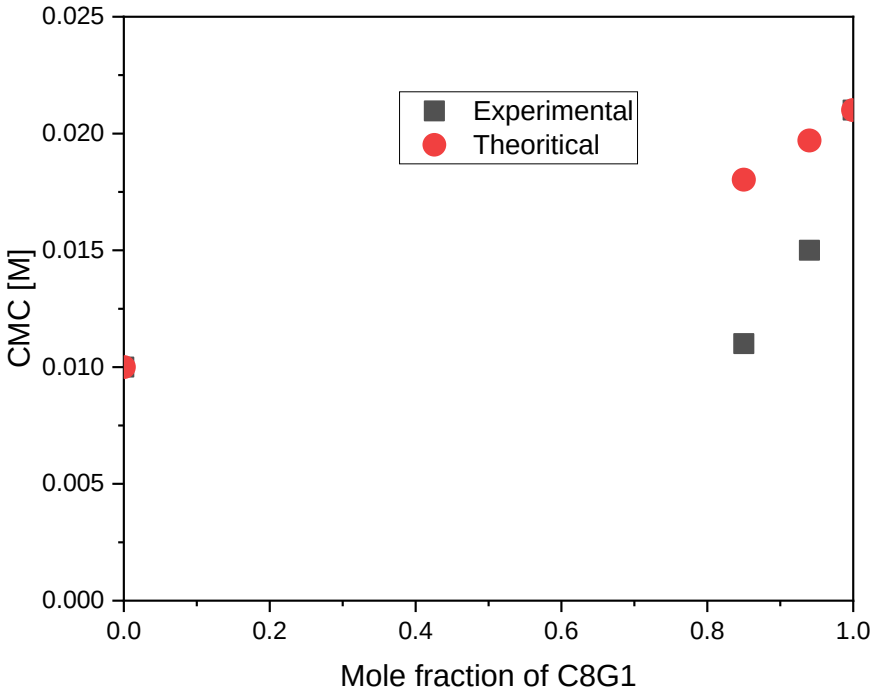

Figure 15. A plot of the critical micelle concentration of the aqueous solution of C8G1 and COSAN mixtures (CMC) as a function of the C8G1 mole fraction using equation 1.

As observed in Fig. 15, this model does not fit the experimental data, this means that there is no ideal mixing of C8G1 and COSAN in the mixed micelles, which means that the mole fraction of C8G1 and COSAN in the bulk phase is not the same in the mixed micelles.[Jańczuk, 2019]

The suitable equation for this case is the following: [Jańczuk, 2019]

$$\frac{(X_1)^2 \ln(\frac{\alpha_1 CMC}{X_1 CMC_1})}{(1-X_1)^2 ln\left[\frac{(1-\alpha_1)CMC}{(1-X_1)CMC_2}\right]} = 1 \qquad Eq.12$$

Where X_1 is the mole fraction of C8G1 in the mixed micelles. To solve this equation, I plotted the numerator and denominator as two different functions, $F(X_1)$ and $F'(X_1)$ respectively (where

α_1 and CMC are known for each C8G1 mole fraction). Changing X_1 between 0 and 1, the interception of these two different functions give rise to X_1 value for each C8G1 mole fraction (see Fig.16).

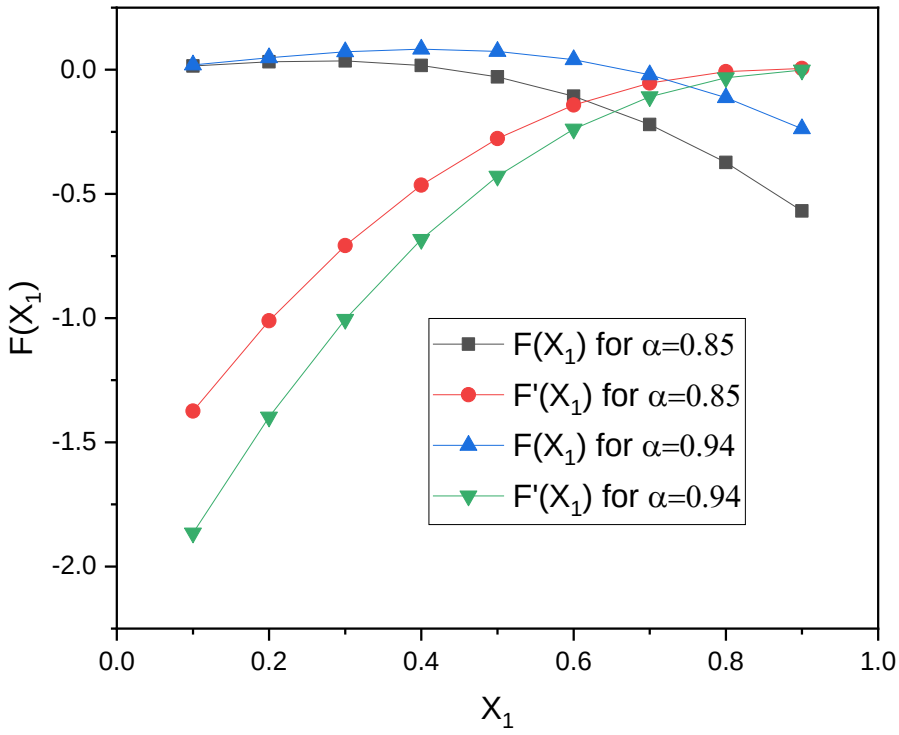

Figure 16. A plot of the functions from equation 12.

For $\alpha_1 = 0.85$, $X_1 = 0.62 \Longrightarrow$CMC = 0.01130656; for $\alpha_1 = 0.94$, $X_1 = 0.75 \Longrightarrow$ CMC = 0.01495851. CMC can then be calculated from the equation 12 where α_1, X_1, CMC_1 and CMC_2 are known (see Fig. 17).

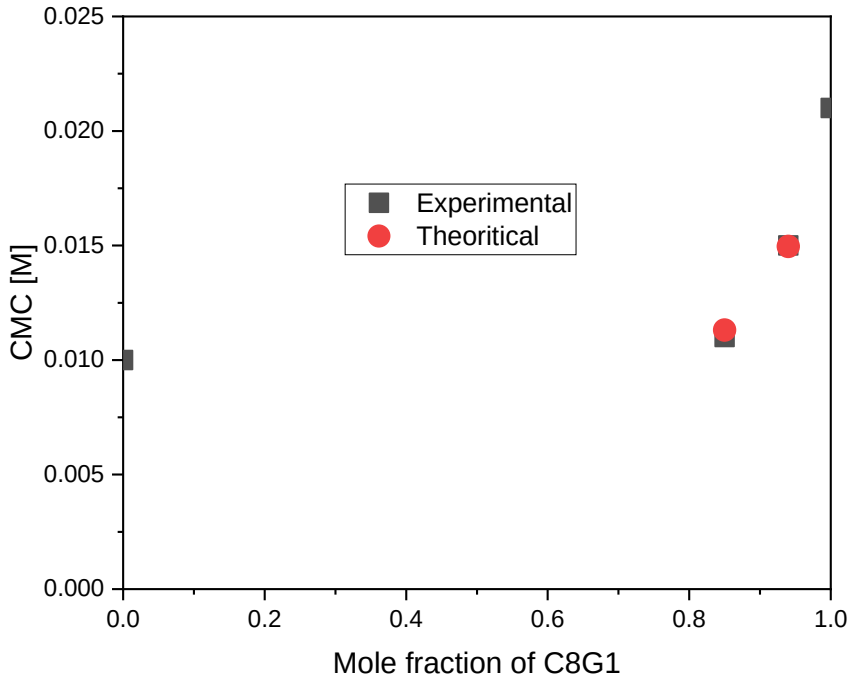

Figure 17. A plot of the critical micellar concentration of the aqueous solution of C8G1 and COSAN mixtures (CMC) as a function of the C8G1 mole fraction using equation 12.

However, here, in C8G1 mixtures with low COSAN contents, another assumption is to consider that the location of COSAN in C8G1/COSAN mixed micelles is not straightforward, that means between the C8G1 molecules, considering that COSAN has neither a hydrophobic chain nor a pronounced amphiphilic structure.

It is important to remind that

i) COSAN adsorbs to hydrophobic interfaces e.g. water/air or water/alkane interfaces owing to its surface activity but

ii) COSAN is not miscible in bulk alkanes.

Consequently, it is expected that COSAN bind to hydrophobic moieties (surfaces) but it is not expected to be distributed in an alkane riche phase i.e. it is not expected to be located within the oily core of surfactant micelles. As suggested by the NMR results (see Fig.12), COSAN-C8G1 nano-assemblies form in the pre-CMC region. The formation of these assemblies results from the binding of COSAN to C8G1 monomer, which is likely to take place through the hydrophobic effect between COSAN and the C8G1 alkyl chains (in monomeric state). Such a

binding of COSAN with a hydrophobic moiety was previously reported with octadecylmercaptan.[Errachid, 2007]

In the next section small angle X-ray and neutron scattering was used in order to shed light on the structures of the C8G1-COSAN assemblies in water, i.e. (i) the C8G1 micelles at low COSAN content, (ii) the nano-assemblies in the pre-CMC region and (iii) other aggregates types at high COSAN content.

III-5. Supramolecular C8G1/COSAN structures.

Small and wide angle X-ray scattering (SAXS/WAXS – see Annex V-5) is a powerful technique to investigate molecular aggregation in a solvent, as it probes electron density heterogeneities from the inter-atomic to the supra-molecular scales. COSAN has an electron density very close to those of water and therefore the x-ray contrast in water is weak. COSAN micelles, with a radius of around 1 nm and an aggregation number of 12-14, are typically detectable with a lab setup only at high concentrations above 100-130 mM. Regarding C8G1 micelles, the SAXS signal obtained on a lab setup is satisfactory for C8G1 concentrations above 100 mM, i.e. around five times the CMC. Thus, in the following parts SAXS was performed on 150 mM (2.97%v/v) C8G1 solutions in order to have a sufficiently high signal/noise ratio with our lab setup and to investigate C8G1 micelles upon COSAN addition. C8G1 micelles are usually described by using core-shell elliptical models (form factor) with an excess electron density in the glucose rich shell.[Giordano, 1997; Zhang, 1999; He, 2000] The typical SAXS spectrum of C8G1 micelles, arising mainly from the micelle form factor, shows an upturn intensity at low q values and a large oscillation at high q values, see the SAXS spectrum obtained for 150 mM C8G1 in Fig. 18-a-b (dark squares).

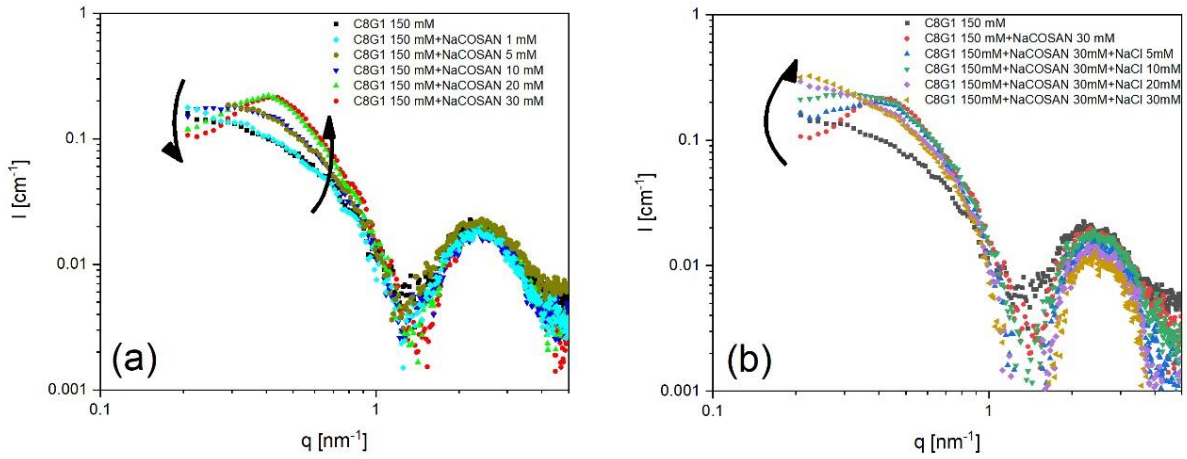

Figure 18. SAXS spectra of (a) C8G1 150 mM in the presence of [NaCOSAN] = 1, 5, 10, 20 and 30 mM, (b) C8G1 150 mM and NaCOSAN 30 mM in the presence of [NaCl] = 5, 10, 20 and 30 mM. All experiments were performed at room temperature.

SAXS was measured on C8G1 mixed micelles (150 mM) with different COSAN concentrations, at 1, 5, 10, 20 and 30 mM, see Fig. 18-a. In such a C8G1/COSAN composition range, the scattering is governed by C8G1 micelles, i.e. the scattering of COSAN monomers or micelles can be neglected (too low scattering contrast and too low concentration). This enables to obtain information on the evolution of C8G1 micelles structure, i.e. their shape/size/interactions and internal structure (core-shell structure), upon addition of COSAN. The increase in the COSAN concentration strongly affects the SAXS spectra in the low q regime ($q < 0.8$ nm^{-1}) showing a decrease in the scattered intensity and the appearance of a broad scattering peak shifting from 0.3 to 0.4 nm^{-1}. This evolution can be attributed to (i) a possible shortening of the micelles and to (ii) a clear rising of strong intermicellar repulsions. In the medium q-range ($1 < q < 1.5$ nm^{-1}) a slight shift of the first minimum towards the larger q-values may be related to some slight changes in the micelle size. Otherwise the SAXS spectra in the medium and high q-region remain mostly unchanged by addition of COSAN. For COSAN concentrations from 1 to 30 mM, the alkyl chain correlation peak (centered at around 15 nm^{-1}, i.e. 4.2 Å ($2\pi/q$) in real space) is observed at the same position as in the spectrum of 150 mM C8G1 in water (see Fig. 19). This observation indicates that the (liquid like-) alkyl chains in the micelle core are not affected by the COSAN and confirms that COSAN anion is adsorbed on or within the polar head corona.

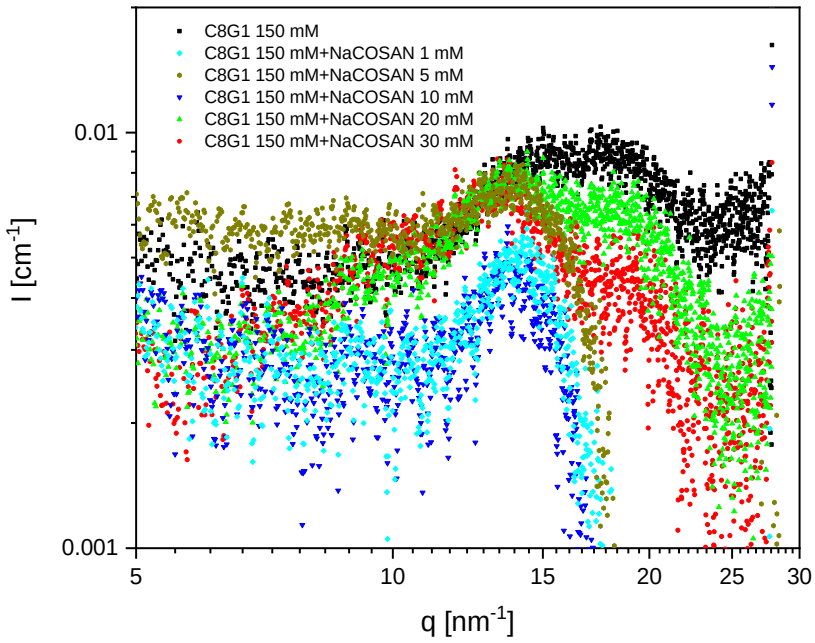

Figure 19. WAXS spectra of C8G1 150 mM in the presence of [NaCOSAN] = 1, 5,10, 20 and 30 mM. The broad peak centered at around 20 nm^{-1} arises from the signal of water which is still visible even after subtraction of the spectrum of water.

Very recently, all types of superchaotropic nano-anions investigated so far, were studied in a consistent way regarding their effect on the phase behavior on polyethoxlylated surfactants.[Assaf, 2018] It was shown that the adsorption of nano-ions at the surface of non-ionic micelles leads to profound effects, comparable to the effects produced by the addition of an anionic surfactant: lyotropic lamellar phase to vesicle transition, decrease in the micellar size and increase in the intermicellar repulsions. Based on these considerations and on the experimental evidence exposed here, it can be concluded that COSAN adsorb on the surface of C8G1 micelles which leads to the rising of strong electrostatic intermicellar repulsions.

In order to probe these electrostatic intermicellar repulsions, salt (NaCl) was added to the system showing the strongest repulsions, i.e. in the presence of 30 mM COSAN, see Fig. 18-b. Addition of salt at low concentrations (5-10 mM), clearly leads to the suppression of the repulsive interactions, by showing the disappearance of the scattering peak and the increase in the scattered intensity at low q values. This evolution by addition of salt is typical of the electrostatic screening of charged colloids and therefore proves that the intermicellar repulsions are of electrostatic origin. Full screening of the electrostatics between the COSAN decorated C8G1 micelles seems to be achieved at 10 mM NaCl, i.e. when the scattered intensity reaches a constant value at low q values, which is observed when there are no inter-

aggregate interactions. By increasing further NaCl concentrations above 10 mM, the scattered intensity at low q values keeps increasing, which can be assigned to the rising of attractive interactions and/or to an increase in the micellar size. These two latter effects are fully consistent with (i) the dehydration of the micellar surface upon COSAN adsorption, i.e. which is the classical mechanism proposed to explain the strong binding/adsorption of chaotropic nano-ions, and with (ii) the screening effect by salt leading the intermicellar attraction interactions, arising from van der Waals forces, to become predominant over repulsions, arising from electrostatics and hydration.

III-6. C8G1/COSAN at high salt concentration

Interestingly, adding NaCl at higher concentrations (50, 100 and 150 mM), a phase separation is observed with a transparent upper phase and a dark orange viscous lower phase (see Fig. 20). As the NaCl concentration increases, the volume of the lower phase decreases, the viscosity increases and the phase color becomes darker (dark orange) indicating that the lower phase is getting more concentrated by COSAN.

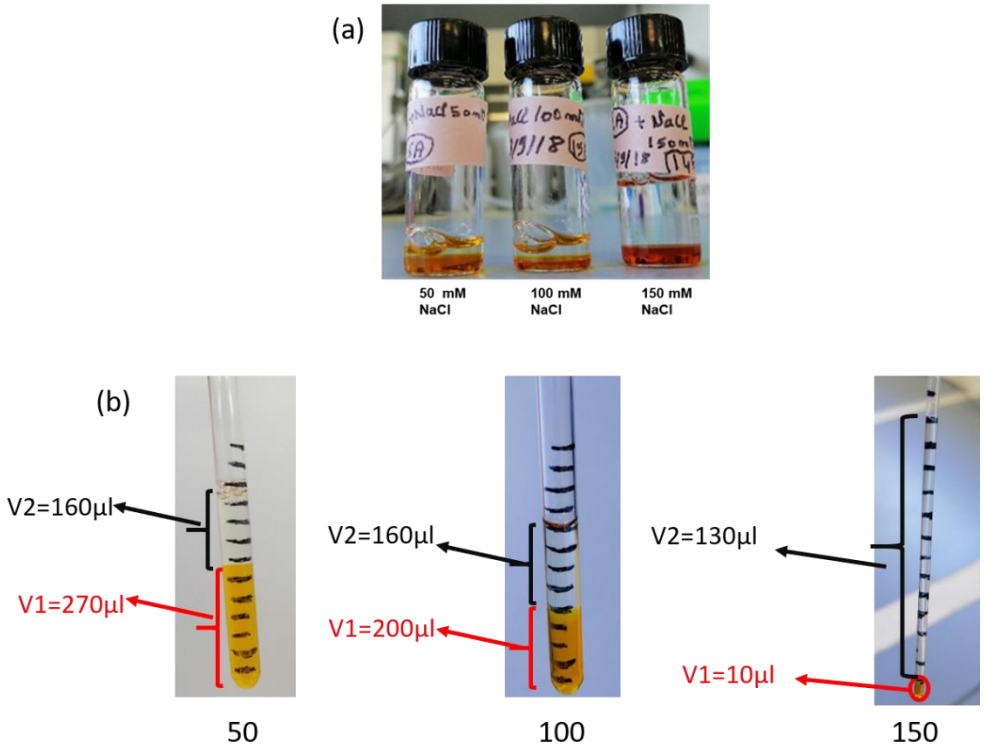

Figure 20. Three solutions of C8G1 150 mM in the presence of NaCOSAN 30 mM and [NaCl] = 50, 100 and 150 mM. The same solutions prepared in capillaries in order to determine the volume ratio between the lower and upper phases.

The composition of the upper and lower phases was investigated. In the upper phase, COSAN concentration was determined using UV-vis spectroscopy analysis. Knowing the global COSAN concentration, the COSAN concentration in the lower phase was calculated (substraction). C8G1 concentration was determined using the total organic carbon analyzer technique (TOC). TOC is a technique based on the oxidation of organic carbon atoms giving rise to CO_2 that will be analyzed in infrared in order to quantify the carbons in the analyzed solution. Noting that, for this measurement only the organic carbons were analyzed i.e. the carbon atoms of C8G1. The TOC analysis was calibrated by analyzing a C8G1 solution with a known concentration about 22.98 ppm where the obtained concentration was about 23.3 ppm. It was found that the amount of COSAN and C8G1 in the upper phase is negligible (see Table. 2). Therefore, after phase separation, the majority of C8G1 and NaCOSAN are concentrated in the lower phase. In addition, since the phase separation was observed upon charge screening by NaCl, it is supposed that the salt is concentrated mostly in the lower phase.

The volume ratio $\frac{V_1}{V_1+V_2}$ i.e. $\frac{V_{lower\ phase}}{Total\ volume}$ was determined by preparing the solutions in graduated capillaries (see Fig. 20 and Table. 2). A pseudo-ternary phase diagram was drawn in order to indicate the different phases that can exist by mixing C8G1 and NaCOSAN in H_2O in the presence of 150 mM NaCl (see Fig. 21). 419 mM of COSAN corresponds to a weight fraction about 14.2 wt% and 1.92 M of C8G1 corresponds to 55 wt%.

Table 2. Volume ratio and composition of the upper and lower phases.

		[NaCl] = 50 mM	[NaCl] = 100 mM	[NaCl] = 150 mM
[C8G1] / mM	Upper phase	14.15	20.3	13.5
	Lower phase	230.5	253.8	1924
[NaCOSAN] / mM	Upper phase	-	-	0.086
	Lower phase	-	-	419
$(\frac{V_1}{V_1+V_2}) \times 100$		63%	56%	7%

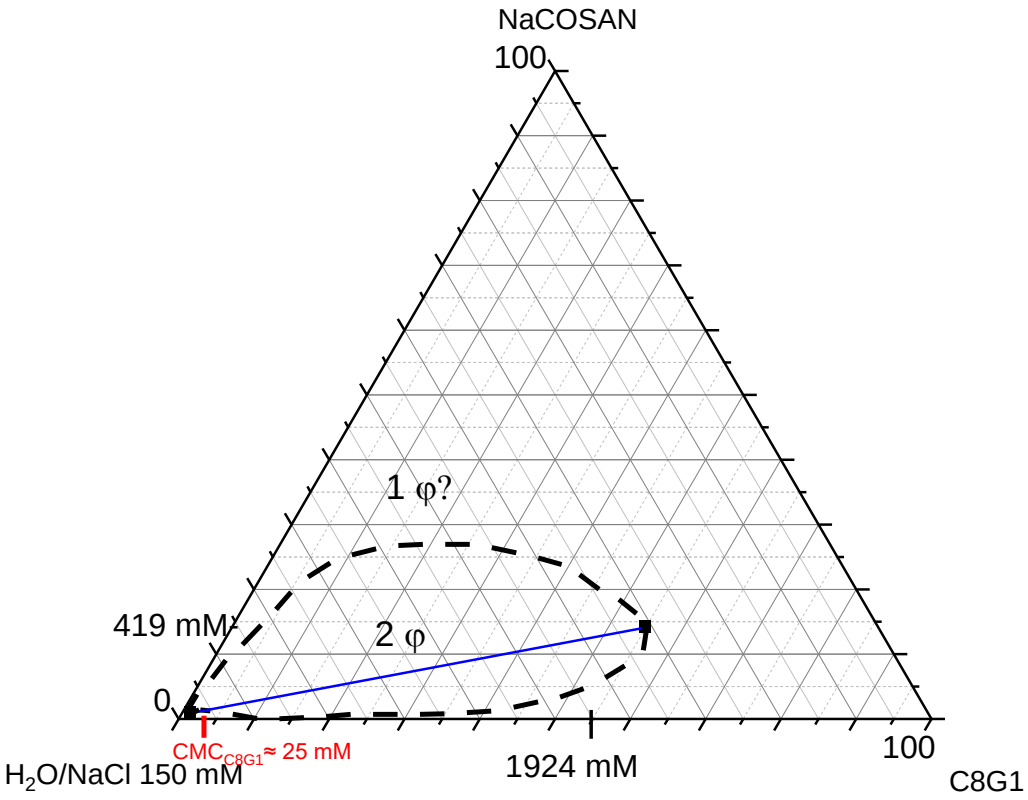

Figure 21. Pseudo-ternary phase diagram of the system C8G1/COSAN/H_2O-NaCl 150 mM. The bold doted black delimited region corresponds to the presence of the two phases. The blue line is a tie-line that connect the two equilibrium phases (the upper and the lower phases).

What is interesting here is that, increasing the NaCl concentration in the C8G1/NaCOSAN solution decreases the volume fraction of the upper phase (see Table. 2). The extension of the monophasic phase as well as the biphasic region have to be further investigated. Indeed, COSAN/C8G1 mixtures in brine solution can be a new solvent or a new ionic liquid? This would be interesting for further investigations.

The three lower phases (at 50, 100 and 150 mM of NaCl) were analyzed by SAXS in order to investigate whether the C8G1 micelles structure and size are affected (see Fig. 22).

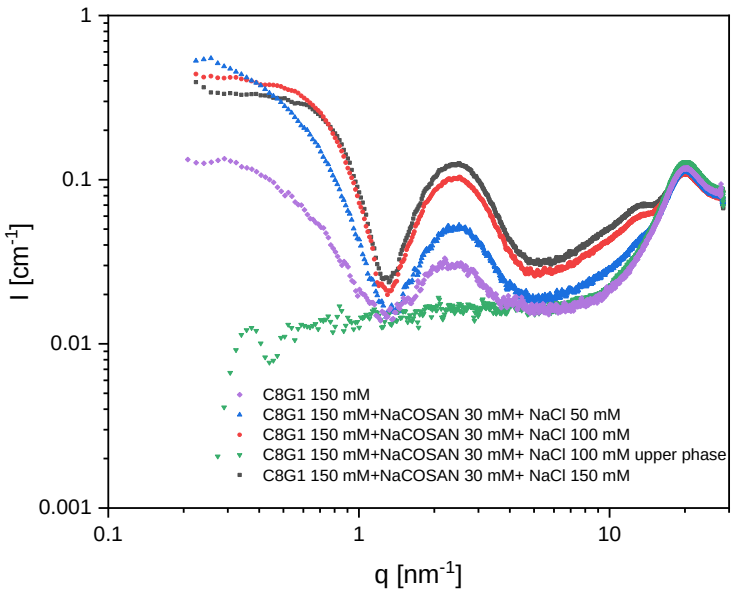

Figure 22. SAXS spectra of the lower phases after the phase separation of theC8G1 150 mM + NaCOSAN 30 mM solutions upon adding [NaCl] = 50, 100 and 150 mM. The green curve is the SAXS spectra of upper phase of the solution containing 100 mM NaCl. Water contribution to the scattering was not subtracted since the volume fraction of water is unknown.

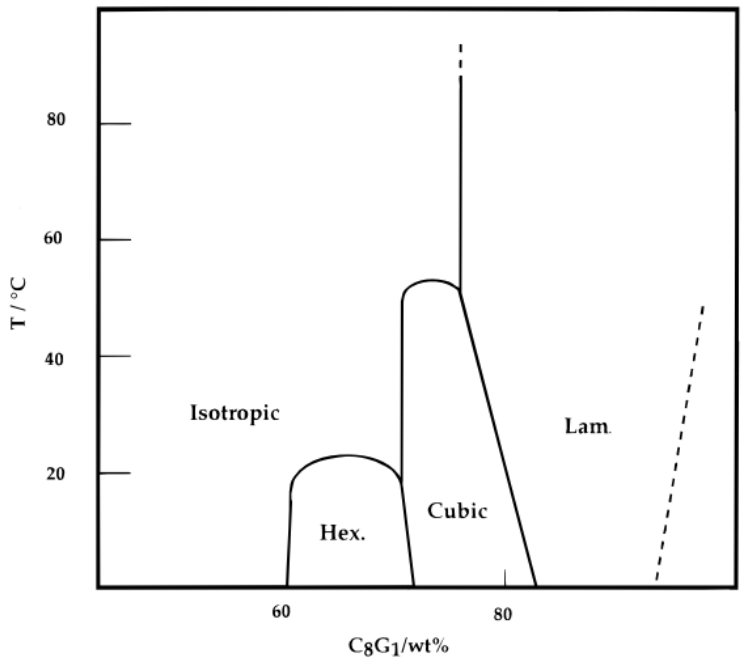

Figure 23. C8G1 phase diagram extracted from the paper of Nilsson 1996.[Nilsson, 1996]

The typical SAXS spectrum of C8G1 micelles, arising mainly from the micelle form factor is obtained here. The C8G1 concentration (1.924 M) in the lower phase of the solution containing 150 mM NaCl corresponds to around 55 %wt. that should be an isotropic phase (see C8G1

phase diagram in Fig. 23). Therefore, the C8G1 core-shell micelles are present in the lower phase. When increasing NaCl concentration, the scattered intensity is increased. This can be due to the increase of C8G1 concentration in the lower phase when increasing NaCl concentration (see Table. 2).

At low q values, the SAXS spectra for C8G1 in pure water indicate a core-shell structure with an ellipsoidal shape of the micelles.[Giordano, 1997; Zhang, 1999; He, 2000] The SAXS spectra of the lower phases at the same q range may indicate that the core-shell structure is maintained ($1< q <5$ nm^{-1}) and that the ellipsoidal C8G1 micelles evolved into spherical shape ($q < 1$ nm^{-1}).

The peak at 20.3 nm^{-1} corresponds to the distance between two water molecules (O-O). Here, the water contribution wasn't subtracted from the scattered intensity because of the unknown quantity of water. The alkyl chain correlation peak is expected at around 15 nm^{-1}, i.e. 4.2 Å ($2\pi/q$) in real space. However, a peak around 13.3 nm^{-1} (i.e. 4.7 Å nm in real space) corresponds to the interactions between the octyl chains of the C8G1 surfactant or to a couple COSAN/alkyl chains interactions. Although the COSAN concentration is relatively high in the lower phase ($\approx$ 419 mM), the peak corresponding to the closest accessible Co-Co distance that should be around 10.8 nm^{-1} is not observed.

As a conclusion here, the addition of salt to the C8G1 150 mM/COSAN 30 mM solution screens the repulsive interactions between the micelles up to a NaCl concentration below 50 mM. Above 50 mM, a phase separation is observed. This observation can be interpreted by the fact that the adsorption of COSAN anions onto the C8G1 micelles is a water mediated interaction. Therefore, since both COSAN anions and C8G1 micelles are dehydrated upon interaction, the charge screening by NaCl i.e. the suppression of the electrostatic repulsive interactions leads to a phase demixion.

According to a recent model[Girard, 2019] which is based on a lateral equation of state taking into account electrostatic contributions and adsorption of charged nano-ions on non-ionic micelles, the Gibbs free energy of adsorption of COSAN onto C8G1 micelle, ΔG_{ads}, can be estimated, details on the method are described in Annex V-4. With this method, ΔG_{ads} was found to be between -6.5 ± 0.5 kT which is quite well in agreement with the results obtained from UV measurements and by using the Langmuir isotherm model, $K = 0.16$ mM^{-1} which corresponds to -5.1 kT.

III-7. Effect of high COSAN content on C8G1 micelles.

By further increase in the COSAN concentration (≥ 50 mM), the SAXS spectra in Fig. 24-a show:

(i) A pronounced shift in the scattering pattern of the (COSAN decorated) C8G1 micelles to high q values, i.e. to smaller structures, and

(ii) A decrease in the overall scattering intensity.

This evolution in the spectra upon COSAN addition can be attributed to a continuous disruption of the micelles into smaller aggregates (see the sketches in Fig. 24-a) but keeping a core-shell structure up to 150 mM COSAN, with an excess electron density in the shell, as indicated by the large oscillation at high q values and the intensity upturn at low q values. It is interesting to note that COSAN at 150 mM in water (without C8G1) forms small micelles with a radius of 1 nm, which is around the maximal length of a COSAN anion, and shows the typical scattering pattern of small globular objects with homogeneous electron density, i.e. without a core-shell structure, see red symbols in Fig. 24-a. Therefore, it is expected for higher COSAN concentrations, that C8G1 micelles are fully disrupted, i.e. losing the core-shell structure. Let us remark also that COSAN micelles present at 150 mM in pure water are fully disrupted in the presence of 150 mM C8G1 to form mixed micelles, i.e. COSAN decorated C8G1 micelles. This may suggest that C8G1 micelles are more stable than COSAN micelles.

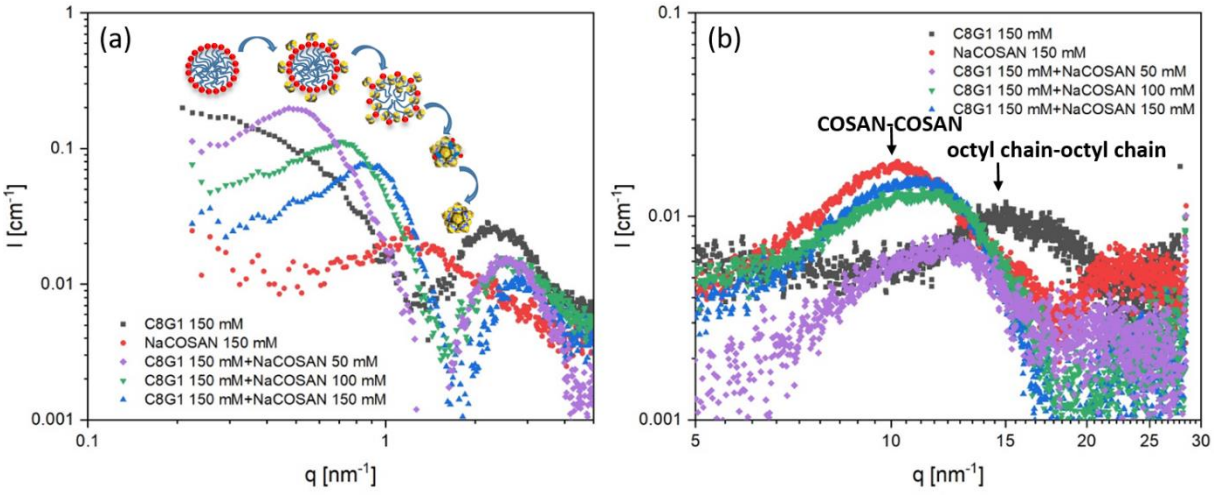

Figure 24. SAXS (a) and WAXS (b) spectra of C8G1 150 mM in the presence of [NaCOSAN] = 50, 100 and 150 mM. The ordinate axis is the absolute intensity. All experiments were performed at room temperature.

In the WAXS region, from 5 to 27 nm^{-1} where intermolecular and interatomic distances are probed (from around 2 to 12 Å), the spectrum of C8G1 micelles (150 mM C8G1) in pure water, see dark symbols in Fig. 24-b, show a unique and intense broad peak centered at around 15 nm^{-1}, i.e. 4.2 Å ($2\pi/q$) in real space corresponding to the typical average chain-chain distance

measured in liquid alkanes. Therefore, this correlation peak at $q_{C8-C8}^{C8G1\ micelle}$, corresponds here to correlation in space between octyl chains in the micellar core. The contribution of water in the SAXS spectra, showing a broad and intense signal centered at around 20 nm^{-1} and arising from O-O correlations in liquid water, was subtracted on all spectra proportionally to the volume fraction of water in the measured sample. In the presence of high COSAN concentrations, the broad "alkane" peak is not present, see in Fig. 24-b, but a correlation peak at lower q values is observed at 12.2, 11.1, and 10.5 nm^{-1}, respectively for COSAN concentrations of 50, 100 and 150 mM, which correspond in real space to 5.1, 5.7 and 5.9 Å. In order to understand the origin of this correlation peak, it is informative to make comparison with the spectrum of a concentrated COSAN solution at 150 mM, see red symbols in Fig. 24-b. At such high concentrations the large majority of the COSAN anion form small micelles and a correlation peak is observed at around 10 nm^{-1} ($q_{COSAN-COSAN}^{COSAN\ micelle}$), which corresponds to 6.3 Å in real space and which was previously attributed to COSAN-COSAN correlations in the COSAN micelles.[Bauduin, 2011] Therefore the correlation peaks in WAXS in C8G1/COSAN mixtures, which are observed at q values between $q_{C8-C8}^{C8G1\ micelle}$ and $q_{COSAN-COSAN}^{COSAN\ micelle}$, corresponds to average correlations between octyl chain and COSAN. Consequently, in the concentration range investigated here, COSAN and alkyl chains of C8G1 are intimately mixed in a liquid state in the mixed aggregates.

III-8. Effect of COSAN on C8G1 micelles at low C8G1 concentrations

In SANS experiments (see Annex V-5), samples were prepared in D_2O, and not H_2O as for the other techniques used here, and the major contrast arises then from hydrogenated part (C8G1 and COSAN) and deuterated part (D_2O solvent). This sensitive technique enables the investigation of supramolecular assembly (C8G1/COSAN micelles) at low C8G1/COSAN concentrations. SANS measurements were performed at low C8G1 concentrations (15, 30, 40 mM), i.e. above and below CMC_0^{C8G1}, in the presence of COSAN at 2 and 10 mM (Fig. 25). The spectrum of C8G1 at 40 mM, around 2 times CMC_0^{C8G1}, shows the typical scattering of elliptical micelles, in good agreement with previous literature.[Giordano, 1997; Zhang, 1999; He, 2000] In the presence of 10 mM COSAN (red circles), the SANS spectrum shows (i) a stronger excess scattering as expected from the adsorption of COSAN on C8G1 micelles which increases the hydrogen content of the micelles, and (ii) the appearance of a scattering peak indicating repulsive interactions between COSAN decorated C8G1 micelles, as observed above by SAXS measurements. Similar conclusions can be drawn at C8G1 30 mM (blue triangles in Fig. 25).

Interestingly the spectra at 15 mM C8G1, which is below CMC_0^{C8G1}, with 2 and 10 mM COSAN show at high q values a strong scattering signal similar (> 0.1 $Å^{-1}$) to the signal of bare C8G1 micelles at 40 mM in water. At low q values (q < 0.1 $Å^{-1}$) a strong decrease in the scattered intensity as well as a broad scattering peak centered at 0.03-0.04 $Å^{-1}$ indicate a strong repulsive micelles-micelles interactions. C8G1 in water at 15 mM is only present as monomers, which do not produce sufficient scattered intensity to be measured. Therefore, it can be concluded that COSAN decorated C8G1 micelles, with a size comparable to the size of bare C8G1 micelles, are present at C8G1 concentrations below CMC_0^{C8G1}. This result suggests that the CMC of C8G1 is decreased below 15 mM in the presence of 2 and 10 mM COSAN, which is in full agreement with the shift to lower concentrations in the surface tension break (at least for 2 mM COSAN) and with the conclusion made in the UV/NMR section. This confirms that COSAN at low concentrations, i.e. below or at the CAC of COSAN, stabilizes C8G1 micelles as they form at concentrations lower than CMC_0^{C8G1}. Nevertheless, the results obtained from DLS measurements (page 50 Fig. 3-b) show that at 15 mM C8G1 in the presence of 2 mM COSAN, only COSAN vesicles are detected in the solution. However, since DLS technique is more sensitive to large objects, when the micelles concentration is too low and when both coexist (COSAN vesicles and C8G1 micelles), the results are not fully conflicting. At 15 mM C8G1 in the presence of 2 mM COSAN, the number of C8G1 micelles is not sufficient to make them detectable in DLS. The transition for the coexistence between C8G1 micelles and COSAN vesicles is perhaps at a lower value of C8G1 concentration.

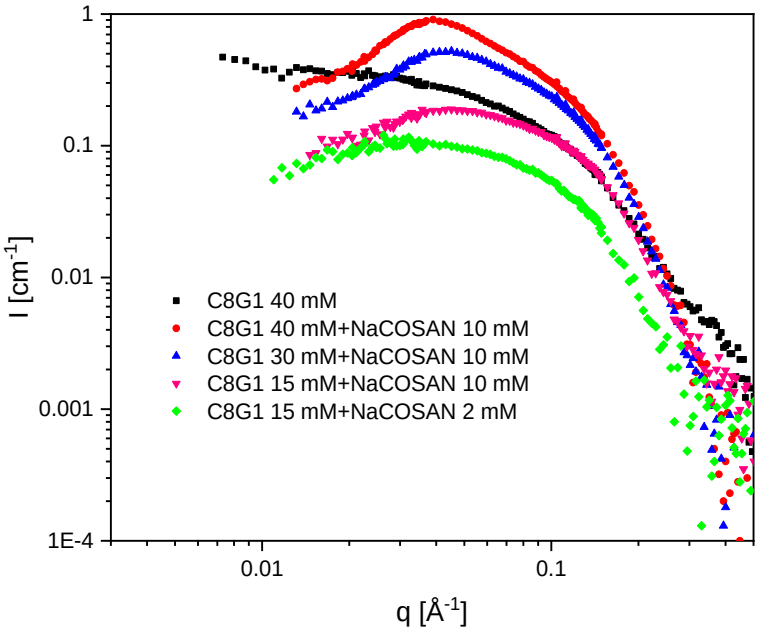

sure 25. SANS spectra of C8G1 in the presence of COSAN. The ordinate axis is the absolute intensity. All experiments were performed at room temperature.

IV. Conclusion

It was shown here in many aspects that COSAN strongly interact with C8G1 to form mixed aggregates in equilibrium. As a conclusion the type of C8G1/COSAN assemblies depends exclusively on the concentrations of both species:

1) **At low COSAN content (below the CAC)**, where COSAN vesicles and non-aggregated COSAN (i.e. monomers) coexist, COSAN vesicles are destroyed by addition of C8G1 in monomeric form i.e. at concentrations below the CMC of C8G1. Note that the limit of the coexistence region between COSAN vesicles and C8G1 micelles depends on the technique used. In this concentration region, COSAN-C8G1 nano-assemblies, highlighted by NMR, are formed through the hydrophobic effect between COSAN and the alkyl chain of C8G1.
2) **At low COSAN content (below the CAC) and at high C8G1 concentrations (above the CMC)**, COSAN adsorbs to the hydrated surface of C8G1 micelles. The binding of COSAN at the micellar surface leads to a decrease in the CMC of C8G1, i.e. to a stabilization of the C8G1 micelles. Adsorption of COSAN arises from collective interactions with a glucose covered surface, where local interactions between COSAN with many glucose units appear. This was confirmed by the investigation of mixtures of COSAN with simple mono- and di-sugars in water that has shown no binding whereas a strong binding to linear oligosaccharide (maltodextrin) was observed. Therefore, many sugars, presumably more than 3 to 5, in a local environment, are required to observe a significant binding of COSAN. Depending on the experimental approach the binding constant is roughly estimated between 0.2 and 0.5 mM^{-1}. This result is interesting to compare with the formation of well-defined stoichiometric complex, i.e. 1:1 host-guest complex, of COSAN with the glucose-based macrocycles, β or γ-cyclodextrins containing respectively 7 and 8 glucose units, for which binding constants of 0.026 and 0.191 mM^{-1} were obtained. The strong binding of nanometric sized ions at non-ionic micellar surfaces [Naskar, 2015] or in the cavity of macrocycles [Assaf, 2015] has been previously explained to originate from a water-mediated effect named the chaotropic effect or superchaotropicity regarding its reinforced effect compared to classical chaotropic ions such as SCN^- or I^-. In the present work, the superchaotropic behavior of COSAN is shown by its spontaneous adsorption on the surface of C8G1 micelles, comparably to POMs nano-ions.[Naskar, 2015; Buchecker, 2018; Hohenschutz, 2020] Therefore, at high C8G1 concentrations, the superchaotropic effect is predominant over the hydrophobic effect observed between C8G1 and COSAN at low concentrations.
3) **At high COSAN content (above the CAC)**, the addition of COSAN disrupts continuously C8G1 micelles, i.e. with the COSAN penetrating in the micellar surface. By further increase in the COSAN concentrations, i.e. at higher COSAN/C8G1 ratios, the COSAN-C8G1

assemblies become similar in size and shape to COSAN micelles but containing small amount of solubilized C8G1 molecules. Such COSAN micelles containing molecularly dissolved C8G1 molecules presumably also form at low C8G1 concentrations and at high COSAN concentrations. COSAN differs here from POMs due to the surfactant properties of COSAN, i.e. mainly surface activity and micelle formation. Indeed, at high POM content, POMs neither penetrate nor disrupt C8G1 micelles.[Naskar, 2015]

The general superchaotropic property of nanometric sized ions, POMs, boron clusters including COSAN, takes place in many different chemical systems and is therefore likely to be related to their effect on biological systems including antiviral activities,[Rhule, 1998; Cígler, 2005] effect on cells.[Tarrés, 2015] In addition to the superchaotropic property, COSAN and its derivatives show some additional surfactant properties, associated to a more hydrophobic character (lower charge density),[Masalles, 2002] which brings some exceptional ability to cross through biological membranes, model phospholipids and cell membranes,[Verdiá-Báguena, 2014; Tarrés, 2015; Rokitskaya, 2017] opening opportunities in the pharmaceutical field.

Part of the data in this chapter was published in Chemistry-A European Journal.[Merhi, 2020]

V. Annex of chapter 2

V-1. DLS measurements

The DLS was performed using an ALV-CGS3 goniometer equipped with a 22 mW HeNe laser (632.8 nm) and an APD-based single-photon detector coupled to an ALV/LSE-5004 auto-correlator. It has a minimum real time sampling time of 0.1 µs and a maximum of about 50 s. For all the light scattering experiments, the temperature was maintained at 25°C. The experimental autocorrelation function was measured at different angles from 30 to 150° with a 10° step. The autocorrelation functions that correspond in our case to multi-exponential functions were fitted by the least-squares method using the Microsoft Excel Solver.

Figure 1. A picture of the DLS apparatus used for the measurements in this chapter.

V-2. Determination of the diffusion coefficient and the hydrodynamic radius-DLS.

From the fit of the correlation function (equal to a sum of exponentials), we obtain the gamma (Γ) values for the slow mode (large particles) and fast mode (small particles). Gamma values are plotted as a function of the square of the scattering vector q in order to determine the diffusion coefficient D:

$$\Gamma = D\, q^2 \quad (Eq.\ 1)$$

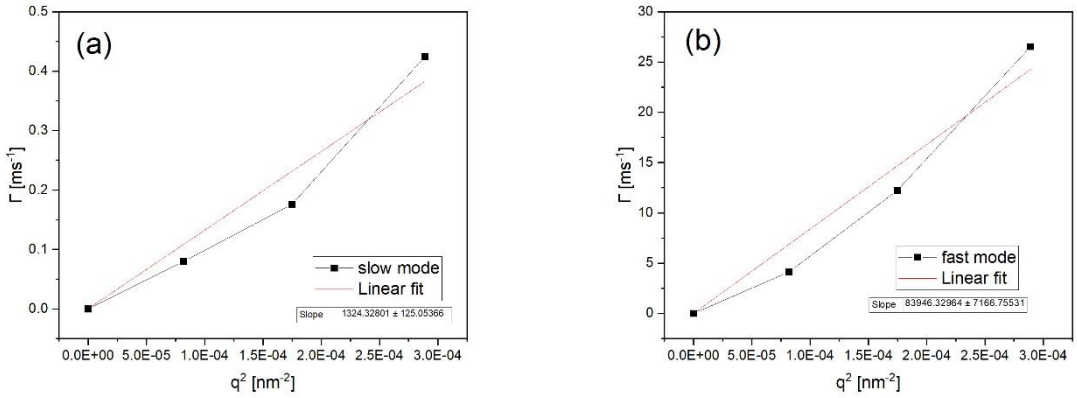

Figure 2. Gamma values of slow (a) and fast (b) modes obtained from fitting DLS correlation function for [NaCOSAN]= 1 mM in the presence of C8G1, as a function of the square of the wave vector. The slope of the linear fit represents the diffusion coefficient of aggregates.

The slope is related to the diffusion coefficient of the COSAN vesicles, 1324.3 nm^2/ms, which corresponds to a hydrodynamic radius about 183.226 nm that can be attributed to COSAN vesicles. While for the fast mode D = 83946 nm^2/ms, which corresponds to a hydrodynamic radius about 2.89 nm.

V-3. UV-visible spectroscopy

UV–visible absorption spectra were recorded from 190 to 600 nm using a Shimadzu UV–vis–NIR spectrophotometer UV-3600 equipped with deuterium and halogen lamps. The experiments were performed in a dual-beam mode with a slit width of 8 nm and a step of 0.5 nm. Samples were prepared in quartz tubes of about 2 mm in thickness.

V-4. Determination of ΔG_{ads} for NaCOSAN molecules adsorbed on C8G1 micelles.

A thermodynamic model based on the pseudo-phase model[Shinoda, 1962] is used to explain the decrease of the CMC of C8G1 in the presence of COSAN anions and to determine the association energy ΔG_{ads} of COSAN molecules on C8G1 micellar surface. In this case, the C8G1 micelles are stabilized by the COSAN adsorption at their surface and different species could be considered: the C8G1 monomer *m*, the C8G1 micelle *M*, the COSAN *c* and the C8G1 micelle associated with the COSAN M_a.

$$m \overset{(1)}{\Leftrightarrow} m \text{ in M} \quad \text{and} \quad m \overset{(2)}{\Leftrightarrow} m \text{ in } M_a$$

The equilibrium constant K_1^0 of the Equilibrium (1) can be expressed as:

$$K_1^0 = \frac{1}{C_{\mathrm{m}}} = \mathrm{e}^{-\frac{\mu_{\mathrm{M}}^0 - \mu_{\mathrm{m}}^0}{k_B T}} = \mathrm{e}^{-\frac{\Delta G_{\mathrm{mic}}^0}{k_B T}} \qquad \text{(Eq. 2)}$$

For the Equilibrium (2), the equality of the chemical potentials can be expressed as:

$$\mu_{\mathrm{m}}^0 + k_B T \ln c_{\mathrm{m}} = \mu_{\mathrm{M_a}}^0 \qquad \text{(Eq. 3)}$$

With the defined equilibrium constant K_2^0 as:

$$K_2^0 = \frac{1}{C_{\mathrm{m}}} = \mathrm{e}^{-\frac{\mu_{\mathrm{M_a}}^0 - \mu_{\mathrm{m}}^0}{k_B T}} = \mathrm{e}^{-\frac{\Delta G_{mic,a}^0}{k_B T}} \qquad \text{(Eq. 4)}$$

Equations (1) and (2) are not compatible, as the Equilibrium (1) cannot be present together with Equilibrium (2). In other words, only the most stable micellar aggregates, either the micelles without COSAN (Equilibrium 1) or the micelles with COSAN (Equilibrium 2) can be present as a pseudo-phase. Thus, in our case where the CMC of C8G1 is decreased in the presence of COSAN i.e. COSAN stabilizes C8G1 micelles, $\mu_{\mathrm{M}}^0 > \mu_{\mathrm{M_a}}^0$, and Equilibrium (2) take place according to Eq. (4).

The free energy of micellization ΔG_{mic} in the presence of COSAN can be written as follow:

$$\Delta G_{\ mic} = F_{\mathrm{L}/\mathrm{W}} + F_{\mathrm{head-rep}} + \frac{(F_{\mathrm{ads}} + F_{\mathrm{elec}})}{N_{\mathrm{agg}}}$$

Where $F_{\mathrm{L}/\mathrm{W}}$ term represent the free energy of hydrocarbon (C8G1 tail)/water, $F_{\mathrm{head-rep}}$ term represent the steric repulsion between C8G1 headgroups, F_{ads} term account for the adsorption of COSAN onto C8G1 micelles and F_{elec} term account for the repulsion interactions between COSAN anions on the C8G1 micellar surface. For more details see L. Girard et al. 2019.[Girard, 2019] A first minimisation of micellization energy ΔG_{mic} as a function of N_{ads} method is used in order to determine the association energy ΔG_{ads} of COSAN molecules on C8G1 micellar surface. In the present model, the input parameters are: the aggregation number of C8G1 micelles (between 50 and 100 depending on C8G1 concentration, here we have shown that C8G1 micelles become spherical upon adsorption of COSAN suggesting an aggregation number around 35-40), the surface per surfactant headgroup within the micelle in pure water solution (a = 0.49 nm^2),[Bauer, 2012] the minimal headgroup area from pure steric considerations (a_0 = 0.36 nm^2), COSAN concentration in $mol.L^{-1}$, the energy associated to the binding of one COSAN on a micelle, ΔG_{ads} (kT), and the alkane/water surface tension 45 $mN.m^{-1}$. The surface permittivity (ε_r) depends on the number of COSAN molecules adsorbed at the micellar surface (see SI of L. Girard et al. Journal of Molecular Liquids, 2019, 293, 111280). In this model ΔG_{ads} is obtained by fitting the CMC of C8G1 by considering a reasonable number of COSAN adsorbed at C8G1 micellar surface, i.e. 5 COSAN molecules

per C8G1 micelle as estimated from the UV-visible measurements for 1 mM COSAN and at [C8G1] = 50 mM the concentration for which saturation is reached. As a result, ΔG_{ads} is found to be in the range of -6 to -7 kT.

V-5. Small angle X-ray and neutron scattering (SAXS-SANS)

Small Angle X-ray Scattering (SAXS) measurements using a Mo radiation source (λ = 0.071 nm) were performed on a bench built by XENOCS at the ICSM institute. The scattered intensity I (q), obtained by radial averaging of the 2D images, is plotted in absolute scale as a function of wave vector q, defined as $q = {}^{2\pi}/_{\lambda} \sin {}^{\theta}/_{2}$, where θ is the scattering angle and λ is the X-ray wavelength. Samples were prepared in quartz tubes of about 2 mm in diameter. Standard calibration procedure of the scattered intensity was made with high density polyethylene and the absolute scattered intensity was checked by measuring water (1.6 10^{-2} cm^{-1}).

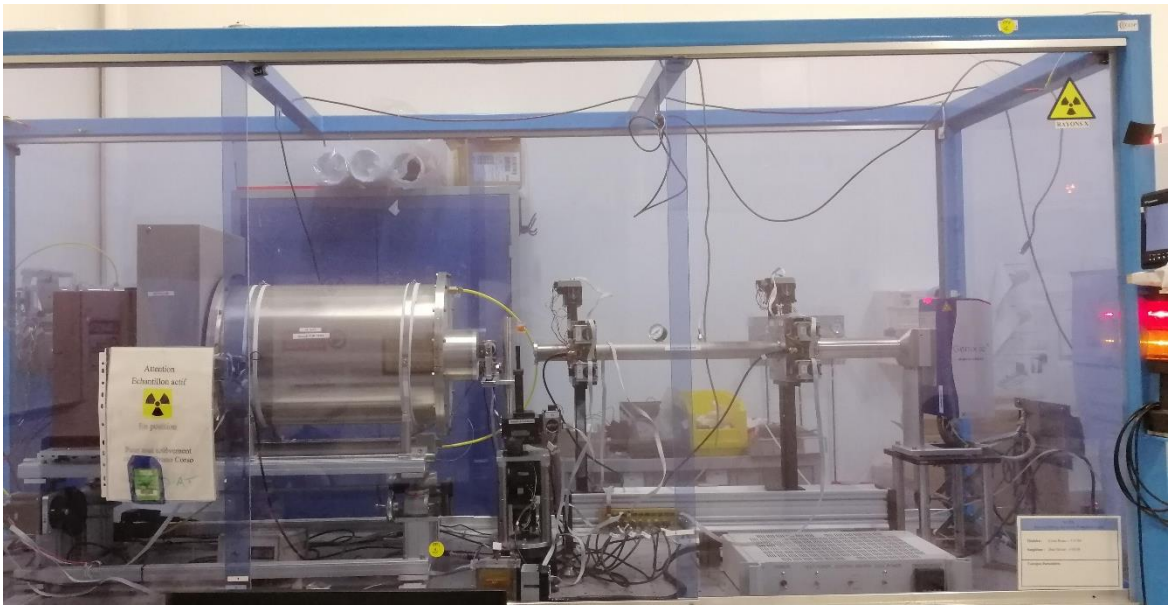

Figure 3. SAXS instrument at the ICSM institute.

Small angle neutron scattering (SANS) measurements were performed on the SANS spectrometer “PAXY” at LLB-Cea Saclay. For each sample, the sample-multidetector distance was 1 m, 3 m and 5 m with an incident wavelength λ = 4, 5 and 8.5 Å respectively.

Chapter 3

Interaction between COSAN anion and glycolipid monolayers at the air/water interface

I. Introduction

As mentioned in the second chapter of this manuscript, the thermodynamical equilibrium that drives the partitioning of the COSAN nano-ions between the bulk solution and the micellar surface, fixes the surface charge per micelles and thus the surface area per headgroup. Therefore, the question is, is it possible to regulate the nano-ion adsorption by tuning the surface per polar head of the amphiphilic molecules? One way to do it, is to perform pressure isotherms using a Langmuir trough where low soluble amphiphilic molecules are spread on and compressed at the water surface, varying the concentration of the nano-ions in the subphase. In the continuity of our first study with sugar-based surfactant, we decided to consider lipids with sugar-based polar heads such as the glycolipids. Moreover, glycolipids are essential components of biological membranes and they exhibit highly specific interactions with other saccharides [Bucior, 2004] and with proteins.[Lis, 1998]

At the time of this musing, a similar study was carried out at the Max Planck Institute in Potsdam under the supervision of E. Schneck. His project was indeed focusing on the preferential interaction of ions with glycolipids. Interestingly, ions seem to promote specific interactions with saccharide headgroups even if they are neither charged nor of zwitterionic character. These latter features have therefore motivated our investigation in the continuity of our first studies on micelles.

There are very few papers on nano-ions in interaction with monolayers of insoluble amphiphiles. The works on POMs nano-ions in interaction with model cell membranes and lipid monolayers from Nabika et al in 2013 [Nabika, 2013] and from Kobayashi in 2017 seems for us the most pertinent.[Kobayashi, 2017]

To summarize these works, POMs showed destructive activity on lipid (egg yolk phosphatidylcholine or egg-PC) bilayer vesicles as model membranes self-assemblies. Egg-PC diglycerides are zwitterionic phospholipids where ammonium groups (positively charged, weakly hydrated) are located at the outer region of the bilayer assemblies and exposed to surrounding water molecules. Langmuir isotherm measurements of the egg-PC monolayer showed an increase of the molecular area per lipid molecules in the presence of POMs anions. It was suggested that the interactions of nanometer sized POMs (1-2 nm) force the lipid molecules to be arranged in a tilted configuration, which then increases their molecular area and to induce at higher concentration the disruption of the monolayer. New POMs-lipid conjugates self-assemblies can then be formed and solubilized.[Nabika, 2013] The interactions of POMs with egg-PC monolayer are shown to be electrostatic- or hydrophobic-predominant depending on the charge density of the POM and the density of the lipid monolayer. The

hydrophobic interactions are predominant only in the compressed state of the monolayer (surface pressure of 40 $mN.m^{-1}$), where the lipid density is high enough to form a hydrophobic environment. In this case, the POMs with lower charge density, i.e. more chaotropic, exhibit the stronger effect.[Kobayashi, 2017] Moreover, the interaction of POMs with the lipid monolayer increases the tilt of lipid molecules at high pressure.

Other studies were also investigated within our group using POMs in interaction with multi-lamellar vesicles made of zwitterionics or mixture of anionics and zwitterionics phospholipids. We performed similar experiments using COSAN anions with phospholipids in order to compare their effect of interaction with POMs nano-ions. For these experiments I did not participated to some current investigations that show the full solubilization of the phospholipids.

However, to be coherent with my first study of sugar-based surfactant and trying to draw our study following the E. Schneck studies, I have worked with two different types of glycolipids: mono- and di-galactosyldiacylglycerol (MGDG-sat and DGDG-sat) (see Fig. 1). For the MGDG-sat system, we find back the similar sugar function than for the C8G1 polar head. It is doubled for the DGDG-sat molecule that is therefore much more bulky. In both cases, the aliphatic double chains were saturated. Langmuir monolayers made with these neutral glycolipids were prepared in a Langmuir trough in order to vary the lateral packing (see Annex for details of the preparation). Pressure-area (π-a) isotherms were recorded as a function of the nano-ion concentration in the bulk phase. Several features such as the average molecular area A_0 corresponding to the closest packing (called also in the literature the limiting area) as well as the molecular area or the lift-off area A_1 at which a phase transition from gas to liquid expanded (LE) occurs will be noted and discussed. A_0 is determined from the Langmuir isotherm at high pressure (see an example in Annex VII-4). A_1 was determined as the surface area per molecule at a surface pressure about 0.5 $mN.m^{-1}$ since the transition gas-LE was not pronounced enough to consider the slope at which we can observe the LE phase.[Ładniak, 2019] The isothermal surface compressibility C, defined as:

$$C = -\frac{1}{A}.\left(\frac{dA}{d\pi}\right)_T$$

By analogy with the bulk compressibility modulus, will be also displayed as C^{-1} versus the surface pressure characterizing the evolution of the relative elasticity (or fluidification) of the monolayer when the nano-ions interact with the glycolipids layer. Using synchrotron radiation, we have also probed the water/air interface covered by the glycolipids through grazing incidence x-ray diffraction (GIXD) technique to characterize the molecular ordering at the surface. We used also the total-reflection x-ray fluorescence (TXRF) to estimate the preferential accumulation of the nano-ions (excess fluorescence) at the interface and finally

the off-specular x-ray reflectivity (GIXOS) to check if we can evaluate the ion distribution along the normal axis (see Annex VII-1).

As described in the general introduction, the interactions of nano-ions with neutral (and not zwitterionic) glycolipids that were never investigated were expected to be of superchaotropic nature. In addition, this system allows us to extent the study of interaction between COSAN and glucose molecules from a system in equilibrium between monomers and micelles in the bulk phase (chapter 2) to a monolayer of sugar functions at an air/water interface.

II. MGDG-sat and DGDG-sat in interaction with classical ions.

The mono- and di-galactosyldiacylglycerol are uncharged amphiphilic glycolipid molecules with sugar headgroups consisting of one and two galactose moieties respectively and two fatty acyl chains as hydrophobic part (see Fig. 1). [Stefaniu, 2019]

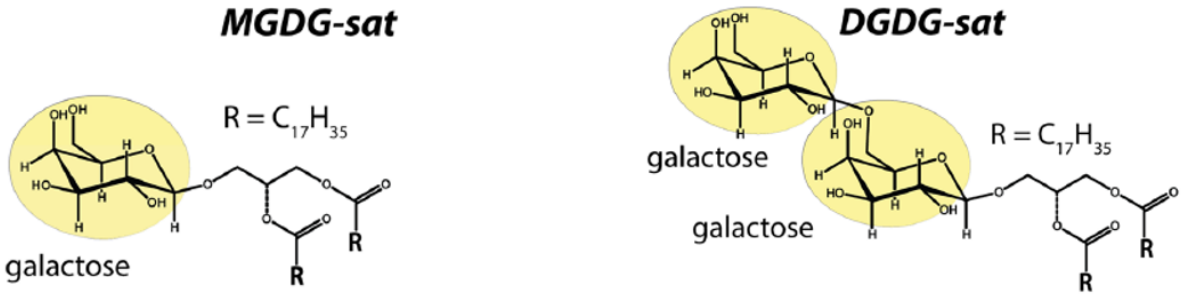

Figure 1. MGDG-sat (left) and DGDG-sat (right) molecular structures with 1 and 2 galactosides polar group respectively.

Pressure-area (π-a) isotherms display different behavior for both systems (see Fig. 2-a). The π-a curve for the MGDG-sat is rather flat and close to zero mN.m^{-1} over a large variation of the surface per polar heads until a steep increase is observed above around A_1= 50 Å. It was mentioned in the literature [Hoyo, 2016] the formation of a liquid condensed phase under compression for MGDG-sat system and a 1st order transition toward a solid phase between 10 and 15 mN.m^{-1} surface pressure.

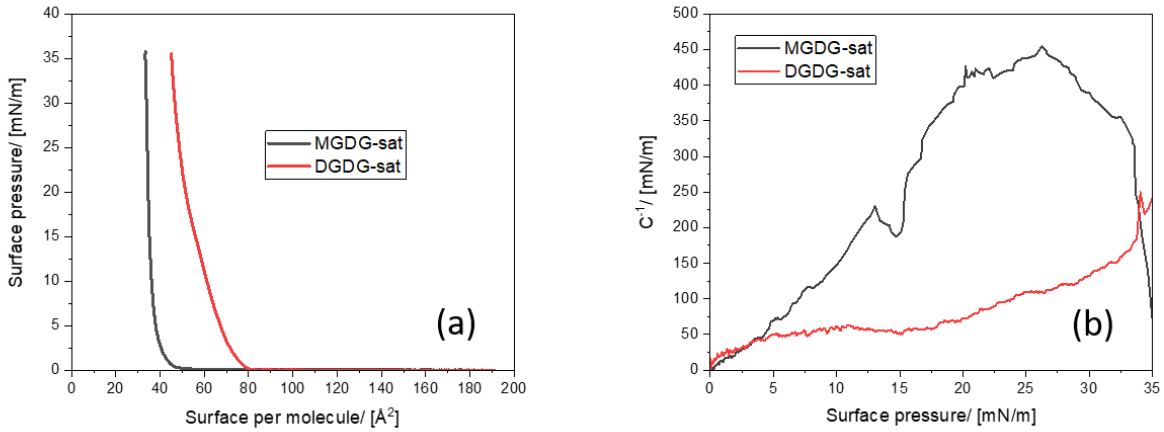

Figure 2. (a) Langmuir isotherms of MGDG-sat and DGDG-sat on pure water (see Annex VII-2). (b) Inverse of the compressibility modulus versus surface pressure for the same systems.

From the E. Schneck group investigations, [Stefaniu, 2019] it was confirmed using GIXD that above a surface pressure of 10 $mN.m^{-1}$ a 2D-ordering at two levels within the monolayer exist (see Fig. 3): First, between the galactoside heads via H-bonds [Hinz, 1991] that forces in a second step, the ordering of the aliphatic chains with a defined orientation tilt angle of about 30°. This strong ordering observed even at low surface pressure means that perhaps, a crystalline structure pre-exists at lower surface pressure under the form of solid islands in equilibrium with the gas-phase of glycolipids and that the surface pressure lifts off at low surface area when the solid islands are in close contact. Looking at the evolution of the inverse compressibility (see Fig 2-b, black curve) as a function of the surface pressure it does not seem that a liquid state exists along the compression. The increase in C^{-1} is rather continuous up to a large value of about 400 $mN.m^{-1}$ (C^{-1}) at its highest value, characteristic of a solid phase.

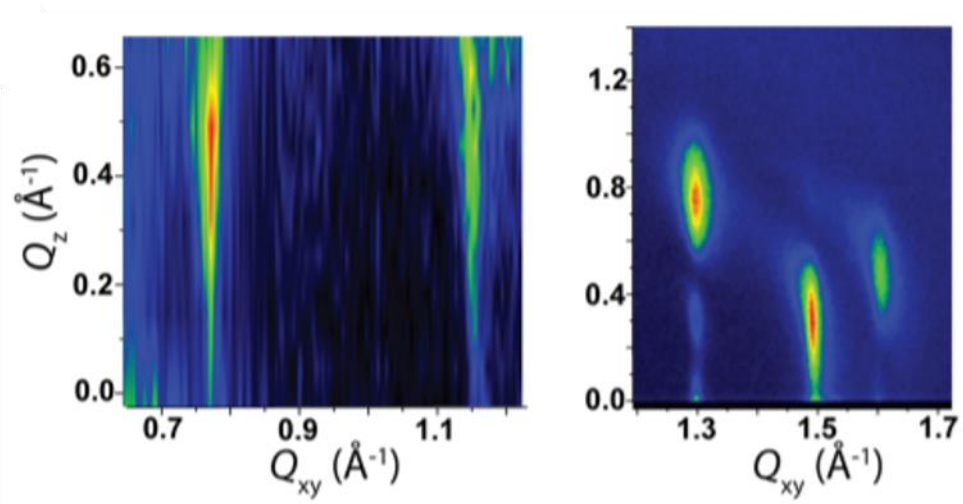

Figure 3. GIXD plots displaying the scattered intensity versus the in-plane and the out-plane components of the scattering vector, Q_{xy} and Q_z, for MGDG-sat (30 mN.m^{-1}) monolayers on 1 mM CsBr. A caption from the paper of Stefaniu et al. 2019.[Stefaniu, 2019] The 2 Bragg peaks in the mid-angle region indicate an ordering of weakly hydrated galactose moieties. The 3 diffraction peaks in the wide-angle region characterize an oblique lattice structure of tilted chains.[Stefaniu, 2019]

DGDG-sat system at the water/air interface presents a slightly different behavior under compression as mentioned previously. The corresponding π-a curve (red curve in Fig. 2-a) is less abrupt. DGDG-sat monolayer on pure water is known to be characterized by liquid expanded (LE) phase at low surface pressure (until 8-10 mN.m^{-1}). Above 10 mN.m^{-1}, DGDG-sat monolayer change to form a liquid condensed (LC) phase.[Hoyo, 2016] The inverse of the surface compressibility versus π appears to be more appropriate to characterize these transitions (see Fig. 2-b, red curve) with first a plateau around 50 mN.m^{-1} (C^{-1}) at a surface pressure around 10 mN.m^{-1} before to re-increase to larger values close to 200 mN.m^{-1} and comparable to values for more classical phospholipid monolayer under compression in its LC phase. The structural works of E. Schneck group have confirmed this state demonstrating using GIXD that, above 10 mN.m^{-1}, the DGDG-sat molecules are organized in a structured monolayer with ordered alkyl chains but disordered headgroups sublayer with a tilt angle of the chains that decreases slightly as a function of surface pressure (from 40° down to 30°).[Stefaniu, 2019]

Interactions of ions such as K^+I^-, Cs^+Br^- or $Ca^{2+}Br^-$ (1 mM) with MGDG and DGDG glycolipids monolayers were investigated by C. Stefaniu et al.[Stefaniu, 2019] It was interesting that among the investigated salts, it was shown that preferential interaction was observed (highlighted using TRXF) whereas the lipids are non-charged. This type of selective interaction is usually expected and observed for non-charged crown ether functions as already mentioned in chapter 2 and often assigned to size-matching between the cavity dimension and the ion diameter. For sugar functions, this was also observed as a function of the orientation of the

OH groups around the carbohydrate ring [Allscher, 2008] in interaction with multivalent ions. Therefore, structural motifs displayed by the headgroups can be responsible for the ion selectivity. Glycolipids with ordered headgroups exhibit preferential interactions with at least one ion species (K^+ at the expense of I^- or Br^- at the expense of Cs^+), whereas glycolipids with non-ordered headgroups such as DGDG-sat does not display any ion selectivity.[Stefaniu, 2019]

The effect of the investigated nano-ions (POMs and COSAN) on the glycolipid monolayers was also assessed in our study by measuring the surface pressure, the total X-ray fluorescence (XRF), the grazing incidence X-ray diffraction (GIXD) and the grazing incidence X-ray off specular (GIXOS) in order to analyze the monolayer in the absence and the presence of nano-ions in aqueous phase. Two Keggin POMs, the phosphotungstic acid HPW ($3H^+$,$PW_{12}O_{40}^{3-}$) and the tungstosilicic acid HSiW ($4H^+$,$SiW_{12}O_{40}^{4-}$), were investigated here in their acid form. In addition, a reference inorganic anion with a similar atomic composition, the ammonium metatungstate AMW ($6(NH_4)^+$,$W_{12}O_{40}^{6-}$) that is not considered as chaotropic due to its high charge density (6 negative charges onto ≈ 1 nm-size anion and its ammonium form, was investigated for comparison. Theoretically, the chaotropicity of the nano-ions investigated here follows the following order: HSiW < HPW < NaCOSAN according to their charge density that decreases from HSiW to NaCOSAN (see Table. 1). The choice of POMs in supplement to COSAN was done because we expected a more complex behavior with COSAN due to its surface activity feature that is not observed for POMs.

Table 1. Charge, molecular volume and charge density of the investigated nano-ions.

Nano-ion	Charge [e^-]	Molecular volume [nm^3]	Charge density [charge/nm^3]
AMW	6	0.46	13
SiW	4	0.48*	8.7
PW	3	0.48*	6.5
COSAN	1	0.45**	2.2

*:[Buchecker, 2018]
**:[Bauduin, 2011]

III. Effects of nano-ions on MGDG-sat monolayer

In Fig. 4 are shown the pressure isotherms for MGDG-sat in the presence of the different nano-ions species in the sub-phase at a fixed concentration of 0.5 mM.

The first observation is a strong effect compare with the system without salt (black curve) with a large shift of the lift-off values A_1 to much larger values between 120 and 180 Å. In addition, the slope variation of the surface pressure under compression is much smooth when nano-ions are in the sub-phase. If we translate this effect in term of compressibility variation (see Fig. 4-b), we obtain a level-off of C^{-1} at less than 50 $mN.m^{-1}$ at high surface pressure, so much below than for the MGDG-sat glycolipids without salt. We can assign this observation to a strong fluidification of the monolayer in presence of salt and with a low nano-ions concentration, below the mM range.

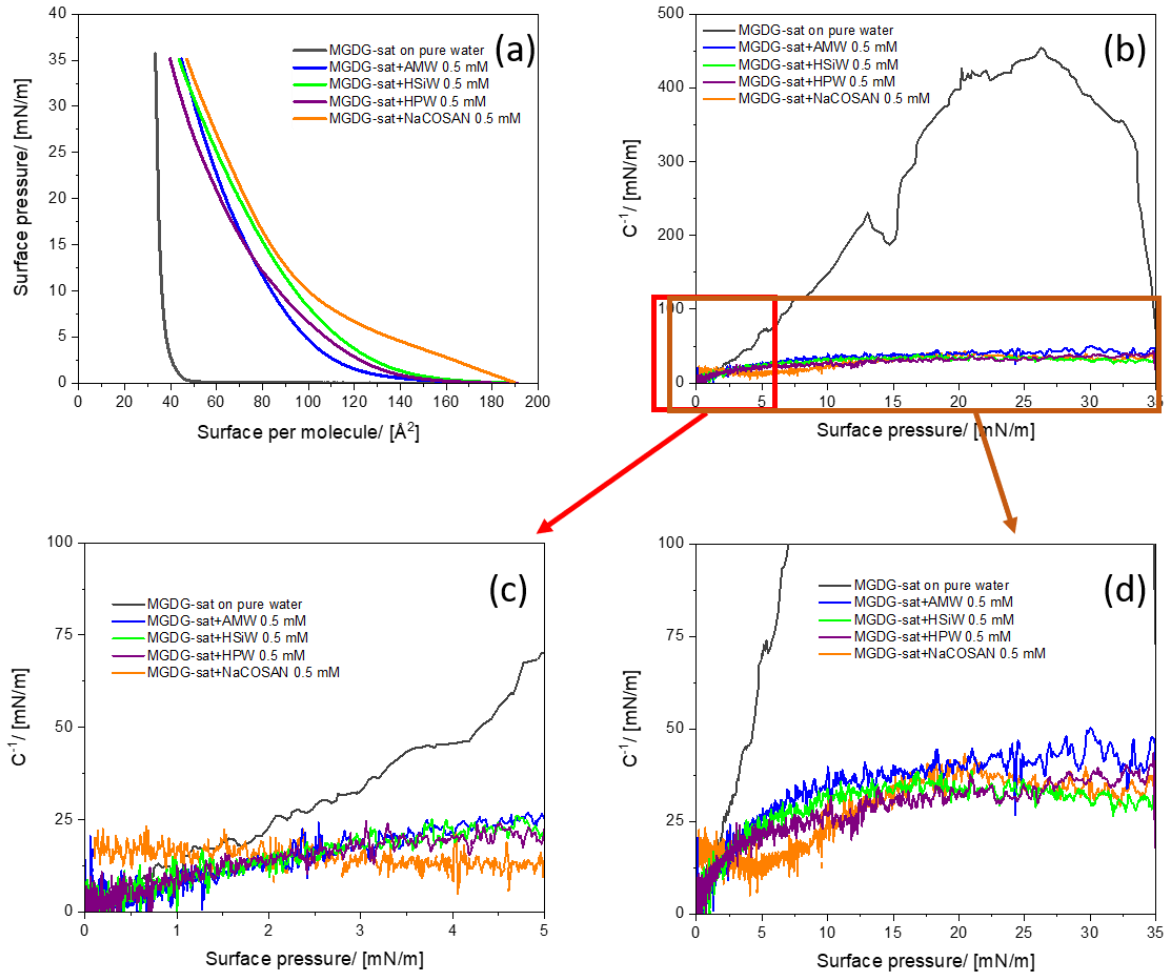

Figure 4. (a) MGDG-sat isotherms for first compression in pure water and in the presence of nano-ions at 0.5 mM. (b) Inverse of the compressibility modulus versus surface pressure for the same systems. (c) and (d) A zoom of the inversed compressibility graphs to show that COSAN does not start from zero $mN.m^{-1}$ like other nano-ions.

Although the limiting area for all the nano-ions is around 90 Å, a value nevertheless two times higher than the system without salt, we can observe some differences between COSAN and the other nano-ions. Indeed, the lift-off area for COSAN is about 180 Å, so about 20% larger than the lift-off area of the other nano-ions. Second, the variation of the inversed compressibility at low surface pressure does not start at zero but with a non-zero value before to decrease slightly and then overlap the other curves at higher surface pressure (see Fig. 4-b and –c).

At this stage, it is difficult to highlight some trends as a function of the superchaotropicity character or more especially to the charge density of the nano-ion.

Varying the nano-ion concentration in the sub-phase we can nevertheless discretized some behaviors (see Fig. 5 to 8) in three categories.

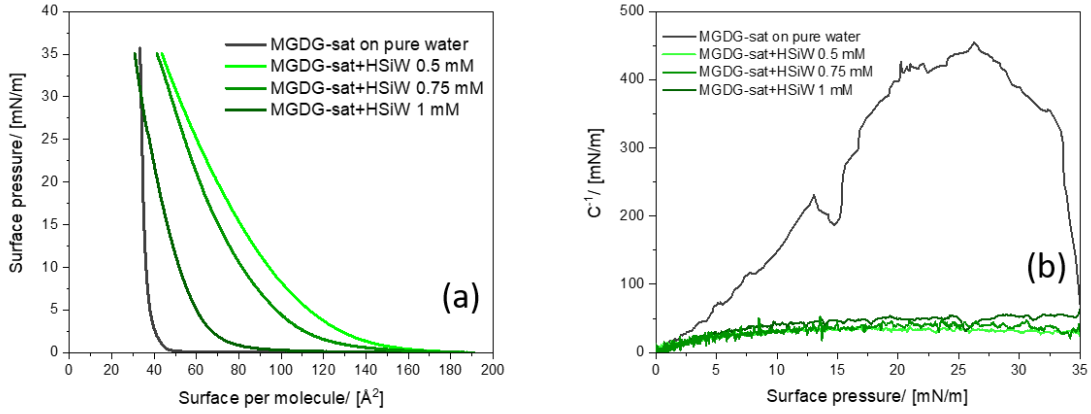

Figure 5. (a) Langmuir isotherms of MGDG-sat in the presence of HSiW (Potsdam). (b) Inverse of the compressibility modulus versus surface pressure for the same systems.

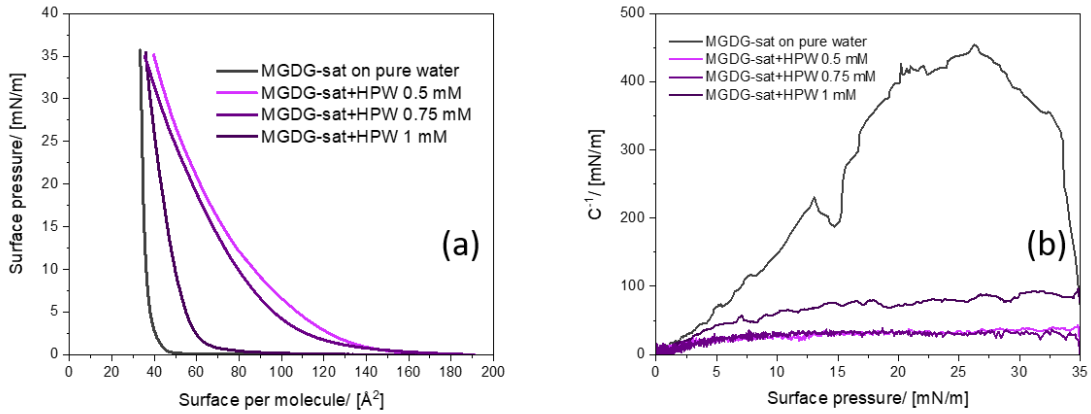

Figure 6. (a) Langmuir isotherms of MGDG-sat in the presence of HPW (Potsdam). (b) Inverse of the compressibility modulus versus surface pressure for the same systems.

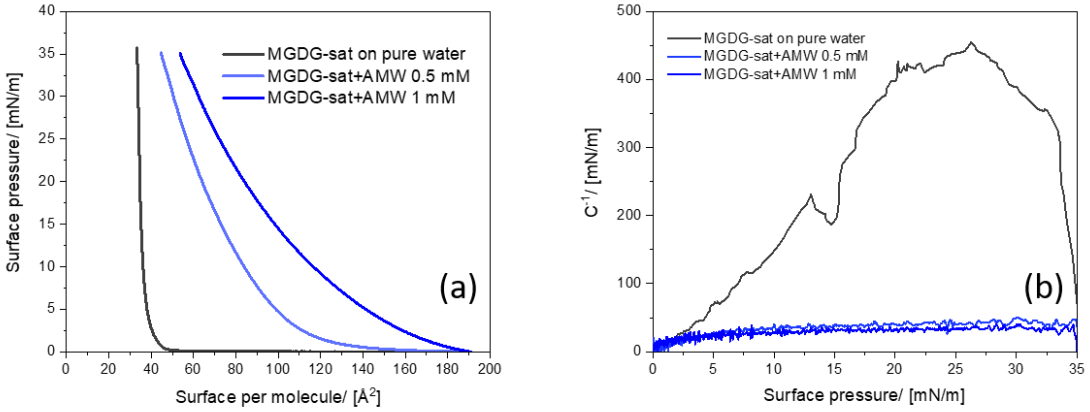

Figure 7. (a) Langmuir isotherms of MGDG-sat in the presence of AMW (Potsdam). (b) Inverse of the compressibility modulus versus surface pressure for the same systems.

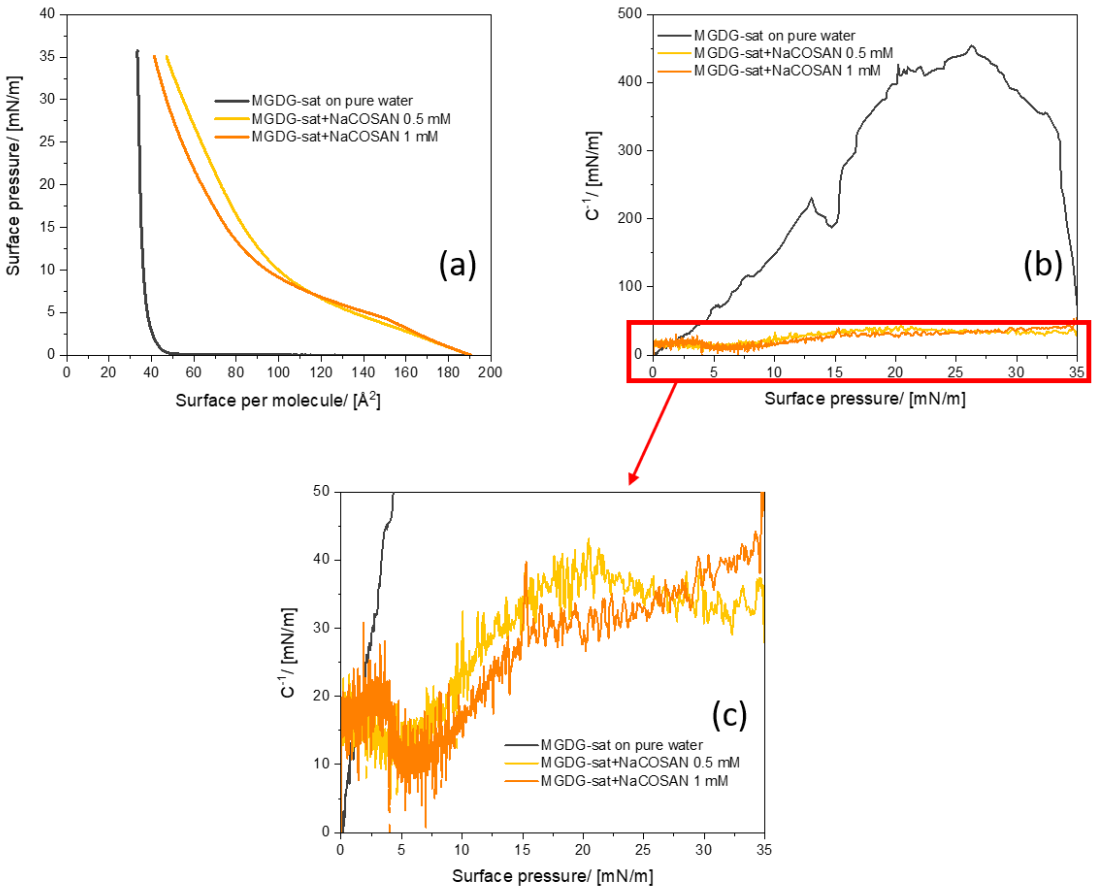

Figure 8. (a) Langmuir isotherms of MGDG-sat in the presence of NaCOSAN (Potsdam). (b) Inverse of the compressibility modulus versus surface pressure for the same systems. (c) A zoom on the y axis of the inversed compressibility graph.

For SiW^{4-} and PW^{3-} nano-ions we observe first an expansion of the monolayer as a function of the concentration (see Fig. 5 and 6) – Some data were recorded at concentration lower than 0.5 mM but were unfortunately not saved - and then above a threshold around 0.5 mM a compression of the monolayer. At the contrary, for AMW, the expansion was observed until 1 mM (Fig. 7). Of course, some acquisitions at higher concentrations are required to confirm this difference in trend. On the other hand, in the presence of $COSAN^{-1}$, the slope variation of surface pressure is not monotonous which can be a sign of a transition between different surface states at around 150 $Å^2$/molecule or at surface pressure between 5 and 7 $mN.m^{-1}$.

The lift-off area and the limiting area are plotted in one graph in figure 9 by trying to correlate both dimensions.

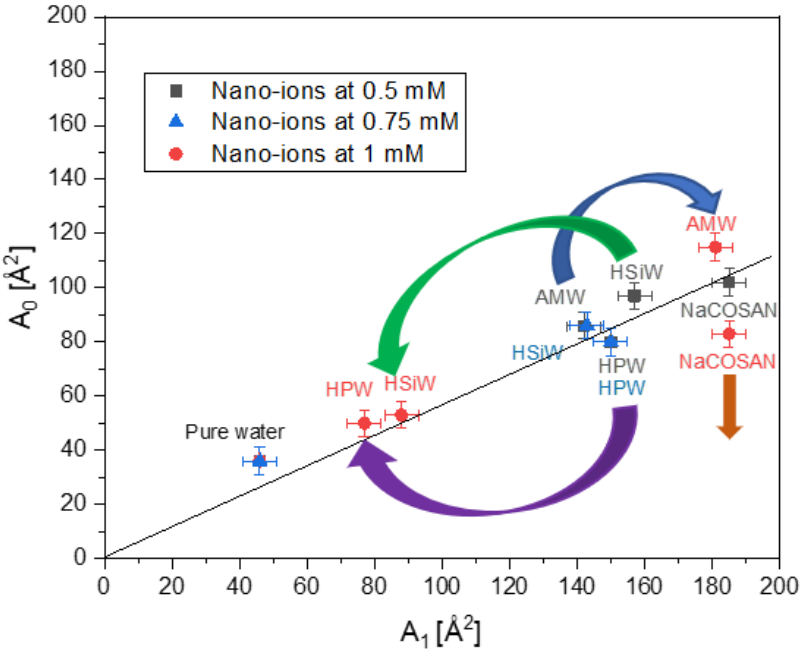

Figure 9. Limiting area (A_0) as a function of the lift-off area (A_1) of the MGDG-sat monolayer in the presence of 0.5, 0.75 and 1 mM nano-ions from experiment in MPI-Potsdam. Arrows represent an increase of the nano-ions concentrations.

The fact that changing the nano-ion concentration we shift the data along the same axis means that the compression or expansion mechanism has the same physical origin. We find back the three different cases noticed previously. For SiW^{4-} and PW^{3-} nano-ions, the shift of the value increasing the concentration goes to the left, towards those without salt, whereas for MW^{6-} it

goes to the right. For COSAN the shift is out of the axis. We should confirm these variations varying more largely the concentration range.

Before to try any interpretation of the data, other structural data were first collected from GIXD and TRXF.

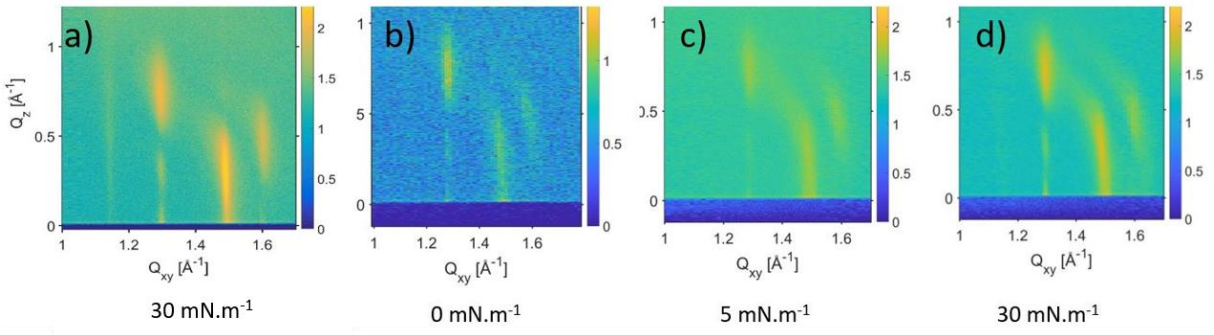

Figure 10. GIXD MGDG-sat monolayer (a) in pure water at 30 mN.m^{-1} and (b)-(d) in the presence of HPW 0.5 mM at different surface pressures - experiment performed in December 2018.

As already written, grazing-incidence x-ray diffraction (GIXD) reveals the structural ordering of the monolayers down to an Angstrom level. The monolayer of MGDG-sat is defined by mainly three diffraction peaks above the horizon (Qz > 0) in the wide-angle region (at high Qxy between 1.2 and 1.6), characterizing an oblique lattice structure of tilted chains.[Stefaniu, 2019] We did not observe any modification of the scattering signature at this q-range with or without HPW in the subphase at 0.5 mM and at different surface pressure (see Fig. 10). Similar results were obtained using HSiW and also varying the concentration from 0 up to 1 mM.

However, some differences were observed for the effect of COSAN (Fig. 11-d) that was not yet quantified in term of chain orientation but qualitatively can assigned to a slightly loss of lateral position correlation.

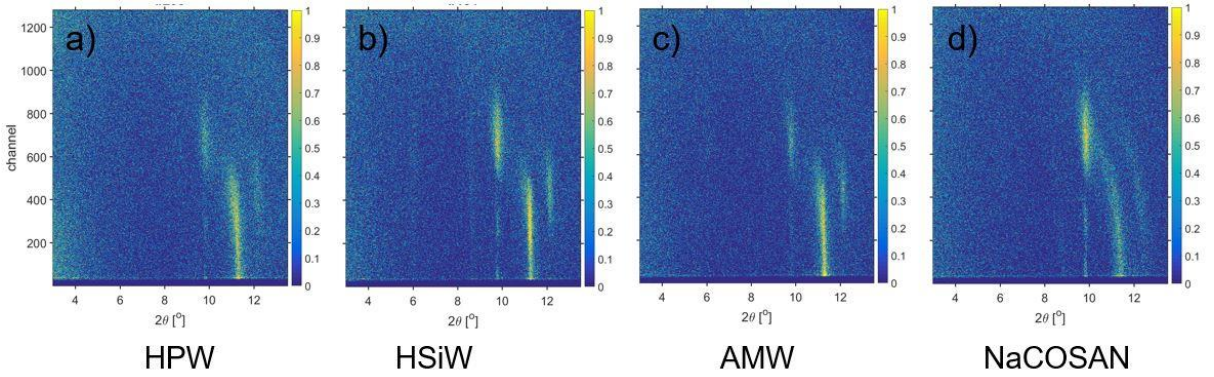

Figure 11. GIXD measurement of MGDG-sat monolayer in the presence of nano-ions at 1 mM at 30 mN.m^{-1} - experiment performed in December 2018.

The variation of peak intensity comes just from either the acquisition time, the scan resolution or the concentration of lipids at the surface.

Total-reflection x-ray fluorescence (TRXF) measurements enable the quantification of the monolayers' preferential interactions with ions in order to get the total overview of the monolayer.

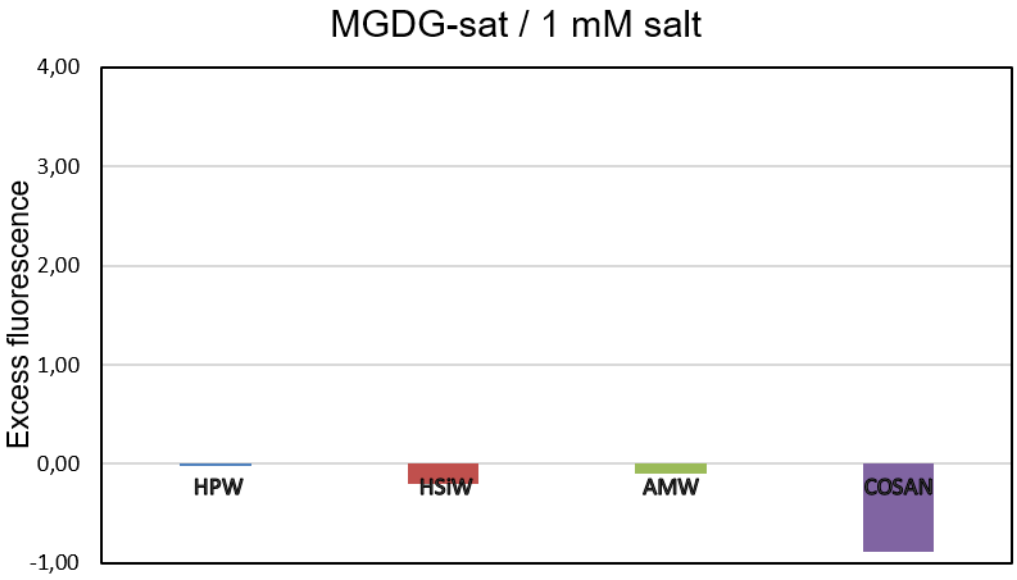

Figure 12. Excess fluorescence for tungstate and cobalt elements at MGDG-sat monolayer at 30 $mN.m^{-1}$ for nano-ions concentration 1 mM. Experiment performed in December 2018. The scale on the y-axis is kept until 4 in order to compare with the excess fluorescence form DGDG-sat monolayer (see Fig. 18).

The excess fluorescence at MGDG-sat monolayer was measured at 30 $mN.m^{-1}$ in the presence of 1 mM nano-ions (see Fig. 12). All the values are negative, the sign of no preferential adsorption of the nano-ions at the glycolipid interface. The values for HPW, HSiW and AMW being rather weak, we cannot really assign these data to a nano-ion depletion as well.

It is important to remind that the fluorescence excess is determined in reference to the bare surface with water containing the salt. For COSAN, because this nano-ion is surface active, the bare surface is already partially covered by the COSAN and once the glycolipids are spread over the surface, both amphiphilic molecules will share the interface. Under compression there is certainly a desorption of the COSAN that can explain the apparent strong lack of COSAN at the surface or in the sub-surface probed by the grazing incident x-rays.

At that stage for MGDG-sat, it seems to have a contradiction between the isotherms that suggest a strong interaction between the nano-ions and the monolayers whereas neither an

excess of nano-ions at the surface nor a change in the glycolipid surface structure seem to be detectable (except for COSAN).

Similar experiments were performed using a slightly more de-organized monolayer formed by DGDG-sat molecules under compression.

IV. Effects of nano-ions on DGDG-sat monolayer

Whereas all the surface pressure isotherms experiments on MGDG-sat were performed at the MPI-Potsdam, the surface pressure isotherms experiments on DGDG-sat were performed at the MPI-Potsdam and at the IEM in Montpellier. Our Langmuir set-up having some mechanical problems.

This point is mentioned because we had some reproducibility issues between both series and we suspect some differences due to the different batch used at Potsdam and DESY synchrotron and those used in Montpellier. We can indeed observe that the DGDG-sat isotherms performed on both sites and plotted in Fig.13-a (solid and doted red curves) are different. In comparison with published data[Hoyo, 2016] we are more confident with those collected at Potsdam and at DESY, nevertheless we have kept plotted also the Montpellier data since we did not have time to perform a third measuring campaign.

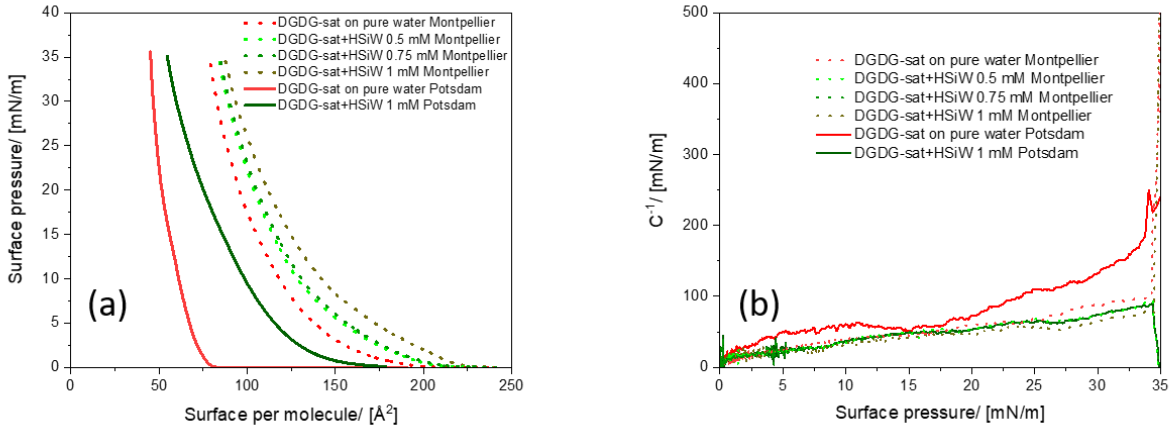

Figure 13. (a) Langmuir isotherms of DGDG-sat in the presence of HSiW. (b) Inverse of the compressibility modulus versus surface pressure for the same systems. Dots are the measurements performed in Montpellier.

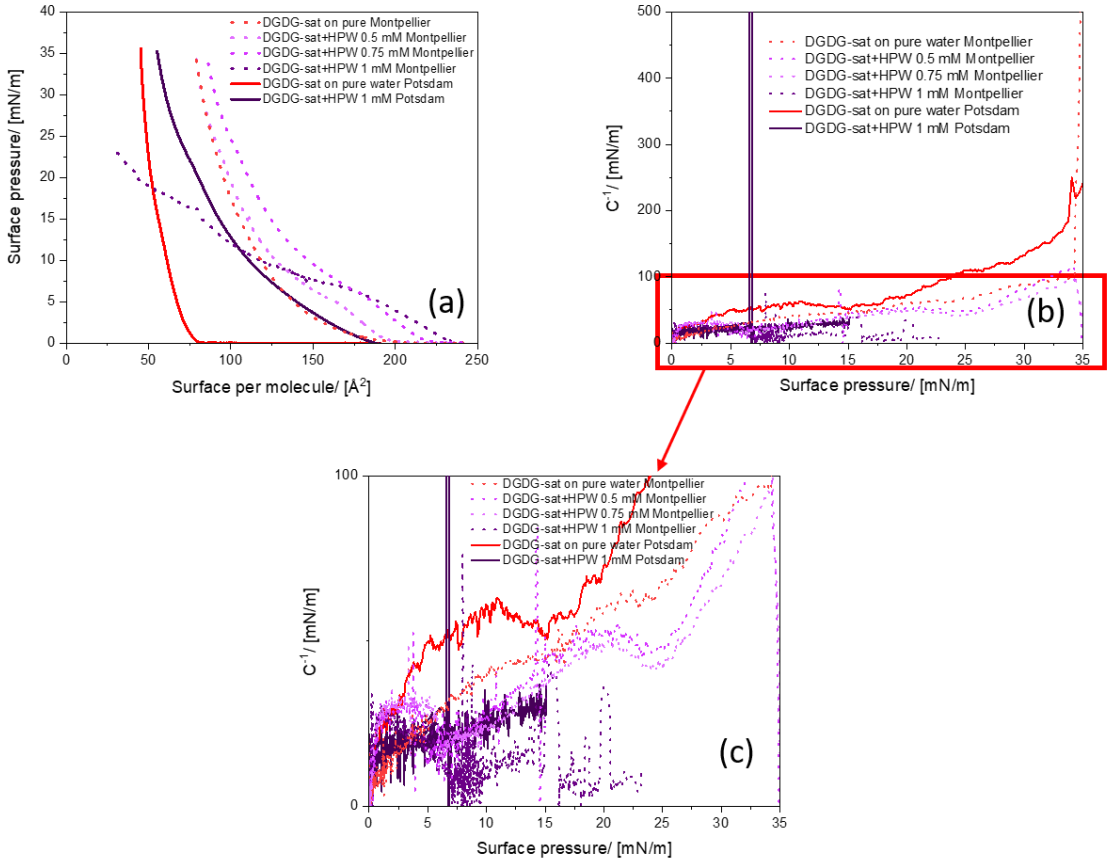

Figure 14. (a) Langmuir isotherms of DGDG-sat in the presence of HPW. (b) Inverse of the compressibility modulus versus surface pressure for the same systems. Dots are the measurements performed in Montpellier. (c) A zoom on the y axis of the inversed compressibility graph.

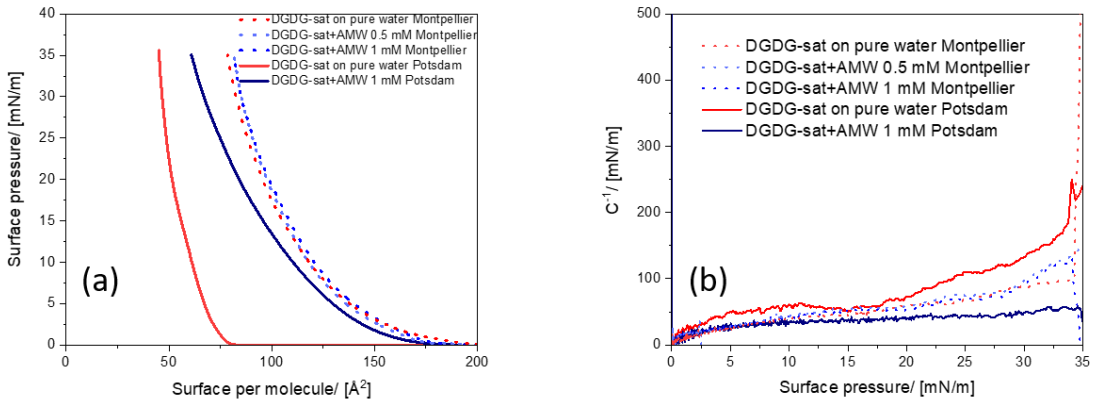

Figure 15. (a) Langmuir isotherms of DGDG-sat in the presence of AMW. (b) Inverse of the compressibility modulus versus surface pressure for the same systems. Dots are the measurements performed in Montpellier.

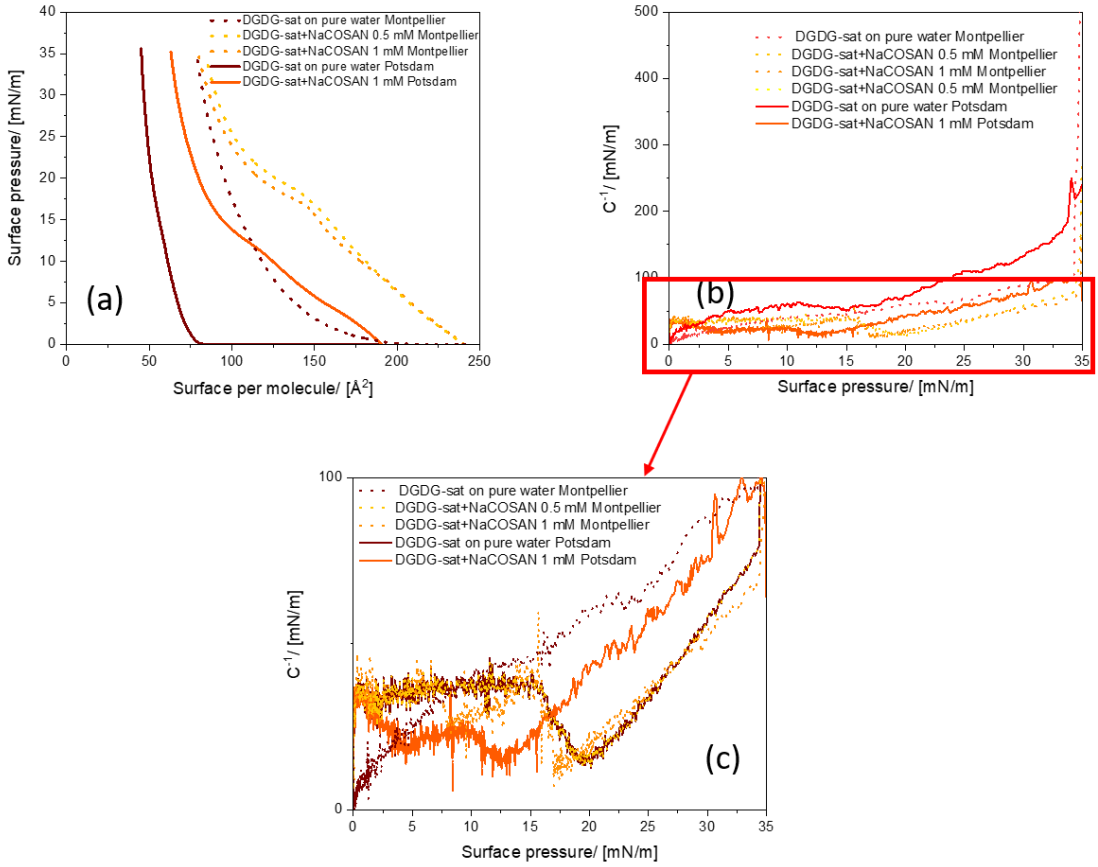

Figure 16. (a) Langmuir isotherms of DGDG-sat in the presence of NaCOSAN. (b) Inverse of the compressibility modulus versus surface pressure for the same systems. Dots are the measurements performed in Montpellier. (c) A zoom on the y axis of the inversed compressibility graph.

DGDG-sat monolayer on pure water is characterized by liquid expanded (LE) phase at low surface pressure (until 8 $mN.m^{-1}$) and a formation of a liquid condensed (LC) phase at higher surface pressure.[Hoyo, 2016] This transition is much more visible when the inversed compressibility is plotted versus the surface pressure. However, adding nano-ions in the subphase, this transition is much less visible like if the system under compression shift continuously toward the formation of the condensed phase with a C^{-1} closer to 100. The data from Montpellier experiments are more chaotic and it is more difficult to find a coherence.

A plot of the two characteristic surfaces, A_0 and A_1, on the same graph like for the MGDG-sat is shown in Fig. 17. The first remark is that the values are still aligned on the same axis with again the COSAN shift is out of the axis.

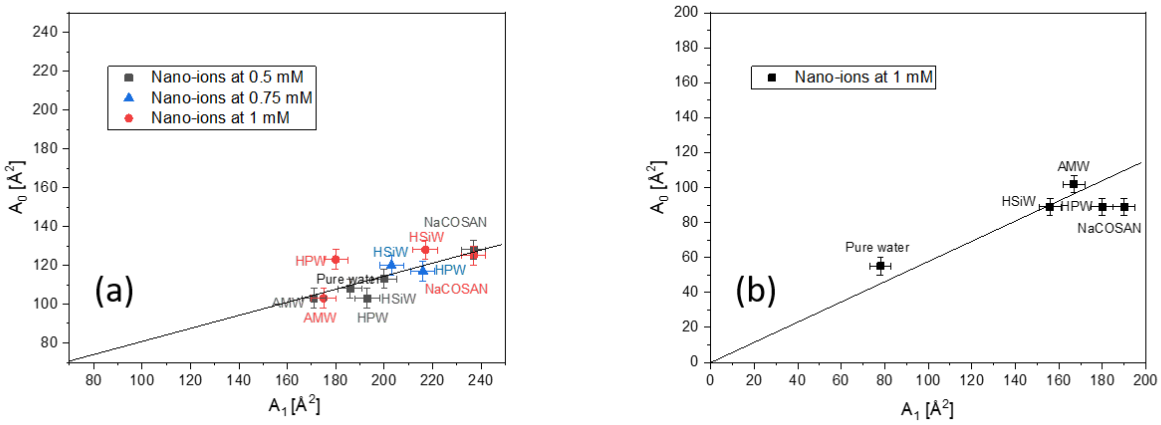

Figure 17. Limiting area (A0) as a function of the lift-off area (A1) of the DGDG-sat monolayer in the presence nano-ions from experiment in (a) Montpellier and (b) MPI-Potsdam.

However, whereas for the MGDG-sat the data at 1 mM for SiW^{4-} and PW^{3-} were much closer to those of pure water (see Fig. 5 and 6), the data for the same concentration for DGDG-sat are located at much higher surface values, similar to those corresponding to 0.5 mM for MGDG-sat. We will come back on this point once we will gather all the information at the end of this chapter.

Data from TRXF at the DGDG-sat monolayer obtained at 30 $mN.m^{-1}$ and with 1 mM of nano-ions in the sub-phase are summarized in Fig.18.

We can clearly notice an excess of the HPW concentration at the interface, a weak tendency for the adsorption for HSiW and like in the case of the MGDG-sat, a negligible adsorption for AMW and COSAN is observed. Therefore, the loss of the organization at the polar head level of DGDG-sat seems to have an influence on the adsorption of the most superchaotropic nano-ions. Again, the reference of the COSAN at the bare interface being not the right one due to its surfactant character, the comparison between COSAN and the other nano-ions cannot be applied on this graph.

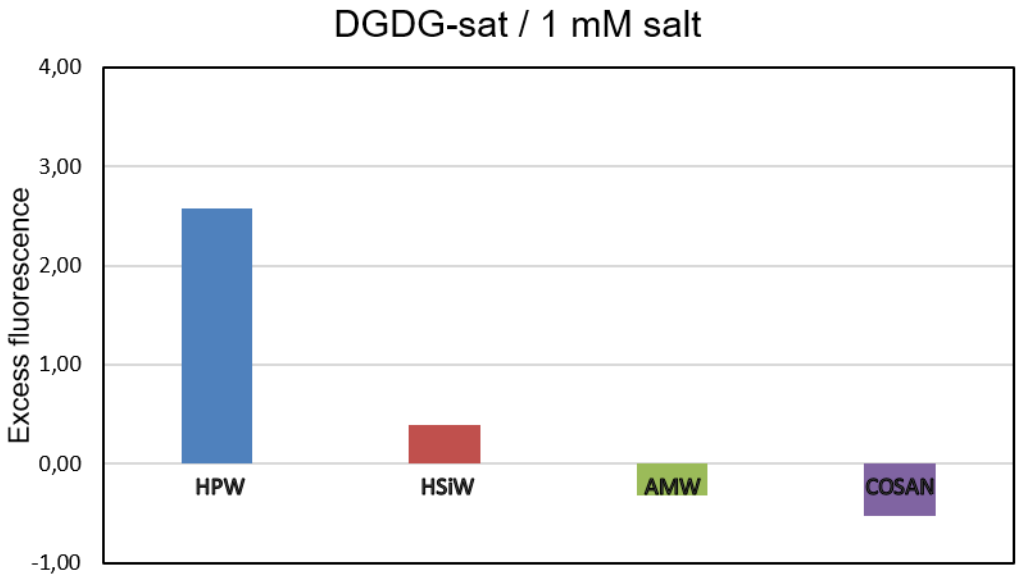

Figure 18. Excess fluorescence for tungstate element at DGDG-sat monolayer at 30 mN.m^{-1} for nano-ions concentration 1 mM. Old results obtained from experiment performed in December 2018.

Another set of TRXF experiments were carried out during a different synchrotron run. Even if the absolute values of fluorescence are different, the trend was confirmed. Indeed, as observed in Fig. 19 and by recording the fluorescence and plotting the excess (or default) at a function of the DGDG-sat surface area for each tungstate nano-ion (at 0.5 mM in the sub-phase) we observed a more pronounced signal or HPW, then for HSiW and a signal quasi-null for AMW.

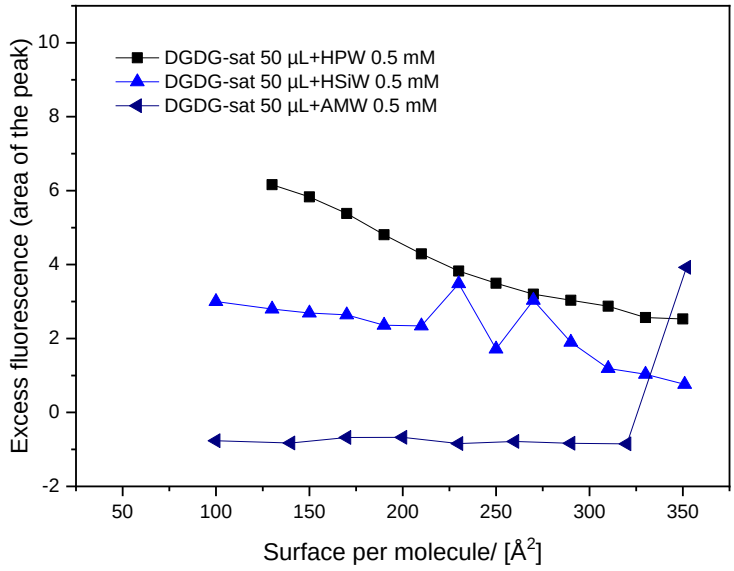

Figure 19. Excess fluorescence per unit area from area of the peak around 8.3 Kev for tungstate element at DGDG-sat monolayer.

The data from GIXD for DGDG monolayer, collected at DESY, are now shown in Fig. 20.

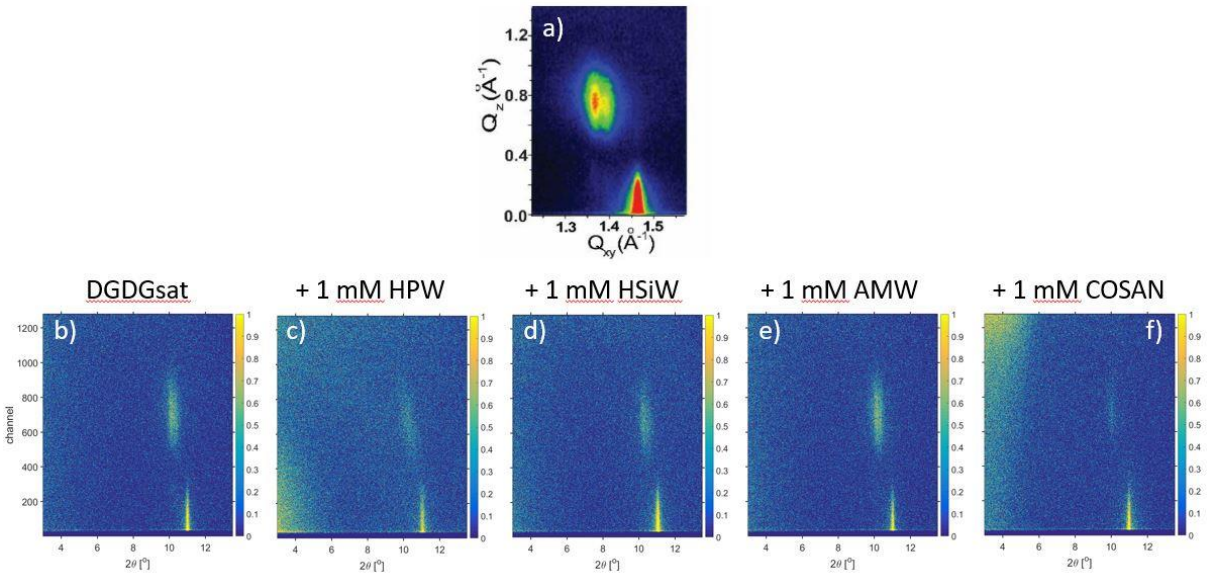

Figure 20. GIXD from DGDG-sat monolayer, nano-ions concentration 1 mM. (a) High resolution scan for DGDG-sat under compression at 30 mN.m^{-1} and from the paper of Stefaniu et al. 2019.[Stefaniu, 2019] (b) - (f) Fast scans experiments in the same conditions, 1 mM of salt and at a surface pressure about 30 mN.m^{-1}. The 3 diffraction peaks in the wide-angle region characterize the alkyl chain lattice. The absence of the diffraction peaks in the mid-angle region indicates the absence of headgroup order.[Stefaniu, 2019] Experiments carried out in December 2018 and April 2019.

As a difference from the previous spectra collected for the MGDG-sat, we observed an apparent impact that depends clearly on the charge density of the nano-ions. This impact is not really onto the chain ordering with perhaps a slight effect on the orientation distribution of the scattering peak at $Q_z \approx 0.8$ Å^{-1} and $Q_{xy} \approx 1.37$ Å^{-1} and related to the chain tilt. However, the most apparent difference is visible at much weaker Q-values for HPW with a scattering upturn at Q reaching 0 and for COSAN with an excess of scattering also at low Q but for large Q_z above 1 Å^{-1}.

For HPW system, we could link these observations to the strong increase of the surface compressibility observed in presence of the nano-ion that can be correlated to larger fluctuation of surface undulation due to surface fluidification. However, the surface compressibility decreases also for the MGDG system and no excess of scattering at low q-values was observed. Therefore, we can consider that more inhomogeneities such as glycolipidic islands exist over the surface pressure are at the origin of the scattering excess. To go further in this analysis more experiments are nevertheless required. In the case of COSAN, the excess of scattering appears at low Q_{xy} and $q_z \neq 0$ but at relatively high Q_z that seems to correspond to the inverse of the monolayer thickness could be related to the interaction between COSAN

nano-ions at the surface. But again, too few experiments have been performed to get a reasonable conclusion.

We succeed to collect also some data for the unsaturated MGDG (MGDG-unsat), a glycolipid which was not listed at the beginning of this chapter but studied by the group of E. Schneck. The unsaturation on the chains of MGDG-unsat makes that, under compression no structural organisation was detected. The position order does not exist anymore neither at the head nor at chains levels.

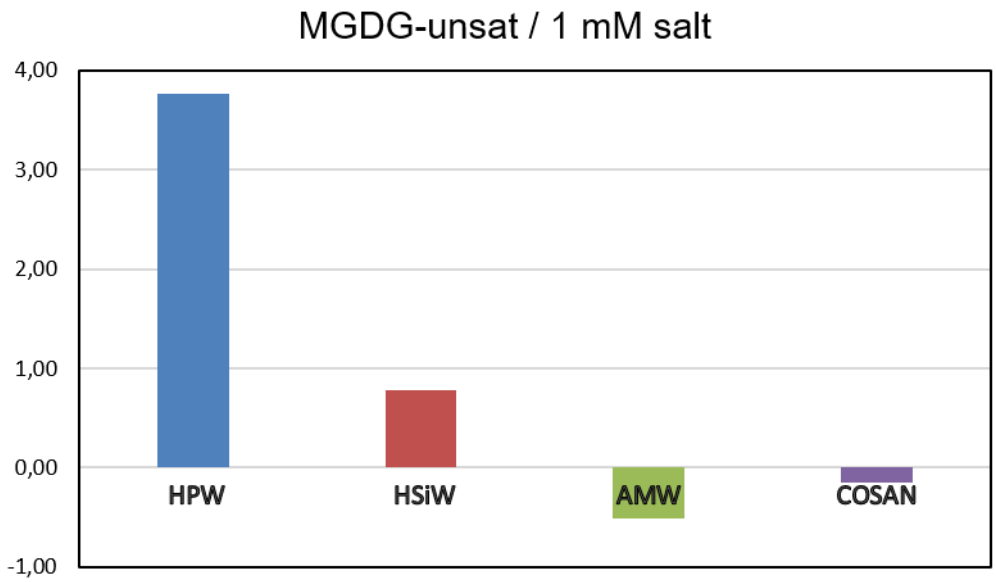

Figure 21. Excess fluorescence for tungstate element at MGDG-unsat monolayer at 30 mN.m^{-1} for nano-ions concentration 1 mM. Old results obtained from experiment performed in December 2018.

Moreover, as observed in Fig. 21 for the TRXF results, the trend that was observed for DGDG-sat is reinforced with MGDG-unsat. This means that PW^{3-} appears to be much more condensed at the interface that SiW^{4-} that now present a significant adsorption unlike for MW^{6-}. COSAN is still also peculiar due to its amphiphilic nature that mismatches the calculation of concentration excess.

V. Grazing incidence X-ray off-specular analysis of the MGDG-sat and DGDG-sat monolayers

The structure of MGDG-sat and DGDG-sat monolayers were analyzed by Grazing incidence X-ray off-specular (GIXOS) technique that can inform about the averaged density along the normal axis at the air/water interface. Results of the GIXOS intensity as a function of the wave vector (q) are presented in Fig. 22 and 23. In addition, by fitting the GIXOS data using an IDL

software provided by E. Schneck (Annex VII-1 and Fig. VII-2 and Fig. VII-3), we obtain the electron density profile at the interface, with and without nano-ions.

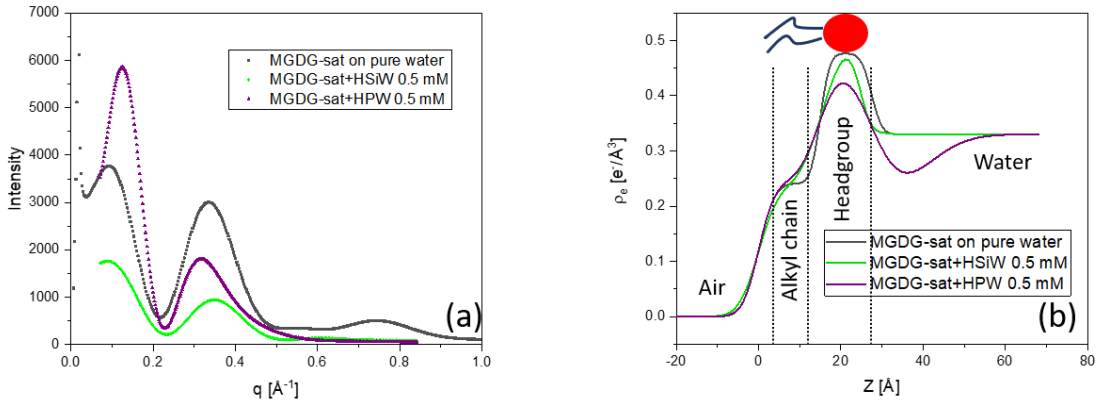

Figure 22. (a) GIXOS spectra of MGDG-sat monolayer in pure water and in the presence of 0.5 mM HSiW and HPW at 30 mN.m^{-1}. (b) Electron density profile along the Z-axis, obtained by fitting the GIXOS spectra.

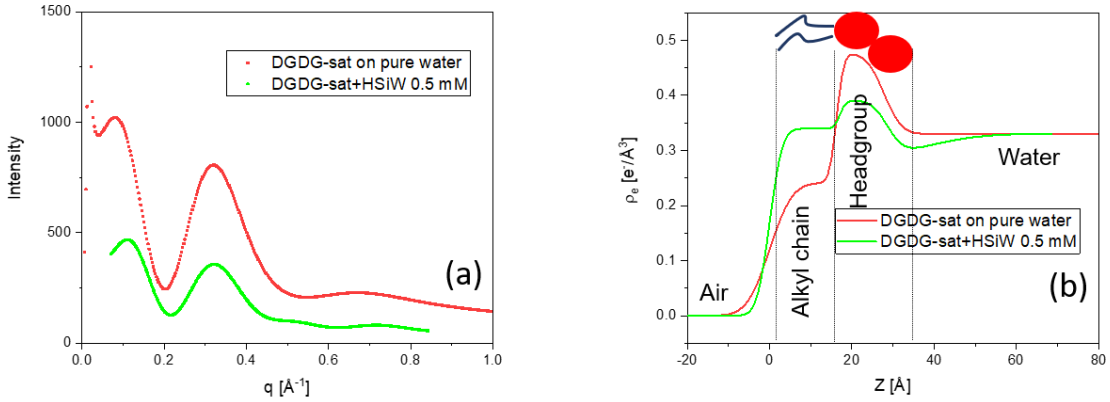

Figure 53. (a) GIXOS spectra of DGDG-sat monolayer in pure water and in the presence of 0.5 mM HSiW at 30 mN.m^{-1}. (b) Electron density profile along the Z axis, obtained by fitting the GIXOS spectra.

What was interesting in the electron density profile graph is the smoothing of the electron density near the interface compare to the bare profile without nano-ions in the subphase. Indeed, for glycolipids on pure water, the electron density near to the interface varies between 0 for air and about 0.33 e$^-$/ Å^3 for water through two steps, a layer characterizing the aliphatic chains with a typical electron density of oil in contact with air and the polar heads oriented towards water with an electron density between 0.45 and 0.5 e$^-$/ Å^3. In the presence of nano-ions which interact with glycolipids in gas-phase via hydrophobic interaction as supposed for COSAN with C8G1 at low concentration, the different steps in electron density becomes of the same order like if some of the glycolipids are flip-flop mixing aliphatic tails and polar heads along the z-axis due to the presence of adsorbed nano-ions.

Table 2. Electron density of all investigated nano-ions.

Nano-ion	Electron density [e^-/ Å^3]	Molecular volume [nm^3]
MW^{6-}	2.64	0.46
SiW^{4-}	2.55	0.48*
PW^{3-}	2.55	0.48*
$COSAN^-$	0.36	0.45**

*:[Buchecker, 2018]; **:[Bauduin, 2011]

VI. Discussion

Finally, the question is, can we draw a coherent scenario with this entire data collection on the interaction of the different nano-ions with various states of compression of the glycolipids?

First for the two main types of glycolipids investigated in this work and for which we did not have enough structural references of the monolayer under compression, we observed a first order transitions between a gas phase at very low surface pressure to either a condensed phase that appears quasi-solid for MGDG-sat or to a first liquid condensed (LC) and then a solid phase for DGDG-sat. In fact, this transition was a first order transition which means that practically over all the compression, both states coexist. The pure system being non-charged, the surface pressure increases under compression only at surface per molecule below 100 Å^2. The presence of nano-ions has only a weak effect on the glycolipid molecular packing (GIXD results). Indeed, we did not observe a strong modification of the Bragg peak positions for both MGDG-sat and DGDG-sat independently of the nano-ions type and concentration in the investigated concentration range between 0.1 and 1 mM in the subphase.

However, we systematically observed a strong effect on the isotherm surface pressure with a lift-off at much higher surface area (A_1). Therefore, we can reasonably suppose that the nano-ions interact with the single molecules at the surface. Indeed, when the glycolipids interact too strongly (the case of MGDG-sat) with each other through H-bonds, the hydration of the polar heads is minimized and the interaction of the nano-ions with the glucoside surface is then unfavourable.

The glycolipids in monomeric form are charged upon their interactions with the nano-ions (POM and COSAN) as was underlined in the chapter 2 for C8G1 below its CMC in the presence of COSAN. Lateral electrostatic repulsion can be responsible of the surface pressure increase. This induces a shift of the equilibrium between gas (or LE) phase with LC or solid phase and delays the formation of the condensed phases by forming a larger number of 2D-ilands. This remains some assumptions because tentative BAM pictures were performed but they were not really conclusive.

When the entropy of the system is increased from MGDG-sat to DGDG-sat and MGDG-unsat i.e. from solid to liquid, nano-ions interact with both gas and LE phases, especially the most superchaotropic ions, PW and COSAN.

These scenarios can be summarized with schematic pictures as followed:

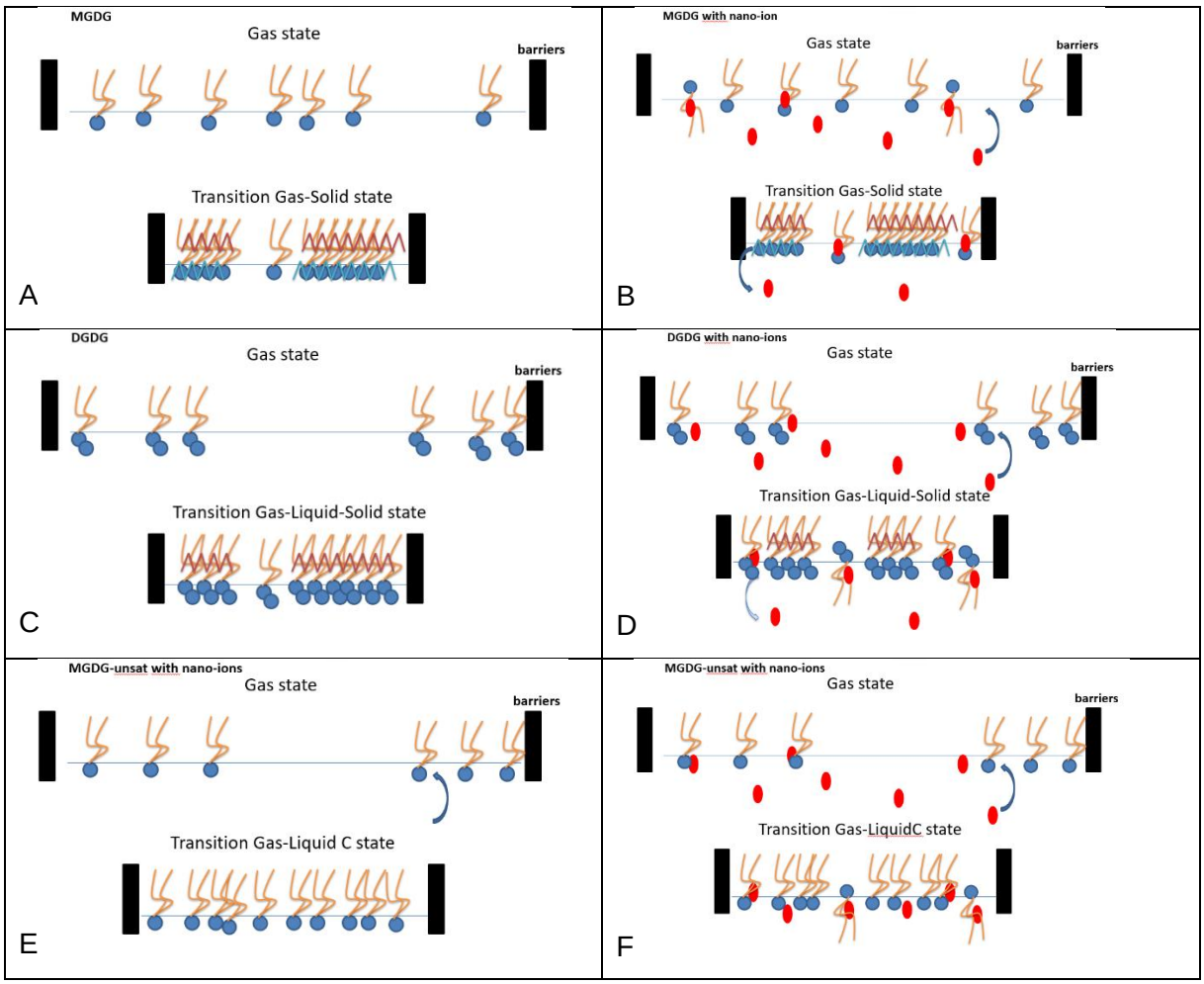

Figure 14. Glycolipids under compression in a Langmuir trough. A and B for MGDG-sat, C and D for DGDG-sat and E and F for MGDG-unsat. Right with nano-ion in the subphase, Left without. The difference between the different nano-ions is related to the strength of their interaction with the glycolipid's interface. Zig-zag sign qualifies the crystalline ordering either at the aliphatic chain level or at the polar-head level. Concerning the MGDG-unsat case, the representation is a prediction since too few experiments exist for this system.

The difference between COSAN and POM is not drawn on this sketch. At the initial state without compression, COSAN is surface active and should be distributed between the glycolipids at the surface

As already explained in our chapter 2 and also within previous publications in our group [Girard, 2019] the mechanism of NI adsorption is characterized by a constant that defines the strength of the interaction and therefore the surface of the lift-off. Once this lift-off is achieved, the addition of NIs in the subphase will screen the electrostatic interactions (lateral repulsion)

induced by the adsorption. This is exactly what we observed for MGDG-sat system between 0.5 and 1 mM of SiW or PW, when the charge screening effect shifts back the surface pressure isotherms toward the curve of the system on pure water. We should observe a similar effect for DGDG-sat and also with the MGDG-unsat systems at higher nano-ion concentrations.

The only point, which appears hard to explain, refers to AMW, the supposed “kosmotropic” nano-ion (cloud point measurements in our group of C8E4 demonstrated the kosmotropic nature of AMW) that is expected to not adsorb due to its high charge density. Indeed, TRXF data show a weak excess of its concentration at the interface whereas a strong effect on the surface pressure is observed, an effect that we have attributed to the nano-ion/glycolipids interaction.

Therefore, complementary experiments are required to clear up this inconsistency. We have focused numerous of our investigation at large surface pressure whereas we should work in a future investigation at low pressure within the gas or LE phase, below 5 $mN.m^{-1}$ and in a larger range of concentration of the nano-ions. Moreover, extension of these investigations at higher surface pressure should be applied on the MGDG-unsat where no solid-phase islands are formed.

VII. Annex of chapter 3

Remark: for the graphs of the inverse of the compressibility modulus: The compressibility curves were smoothed using Adjacent-Averaging method in Origin with a “points of window” about 10.

VII-1. GIXD, TRXF and GIXOS analysis

GIXD

Synchrotron GIXD is the main technique to study the arrangement of amphiphiles at the air/water interface on molecular level. We used GIXD at the DESY synchrotron in Hamburg (see Fig. 1). A monochromatic X-ray beam with $\lambda = 1.304$ Å hit the water with an angle under the critical angle for the total reflection to produce an evanescent wave with a penetration depth about 8 nm. The illuminated are is in the order of 100 mm^2. Q_Z is the vertical component of the wave vector Q. Q_X and Q_y are the in-plane components of Q with $Q_{xy} = \sqrt{(Q_x^2 + Q_y^2)}$.

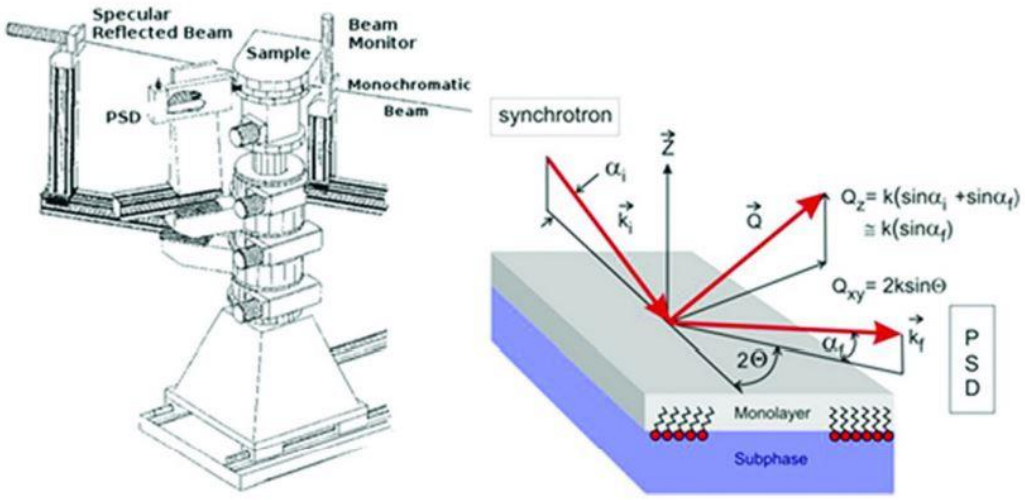

Figure VII-1. Representation of the configuration of X-ray diffraction at small angles, GIXD. PSD is a position sensitive detector for the diffracted beam.

TXRF

The total reflection X-ray fluorescence informs about the density profiles of an element perpendicular to the interface at sub-nm resolution.

X-ray fluorescence performed at the MGDG-sat and DGDG-sat monolayers at an angle of detection of 90° allows the detection of nano-ions adsorbed at the interface. For HPW, HSiW and AMW, we considered the tungstate peak around 8.3 Kev for XRF results. For NaCOSAN, we considered the cobalt peak around 6.84 keV for XRF results. Channel numbers are converted into energy (Kev) according to this calibration: channel number 334 corresponds to energy of 2.96 Kev, and channel number 730 corresponds to energy of 6.49 Kev (from Matlab

program). By plotting these values, we obtain a line and we can determine the slope and the intercept:

E= (slope × channel number) - intercept

Excess fluorescence is normalized to the fluorescence of POM at bare water interface via:

$$Excess\ fluorescence = \frac{I-I_0}{I_0} \quad Eq.VII-1$$

With I_0 is the fluorescence intensity of the nano-ion solution at the bare water interface.

In the case of area of the peak, it is obtained by fitting the peak at 8.3 Kev by Gaussian fit in sigma plot (see equation below) and then calculating the integral of the peak. The excess fluorescence is normalized by the area of the peak for the bare water interface.

$$y = y_0 + ae\left[-0.5\left(\frac{x-x_0}{b}\right)^2\right] \quad Eq.VII-2: Gussian\ fits$$

GIXOS

The intensity of the scattered beam is detected by a position sensitive detector (PSA). The measured diffuse intensity is given as:

$$I(q_z) \propto |T(k_{in})|^2 |T(k_{out})|^2 \frac{R(q_z)}{R_F(q_z)} \quad Eq.VII-3$$

$I(q_z)$ is the intensity measured, $R(q_z)$ is the corresponding specular reflectivity, $R_F(q_z)$ is the specular reflectivity from a flat surface (ideal), $T(k_{in})$ and $T(k_{out})$ are the characteristic Vineyard functions for the grazing incidence configuration.[Oliveira, 2010] The data are fitted using an IDL software provided by E. Schneck based on the master formula for specular reflectivity (see parameters in Fig. VII-2 and VII-3):[Oliveira, 2010]

$$R(q_z) = R_F(q_z)\left|\frac{1}{\rho}\int \frac{d\rho(z)}{dz} exp(iq_z z)dz\right|^2 \quad Eq.VII-4$$

For MGDG-sat in pure water (December 2018) sample test s70

Fixed parameters:
- Upper limit of q_z range: 261
- Scaling: 2200
- Background: 100
- E-density bulk & slab 3: 0.33
- Roughness slab 2/slab 3 & slab/bulk: 2
- Thickness slab 3: 10

Fitted parameters:
- E-density slab 1: 0.241084
- E-density slab 2: 0.476527
- Roughness air/slab 1: 3.06651
- Roughness slab 1/slab 2: 1.83739
- Thickness slab 1: 14.9609
- Thickness slab 2: 12.4773

For MGDG-sat +HPW 0.5 mM at 30 mN/m (April 2019)

Fixed parameters:
- Upper limit of q_z range: 331
- Scaling: 3400
- Background: 50
- E-density slab 1: 0.241084
- E-density slab 2:0.476527
- E-density bulk: 0.33
- Thickness slab 1: 14.9609
- Thickness slab 2: 12.4773

Fitted parameters:
- E-density slab 3: 0.188647
- Roughness air/slab 1: 3.09089
- Roughness slab 1/slab 2: 4.25592
- Roughness slab 2/slab 3: 5.78447
- Roughness slab/bulk: 8.45774
- Thickness slab 3: 11.4489

Figure VII-2. Fixed and fitted parameters for GIXOS data on the MGDG-sat in pure water and in the presence of 0.5 mM HPW at 30 $mM.m^{-1}$.

For DGDG-sat in pure water (December 2018) Sample 10

Fixed parameters:
- Upper limit of q_z range: 261
- Scaling: 630
- Background: 100
- E-density slab 1: 0.241084
- E-density slab 2: 0.476527
- E-density bulk & slab 3: 0.33

Fitted parameters:
- Roughness air/slab 1: 4.33004
- Roughness slab 1/slab 2: 1.39403
- Roughness slab 2/slab 3: 3.37353
- Roughness slab/bulk: 10000
- Thickness slab 1: 16.2696
- Thickness slab 2: 11.5226
- Thickness slab 3: 27.1157

For DGDG-sat +HSiW 0.5 mM (April 2019) Sample s621

Fixed parameters:
- Upper limit of q_z range: 338
- Scaling: 280
- Background: 50
- E-density bulk: 0.33

Fitted parameters:
- E-density slab 1: 0.339589
- E-density slab 2: 0.389056
- E-density slab 2: 0.289650
- Roughness air/slab 1: 2.43593
- Roughness slab 1/slab 2: 1.10733
- Roughness slab 2/slab 3: 3.05146
- Roughness slab/bulk: 9.83965
- Thickness slab 1: 17.0623
- Thickness slab 2: 11.5323
- Thickness slab 3: 10.7235

Figure VII-3. Fixed and fitted parameters for GIXOS data on the DGDG-sat in pure water and in the presence of 0.5 mM HSiW at 30 $mM.m^{-1}$.

The Langmuir trough used has a total surface about 457.6 cm^2. The concentration of MGDG-sat and DGDG-sat was 2 mg/ml prepared in chloroform. The trough was filled with 300 ml of the solvent (water) or the aqueous solution containing nano-ions at 20°C. For stability reason, the pH of HPW and AMW solutions should be below 3 and 4 respectively. The glycolipids were deposited at the air/water interface using Hamilton needle of 50 µL. the glycolipids were spread such the pressure before compression is not above 0 $mN.m^{-1}$. The measurement chamber (see Fig. VI-1) was then sealed and flushed with Helium until pO_2 dropped below 0.5. The beam shutter was then opened. The barrier is moved to compress the glycolipids at the air/water interface to a steady position where the surface pressure is about 30 $mN.m^{-1}$. Then, GIXD and TRXF measurements were recorded at 30 $mN.m^{-1}$.

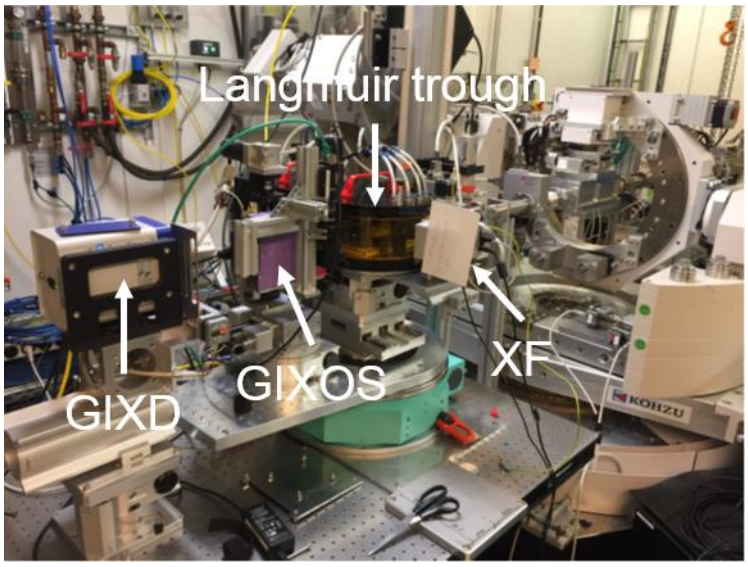

Figure VII-4. Experimental setup used at the DESY-synchrotron in Hamburg.

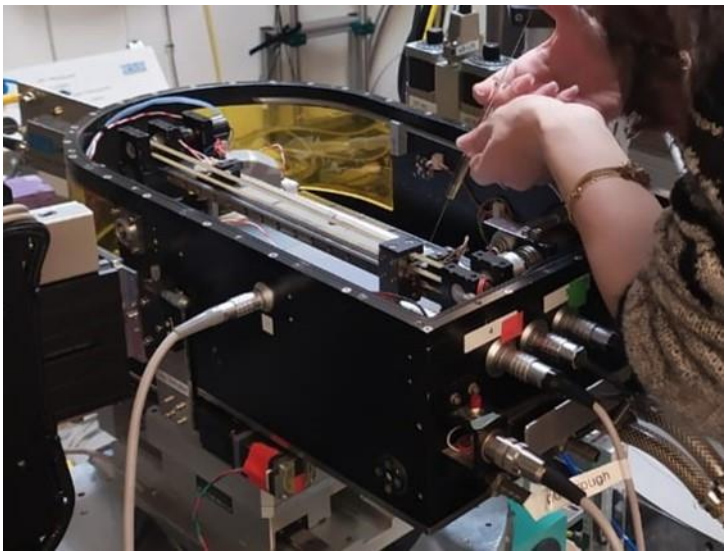

Figure VII-5. While depositing the glycolipid at the air/water interface in the Langmuir trough used at DESY-synchrotron in Hamburg.

In a second run time, also at DESY-synchrotron in Hamburg, the GIXD and TRXF measurements were performed at different surface pressure.

Finally, in a third run time, almost all the GIXD and TRXF measurements were recorded at different low surface pressures.

VII-2. Langmuir isotherms at the Max Planck Institute in Potsdam

The Langmuir trough that we used has a total surface about 41 × 7.5 = 307.5 cm^2. 41 cm corresponds to the trough length between the barrier that we will use to compress and the other limit of the trough (see Fig. VI-3). The concentration of MGDG-sat and DGDG-sat was 2 mg/ml prepared in chloroform. The trough was filled with 200 ml of the solvent (water) or the aqueous solution containing nano-ions at 20°C. The glycolipids were deposited at the air/water interface using Hamilton needle of 50 µL. 20 and 10 µL of MGDG-sat and DGDG-sat solutions (2 mg/ml prepared in chloroform) were deposited at the interface respectively. To form a glycolipid monolayer, we used one barrier to compress with a velocity of 5 $Å^2$/Molecule/min. The measurements were made in three successive steps: compression until 35 $mN.m^{-1}$, decompression to around 0 $mN.m^{-1}$ and recompression again until at least 35 $mN.m^{-1}$.

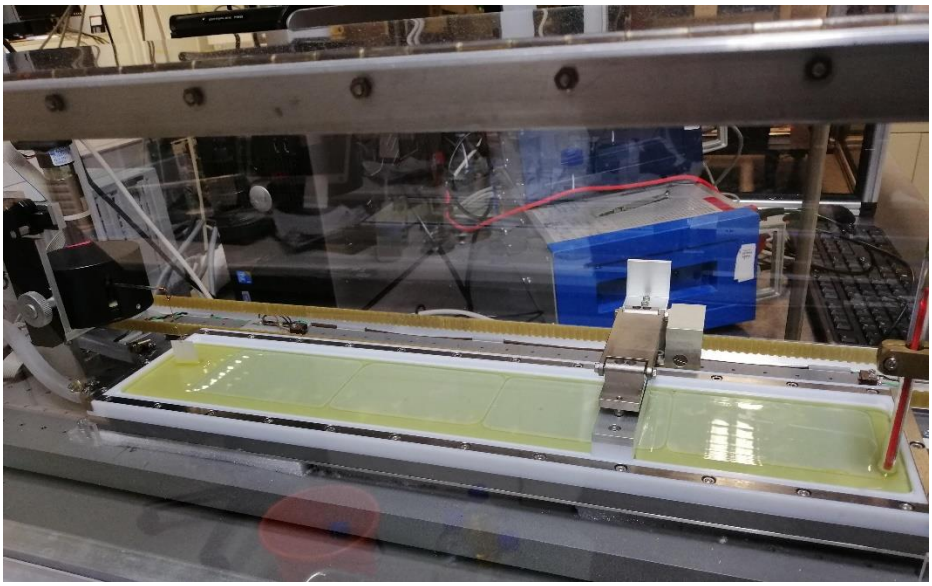

Figure VII-6. Langmuir trough used at Max Planck Institute in Potsdam, filled with aqueous solution of COSAN. Some glace plates were added in order to decrease the solution volume needed.

VII-3. Langmuir isotherms of DGDG-sat at IEM institute in Montpellier

Experiment conditions and parameters were fixed basing on those used for the experiment of Langmuir trough at the Max Planck Institute in Potsdam:

The Langmuir trough in Montpellier has a total surface between the barriers about 30 × 5.4 = 162 cm^2 (we adjust the barrier in a way to adjust the length at 30 cm) (see Fig. VI-4). Only DGDG-sat was investigated because of lack of time. The concentration of DGDG-sat was 2 mg/ml prepared in chloroform. The trough was filled with 200 ml of the solvent (water) or the aqueous solution containing nano-ions at around 20°C. The temperature was not stable all the time, we should add ice from time to time to the thermostat in order to be around 20°C. 5.3 µL of DGDG-sat were deposited at the air/water interface using Hamilton needle of 50 µL (comparable to 10 µL DGDG-sat deposited on a surface about 307.5 in the Langmuir trough in the Max Planck Institute). To form a glycolipid monolayer, we used two barriers to compress with a velocity of 3.115 mm/min that is comparable to 5 $Å^2$/Molecule/min for one barrier (see below how I convert the velocity from $Å^2$/Molecule/min to mm/min). The measurements were made in three successive steps: compression until 35 $mN.m^{-1}$, decompression to around 0 $mN.m^{-1}$ and recompression again until at least 35 $mN.m^{-1}$

I calculate the velocity that I should use for the compression-expansion in mm/min as follow:

5 $Å^2$/Molecule/min or 5×10^{16} cm^2/Molecule/min corresponds to a surface decrease about 5×10^{16} cm^2 × 6.73 $\times10^{15}$ molecules (5.3 µL of DGDG-sat corresponds to 6.73 $\times10^{15}$

molecules). The surface decrease (ΔS) should be constant for the experiments at the MPI and IEM. Therefore,

$$v = \frac{\Delta S}{\Delta t \times d}$$

Where d corresponds to the width of the trough (5.4 cm) and Δt = 1 min.

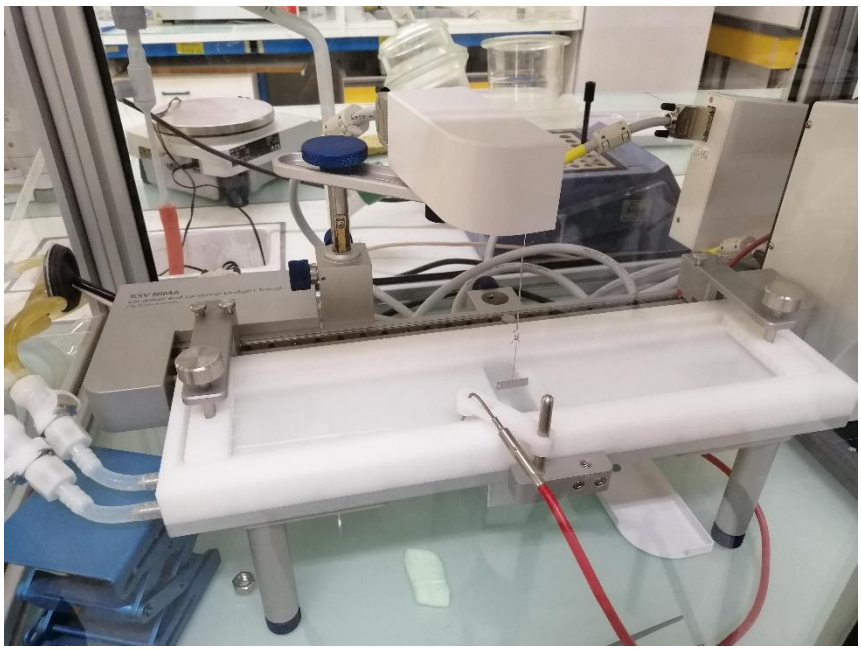

Figure VII-7. Langmuir trough used at IEM Institute in Montpellier.

VII-4. Determination of the closest packing A_0 and the lift-off area A_1

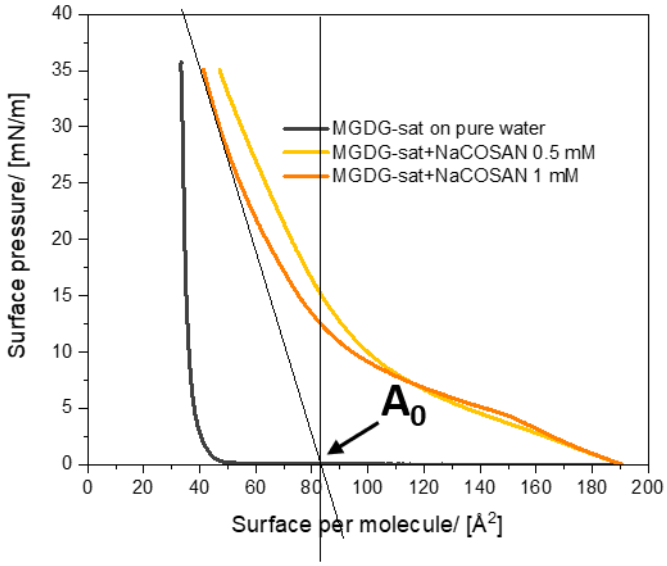

Figure VII-8. Determination of the limiting area of the MGDG-sat Langmuir isotherm in the presence of 1 mM NaCOSAN.

The lift-off area A_1 was determined when the surface pressure was recorded above 0.5 $mN.m^{-1}$.

Chapter 4

Interactions of COSAN anion with proteins

I. Introduction

The effect of ions on proteins was largely investigated in the literature. As described in the first chapter, Franz Hofmeister was the first one to show the notable capacity of ions to solubilize or to precipitate proteins in aqueous solution. The research works that ensued afterwards in this domain have highlighted the strong interest of controlling the salt formulations for tuning the protein-protein interactions either for protein crystallization challenges or for the understanding of the physical-chemistry mechanism taking part of a variety of diseases. The studies of protein interactions in presence of nano-ions for which the superchaotropic features are observed at very low concentration contrary to the classical are expected to open new horizons. Some examples exist already but perhaps not analysed via the "superchaotrope" prism.

It is known that the infectious form (PrP^{sc}) of the prion protein whose its secondary structure has evolved mainly under β-sheets configuration whereas the native physiological form (PrP) is rather an α-helix polymerizes into rods that create amyloids fibers, responsible for the neurodegenerative Creutzfeldt-Jacob disease [Kuznetsov, 1997] and resistant to enzyme degradation. The stabilization of the three-dimensional structure is mainly due to van der Waals and electrostatic forces and approximately 25% of the protein surface is made with uninterrupted hydrophobic amino acids which lead to the formation of intermolecular beta-sheet secondary structure caused by fibrillization.[Chen, 2017] It has been shown that the polyoxometalate (POM) nano-ions precipitate selectively the infections form of the prion protein [Lee, 2005] and also that the POMs charge density drives the interaction between the PrP^{Sc} enabling the selection of the different form of PrP^{sc}. Prion rods are favored by POMs with low charge density whereas 2D crystals are favored by POMs with higher charge density.[Wille, 2009]. Indeed, the protein secondary and tertiary structure depends on its charge distribution that also determines their interactions with POMs. Electrostatic interactions were suggested to be at the origin of the interactions between POMs anions and the positively

charged sites of the infectious prions located in the N-terminal helix.[Lee, 2005; Norstrom, 2006] Therefore, the biological interest in that case is that the precipitation of the infectious form of this protein by interactions with POMs could allow an early detection of the disease.

Another similar example is that depending on the charge and the size of the POMs, these nano-ions inhibit the amyloidogenesis of the amyloid β peptides at the origin of the amyloid plaques in the neurodegenerative Alzheimer Disease.[Geng, 2011]

Polyoxometalate nano-ions showed also an inhibition activity toward HIV protease[Hill, 1990; Rhule, 1998; Judd, 2001] and toward protein kinase CK2.[Prudent, 2008] Kinase protein catalyze protein phosphorylation which is responsible for several cell functions such as proliferation and growth [Cicenas, 2018] and in that case, the presence of POMs disrupt the contact between the N-terminal and the activation segment of the kinase protein CK2 that is stabilized by N-terminal and maintained in an active state. This locks the CK2 in an inactive conformation.[Hill, 1990; Rhule, 1998; Judd, 2001] However, the investigations of POM activity toward protein kinase in living cells showed non-inhibition effects. These observations were interpreted by the degradation of POMs in the cellular environment,[Prudent, 2008] knowing that POMs structure depends on the pH, the temperature and the solution composition.[Pope, 2003]

Different types of POM/proteins binding mechanisms have been considered depending on the POMs size and charge, and on the protein structure.[Arefian, 2017] The non-covalent interaction such as electrostatic forces, hydrogen bonding, or van der Waals forces are the main types of POMs binding to proteins. However, the POMs can also be directly linked to a metallic center as a ligand or an electrophilic group of a protein. The proteins building blocks or the amino acids have two coordination sites that favor their coordination (N and O) with a transition metal. Depending on the nature of the amino acid side chain, amino acids can be charged (positive or negative), neutral and polar or hydrophobic (aromatic and aliphatic side chain). So to summarize, interactions between POMs and amino acids can be classified in two types: (i) interactions with amino-acids via noncovalent interactions that are the electrostatic

forces due to the anionic nature of POMs, Van der Waals interactions and possible H-bonding and (ii) covalent binding of POMs to amino acids to form hybrid complexes via covalent/coordination bonding (see Scheme 1). For that, these nano-ions can be used for crystallography, protein precipitation and extraction and even could be used for potential medicine formulations.[Arefian, 2017]

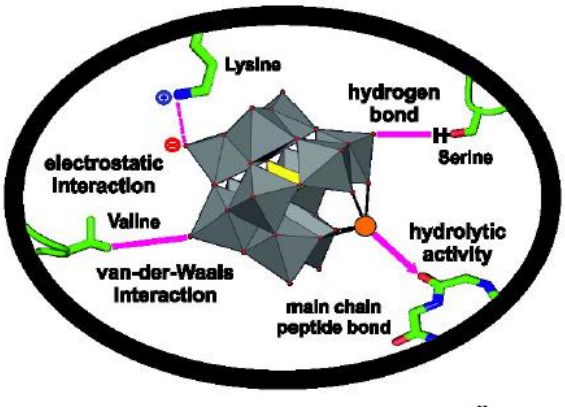

Scheme 6. A caption of the Fig. 9 in the paper of Arefian et al. 2017.[Arefian, 2017] Reproduced from Bijelic and Rompel 2015.[Bijelic, 2015] Lysine is a positively charged amino acid at physiological pH. Serine is a polar amino acid carrying a hydroxyl group. Valine is a hydrophobic amino acid.

As mentioned in the first chapter, COSAN nano-ion is stable in biological systems and have already showed interesting biological activities. Having similar superchaotropic properties as POMs, COSAN is for example currently investigated as kinase inhibitor in living cells where the POMs anions were shown to be degraded.[Prudent, 2008] (And a project initiated by C. cochet team-CEA Grenoble). I am just reminding also that very interestingly, it has been shown that COSAN pass through cell membranes and stop cell growth and proliferation.[Tarrés, 2015]

Few studies, found in the literature, deciphered the features of the interactions of COSAN with proteins. It has been shown that COSAN and its derivatives interact with proteins such as HIV protease,[Cígler, 2005; Kožíšek, 2008; Řezáčová, 2009] human serum albumin (HSA),[Rak, 2011; Rak, 2013] fetal bovine serum (FBS) protein[Fuentes, 2018] and bovine serum albumin (BSA).[Goszczyński, 2017] COSAN and its derivatives interact strongly with the BSA molecule with a binding constant around 10^5 M^{-1} preventing thermal induced aggregation.[Goszczyński,

2017] Fluorescence quenching measurements showed that COSAN and its derivatives exhibit dynamic (collision between the fluorophores of BSA and COSAN as quenchers) and static (a ground state complex formation) quenching with the BSA fluorophores.[Goszczyński, 2017] BSA has three fluorophores residues, the tryptophan residue with the stronger intensity is located in the hydrophobic pocket of the BSA molecule. It was demonstrated on the basis of thermodynamic calculations that COSAN and its derivatives interact with the hydrophobic pocket of the BSA with a hydrophobic interaction mode at low COSAN content (a µM range).[Goszczyński, 2017] in addition, it was demonstrated by Stoica et al. that COSAN interacts with tryptophan via unconventional di-hydrogen bonds.[Stoica, 2009] It was also shown that COSAN interacts with HSA (human serum albumin) via hydrophobic interactions.[Rak, 2011; Rak, 2013] In contrast, at high content, COSAN and its derivatives interact with the BSA protein surface suggesting polar interactions.[Goszczyński, 2017] Dynamic light scattering (DLS) measurements of BSA in the presence of COSAN showed that the hydrodynamic size of BSA increase with increasing COSAN concentration above a molar ratio COSAN/BSA about 10. COSAN/BSA complexes are suggested to be formed.[Goszczyński, 2017]

Therefore, it seems evident that COSAN is a promising nano-ion for the medical and pharmaceutical applications. However, the mechanism of interactions of COSAN with biological molecules is needed to develop its applications in the biological domain. Proteins molecules are one of the main constituents in biological systems. Therefore, the study of COSAN/proteins interactions is mandatory. Due to the hydrophobic character of COSAN, arising from its low charge density, it can be expected that COSAN interact with hydrophobic amino acids and hydrophobic pocket of proteins. To understand the mechanism of COSAN interactions or binding, it is necessary to find out what structural parameters of the proteins determine their interactions with COSAN nano-ions. Therefore, the aim of our studies is to investigate the interactions of COSAN not only with specific type of protein, but with the whole

cytoplasm proteins in order to get further understanding of COSAN interactions mode, and if possible, to understand COSAN/proteins selectivity.

To study the interaction between COSAN and proteins, the strategy was based on the modification of the protein charge analysis. The Hypothesis was that COSAN bound to the protein modifies their global charge. To investigate these modifications, iso-electrofocalisation was used. Changes in protein migration in a gel, upon an electric field enabled to identify proteins interacting with COSAN in comparison with the migration of their corresponding native proteins. Proteins which migrate to their *pI* (Isoelectric point = neutral global charge) in the gel are supposed to migrate to a new Isoelectric point as proteins interacts with COSAN by changing their global charge. Two kinds of samples were analyzed with this methodology:

i) A first sample made of a known standard protein's mixture well controlled with the IEF marker 3-10 that contains a mixture of nine proteins whose feature are well known and,

ii) The proteome extracted from a cell line. Since COSAN exhibit inhibition activity of proliferation and growth of cancer cells, and being a good candidate for BNCT treatment, HeLa cells would be appropriate for this study.

Hela cell line is the oldest and the most commonly used human cancer cell line which is originated from cervical epithelial carcinoma cells of an African-American woman, Henrietta Lacks in 1951.[Scherer, 1953; Rahbari, 2009] This cell line differs from other somatic human cell lines by the fact that it is immortal, unlike the other cell lines that survive only for few days. Therefore, HeLa cell line is widely used in cellular biology and medical researches[Rahbari, 2009] Thus, its features are well known.

II. Material and method

II-1. HeLa cells culture

HeLa cells were cultivated in a DMEM (Dulbecco's Modified Eagle Medium) culture medium (see Fig. 1). The percentage of CO_2 was 5% at a pH of 7.4 (physiological pH) and at 37 °C (human body temperature). DMEM added with 10 % of new born calf serum (SVF) contains the factors necessary for their growth (amino acids, vitamins, inorganic salts, growth factors and others). Combined with a GlutaMAX ™ supplement (Stabilized Glutamine), DMEM limits the buildup of toxic ammonia and improves cell growth and viability in an easy-to-use format.

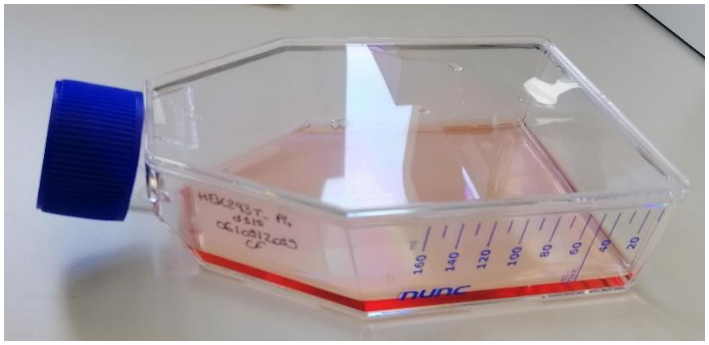

Figure 1. Flask in which cells are cultured in a controlled atmosphere in DMEM/GlutaMax culture medium. The red color comes from the phenol red pH indicator.

II-2. Cell lysate preparation

When the cells have reached the 80 % of confluence (revealed using a microscope), the Flask is rinsed with Phosphate Saline Buffer (PBS) to remove the culture medium, leaving only the viable cells which adhere to the Flask. PBS is a commonly used buffer in biological researches as it maintains the osmolarity, the physiological pH around 7.4. It contains disodium hydrogen phosphate (Na_2HPO_4), sodium chloride (9 g/L), potassium dihydrogen phosphate (KH_2PO_4). Therefore, using PBS as a solvent enables to maintain the physiological conformation of proteins. Moreover, the cells the cells will be detached from the Flask using the trypsin enzyme for 5 min. Then, the activity of the enzyme was stopped by adding DMEM + 10 %SVF. After trypsinization, the cells were centrifuged to eliminate the medium and then suspended in PBS. Cell lysate is obtained after cells disruption to release soluble proteins without denaturation.

This is done mechanically with the Dunn Homogenizer (see Fig. 2). Using the Dunn Homogenizer, cells were crushed in order to break membranes. Then the lysate was centrifuged to pellet the membrane and keep the supernatant containing the soluble proteins released from the cells, representing the soluble protein fraction of the proteome. Proteome is the whole proteins expressed by a cell. It is an expression of the genetic material of an organism that is consisting of the DNA. Therefore, the proteome obtained here contains only cytoplasmic proteins, since the membrane proteins remain aggregated in the lipids of the membranes, otherwise a specific protocol is required in order to extract them.

Figure 7. Dunn Homogenizer tool.

The concentration of proteins of the extracted proteome was determined following the conventional procedure of the Bradford method (see Annex VI-1). As a result, proteins concentration is about 3 mg/ml.

II-3. Isoelectric focusing gel (IEF)

The interactions of standard protein's mixture and HeLa cells proteome with NaCOSAN were investigated using isoelectric focusing gel (IEF). IEF is an electrophoretic technique that is used for the vertical native denaturating separation of proteins based on their isoelectric point (pI). In our case, we used Novex 3-10 IEF gel (thickness about 1 mm) which have a pI performance range from 3.5 to 8.5 where pH 10 corresponds to the top of the gel and pH 3

corresponds to the bottom. The IEF gel have 10 wells, which mean that if an empty well should be kept between 2 samples, 5 samples maximum can be loaded per gel.

Different solutions of proteome/standard proteins in the presence of COSAN were prepared in PBS. The solutions were incubated for one hour at low temperature (using ice). After incubation and just before loading the samples into the wells, sample buffer containing glycerin were added. Glycerin help to densify the proteins and then facilitates their migration along the gel. Then, samples were loaded onto the polyacrylamide gels and migrate upon the applied electric field with a pH gradient. For each experiment, two gels were performed in parallel. The inner chamber (between the 2 gels) was filled by the cathode running buffer and the 2 outer chambers was filled by the anode running buffer (see Fig. 3 and Annex VI-2 for details). This configuration enables the protein migration from the cathode to the anode, driving proteins with the higher negative global charge to the bottom of the gel.

IEF is performed by gradually increasing the voltage, then maintaining the final focusing voltage for 30 minutes. Indeed, applying high voltage during the initial stages of IEF leads to the generation of excessive heat due to the movement of carrier proteins. For that and for best results, we applied a voltage of 100 mV for 45 min followed by 200 mV for 45 min and the final focusing voltage was 300 mV for 30 min. The high finishing voltage help to focus the proteins into narrow zones.

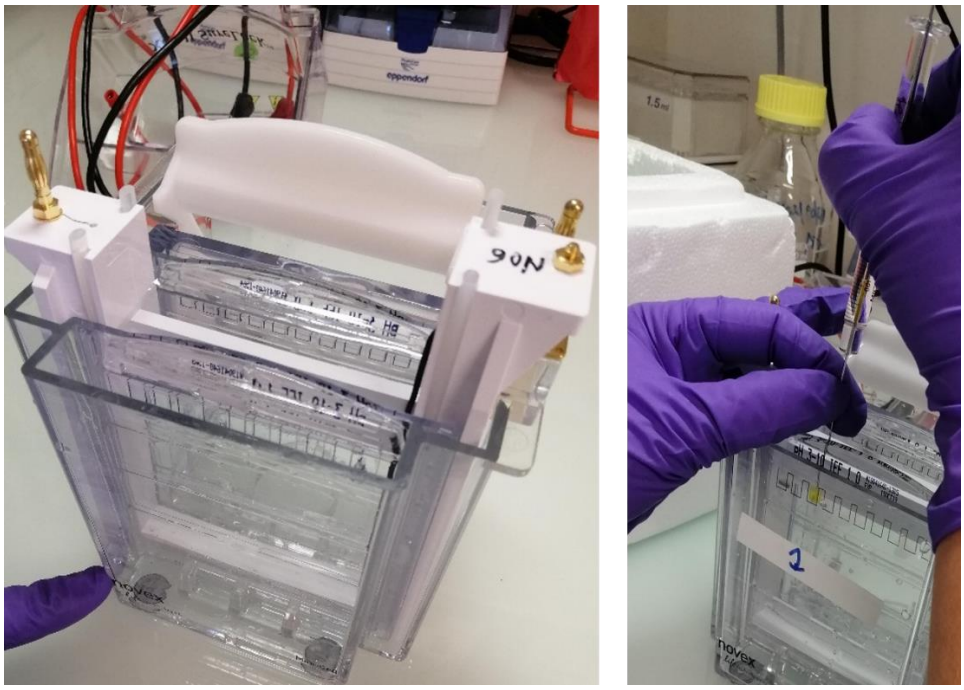

Figure 8. Two cassettes (containing the gels) placed in parallel in a device connected to an electric current generator.

To visualize the bands of proteins after migration, a staining of the proteins was performed using Coomassie Phastgel blue R-350 that interacts with basic amino acids (see Annex VI-3 for details about the procedure).

II-4. Mass spectrometry analysis of selected bands

After gel staining, an analysis software Quantity-One, supplied by BIORAD, was used to localize every band of the gel and calculate the pI of each band by comparing their migration point with the Marker 3-10 supplied by SERVA (see Fig. 4). The interesting bands that exhibit pI modification in the presence of COSAN were selected for their analysis.

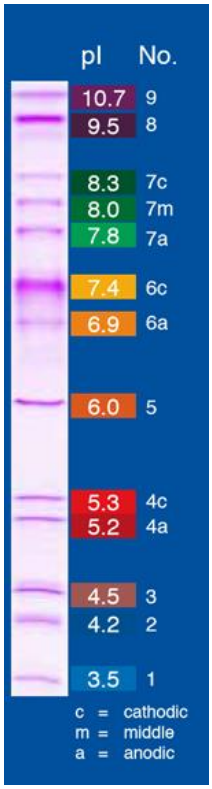

Table 3. Proteins of the IEF marker 3-10, SERVA Liquid Mix

Protein name	**pI* of main band**
Cytochrome C (horse, heart)	10.7
Ribonuclease A (bovine, pancreas)	9.5
Lectin (lens culinaris)	8.3, 8.0, 7.8
Myoglobin (horse, muscle)	7.4, 6.9
Carbonic anhydrase (bovine, erythrocytes)	6.0
ß-Lactoglobulin (bovine, milk)	5.3, 5.2
Trypsin inhibitor (soybean)	4.5
Glucose oxidase (Aspergillus niger)	4.2
Amyloglucosidase (Aspergillus niger)	3.5

Figure 4. Proteins of the IEF marker 3-10, SERVA Liquid Mix.

II-4-i. Peptides preparation

Bands were cut and digested (fragmented into peptides) according to the standard procedure using trypsin gold/proteaseMAX™ Promega (see Annex VI-4 for details). The procedure includes several steps performed in a 96 wells plate, which cover the gel bands destaining, dehydration/rehydration to perform the reduction/alkylation step, then dehydration/rehydration to perform the trypsin digestion helped by the proteaseMax for 1 hour at 56 °C. The digestion was stopped by adding 5 µL of a TFA 1% solution. The final solution contained the peptide released from proteins digested by trypsin in the gel. It's known that more than 10 % of the potential trypsic peptides are released and that the proteins sequence is well covered.

II-4-ii. Mass spectrometry analysis

Tandem Mass spectrometry is a suitable technique for the analysis and identification of proteins. The reverse phase liquid chromatography column (LC) (C_{18} column) coupled to the mass spectrometry separates the peptides obtained after digestion according to their hydrophobicity.

In the case of the Hela proteome analysis, the mass spectrometer used was the Q-Exactive-Orbitrap HF with speed of spectra scan at a 20 Hz frequency. Peptides identification was made with MS/MS methodology including several steps. The process is described briefly. First, the formation of the positive molecular ion or parent ion is done by its vaporization in the ionization chamber. The ion travel through the mass spectrometer to reach the analyzer. Then the full scan of the ion parent is performed before being sent in the collision chamber to induce by collision energy its fragmentation producing randomly several fragment masses, then scanned by the orbitrap analyzer. The methodology used is the top 20 which scan the 20 most abundant ions every second (20 Hz frequency). Mass to charge ratio (m/z) of ions scan from 350 to 1800 m/z is the measure obtained with this analysis technique.

In the case of the standard protein's samples, the mass spectrometry analysis was performed with the LTQ-Orbitrap XL. The principle is the same as the Q-Exactive HF since the analyzer are the same. The only difference between these two mass spectrometer is the scan frequency which is 5 Hz instead of 20 with the Q-Exactive. As the protein mixture sample was not complex, and the number of proteins in the sample is low, it was sufficient to use a mass spectrometer less efficient.

II-4-iii. Peptide Spectra Matching (PSM)

A powerful search engine software, Mascot, was used for the identification of proteins from primary databases obtained by mass spectrometry. The search engine finds in a database the mass of the peptide and so its sequence corresponding to the spectra.

Each protein was identified with at least two peptides. The relative quantification analysis was performed by their spectral count (SC) comparison between proteins with and without COSAN.

III. Interaction between COSAN and standard proteins

III-1. Isoelectric focusing gel of standard proteins

For IEF experiments, an IEF marker should be load on the first or last (or both) well. IEF marker supplied by SERVA was used as the well-controlled. It contains a mixture of nine standard proteins with well-known amino acid sequences and isoelectric points values (see table 1). Therefore, it was interesting to investigate the interactions of NaCOSAN with IEF marker proteins. For that, samples of IEF marker proteins with and without COSAN at different concentrations (0.1-10 mM) were investigated using the isoelectric focusing gel. Here, no need to add the sample buffer since the IEF marker contains already the sample buffer. The amount of IEF proteins was 250 µg and 125 µg for the samples without and with COSAN respectively. The samples were injected into the gel following the procedure described above. IEF is performed by gradually increasing the voltage, a voltage of 100 mV for 45 min followed by 200 mV for 45 min and the final focusing voltage was 300 mV for 11 min (instead of 30 min).

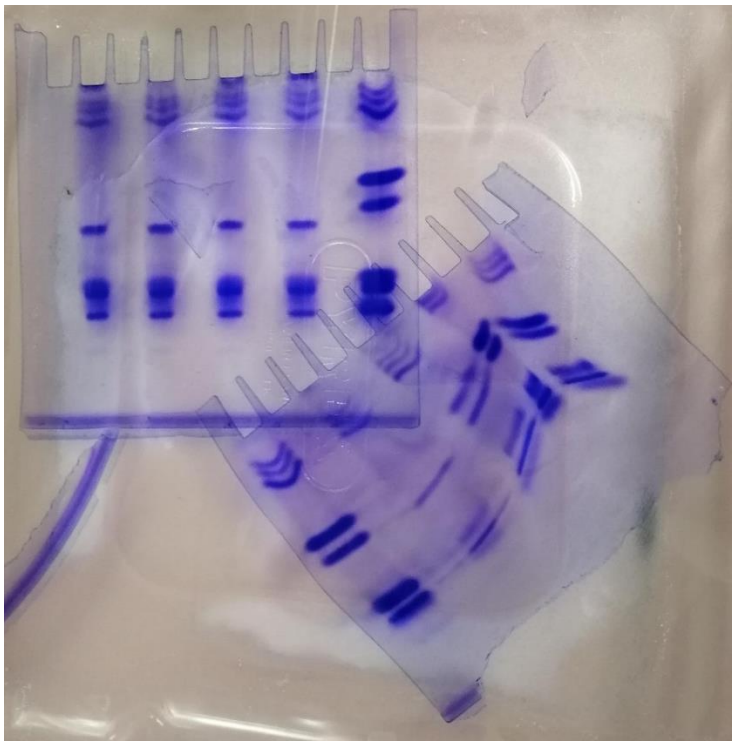

Figure 5. IEF gels for standard sproteins samples with and without [NaCOSAN] = 0.1-10 mM.

The gels are stained by the Coomassie Phastgel blue R-350 (see Fig. 5) and scanned (Fig. 6).

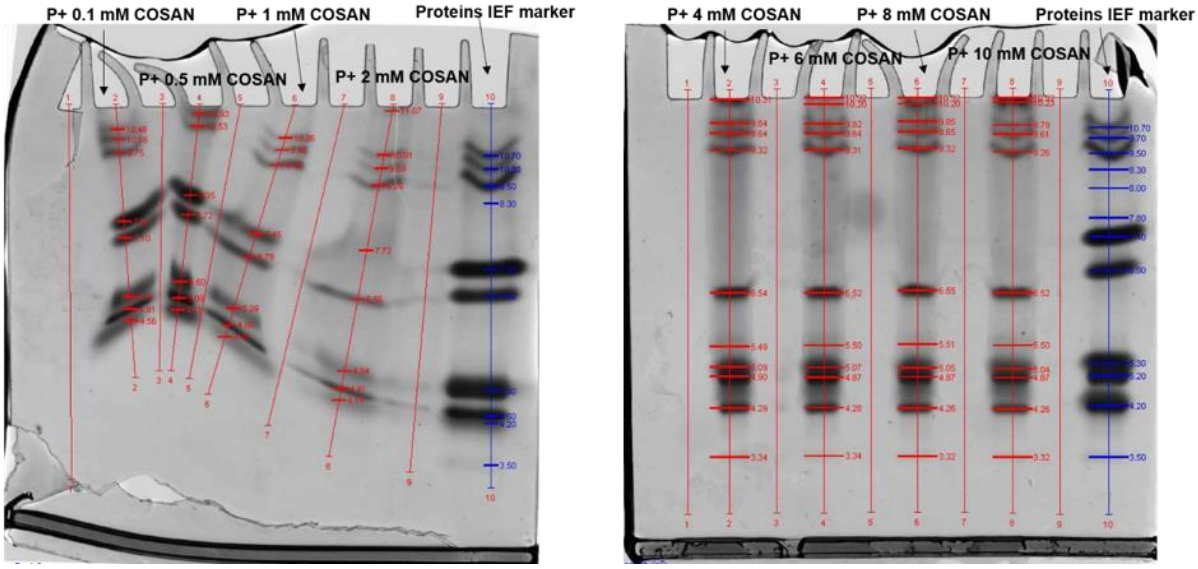

Figure 6. IEF gels scans for IEF marker proteins with and without [NaCOSAN] = 0.1-10 mM. The difference of bands intensity between samples with COSAN and the samples IEF marker without COSAN is due to the difference of the amount of standard proteins.

As can be observed in Fig. 6, significant differences were observed between samples with and without COSAN. As compared to the IEF Marker 3-10 i.e. without COSAN, several bands migrated below their conventional pI. This first observation indicated that COSAN had drastically modify the migration of the proteins driving them lower in the migration lane. The negatively charged COSANs have induced changes in the global charge of proteins. The interactions of COSAN with the proteins can be considered strong enough to resist to the applied electric field that can interrupt the electrostatic interactions. Indeed, the localization in lane of the bands of proteins with a pI = 7.4 and 6.9 changed with the sample prepared with COSAN. New bands appeared around pH= 6.52. On the top of the lanes i.e. at the level of the wells, some proteins did not seem to migrate. This may be due to proteins precipitation that were stuck in the well. The gel at the right in Fig. 6 presented a migration default that was probably due to the gel as both the two gels were run together in the same system. Therefore, only the gel on the left was cut off and analyzed by mass spectrometry. But it was interesting to present it as it is a part of the results of the total COSAN concentration range that was studied. It was important to see that the effect of COSAN appeared between 1 and 2 mM of COSAN. The disappearance of the band localized at the migration level of pI 7.4 started with 2 mM of COSAN. In addition, precipitated proteins in the wells showed that the effect of COSAN was significant from the COSAN concentration 4 mM.

The migration of some other proteins whose pI was around 4.3 did not seem to be changed by the interaction with COSAN informing that potentially no interactions with COSAN.

Interesting bands were selected and analyzed by mass spectrometry. The results of the protein identification are reported in the figure 7.

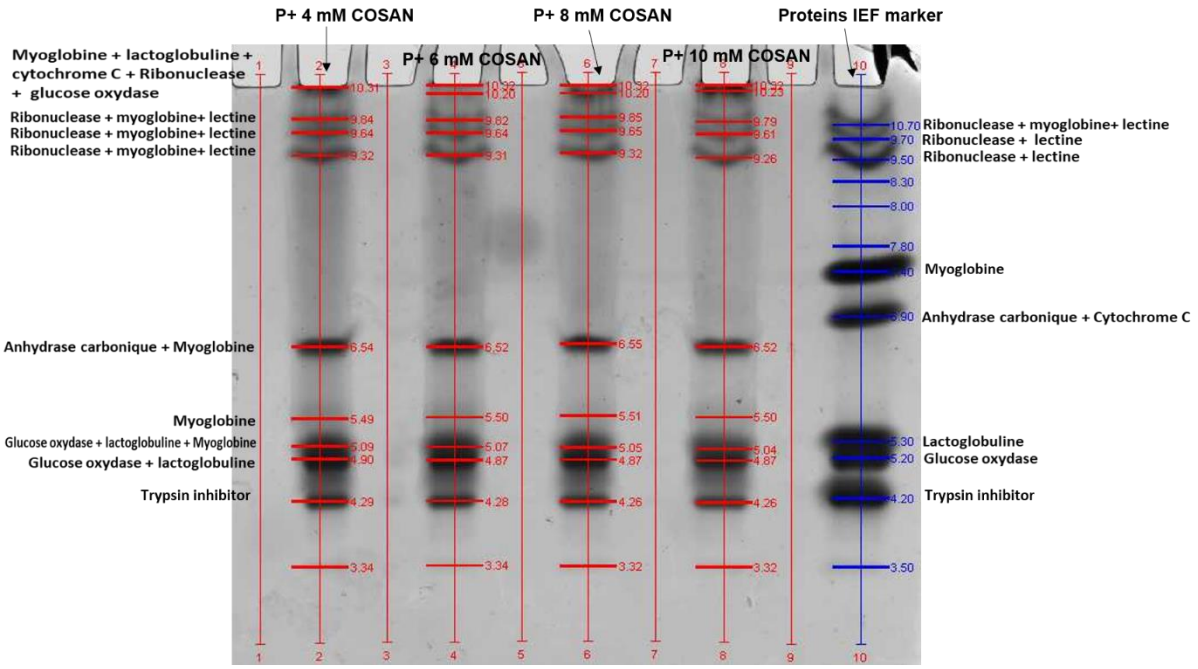

Figure 7. IEF gels scans for IEF marker proteins with and without [NaCOSAN] = 4-10 mM. Proteins labels are the results of mass spectrometry analysis.

First of all, it's interesting to see that NaCOSAN interacts with almost all of the proteins of the marker. Among the nine proteins, seven have their pI modified as their migration point was changed with NaCOSAN. Myoglobin, cytochrome C, ribonuclease, glucose oxidase and lactoglobulin were partially stuck in the wells, i.e. did not migrate in the gel. This may indicate the precipitation of these proteins by COSAN anions. The other part of carbonic anhydrase and lactoglobulin, migrated lower than their conventional pI in the presence of COSAN. Carbonic anhydrase and lactoglobulin pIs evaluated with Quantity-one changed from 6.9 to 6.5 and from 5.3 to 5.1 and 4.9 respectively. The weak effect may be direct, due to the interaction between COSAN and the protein or indirect, due to the interaction of the carbonic anhydrase or lactoglobulin with a complex protein/COSAN primary formed.

In control lane (marker without COSAN), myoglobin was found in two bands, indicating that two forms of myoglobin coexist in the marker or that myoglobin interacts with ribonuclease and lectin, the first with pI at 10.7 and the second, the physiological one with a pI at 7.4. In all the lanes where samples prepared with COSAN migrated, six forms of myoglobin migrated, from

which, five migrating at different Isoelectric point level and one stuck at the top of the gel unable to migrate.

On the contrary, Trypsin inhibitor and lectin proteins did not exhibit pI modification in the presence of COSAN i.e. did not interact with COSAN (see Fig. 7). Therefore, to investigate further the COSAN interactions, three proteins, were selected, myoglobin and carbonic anhydrase that have interacted with COSAN, and the trypsin inhibitor, which did not seem to have COSAN interaction. Unfortunately, because of some problems (see some difficulties section) I did not have time to investigate the interactions between COSAN and carbonic anhydrase or trypsin inhibitor.

III-2. Chemical and physical features of the three proteins

Myoglobin (Mb) is a surface-active globular oxygen-binding protein that is water soluble with a dimension about 4.5 × 3.5 × 2.5 nm.[Essa, 2007] Mb is a cytoplasmic protein found in the muscle tissue of vertebrates. It consists of 153 amino acids residues, 8 alpha helices and a hydrophobic core (see Fig. 9). Each myoglobin molecule possesses one heme or a prosthetic group which is a non-amino acid compound of the protein, inserted in the hydrophobic cleft.[Essa, 2007; Mondal, 2015] A heme is a coordination complex responsible of the binding with oxygen. It consists of a central iron atom in the +II oxidation state coordinated with a heterocycle macrocycle organic compound (porphyrin).[McNaught, 1997] The most abundant negatively charged groups in proteins are the aspartic and glutamic acids (Asp and Glu), and the most abundant positively charged groups are the arginine (Arg), lysine (Lys) and histidine (His). Myoglobin protein contains 13 Glu, 7 Asp, 2 Arg, 19 Lys and 11 His.[Patrickios, 1995] The experimental isoelectric point of myoglobin at 25°C (from IEF) is about 7.33 and 7.45 (the presence of two values maybe due to the presence of different isoforms of the myoglobin that differ by few number of amino acids).[Righetti, 1976; Patrickios, 1995] For pH above the pI, Glu and Asp are negatively charged while Arg, Lys and His are neutral. For pH below the pI, Arg, Lys and His are positively charged while Glu and Asp are neutral.

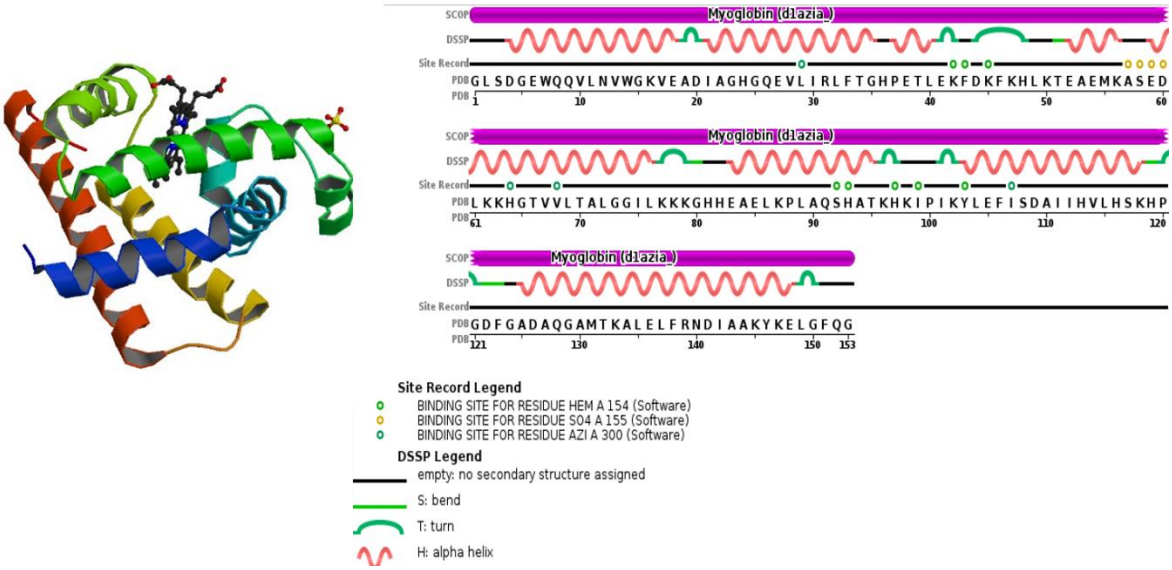

Figure 8. Myoglobin horse of muscle structure and residues sequence from PDB (protein data bank). This protein consists of 153 residues and its secondary structure is composed of 71% helical (8 helices; 110 residues).

Noting that α-helix are more flexible than β-sheet that are stable, rigid and mainly hydrophobic.

However, the myoglobin protein that consists of 71% of α-helix is a globular flexible protein.

Carbonic anhydrase (bovine) consist of 259 residues and its secondary structure is composed of 15% helical (10 helices; 40 residues) and 30% beta sheet (18 strands; 78 residues).

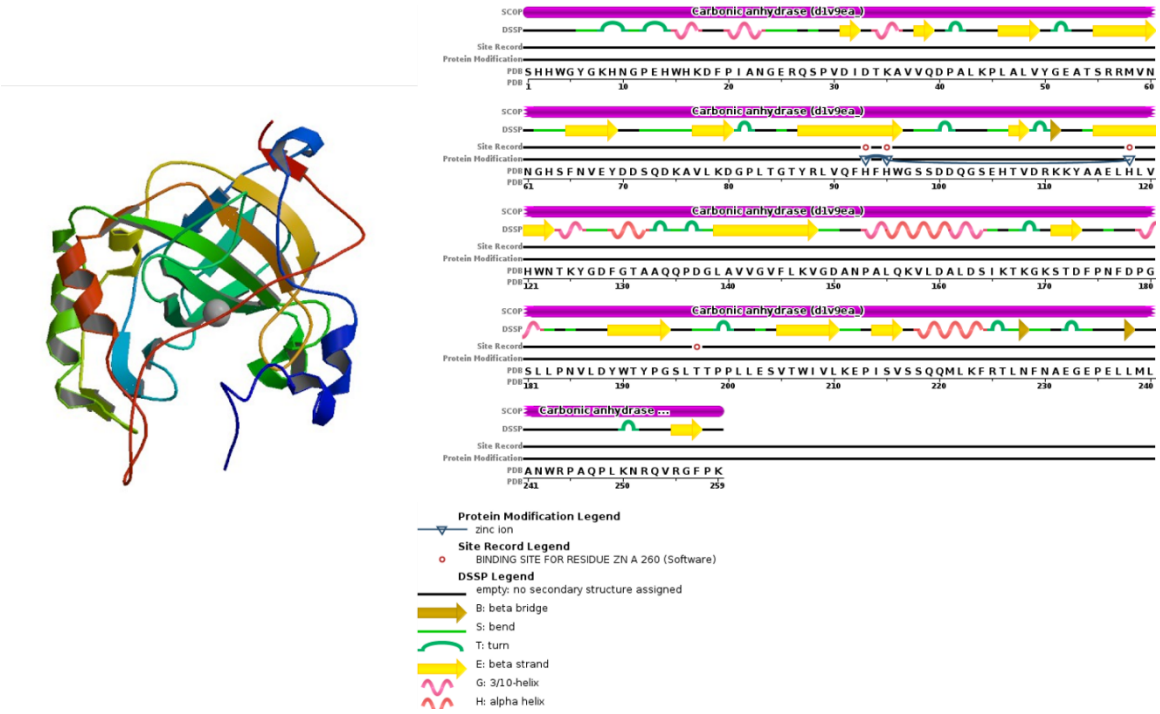

Figure 9. Carbonic anhydrase (bovine) structure from PDB. This protein consists of 259 residues and its secondary structure is composed of 15% helical (10 helices; 40 residues) and 30% beta sheet (18 strands; 78 residues).

The Soybean kunitz trypsin inhibitor (SKTI) is a small, stable monomeric, non-glycosylated, globulin type protein present in the soybean seeds. SKTI protein consists of 181 amino acid residues with a molecular weight of 21.5 kDa and an isoelectric point at pH 4.5 (Kunitz, 1947).[Kunitz, 1947] The overall structure of SKTI is spherical with a diameter of 4-5 nm consisting of 12 criss-cross antiparallel β strands, stabilized by hydrophobic side chains as shown in Fig. 11 (Song & Suh, 1998).[Song, 1998]

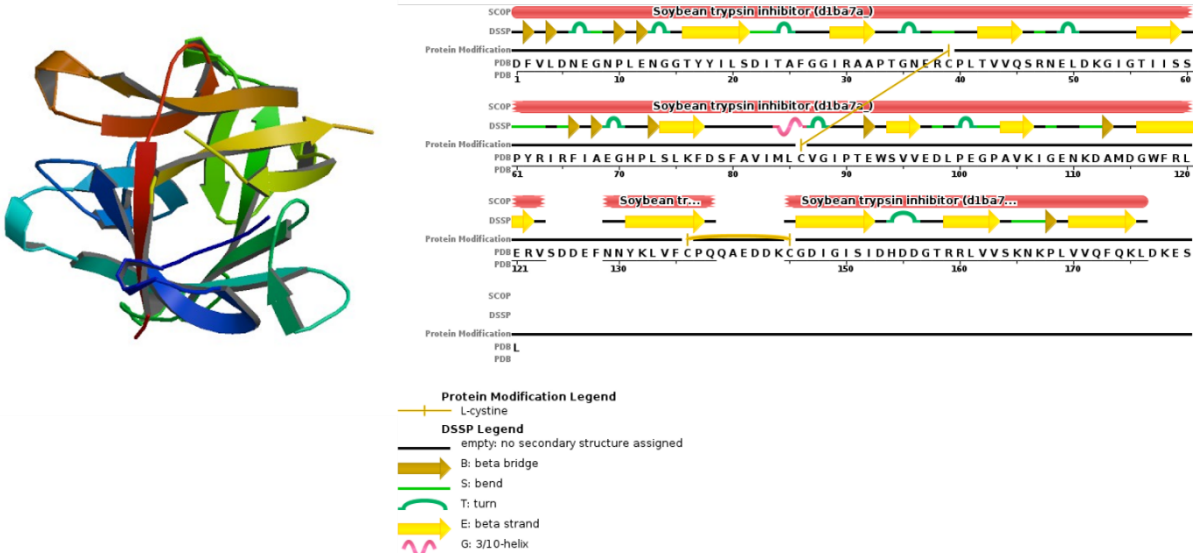

Figure 10. Trypsin inhibitor (soybean) structure and residues sequence from PDB. This protein consists of 181 residues and its secondary structure is composed of 1% helical (1 helice; 3 residues) and 38% beta sheet (22 strands; 70 residues).

III-3. Interaction between Myoglobin horse muscle and COSAN at different pH values.

Dynamic light scattering (DLS) and zeta potential measurement were used to investigate whether the COSAN induces the modification of the global charge and the precipitation of Myoglobin as shown in Fig. 7 by IEF gel electrophoresis.

The DLS, here measured at an angle about 173°, informs about the scattering particle size. This technique analyzes the size and shape of particles based on their Brownian motion and translational displacement. Einstein demonstrated that the mean squared displacement of particles due to Brownian motion is proportional to time leading to the diffusion coefficient. The diffusion coefficient, and hence the hydrodynamic radii calculated from it, depends on the size and shape of macromolecules.

Zeta potential (ζ-potential in mV) is a technique used for the determination of surface charge of particles in solution. Zeta potential term is used for the description of the electrokinetic potential of dispersed charged particles. When a charged particle is in solution, ions with

opposite charges are attracted and form a layer around the particle (Stern layer). When this particle undergoes the effect of an electric field, it moves in the solution and this layer remains attached. The interface between the attached layer and the counter ions that do not migrate with the particle is called the slipping plane. The electric potential at the slipping plane is the zeta potential.[Hanaor, 2012] Zeta potential value of a particle is predictive of the stability. In general, for high values (higher than 25 mV), the particles are highly enough charged to be dispersed and stable in the solution. For small values (less than 25 mV), a flocculation or agglomeration may occur due to the attractive forces that exceed the repulsive interactions, such as the van der Waals and the hydrophobic interactions, and hydrogen bonding.[Greenwood, 1999; Kumar, 2017]

The concentration of Myoglobin solutions was about 0.032 mM, which could be comparable to the concentration of this protein in the IEF marker considering that the 9 proteins are in equal concentration. In the IEF gel experiments using IEF marker proteins, the total amount of proteins (9 protein types) in each well was 125 µg/25 µl. It corresponds to a concentration of 5 mg/ml. Making consideration that the 9 proteins are in equal concentration, the concentration of Myoglobin (molar weight 17000 Da) was 5/9 = 0.56 mg/ml which corresponds to around 0.032 mM. Solutions of Myoglobin 0.032 mM in (i) pure water (ii) 1 mM NaCOSAN aqueous solution (iii) PBS solution (iv) 1 mM NaCOSAN in PBS solution were prepared and filtered using cellulose acetate filters 0.2 µm (see Fig. 11) and centrifuged for 5 min at 7000 rpm.

Figure 11. Filtration of a solution containing a mixture of myoglobin and COSAN using cellulose acetate 0.2 µm filter.

DLS measurements were performed in order to estimate the hydrodynamic size (diameter, nm) of the protein. The hydrodynamic diameter of myoglobin in pure water was found to be ≈ 4.5 nm which is in according with the literature.[Wilkins, 1999; Ali, 2010] We observed that in general, decreasing the pH of the solution lead to the formation of large aggregates as the protein is getting closer to its isoelectric point. However, for the system in pure water, large aggregates start to form once the solution reach its pI but no turbidity was observed. In the presence of 1 mM COSAN, large particles start to form earlier, even for pH values above the pI, i.e. from pH between 5.79 and 4.899 where the solution was visually turbid for pH ≈ 4.899 (see Fig. 12). Mention that DLS and zeta potential measurements are not representative of the solution when it is turbid, which is the case of the DLS/zeta potential measurements of the myoglobin solution in the presence of 1 mM NaCOSAN at pH 4.899. The increase of myoglobin aggregates size in the presence of COSAN may suggest that COSAN anions interacts with the hydrophobic inner parts of the myoglobin. Repulsive interactions between different COSAN anions inside the protein may occurred leading to the swelling of the aggregates. This may

explain the precipitation of myoglobin in the wells of IEF gel in the presence of COSAN (Fig. 7).

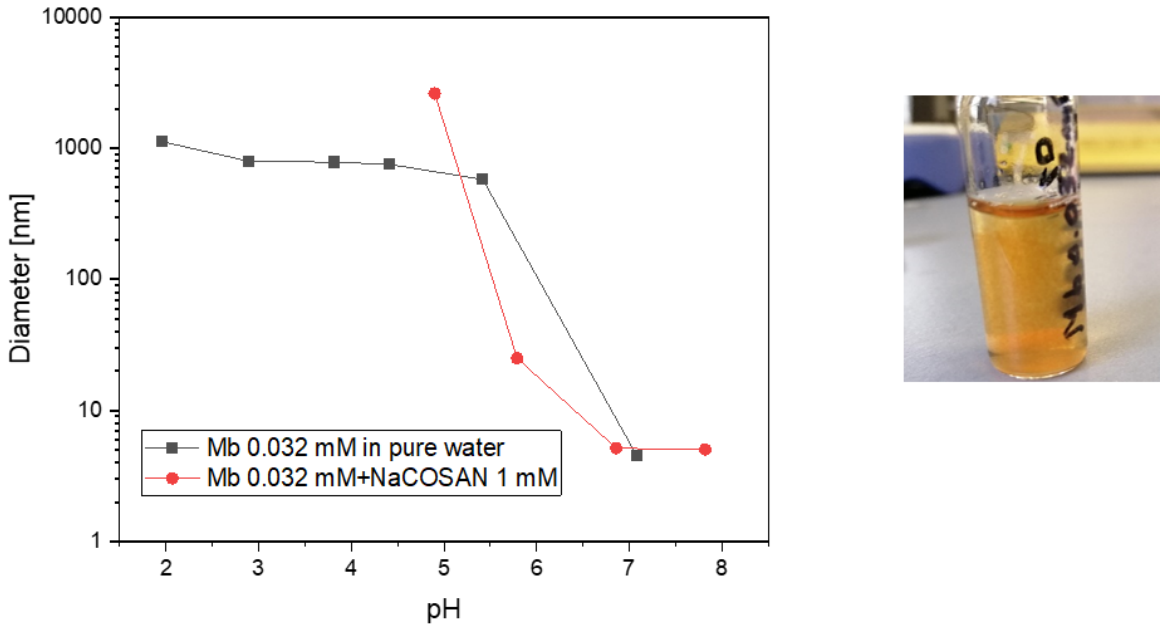

Figure 12. Hydrodynamic diameter of Myoglobin 0.032 mM with and without NaCOSAN in pure water. On the right side a photo of the turbid solution containing Mb 0.032 mM in the presence of 1 mM NaCOSAN at pH around 4.899.

Zeta potential measurements were performed in parallel to DLS in order to investigate the protein charge modification in the presence of COSAN as well as to estimate the myoglobin isoelectric point. Zeta potential values indicate that the protein in pure water is not stable since the values are below 25 mV (in absolute values). On the other hand, in the presence of 1 mM NaCOSAN the protein is stabilized at high pH (7.82-6.86) due the increase of its global charge upon interactions with COSAN anions, and destabilized at lower pH as the protein get closer to its isoelectric point at which its global charge is neutral. Indeed, the experimental isoelectric point of myoglobin in pure water (natural pH ≈ 7.08) obtained from zeta potential measurements was found around 5.4. In the presence of NaCOSAN in water (natural pH ≈ 7.82), the isoelectric point decreased to around 4.5 (see Fig. 13). COSAN was added to the myoglobin at its natural pH in water which is above its PI, this means that the positively charged

groups (Arg, Lys and His) should be neutral. This decreasing in pI value in the presence of NaCOSAN anions demonstrates that NaCOSAN increases the negative charges of the protein by binding with neutral or negative sites.

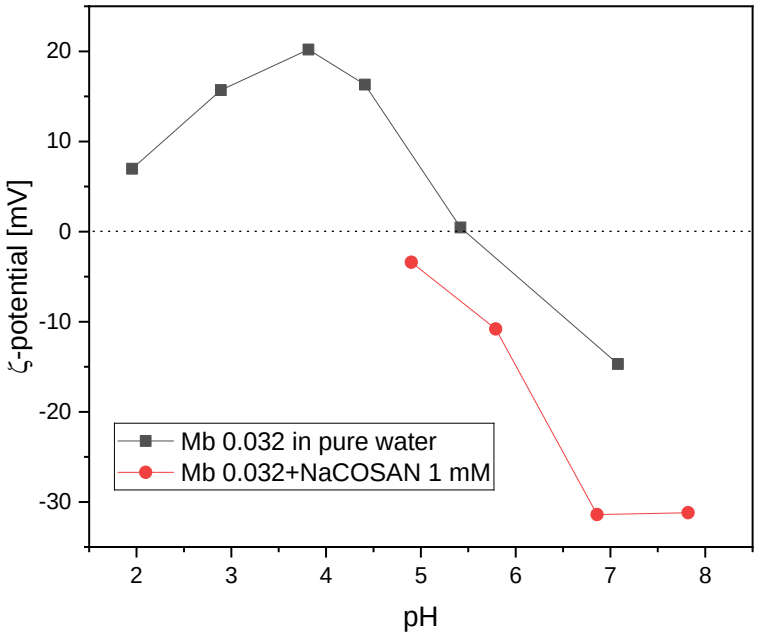

Figure 13. Zeta potential measurements for Myoglobin 0.032 mM with and without NaCOSAN in pure water.

III-4. Interaction between Myoglobin horse muscle and COSAN at different concentrations.

As observed above, a precipitation of myoglobin in the well was observed in the presence of COSAN (Fig. 7). Investigation of the precipitation of myoglobin by COSAN anions was performed using DLS, zeta potential and UV-visible spectroscopy techniques. For that, solutions at fixed concentration of myoglobin at 0.032 mM in the presence of different concentrations of COSAN (0.01-5 mM) were analyzed. The results are presented in the following Fig. 14 and 15.

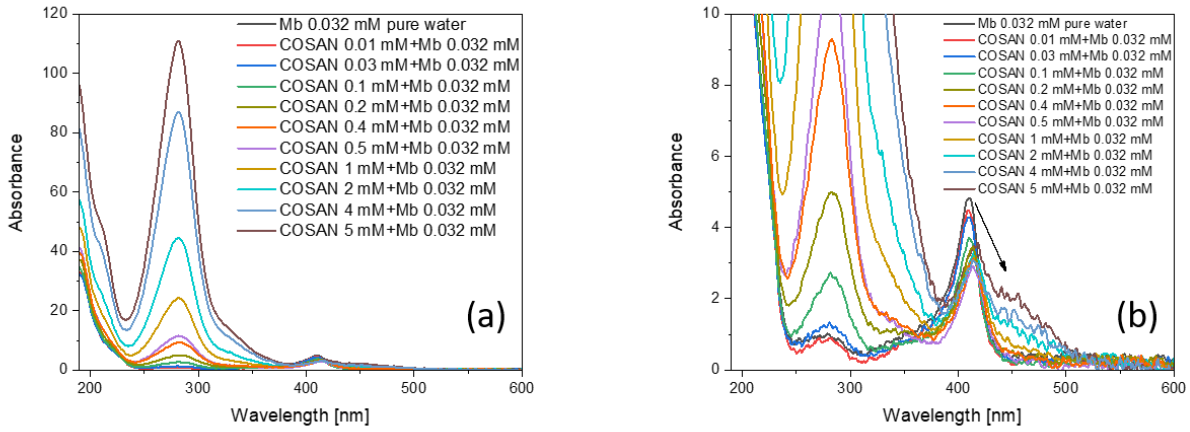

Figure 14. (a) UV-visible spectra of myoglobin 0.032 mM and COSAN at different concentrations. (b) A zoom on the absorption peak of porphyrin in the visible region showing a hypochromic and a bathochromic effect as the COSAN concentration increases. The measurements were performed using Nano Drop One absorption spectroscopy (thermo scientific) where the solution volume needed is 2 µl.

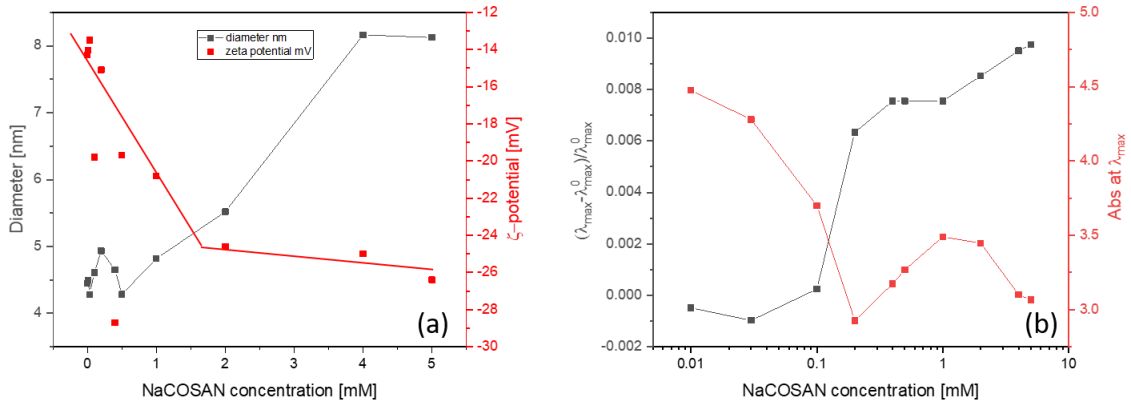

Figure 15. (a) Hydrodynamic diameter (black curve) and zeta potential (red points) measurements of Myoglobin 0.032 mM in the presence of different concentrations of NaCOSAN. (b) A plot of the normalized shift of the wavelength at the maximum absorbance of Myoglobin 0.032 mM in the visible region (around 410 nm) as a function of NaCOSAN concentration.

As observed from DLS measurements, i.e. the hydrodynamic diameter of the scattering particles increases from around 4.5 nm to around 8 nm with increasing COSAN concentration after 1 mM. The particle size is relatively stable at 4 and 5 mM of COSAN. Here, the precipitation myoglobin by COSAN in the wells of the IEF gel that we mentioned before is not confirmed. As the size of the protein is doubled the investigated concentration range of

COSAN, we can assume that there is dimerization of myoglobin. In addition, myoglobin interacts with ribonuclease and lectin as can be concluded from the band at 10.7 of the lane of IEF marker (without COSAN, see Fig. 7). This may indicate that the precipitation of myoglobin by the presence of COSAN in the IEF wells is induced by its interactions with ribonuclease and lectin proteins.

On the other hand, increasing COSAN concentration, the zeta potential is getting more and more negative (see Fig. 15-a red points). This can proof the binding of COSAN anions to the myoglobin that becomes more negatively charged. It seems like two regimes exist, one regime below 2 mM of COSAN where the slope of the zeta potential curve is stronger than the one above 2 mM (see Fig. 15).

The UV-visible spectra of myoglobin can give information about the surrounding environment of the heme group. The Soret band of the myoglobin is around 410 nm which is an intrinsic heme-group property.[Gan, 2004; Mrázová, 2008] Another absorption peak is observed in the UV range around 280 nm that corresponds to the absorption of tryptophan units of myoglobin.[Loget, 2011] COSAN has also an absorption peak around 280 nm that cover the peak of myoglobin that is much less intense. However, this peak at 280 nm seems to be unaffected. The UV-vis spectra are not saturated at high COSAN concentrations (above 1 mM) like observed in the second chapter. The measurements here were performed using a Nano drop UV-visible technique. Interestingly, when the concentration of COSAN is increased, an evolution of the Soret band around 410 nm is observed. Indeed, increasing COSAN concentration lead to the decrease of the peak intensity (hypochromic effect) which can indicate that the heme environment can change the myoglobin conformation without destroying it.[Gan, 2004; Loget, 2011] A shift of the wavelength at the maximum absorption toward higher values (bathochromic effect) is also observed (see Fig. 14). These observations are an additional proof of the binding of COSAN to the myoglobin and a possible denaturation or a modification of the conformation. Moreover, the evolution of the absorption peak of myoglobin in the visible range indicates that COSAN interacts with the porphyrin that is located in the

hydrophobic pocket of myoglobin. This does not mean necessary that the COSAN anions does not interact with the surface of the protein or with the residues. Small angle X-ray scattering analysis of the solution COSAN/myoglobin could inform about whether the COSAN adsorb on the protein surface or not.

IV. Interactions COSAN/proteome of Hela cells

IV-1. Isoelectric focusing gel of proteome of HeLa cells

Solutions of 30 µg proteome without NaCOSAN (control) and with 2 different NaCOSAN concentrations, 1 and 5 mM, were prepared in PBS and loaded into the wells. An empty well between two samples was kept in order to avoid contamination between the two samples. An IEF marker (pH marker) was loaded in the first and the last well. The same IEF procedure described above was followed. The obtaining gels were stained using Coomassie Phastgel blue R-350 (see Fig. 16 and scanned using the Quantity-One software (see Fig. 17).

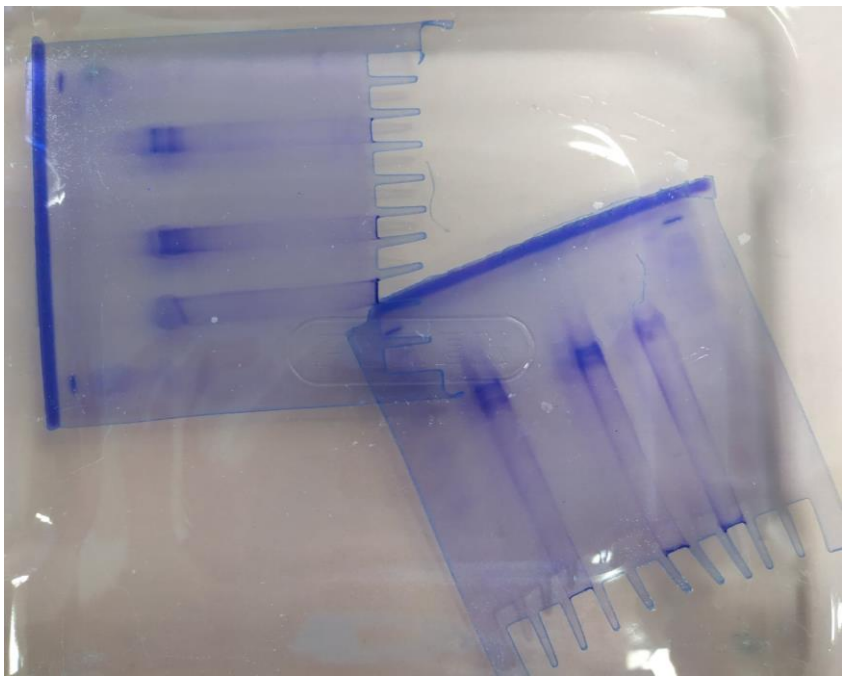

Figure 16. IEF gels for proteome of HeLa cells with and without [NaCOSAN] = 1 and 5 mM. The two gels consist of the same samples and were in parallel during a same experiment.

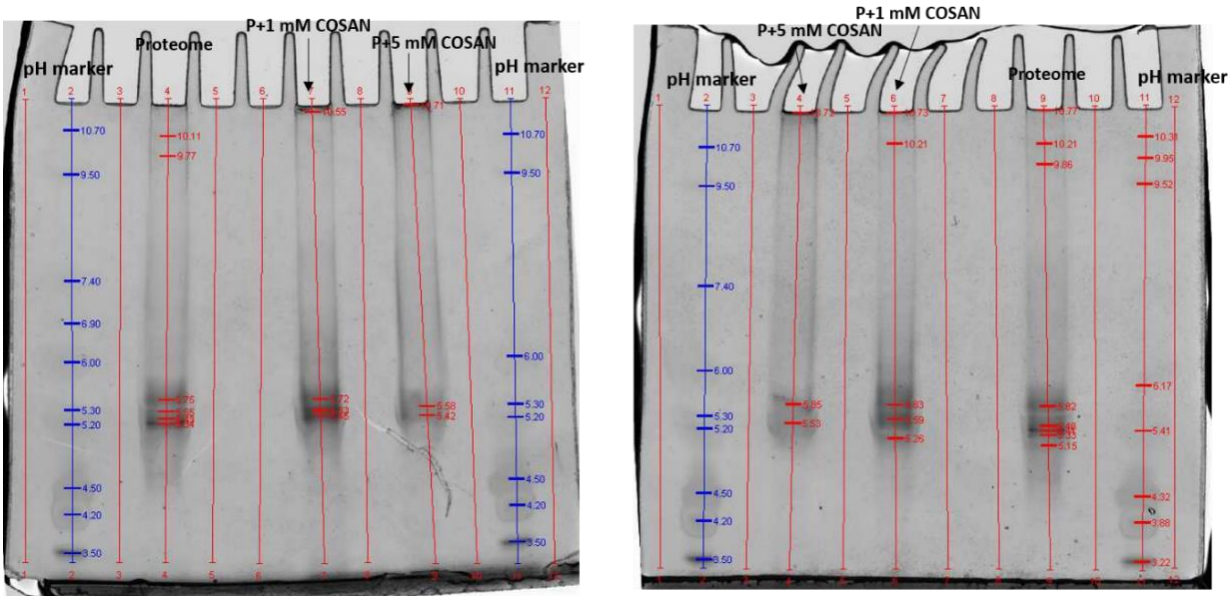

Figure 17. Scans of IEF gels of proteome of HeLa cells with and without [NaCOSAN] = 1 and 5 mM. The two gels consist of the same samples and were in parallel during a same experiment.

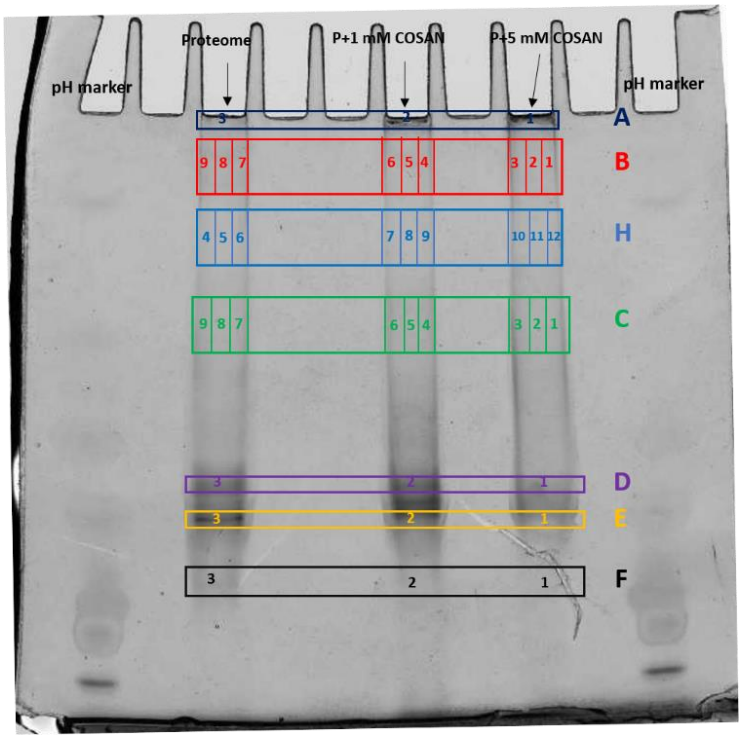

Figure 18. IEF gel scan for proteome of HeLa cells with and without [NaCOSAN] = 1 and 5 mM with representation of the interesting bands that were analyzed by mass spectrometry.

By observation of the proteins bands of the gel scans, several interesting bands were identified. We observed that some bands are affected in the presence of COSAN in comparison to the proteome control (without COSAN). Interesting regions of the gels have been chosen for their further analysis by mass spectrometry in order to identify the proteins that interacted with COSAN. The different bands of the gel that were cut and analyzed are indicated in Fig. 18.

For statistical requirement, IEF experiment of HeLa proteome in interaction with COSAN was repeated. Three gels of the same samples were run at the same time. The only difference was the finishing voltage that was 500 mV instead of 300 mV. We increased the finishing voltage in order to gain resolution and split the bands further. The resulting three gels did not show an enhancement of the resolution (see Fig. 19).

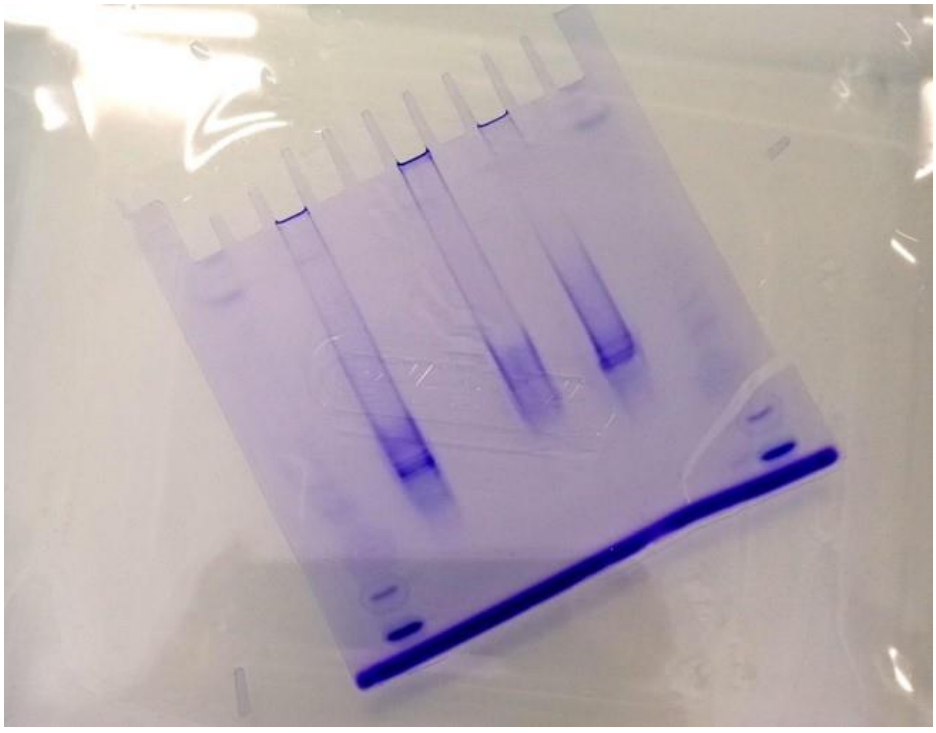

Figure 19. One of the three IEF gels that were run at the same time.

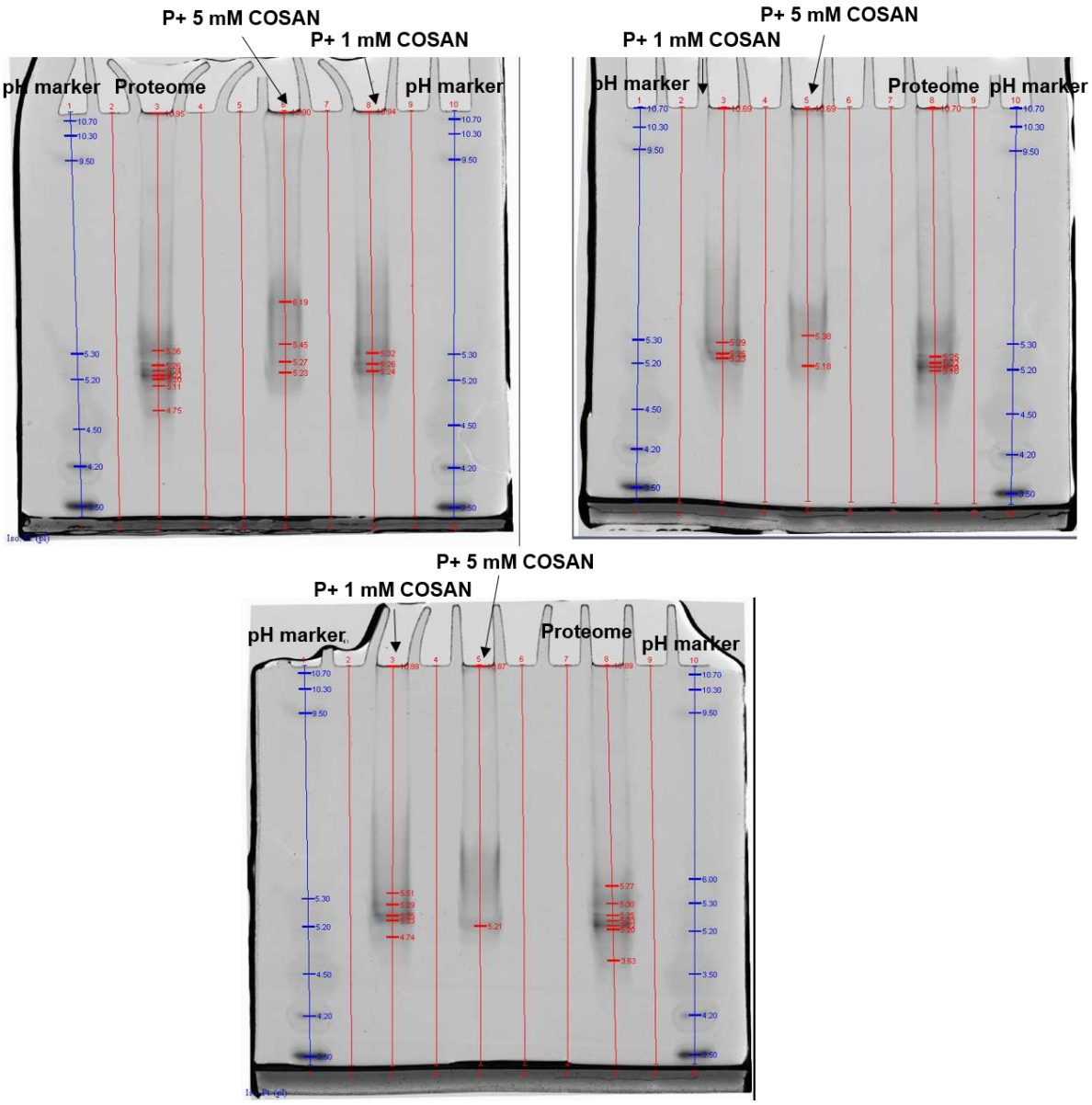

Figure 20. Scans of IEF gels of proteome of HeLa cells with and without [NaCOSAN] = 1 and 5 mM. The three gels consist of the same samples.

Several interesting bands were identified. Like the previous IEF experiment, we observed that some bands are affected in the presence of COSAN in comparison to the proteome control (without COSAN). Interesting regions of the gels have been chosen for their further analysis by mass spectrometry in order to identify the proteins that interacted with COSAN. The different bands of the gel that were cut and analyzed are indicated in Fig. 21-a.

It is essential to ensure that the bands of the three gels will be cut at the same level in order to have comparable results. For that, a manual drawn was put below the glass plate at which the gel will be cut (see Fig. 21-b).

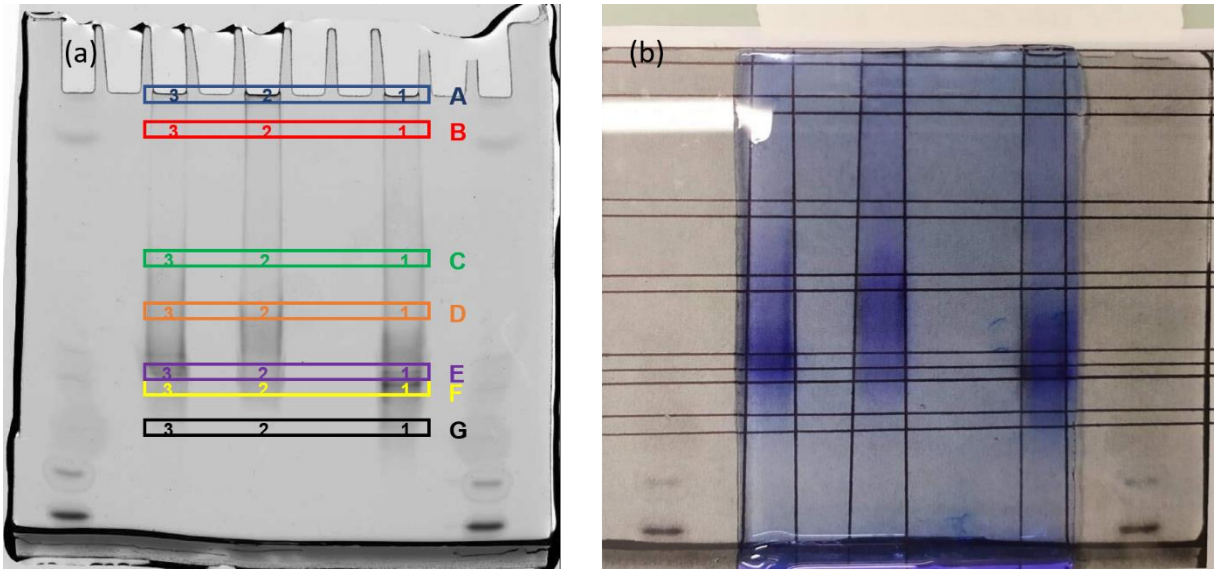

Figure 21. (a) The bands chosen for mass spectrometry analysis. (b) One of the obtained gels during the band cut procedure. A manual drawn was put below the glass plate in order to guide the cut the selected bands.

IV-2. Mass spectrometry analysis of selected bands

After peptides preparation from the selected bands and their analysis by mass spectrometry, 2000-3000 proteins were identified in each sample from the IEF gels of proteome. From an overview of the results, we observed some interesting effects. The results are partially presented in an Excel table that shows the spectral count (SC) of each identified protein in each sample (band) (see a part of this table as an example in Fig. 22). A shade of color was used in order to visualize easily if in the presence of COSAN the spectral count number of a specific protein is modified. If we look to the table in Fig. 22, we can observe that some proteins clearly interact with COSAN. For an illustration, let see at some examples. Indeed, the abundance of the proteins in the lines 13; 14; 16; 17 and 38 to 43 in specific pH range of the IEF gel presents some modifications between the proteins control (without COSAN) and the proteins in the presence of COSAN. 13 and 14 lines correspond to alpha enolase and beta enolase proteins respectively. For these two proteins belonging to the same family, they

precipitate in the wells in presence of COSAN. They are less abundant in the 9.5-10.7 pH region than the control and more abundant at all other pH region than the control except for beta enolase where it is more abundant at 4.5-5 pH range than the control. Another example is for the human actin protein, which corresponds to the lines 16 and 17. The actin protein that was found at pH 5.5-7 for the control was detected at pH 7-8 in the presence of COSAN. Let remark that for some proteins that was affected by the presence of COSAN, we could not detect their migration within the gel because we did not cut in parts all the gel.

A deeper treatment of these results is planned. Very recently, we have repeated this type of experiment and some band shifts were not always reproducible. So it is clear that it requests a high statistic in data collection to be able to define a general tendency. In fact, we are looking to prepare a macro that will be able to treat the data in a way that can help to find out the protein features that are responsible for their interactions with COSAN. For example, it will be interesting when a specific protein interacts with COSAN while the other proteins belonging to the same family (sharing more than 50% of amino acids sequences) does not. In this case, some specific differences in the amino acids sequences or the protein structure could be the key to find out the features that are responsible for the interactions.

Figure 22. A caption of the Excel sheet containing the mass spectrometry results of the IEF gel of the proteome. The red color corresponds to the lower SC. The green color corresponds to the higher SC.

V. Conclusion

In this chapter, we demonstrated that COSAN anion exhibits interactions with some proteins and not with some others. Indeed, some proteins features could be responsible for the interactions and the selectivity of COSAN toward proteins. It will be a great importance to find out what are the specific features that determine COSAN selectivity. This could be a necessary step for the understanding of the biological activities of COSAN as described in the first chapter and the introduction of the present one and therefore the development of its applications in this field.

Moreover, we demonstrated that COSAN interacts with the myoglobin at a pH higher than its isoelectric point, i.e. when the protein is negatively charged. It is interesting to observe that the negatively charged COSAN interacts with the negatively charged protein. These interactions could be strong enough to overcome the repulsions between COSAN anions and the negatively charged myoglobin. Indeed, the protein is not a homogenous macromolecule and it possesses neutral polar and nonpolar fragments, positively and negatively charge regions also. Here, we supposed that COSAN interacts with the hydrophobic pocket of myoglobin where the heme group is located. This might be one of the possible type of interactions between COSAN and the proteins. It has been shown for the analogous strong chaotropic cation guanidium that is also an amphiphilic surface-active ion that it interacts with the polar groups of the protein via hydrogen bonds.[Makhatadze, 1992; Makhatadze, 1999; Matějíček, 2020] COSAN is considered also as a superchaotropic species and therefore we could suppose that it interacts with the hydrated polar fragments of the proteins. In addition, COSAN can finally interact with the positively charged amino acids via electrostatic attractions due to its anionic nature.

VI. Annex of chapter 4

VI-1. Determination of the concentration of the proteins extracted from HeLa cells

The determination of proteins concentration was done according to the Bradford method **(Coomassie Plus (Bradford) Assay Kit-Thermo scientific)** described in the following:

Standard solutions of bovine serum albumin (BSA) with known concentrations and solutions containing the proteome with unknown concentrations were prepared in PBS. A Coomassie plus reagent that absorb at 595 nm and bind to the basic amino-acids was added to all the solutions, in order to measure the absorbance at 595 nm. Therefore, by measuring the absorbance of standard albumin solutions, a calibration curve can be established which will be used to determine the unknown quantity of proteins extracted from HeLa cells. As a result, the concentration of proteins extracted from HeLa cells was found to be 3 mg/ml.

VI-2. Preparation of cathode and anode buffer for the IEF experiment

The anode running buffer (lower buffer chamber) was prepared using 20 mL of IEF Anode Buffer and adding 980 mL of pure water. The cathode running buffer (upper buffer chamber was prepared using 20 mL of the appropriate IEF Cathode Buffer pH 3-10 and adding 180 mL pure water.

VI-3. IEF gel staining

Before staining of the gel, a step of fixation is necessary in order to fix the proteins in the gel. For that, the gel should be impregnated for 30 min in the fixation solution that consists of 20 mL ethanol 200 mL acetic acid and 250 mL pure water.

Once the proteins are fixed, the gel can be stained by the Coomassie Phastgel Blue R-350:

- Preparation of the staining stock solution by mixing a tablet of R-350 with 80 mL water for 5-10 min. Then, add 120 mL methanol.
- The staining solution is prepared by mixing 125 mL of the staining stock solution with 375 mL acetic acid 20% (v/v).

The gel should be impregnated for 1 hour in the staining solution.

to remove nonspecifically bound stain and visualize the proteins bands, a destaining procedure was followed. Therefore, the gel should be impregnated for 2×20 min followed by 1:30 hour in the destaining solution that consists of 250 mL ethanol 80 mL acetic acid and 670 mL pure water.

VI-4. Digestion of the proteins by trypsin gold/proteaseMAX™ Promega

VI-4-1. Washing

1. Destain with 200 µl of methanol:50 mM NH_4HCO_3 (1:1 v/v) for 1 minute with intermittent vortex mixing at 500 tr/min. Discard supernatant. Repeat once.
2. Dehydrate for 5 minutes in 200 µl of acetonitrile:50 mM NH_4HCO_3 (1:1 v/v) with intermittent vortex mixing at 500 tr/min. Discard supernatant. Add 200 µl of 100% acetonitrile, mix and incubate for 1 min at 500 tr/min. Discard the supernatant.
3. Dry in a Speed Vac® vacuum centrifuge for 5 minutes or until sample is dry.

VI-4-2. Reduction/Alkylation

1. Rehydrate in 100 µl of freshly prepared 25 mM DTT in 50 mM NH_4HCO_3, and incubate for 10 minutes at 56°C at 500 tr/min.
2. Discard supernatant. Add 100 µl of freshly prepared 55 mM iodoacetamide in 50 mM NH_4HCO_3, and incubate in the dark for 10 minutes at room temperature at 500 tr/min.
3. Discard supernatant, and wash with 200 µl of MilliQ water by vortex mixing at 550 tr/min for 1 minute. Discard supernatant. Repeat once.
4. Dehydrate for 5 minutes in 200 µl of acetonitrile:50 mM NH_4HCO_3 (1:1 v/v) with intermittent vortex mixing at 550 tr/min. Discard supernatant. Add 200 µl of 100% acetonitrile, mix at 550 tr/min for 1 min. Discard the supernatant.
5. Dry in a Speed Vac® vacuum centrifuge for 5 minutes or until sample is dry.

VI-4-3. Digestion

For 63 wells:

1. Rehydrate in 30 µl of enzymatic solution: ProteaseMAX™ 0.011% (1762.2 µl NH_4HCO_3 + 19.8 µl ProteaseMAX™ 1%) + trypsin gold 0.1 µg/µl in ice. Discard supernatant (excess of trypsin).
2. Add 75 µl of the incubation solution: ProteaseMAX™ 0.01% (4900.5 µl NH_4HCO_3 + 49.5 µl ProteaseMAX™ 1%). Mix for seconds at 200 tr/min. incubate for 1 hour at 50°C.

Collect the condensate from tube walls and transfer the digestion reaction with extracted peptides into a new tube. Add 5 µl TFA to a final concentration of 0.5% to inactivate trypsin. Mix and keep the tube on ice. If the digest is not going to be analyzed within several hours, snap-freeze it in dry ice and store at –20°C.

General conclusion and perspectives

I. Conclusion

In this work, the interactions between COSAN (and occasionally POMs) nano-ions and neutral biological functions and biological macromolecules were investigated.

COSAN is a nanometer-sized anion with a charge density below 3 charges per nm^3 (of the same order than tetraphenylborate anion) and so it's one of the lowest charge values known, while remaining fully water-soluble in its acid or sodium form.

First, we have demonstrated in water the strong interactions between COSAN and the C8G1 surfactant that is composed with a highly hydrated and neutral glucose moieties. The type of interaction, hydrophobic or superchaotropic, depends on the concentration of each species (COSAN and C8G1), which imposes the chemical potential of the species and thus the various equilibrium monomers ↔ (mixed-) aggregation. Below the CMC_0^{C8G1}, the interactions of COSAN with the C8G1 monomers arises mainly from the hydrophobic effect. However, increasing the C8G1 concentration, the COSAN nano-ion stabilizes the self-assemblies of C8G1 and leads to the decrease of the CMC_0^{C8G1}. The interaction of COSAN with C8G1 micelles is thus a water mediated mechanism driven by the superchaotropic nature of COSAN ions. Let mention that both the hydrophobic and the superchaotropic effects are water mediated i.e. characterized by a change in the hydration shells and with a release of the hydration water to the bulk phase upon binding. Indeed, the difference between the hydrophobic and the superchaotropic effect remains subtle. The balance entropically driven/ enthalpically driven process depends on the stoichiometry of the various solutes in water and on the relative difference in polarity between the guest and host molecules, the guest being the nano-ions and the host being the solute in interaction. It was shown by our group that the strength of the binding of nano-ions to surfaces (or to macrocycle [Assaf, 2015]) is related to the charge density of the nano-ions, the lowest the charge density the stronger the binding (see for the classification of POMs according a superchaotropy scale in Buchecker et al. Chem. Comm. 2018 [Buchecker, 2018]). The lower limit for the charge density is zero, which is the case for purely hydrophobic compounds, without considering polarity of surface moieties of the molecule. Therefore, decreasing charge density leads to an increased superchaotropicity as well as an increased hydrophobicity. This brings these two concepts to be intimately

interrelated. The different thermodynamic signatures as proposed by Nau's group [Assaf, 2015] may define the frontier between the two concepts.

Second, we investigated the interactions of different superchaotropic nano-ions (COSAN and POMs) with sugar moieties for which we can control their packing at water/air interface using glycolipids molecules submitted to a surface pressure. Indeed, it was not possible using micelles because the surface per polar head was fixed by the thermodynamical equilibrium. In this chapter, different types of glycolipids but same chemical nature (sugar headgroups and alkyl chains) were investigated, the MGDG-sat, the DGDG-sat and the MGDG-unsat, allowing a variation of the sugar-head density at an interface. The difference between the three glycolipids was indeed the lateral organization between the aliphatic chains and between the polar heads as a function of the surface pressure. MGDG-sat molecules formed the most rigid and less hydrated monolayer under compression whereas the MGDG-unsat molecules formed the most fluid and the more hydrated glycolipid monolayer. It was demonstrated in this project that the different nano-ions interact mainly with the glycolipids in the gaseous and the liquid expanded states of the glycolipids and the lower the charge density the stronger the interaction. Moreover, the adsorption of the nano-ions at the interface fluidifies the interface in delaying the formation of a solid or condensed monolayer. The study with COSAN was difficult because COSAN is also surface active and so different mechanism of interaction were superimposed. However, as with the other POM-type nano-ions, the interaction between COSAN and the glycolipids appears to be more pronounced when a degree of entropy exists at the interface under compression. If the glycolipid/glycolipid attraction via H-bounds is stronger than the COSAN/glycolipid interaction by decreasing the surface per molecules then the nano-ions will be desorbed from the interface.

Finally, we investigated the interactions of COSAN with proteins. COSAN interacts with some proteins and not with some others. The COSAN specificity toward proteins is still under investigation in order to determine the features of the proteins that are responsible for their interactions with COSAN. Even though this study is still under investigation, we realized that COSAN interacts with the myoglobin and does not interact with the trypsin inhibitor. Indeed, the myoglobin consists mainly of α-helices structures whereas the trypsin inhibitor consists mainly of β-sheets structures. It's known that β-sheets are rigid compared to α-helices. This observation is coherent with what was observed with the "first" and "second" parts of this conclusion. The more rigid is the molecule, the less is the interactions with COSAN.

This project highlights the interactions of COSAN with a ubiquitous function in the biological system that are the saccharides. In addition, the investigations of the specificity of COSAN toward proteins could allow the determination of the proteins features that are responsible for

their interactions with COSAN. Indeed, we will gain understanding of the mechanisms of interactions of COSAN with some specific proteins as well as of their effects on the cells growth and proliferation as highlighted in the first chapter. Therefore, I hope that this work could help for the future investigations related to the development of the COSAN applications in the pharmaceutical and medical fields.

II. Perspectives

Due to the limited time of the PhD thesis and the lockdown imposed for almost 3 months because of Covid-19, I did not have enough time to perform some complementary experiments. Therefore, here I will describe some experiments that I could have done.

In the second chapter at high concentration of COSAN and C8G1 we observed a phase demixion using brine at different concentration. The salt has screened the interaction between the charged mixed aggregates and induced a liquid/liquid phase separation with one of the phases very rich in surfactant, COSAN and salt that could be used as a new solvent. The one phase region beyond the 2-phase domain has to be exploited and so first probed in analyzing the corresponding phase boundaries.

We know already that inorganic nano-ions such as COSAN can be used to increase the solubilization of few water-soluble organic molecules, using the sticky charge effect of these nano-ions at low concentration. This is part of a ERC subject in the team. However, at very high concentration, COSAN can offer a new opportunity of solubilization of much less soluble organic molecule via the control of the osmotic pressure adding brine.

We tentatively tried to solubilized lipids by C8G1/NaCOSAN/NaCl solution for their extractions by C8G1/COSAN mixed aggregates by preparing solutions with different lipid concentration. However, the analysis is in progress in collaboration with the Laboratoire d'Etudes du Métabolisme des Médicaments at the Institut des sciences du vivant Frédéric Joliot.

Considering the interactions of nano-ions with the glycolipid monolayers, we have to finalize the P over A experiment on the MGDG-unsat and to analyse the pressure response in the gas or LE monophasic range to quantify the NI adsorption at different concentration of nano-ions in the subphase. MGDG-unsat system is finally expected to be the most suitable system to measure the difference in adsorption constants between each NI.

Another simple experiment that can help to proof the adsorption of the nano-ions on the glycolipid monolayer at the air/water interface would to use solid substrate dipping through the

monolayer and to analyze the coating using an AFM technique. We know that nano-ions have a very good surface contrast with this surface technique and we have an expert of this technique in our institute.

Finally, considering the study of the interactions of COSAN with proteins in the fourth chapter, several important experiments would be complementary for this study. The interactions of COSAN with the porphyrin of myoglobin can be verified by carrying out the study with two types of myoglobin, with and without heme group. A solution of myoglobin/COSAN 1:1 in D_2O was sent to Grenoble at the beginning of August 2020 to be analyzed by Synchrotron SAXS/SANS. This analysis could inform about the particles structure and give supplementary information to investigate whether the COSAN adsorb on the protein surface. A circular dichroism analysis of COSAN/myoglobin mixture could investigate the possible structure modifications of the myoglobin upon its interaction with COSAN. Also, it is worth analyzing a series of samples containing a fix COSAN concentration and varying myoglobin concentration by UV-visible spectroscopy. Therefore, we can check whether the absorption peak of COSAN at 280 nm will be shifted and affected like observed in the presence of C8G1 in the second chapter (see section I-2).
In parallel to the study of the interactions between COSAN and myoglobin, it is interesting to do the same study with a standard protein that does not interact with COSAN like the trypsin inhibitor (see Fig. 7 in section III). Let mention that myoglobin is composed mainly of α-helices while trypsin inhibitor is composed mainly of β-sheets. Moreover, the carbonic anhydrase protein is composed of both α-helices and β-sheets. Therefore, it could be interesting to complete the study with such a protein which structure composition is between myoglobin and trypsin inhibitor.

Also, a deeper investigation of the interactions of COSAN with the identified standard proteins can be performed. Indeed, the standard proteins that were identified for their interactions with COSAN (example myoglobin and carbonic anhydrase) can be digest into peptides before their mixture with COSAN. For each protein (or peptides of a specific protein), the peptides (in mixture with COSAN and without COSAN) can undergo a reversed phase liquid chromatography for their separation basing on their hydrophobicity. The peptides with a modified retention time are supposed to be responsible for the interactions of COSAN with the corresponding protein. Therefore, it will be possible to identify some features of the proteins that are responsible for COSAN specificity.

In addition, IEF gel can be performed in another setup. I used IEF with vertical migration of the proteins on a pH range 3-10 where 10 corresponds to the top of the gel (wells). Another IEF

setup that allows a horizontal migration could be interesting to test. Indeed, this later, is longer than the gel of IEF vertical migration, which allow a longer migration time that can gain in the resolution of the different proteins bands. And also, we can start with a pH lower than 10 to avoid the precipitation of the proteins in the wells (top of the gel).

Some difficulties

The Langmuir isotherms measurements were not performed using the same trough for several reasons and we have lost a lot of time to get reproducible data. We started to record the isotherms of the glycolipid monolayers at the Max Planck Institute in collaboration with Emanuel Schneck who have some expertise on these systems. When we would repeat these experiments at our institute we have got some mechanical problem with our Langmuir machine which are still not solved. Thus, we tried to use another set-up at IEM in Montpellier where unfortunately we did not get the same isotherms for DGDG-sat that made me puzzling and the COVID time prevented to check the problems certainly due to some different spreading concentrations.

For the synchrotron experiments (GIXD, TXRF and GIXOS), we got three campaigns of experiments at the DESY-synchrotron in Hamburg-Germany. However, we did not succeed to perform the experiments as much as we need in order to further investigate the effects of nano-ions on the glycolipid monolayers. Indeed, we had performed three runs at different dates and some surprising and not expected data at that time oriented us towards different experimental configurations that could not be exploited and some time was lost. Now with the hindsight, we would be more efficient.

IEF gel experiments are very delicate. Indeed, handling with the gel itself, which has a thickness of 1 mm, was not at all easy. The gels should be always in solution and can be very easily broken when transferring from a solution to another. The experimental stages are relatively long. Each IEF run lasted almost a week between the gels and samples preparation and the peptide preparation (digestion). Moreover, to cut the gel is not so evident, sometimes the bands cut-off re-stick to the gel. And also, for the region that we chose to cut and that there's no bands, it was hard to cut all the gels at the same level. In addition, some gels had a defect in their manufacture. It is not possible to know in advance that there is a defect until the staining of the IEF gels is complete. This results in the waste of time and finally, the COVID period did not help, one campaign of preparation was totally lost.

All these experiments require some expertise that takes time to learn and unfortunately, the PhD period is too short.

Résumé en français

Les ions sont partout quel que soit le milieu environnant, solide, liquide ou gazeux et parce qu'ils sont chargés, chaque ion est entouré d'une atmosphère ionique qui écrante sa charge et qui est caractérisé par une constante diélectrique. C'est pourquoi la matière est globalement neutre. Leurs interactions avec leur environnement sont caractérisées par des interactions électrostatiques qui peuvent être répulsives ou attractives et également par des interactions attractives dipolaires dues à la fluctuation du champ électrique produit par l'atmosphère ionique. L'une des principales caractéristiques des ions est leur propension à migrer si le milieu environnant le permet, d'où l'origine grecque du terme «ion» qui signifie «aller, bouger». C'est le cas de l'eau, liquide familier et si spécifique du fait de son dynamique réseau de liaisons H qu'elle est considérée comme la source de vie de l'homme. Cependant, cette source de vie est en partie liée aux migrations ioniques à travers les domaines extracellulaires, intracellulaires (dans le cytoplasme) et entre ces deux domaines où elles remplissent des rôles essentiels. Voici quelques exemples : le co-transport d'autres molécules essentielles pour les cellules à travers les membranes cellulaires, un rôle clé dans la transduction du signal pour les ions sodium. L'équilibre salin du corps humain qui joue un rôle clé pour le potentiel membranaire via la différence de charges à l'intérieur et à l'extérieur des cellules (ions sodium, potassium et calcium) est très important pour certaines fonctions (contraction des muscles, pompage du cœur ...), le transport de l'oxygène avec Fe^{2+} ou Fe^{3+} ainsi que étant des composants principaux comme les ions phosphates pour les acides nucléiques (ADN et ARN) et pour les membranes cellulaires (phospholipides).[Ussing, 2013]

Au fil des années, il a été démontré que l'état d'hydratation des ions et plus globalement l'activité des ions et du solvant doit être pris en compte dans de nombreuses propriétés ou caractéristiques physico-chimiques et doit être considéré comme spécifique de la nature ionique.

Les ions ont en effet des effets spécifiques qui semblent dépasser les interactions électrostatiques. Les effets ioniques spécifiques (SIE) ont été décrits dans la littérature depuis les années 1880 pour la première fois par Franz Hofmeister qui a classé les ions en fonction de leur capacité de retirer l'eau.[Hofmeister, 1888; Kunz, 2004] En général, les interactions basées sur des effets ioniques spécifiques avec d'autres composés sont médiées par des molécules d'eau.[Kunz, 2010]

Plus tard, les ions ont été classés en deux classes, les chaotropes et les kosmotropes. Les chaotropes sont des ions faiblement hydratés qui peuvent augmenter la solubilité des protéines dans des solutions aqueuses (salting-in). Par contre, les kosmotropes sont des ions

fortement hydratés qui peuvent diminuer la solubilité des protéines (salting-out).[Collins, 1997; Collins, 2004]

Plus récemment, les effets ioniques spécifiques ont également été étudiés avec des ions de taille nanométrique, c'est-à-dire plus grands que les ions classiques. Les ions de taille nanométrique comprennent différentes variétés de molécules, telles que les clusters du bore et des métal-oxygène. Pour les gros ions, caractérisés par une faible densité de charge, leurs effets de «salting-in» sont beaucoup plus prononcés que pour les ions classiques.[Assaf, 2018] En effet, il a été montré que certains des anions polyoxométalates (ou POM) et les clusters de bore s'adsorbent sur des surfaces ou des molécules hydratées neutres [Naskar, 2015; Buchecker, 2017; Buchecker, 2018; Hohenschutz, 2020] ou se lient aux poches hydrophobes de molécules de macrocycles comme la cyclodextrine à de faibles concentrations dans la gamme millimolaire [Assaf, 2015; Warneke, 2016; Assaf, 2018]

Dans ce projet de thèse, nous avons voulu approfondir l'étude de ces phénomènes, pour caractériser plus profondément la force et les conditions thermodynamiques de ces propriétés spécifiques. Nous avons concentré nos recherches sur les clusters de bore et plus particulièrement sur les composés de type métalla-bis-(dicarbollide). Pourquoi ces composés? Parce qu'ils sont chimiquement et thermiquement très stables quel que soit le milieu.[Gabel, 2015; Grimes, 2016] Par ailleurs, en terme d'objectifs et de forte motivation dans mes recherches, les composés des clusters de bore (dont les métalla-bis-(dicarbollide)) ont plusieurs intérêts dans les domaines médical et pharmaceutique. Par conséquent, les interactions ioniques spécifiques des clusters de bore avec les interfaces biologiques doivent être mieux comprises afin de développer leurs applications dans ces domaines. Nous avons fait le choix d'étudier leurs interactions avec les systèmes carbohydrates et les protéines.

Les carbohydrates ou molécules ou chaînes de glucides et souvent appelés sucres (saccharides) ou sucres polymères sont les biomolécules les plus abondantes sur terre et ont de nombreuses fonctions différentes dans les systèmes vivants. Par exemple, les groupes sanguins ABO correspondant à une classification du sang humain sont déterminés par les sucres sur les cellules sanguines.[Sharon, 1993] Les carbohydrates sont un constituant du squelette des acides nucléiques. [Gabius, 2017] Les cellules et d'autres structures cellulaires (noyau, mitochondries) sont délimitées par des membranes biologiques qui sont responsables de la translocation moléculaire vers et hors des cellules ainsi que des communications intercellulaires et de nombreuses fonctions importantes différentes.[Sharon, 1993] La bicouche lipidique est la structure commune pour toutes ces membranes biologiques. Cependant, les cellules portent également des parties à base de sucre qui sont constituées de glycoprotéines et de glycolipides, deux types de carbohydrates complexes dans lesquels

les groupes sucres sont liés aux lipides et aux protéines membranaires.[Sharon, 1993] Les carbohydrates ont une structure complexe, par exemple, deux monosaccharides peuvent former 11 disaccharides différents et quatre monosaccharides peuvent former 35 560 tétrasaccharides. Par conséquent, les monosaccharides représentent les lettres qui font des mots (signaux) dans notre système avec une capacité de codage élevée faisant des carbohydrates les principaux marqueurs de la reconnaissance cellulaire.[Sharon, 1993; Gabius, 2017] Notant que l'assemblé des carbohydrates sur les cellules cancéreuses est remarquablement différente de celle des cellules normales.[Sharon, 1993]

L'importance et l'abondance des carbohydrates (y compris les glycolipides) dans le corps humain étaient la raison pour laquelle dans ce projet nous avons choisi d'étudier leurs interactions avec le nano-ion cobalt-bis-(dicarbollide) (ou COSAN) (voir Fig. 1). Pour cela, les interactions du COSAN avec les molécules de glucosides sous formes monomères ou agrégées et avec des monocouches de glycolipides ont été étudiées.

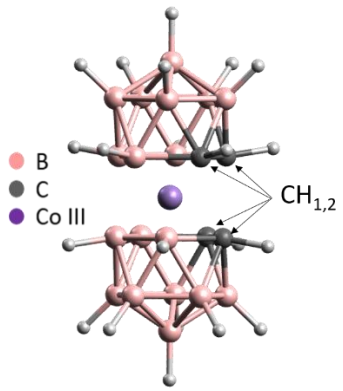

Figure 1. La structure du cobalt-bis-(dicarbollide) ou COSAN.

Dans la première partie, un tensioactif classique neutre à tête en sucre, le n-octyl-β-d-glucopyranoside (C8G1) (voir Fig. 2) a été choisi car il fournit une surface couverte de glucose hydraté en formant des micelles directes dans l'eau, au-dessus de sa concentration micellaire critique (CMC = 19 - 25,8 mM) (page 66 dans la référence [Ruiz, 2008])). De plus, les interactions du cobalt-bis-(dicarbollide) avec les sucres classiques, dimères et oligomères ont été étudiées afin de mieux comprendre les interactions avec les agrégats C8G1. COSAN est un anion qui présente des propriétés tensioactives en solution aqueuse et forme des agrégats (voir Fig. 3). Par conséquent, les mélanges de C8G1 et de COSAN concernent l'étude d'un mélange de deux molécules tensioactives qui forment des agrégats : un tensioactif amphiphile classique (tête polaire queue aliphatique) et un tensioactif non conventionnel respectivement. Différentes techniques ont été utilisées afin d'étudier ces interactions sur les échelles

moléculaires (spectroscopie UV-vis, RMN) et supramoléculaires (diffusion de la lumière, des rayons X et des neutrons) ainsi que les mesures de tension de surface comme technique complémentaire.

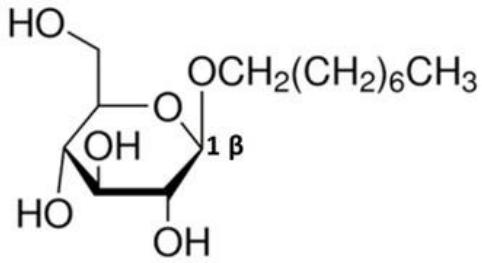

Figure 2. Structure moléculaire de l'octyl-glucopyranoside (C8G1).

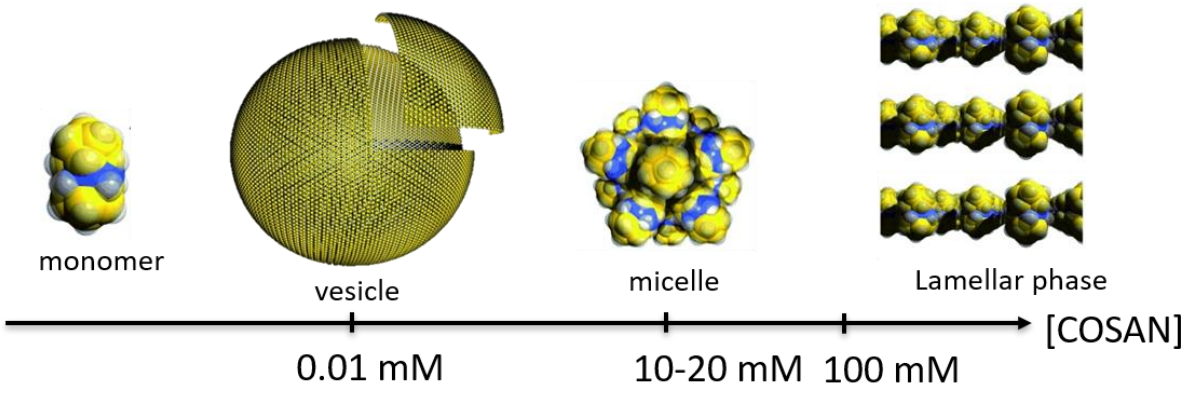

Figure 3. Représentation de l'auto-assemblage du COSAN en solution aqueuse.

Il a été montré ici sous de nombreux aspects que COSAN interagit fortement avec C8G1 pour former des agrégats mixtes en équilibre. En conclusion, le type d'assemblages C8G1 / COSAN dépend exclusivement des concentrations des deux espèces (voir Fig. 4) :

1) À faible teneur en COSAN (en dessous de sa concentration d'agrégation critique CAC), où coexistent des vésicules COSAN et des COSAN non agrégés (c'est-à-dire des monomères), les vésicules COSAN sont détruites par addition de C8G1 sous forme monomère, c'est-à-dire à des concentrations inférieures à la CMC de C8G1. Dans cette région de concentration, les nano-assemblages COSAN-C8G1, mis en évidence par RMN, sont formés par effet hydrophobe entre COSAN et la chaîne alkyle de C8G1.

2) À faible teneur en COSAN (en dessous du CAC) et à des concentrations élevées en C8G1 (au-dessus de la CMC), le COSAN s'adsorbe sur la surface hydratée des micelles C8G1. La liaison du COSAN à la surface micellaire conduit à une diminution de la CMC de C8G1, c'est-

à-dire à une stabilisation des micelles de C8G1. L'adsorption du COSAN résulte d'interactions collectives avec une surface recouverte de glucose, où des interactions locales entre COSAN avec de nombreuses unités de glucose apparaissent. Ceci a été confirmé par l'étude de mélanges de COSAN avec des mono- et di-sucres simples dans de l'eau qui n'a montré aucune liaison alors qu'une forte liaison à l'oligosaccharide linéaire (maltodextrine) a été observée. Par conséquent, de nombreux sucres, probablement plus de 3 à 5, dans un environnement local, sont nécessaires pour observer une liaison significative du COSAN. Selon l'approche expérimentale, la constante de liaison est approximativement estimée entre 0,2 et 0,5 mM^{-1}. Ce résultat est intéressant à comparer avec la formation de complexe stoechiométrique bien défini, c'est-à-dire 1:1 complexe hôte-invité, de COSAN avec les macrocycles à base de glucose, β ou γ-cyclodextrines contenant respectivement 7 et 8 unités de glucose, pour lesquelles les constantes la liaison de 0,026 et 0,191 mM^{-1} ont été obtenues. La forte liaison des ions de taille nanométrique avec des surfaces micellaires non ioniques [Naskar, 2015] ou dans la cavité des macrocycles [Assaf, 2015] a été précédemment expliquée comme provenant d'un effet médié par l'eau appelé l'effet chaotropique ou superchaotropicité concernant son effet beaucoup plus prononcé par rapport aux ions chaotropiques classiques tels que SCN^- ou I^-. Dans le présent travail, le comportement superchaotrope du COSAN est montré par son adsorption spontanée à la surface des micelles C8G1, comparativement aux nano-ions POM [Naskar, 2015; Buchecker, 2018; Hohenschutz, 2020] Ainsi, à des concentrations élevées de C8G1, l'effet superchaotropique est prédominant sur l'effet hydrophobe observé entre C8G1 et COSAN à faibles concentrations.

3) À haute teneur en COSAN (au-dessus du CAC), l'ajout de COSAN perturbe continuellement les micelles de C8G1, c'est-à-dire le COSAN pénètre dans la surface micellaire. En augmentant davantage les concentrations de COSAN, c'est-à-dire à des rapports COSAN / C8G1 plus élevés, les assemblages COSAN-C8G1 deviennent similaires en taille et en forme aux micelles COSAN mais contenant une petite quantité de molécules C8G1 solubilisées. De telles micelles de COSAN contenant des molécules de C8G1 dissoutes de manière moléculaire se forment probablement également à de faibles concentrations de C8G1 et à des concentrations élevées de COSAN. COSAN diffère ici des POM en raison des propriétés tensioactives du COSAN, c'est-à-dire principalement l'activité de surface et la formation de micelles. En effet, à concentration équivalente en POM, les POM ne pénètrent ni perturbent les micelles de C8G1.[Naskar, 2015]

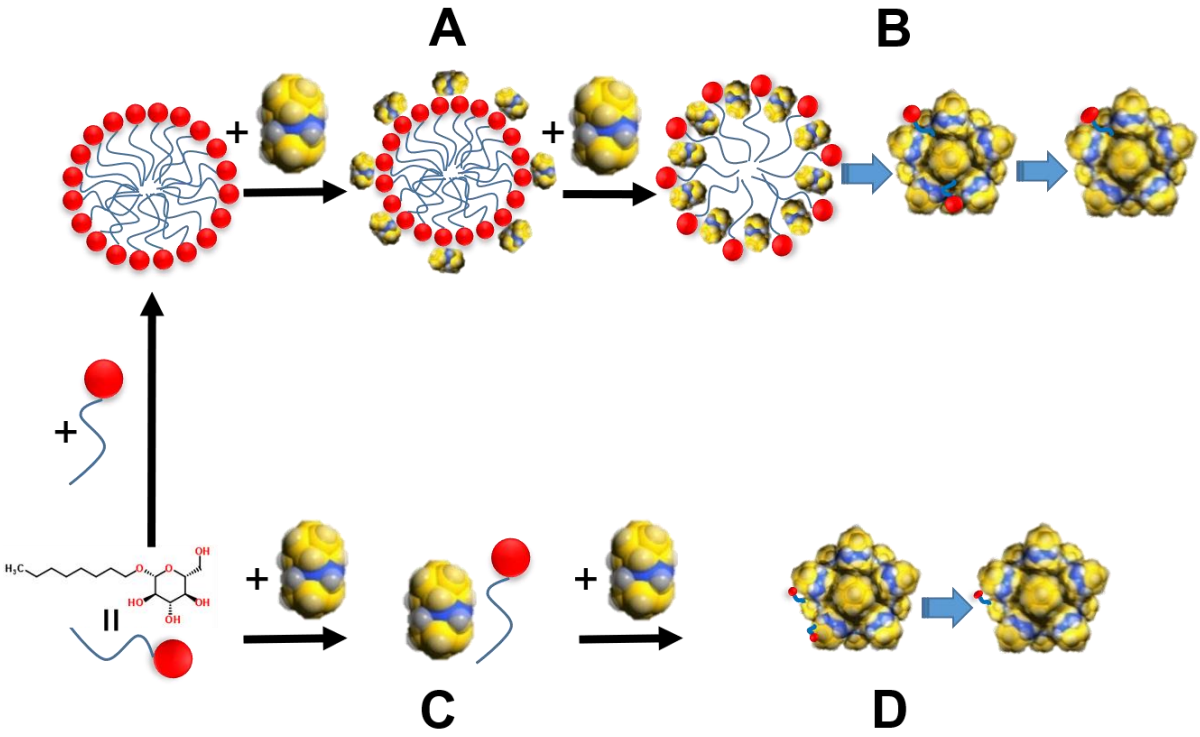

Figure 4. Une représentation qui résume les différents résultats obtenus sur le système COSAN/C8G1. A corresponds to the adsorption of COSAN onto C8G1 micelles by superchaotropicity. B corresponds to the Disruption of C8G1 micelles by COSAN. D corresponds to the co-assembly by the hydrophobic effect and D corresponds to the micellization of COSAN with co-solubilized C8G1.

Dans la deuxième partie, nous avons étendu l'étude de la première partie en étudiant les interactions de l'anion COSAN (et du polyoxométalate, un autre type d'anion de taille nanométrique) avec une monocouche de mono- et di-galactosyldiacylglycérol saturés (MGDG-sat et DGDG- sat) (voir Fig. 4) à divers états de compression 2D.

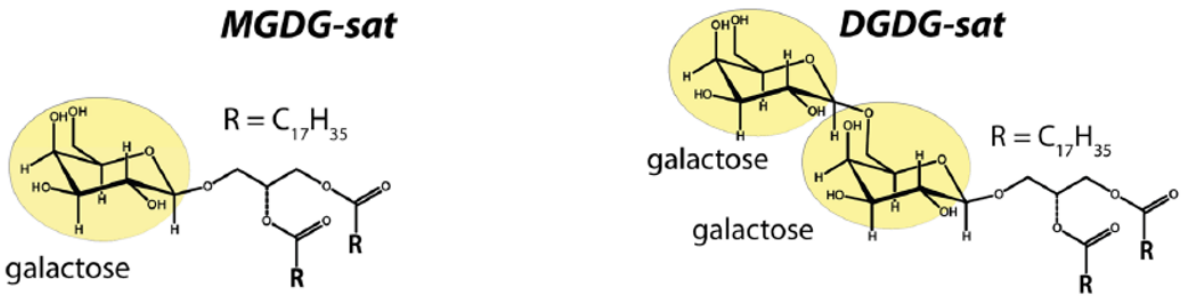

Figure 5. Structure moléculaire de MGDG-sat (gauche) et DGDG-sat (droite).

MGDG-sat et DGDG-sat sont des molécules amphiphiles avec des têtes polaires en sucre et de longues chaînes alkyles hydrophobes. En plus d'être des carbohydrates, les monocouches de glycolipides peuvent être considérées comme un modèle simple pour les membranes biologiques. En phase aqueuse, ils s'adsorbent à l'interface air / eau, et lorsqu'ils sont dans une balance de Langmuir, la compression de la surface augmente la concentration en glycolipides et entraîne la formation de monocouche. Ces interactions ont été étudiées à l'aide des techniques au Synchrotron DESY à Hambourg. Les nano-ions adsorbés sur la monocouche de glycolipide ont été quantifiés en utilisant les mesures de fluorescence X totale (TXRF). Les effets des nano-ions sur l'ordre des molécules de glycolipides ont été étudiés en utilisant la technique de diffraction des rayons X à incidence rasante (GIXD). La technique d'incidence rasante aux rayons X hors spéculaire (GIXOS) a également été appliquée pour déterminer le profil de densité électronique de la monocouche à l'interface. Voir la Fig. 6 qui résume les interprétations des résultats obtenus.

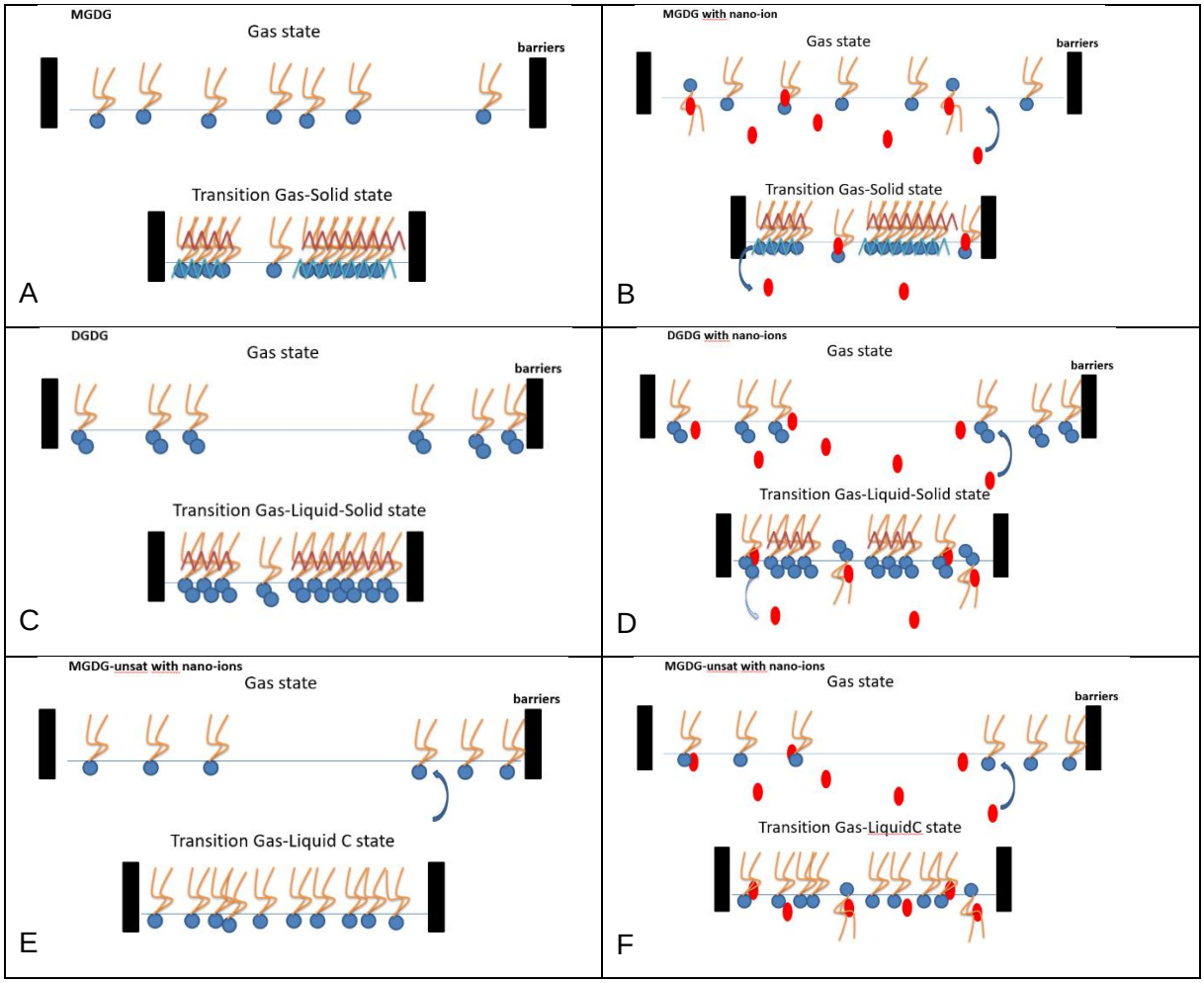

Figure 6. Glycolipides sous compression dans une cuve de Langmuir. A et B pour le MGDG-sat, C et D pour le DGDG-sat et E et F pour le MGDG-unsat. A droite avec nano-ion dans la sous-phase, à gauche sans. La différence entre les différents nano-ions est liée à la force de leur interaction avec l'interface du glycolipide. Le signe zig-zag qualifie l'ordre cristallin soit au niveau de la chaîne aliphatique, soit au

niveau de la tête polaire. En ce qui concerne le cas du MGDG-unsat, la représentation est une prédiction car trop peu d'expériences existe pour ce système.

Dans le dernier chapitre de ce projet, nous avons étudié les interactions du COSAN avec les protéines. Les protéines sont de grandes biomolécules ou macromolécules composées d'une ou plusieurs chaînes de résidus d'acides aminés. Les protéines sont l'un des principaux constituants des systèmes biologiques où elles sont une partie essentielle des organismes et participent à tous les processus au sein des cellules. Par conséquent, l'étude des interactions du COSAN avec les protéines est nécessaire. De plus, des effets intéressants du cobalt-bis-(dicarbollides) sur certaines protéines (comme la protéase du VIH) sont trouvés dans la littérature. L'objectif principal de ce travail était d'aller plus loin dans la compréhension et la spécificité du mode d'interactions du COSAN avec les protéines. Pour cela, les interactions du COSAN avec les protéines des cellules HeLa, c'est-à-dire des cellules cancéreuses humaines, ont été étudiées en utilisant la technique du gel de focalisation isoélectrique (IEF) couplée à une analyse par spectrométrie de masse. L'IEF a été utilisé comme technique pour séparer les protéines en fonction de leurs points isoélectriques (le pH auquel la charge globale d'une protéine est neutre).

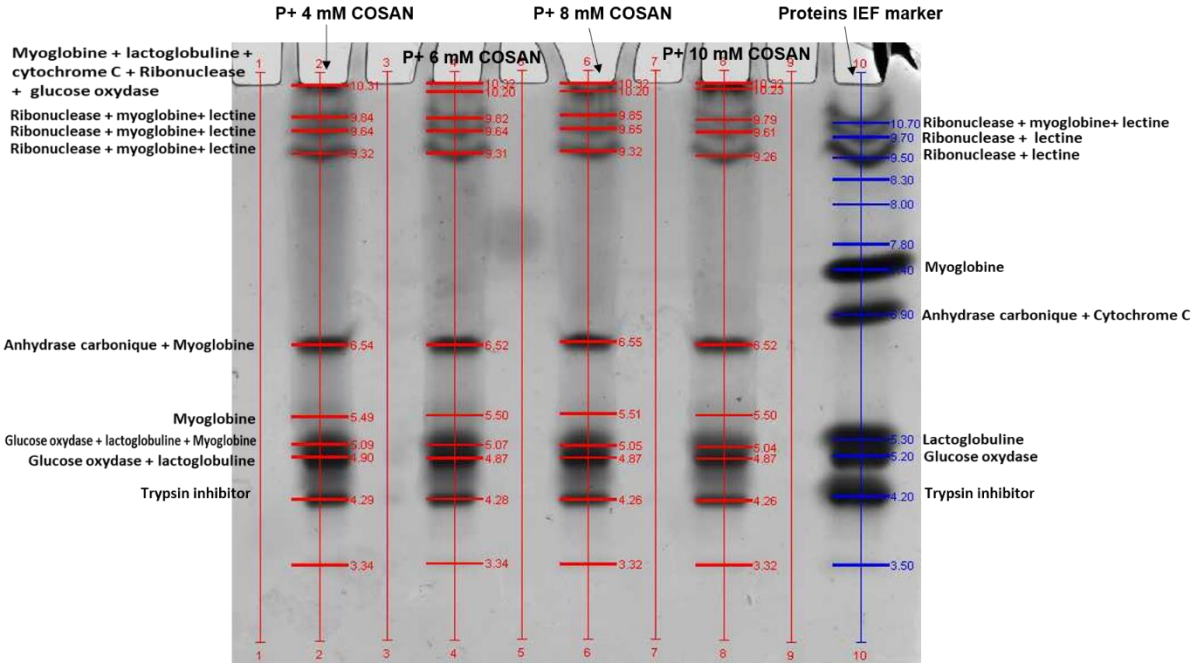

Figure 7. Les gels IEF des protéines marqueurs IEF avec et sans [NaCOSAN] = 4-10 mM. Les annotations des protéines sont les résultats d'une analyse par spectrométrie de masse. Comme résultats, quelques protéines sont précipitées dans les puits en présence du COSAN (exemple la myoglobine). Les points isoélectriques de quelques protéines ont été modifiés en présence du COSAN (exemple l'anhydrase carbonique). De plus, quelques protéines n'interagissent pas avec le COSAN d'où leur point isoélectrique n'est pas modifié (trypsine inhibitrice).

Lorsque les anions COSAN interagissent avec une protéine, la charge globale de la protéine sera modifiée, et donc son point isoélectrique. De plus, nous avons étudié les interactions du cobalt-bis-(dicarbollide) avec un ensemble de neuf protéines standards utilisées

habituellement comme marqueur IEF (référence pour le pH) (voir Fig. 7). D'autres études sur les protéines standard identifiées qui interagissaient avec le cobalt-bis-(dicarbollide) ont été effectuées afin de caractériser davantage leurs interactions en utilisant la spectroscopie UV-visible, la diffusion dynamique de la lumière (DLS) et les mesures du potentiel zêta.

Conclusion en français

Dans ce travail de thèse, les interactions entre les nano-ions COSAN (et parfois les POMs) et les fonctions biologiques neutres et les macromolécules biologiques ont été étudiées.

COSAN est un anion de taille nanométrique avec une densité de charge inférieure à 3 charges par nm^3 (du même ordre que l'anion tétraphénylborate) et donc l'une des plus faibles valeurs de charge connues, tout en restant totalement soluble dans l'eau sous sa forme acide ou sodium.

Tout d'abord, nous avons démontré dans l'eau, les fortes interactions entre le COSAN et le tensioactif C8G1 qui est constitué d'une tête de glucose hautement hydratées et neutres. Le type d'interaction, hydrophobe ou superchaotropique, dépend de la concentration de chaque espèce (COSAN et C8G1), qui impose le potentiel chimique de l'espèce et donc les différents équilibres monomères ↔ agrégats mixtes. En dessous du CMC_0^{C8G1}, les interactions du COSAN avec les monomères C8G1 proviennent principalement de l'effet hydrophobe. Cependant, en augmentant la concentration en C8G1, le nano-ion COSAN stabilise les autoassemblages de C8G1 et conduit à la diminution du CMC_0^{C8G1}. L'interaction du COSAN avec les micelles C8G1 est donc un mécanisme médié par les molécules d'eau entraîné par la nature superchaotropique des ions COSAN. Mentionnons que les effets hydrophobes et superchaotropes sont médiés par l'eau, c'est-à-dire caractérisés par un changement dans les couches d'hydratation et avec une libération de l'eau d'hydratation vers le volume lors de la liaison. En effet, la différence entre l'effet hydrophobe et l'effet superchaotrope reste subtile. L'équilibre processus entropique / enthalpique dépend de la stœchiométrie des différentes espèces dans l'eau et de la différence relative de polarité entre les molécules hôte et guest, le guest étant les nano-ions et l'hôte étant le soluté en interaction. Il a été montré par notre groupe que la force de la liaison des nano-ions aux surfaces (ou au macrocycle [Assaf, 2015]) est liée à la densité de charge des nano-ions, plus la densité de charge est faible, plus la liaison est forte (voir pour la classification des POM selon une échelle de superchaotropie dans Buchecker et al. Chem. Comm 2018 [Buchecker, 2018]). La limite inférieure de la densité de charge est zéro, ce qui est le cas pour les composés purement hydrophobes, sans tenir compte de la polarité des fragments de surface de la molécule. Par conséquent, la diminution de la densité de charge conduit à une superchaotropicité accrue ainsi qu'à une hydrophobicité accrue. Cela amène ces deux concepts à être intimement liés. Les différentes signatures thermodynamiques proposées par le groupe de Nau [Assaf, 2015] peuvent définir la frontière entre les deux concepts. L'effet hydrophobe étant un processus entropique et l'effet superchaotropique étant entraîné par l'enthalpie.

Deuxièmement, nous avons étudié les interactions de différents nano-ions superchaotropes (COSAN et POM) avec des fragments de sucre des molécules de glycolipides pour lesquels nous pouvons contrôler leur état de compression à l'interface eau / air en contrôlant la pression de surface. En effet, il n'était pas possible d'utiliser des micelles car la surface par tête polaire était fixée par l'équilibre thermodynamique. Dans ce chapitre, différents types de glycolipides mais de même nature chimique (tête sucre et chaînes alkyles) ont été étudiés, le MGDG-sat, le DGDG-sat et le MGDG-unsat, permettant une variation de la densité de la tête de sucre à une interface. La différence entre les trois glycolipides était en effet l'organisation latérale entre les chaînes aliphatiques et entre les têtes polaires en fonction de la pression de surface. Les molécules de MGDG-sat formaient la monocouche la plus rigide et la moins hydratée sous compression, tandis que les molécules de MGDG-insat formaient la monocouche de glycolipide la plus fluide et la plus hydratée. Il a été démontré dans ce projet que les différents nano-ions interagissent principalement avec les glycolipides dans les états expansés gazeux et liquides des glycolipides et plus la densité de charge est faible, plus l'interaction est forte. De plus, l'adsorption des nano-ions à l'interface fluidifie l'interface en retardant la formation d'une monocouche solide ou condensée. L'étude avec le COSAN est compliquée car le COSAN est également tensioactif et donc différents mécanismes d'interaction ont été superposés. Cependant, comme pour les autres nano-ions de type POM, l'interaction entre le COSAN et les glycolipides semble plus prononcée lorsqu'un degré d'entropie existe à l'interface sous compression. Si l'attraction glycolipide / glycolipide via les liaisons H est plus forte que l'interaction COSAN / glycolipide en diminuant la surface par molécule, alors les nano-ions seront désorbés de l'interface.

Enfin, nous avons étudié les interactions du COSAN avec les protéines. COSAN interagit avec certaines protéines et non avec d'autres. La spécificité du COSAN vis-à-vis des protéines est toujours à l'étude afin de déterminer les caractéristiques des protéines responsables de leurs interactions avec le COSAN. Même si cette étude est toujours à la recherche, nous avons réalisé que le COSAN interagit avec la myoglobine et n'interagit pas avec la trypsine inhibitrice. En effet, la myoglobine est principalement constituée de structures en hélices α alors que la trypsine inhibitrice est principalement constituée de structures en feuillets β. Sachant que les feuilles β sont rigides par rapport aux hélices α, cette observation est cohérente avec ce qui a été observé avec les «première» et «deuxième» parties de cette conclusion. Plus la molécule est rigide, moins il y a d'interactions avec le COSAN.

Ce projet met en évidence les interactions du COSAN avec une fonction omniprésente dans le système biologique qui sont les saccharides. De plus, les recherches sur la spécificité du COSAN vis-à-vis des protéines pourraient permettre de déterminer les caractéristiques des protéines responsables de leurs interactions avec le COSAN. En effet, nous allons acquérir

une compréhension des mécanismes d'interactions du COSAN avec certaines protéines spécifiques ainsi que de leurs effets sur la croissance et la prolifération des cellules. J'espère donc que ce travail pourra aider pour les futures investigations liées au développement des applications du COSAN dans les domaines pharmaceutique et médical.

References

- [Abe, 2004] Abe, M. (2004). *"Mixed surfactant systems"*. in, CRC Press.
- [Adamson, 2012] Adamson, A. (2012). *"A textbook of physical chemistry"*. in, Elsevier.
- [Ali, 2010] Ali, S., H. Farooqi, R. Prasad, M. Naime, I. Routray, S. Yadav and F. Ahmad (2010). *"Boron stabilizes peroxide mediated changes in the structure of heme proteins."* **International journal of biological macromolecules** 47(2): 109-115.
- [Allscher, 2008] Allscher, T., P. Klüfers and P. Mayer (2008). *"4.7 Carbohydrate-Metal Complexes: Structural Chemistry of Stable Solution Species."*
- [Arefian, 2017] Arefian, M., M. Mirzaei, H. Eshtiagh-Hosseini and A. Frontera (2017). *"A survey of the different roles of polyoxometalates in their interaction with amino acids, peptides and proteins."* **Dalton Transactions** 46(21): 6812-6829.
- [Aroti, 2007] Aroti, A., E. Leontidis, M. Dubois and T. Zemb (2007). *"Effects of monovalent anions of the hofmeister series on DPPC lipid bilayers Part I: swelling and in-plane equations of state."* **Biophysical journal** 93(5): 1580-1590.
- [Aroti, 2004] Aroti, A., E. Leontidis, E. Maltseva and G. Brezesinski (2004). *"Effects of Hofmeister anions on DPPC Langmuir monolayers at the air− water interface."* **The Journal of Physical Chemistry B** 108(39): 15238-15245.
- [Assaf, 2019] Assaf, K. I., B. Begaj, A. Frank, M. Nilam, A. S. Mougharbel, U. Kortz, J. Nekvinda, B. r. Grüner, D. Gabel and W. M. Nau (2019). *"High-Affinity Binding of Metallacarborane Cobalt Bis (dicarbollide) Anions to Cyclodextrins and Application to Membrane Translocation."* **The Journal of organic chemistry** 84(18): 11790-11798.
- [Assaf, 2019] Assaf, K. I., B. Begaj, A. Frank, M. Nilam, A. S. Mougharbel, U. Kortz, J. Nekvinda, B. r. Grüner, D. Gabel and W. M. Nau (2019). *"High-Affinity Binding of Metallacarborane Cobalt Bis (dicarbollide) Anions to Cyclodextrins and Application to Membrane Translocation."* **The Journal of organic chemistry**.
- [Assaf, 2016] Assaf, K. I., D. Gabel, W. Zimmermann and W. M. Nau (2016). *"High-affinity host–guest chemistry of large-ring cyclodextrins."* **Organic & biomolecular chemistry** 14(32): 7702-7706.
- [Assaf, 2018] Assaf, K. I. and W. M. Nau (2018). *"The chaotropic effect as an assembly motif in chemistry."* **Angewandte Chemie International Edition** 57(43): 13968-13981.
- [Assaf, 2015] Assaf, K. I., M. S. Ural, F. Pan, T. Georgiev, S. Simova, K. Rissanen, D. Gabel and W. M. Nau (2015). *"Water Structure Recovery in Chaotropic Anion Recognition: High-Affinity Binding of Dodecaborate Clusters to γ-Cyclodextrin."* **Angewandte Chemie International Edition** 54(23): 6852-6856.
- [Baldwin, 1996] Baldwin, R. L. (1996). *"How Hofmeister ion interactions affect protein stability."* **Biophysical journal** 71(4): 2056-2063.
- [Barth, 1999] Barth, R. F., A. H. Soloway, J. H. Goodman, R. A. Gahbauer, N. Gupta, T. E. Blue, W. Yang and W. Tjarks (1999). *"Boron neutron capture therapy of brain tumors: an emerging therapeutic modality."* **Neurosurgery** 44(3): 433-450.
- [Bastos-González, 2016] Bastos-González, D., L. Pérez-Fuentes, C. Drummond and J. Faraudo (2016). *"Ions at interfaces: the central role of hydration and hydrophobicity."* **Current Opinion in Colloid & Interface Science** 23: 19-28.
- [Bauduin, 2011] Bauduin, P., S. Prevost, P. Farràs, F. Teixidor, O. Diat and T. Zemb (2011). *"A theta-shaped amphiphilic cobaltabisdicarbollide anion: transition from monolayer vesicles to micelles."* **Angewandte Chemie International Edition** 50(23): 5298-5300.
- [Bauer, 2012] Bauer, C., P. Bauduin, L. Girard, O. Diat and T. Zemb (2012). *"Hydration of sugar based surfactants under osmotic stress: A SAXS study."* **Colloids and Surfaces A: Physicochemical and Engineering Aspects** 413: 92-100.

- [Bergström, 2000] Bergström, M. and J. C. Eriksson (2000). *"A theoretical analysis of synergistic effects in mixed surfactant systems."* **Langmuir** 16(18): 7173-7181.
- [Białek-Pietras, 2013] Białek-Pietras, M., A. B. Olejniczak, S. Tachikawa, H. Nakamura and Z. J. Leśnikowski (2013). *"Towards new boron carriers for boron neutron capture therapy: Metallacarboranes bearing cobalt, iron and chromium and their cholesterol conjugates."* **Bioorganic & medicinal chemistry** 21(5): 1136-1142.
- [Biedermann, 2014] Biedermann, F., W. M. Nau and H. J. Schneider (2014). *"The Hydrophobic Effect Revisited—Studies with Supramolecular Complexes Imply High-Energy Water as a Noncovalent Driving Force."* **Angewandte Chemie International Edition** 53(42): 11158-11171.
- [Bijelic, 2015] Bijelic, A. and A. Rompel (2015). *"The use of polyoxometalates in protein crystallography–An attempt to widen a well-known bottleneck."* **Coordination chemistry reviews** 299: 22-38.
- [Borrás-Almenar, 2003] Borrás-Almenar, J. J., E. Coronado, A. Müller and M. Pope (2003). *"Polyoxometalate molecular science"*. in, Springer Science & Business Media.
- [Boström, 2005] Boström, M., F. W. Tavares, S. Finet, F. Skouri-Panet, A. Tardieu and B. W. Ninham (2005). *"Why forces between proteins follow different Hofmeister series for pH above and below pI."* **Biophysical chemistry** 117(3): 217-224.
- [Brady, 1986] Brady, J. E., D. F. Evans, G. G. Warr, F. Grieser and B. W. Ninham (1986). *"Counterion specificity as the determinant of surfactant aggregation."* **The Journal of Physical Chemistry** 90(9): 1853-1859.
- [Brusselle, 2013] Brusselle, D., P. Bauduin, L. Girard, A. Zaulet, C. Viñas, F. Teixidor, I. Ly and O. Diat (2013). *"Lyotropic Lamellar Phase Formed from Monolayered 9-Shaped Carborane-Cage Amphiphiles."* **Angewandte Chemie International Edition** 52(46): 12114-12118.
- [Buchecker, 2017] Buchecker, T., X. Le Goff, B. Naskar, A. Pfitzner, O. Diat and P. Bauduin (2017). *"Polyoxometalate/Polyethylene Glycol Interactions in Water: From Nanoassemblies in Water to Crystal Formation by Electrostatic Screening."* **Chemistry–A European Journal** 23(35): 8434-8442.
- [Buchecker, 2019] Buchecker, T., P. Schmid, I. Grillo, S. Prevost, M. Drechsler, O. Diat, A. Pfitzner and P. Bauduin (2019). *"Self-assembly of short chain poly-n-isopropylacrylamid induced by superchaotropic keggin polyoxometalates: From globules to sheets."* **Journal of the American Chemical Society** 141(17): 6890-6899.
- [Buchecker, 2018] Buchecker, T., P. Schmid, S. Renaudineau, O. Diat, A. Proust, A. Pfitzner and P. Bauduin (2018). *"Polyoxometalates in the Hofmeister series."* **Chemical communications** 54(15): 1833-1836.
- [Bucior, 2004] Bucior, I. and M. M. Burger (2004). *"Carbohydrate–carbohydrate interactions in cell recognition."* **Current opinion in structural biology** 14(5): 631-637.
- [Bühl, 2005] Bühl, M., D. Hnyk and J. Macháček (2005). *"Computational study of structures and properties of metallaboranes: Cobalt bis (dicarbollide)."* **Chemistry–A European Journal** 11(14): 4109-4120.
- [Challa, 2005] Challa, R., A. Ahuja, J. Ali and R. K. Khar (2005). *"Cyclodextrins in drug delivery: an updated review."* **Aaps Pharmscitech** 6(2): E329-E357.
- [Chandler, 2005] Chandler, D. (2005). *"Interfaces and the driving force of hydrophobic assembly."* **Nature** 437(7059): 640-647.
- [Chen, 2017] Chen, G.-f., T.-h. Xu, Y. Yan, Y.-r. Zhou, Y. Jiang, K. Melcher and H. E. Xu (2017). *"Amyloid beta: structure, biology and structure-based therapeutic development."* **Acta Pharmacologica Sinica** 38(9): 1205-1235.
- [Christoforou, 2012] Christoforou, M., E. Leontidis and G. Brezesinski (2012). *"Effects of sodium salts of lyotropic anions on low-temperature, ordered lipid monolayers."* **The Journal of Physical Chemistry B** 116(50): 14602-14612.
- [Cicenas, 2018]

- [Cígler, 2005] Cígler, P., M. Kožíšek, P. Řezáčová, J. Brynda, Z. Otwinowski, J. Pokorná, J. Plešek, B. Grüner, L. Dolečková-Marešová and M. Máša (2005). *"From nonpeptide toward noncarbon protease inhibitors: metallacarboranes as specific and potent inhibitors of HIV protease."* **Proceedings of the National Academy of Sciences** 102(43): 15394-15399.
- [Coderre, 2003] Coderre, J. A., J. C. Turcotte, K. J. Riley, P. J. Binns, O. K. Harling and W. S. Kiger Iii (2003). *"Boron neutron capture therapy: cellular targeting of high linear energy transfer radiation."* **Technology in cancer research & treatment** 2(5): 355-375.
- [Collins, 1997] Collins, K. D. (1997). *"Charge density-dependent strength of hydration and biological structure."* **Biophysical journal** 72(1): 65-76.
- [Collins, 2004] Collins, K. D. (2004). *"Ions from the Hofmeister series and osmolytes: effects on proteins in solution and in the crystallization process."* **Methods** 34(3): 300-311.
- [Dash, 2017] Dash, B. P., R. Satapathy, B. R. Swain, C. S. Mahanta, B. B. Jena and N. S. Hosmane (2017). *"Cobalt bis(dicarbollide) anion and its derivatives."* **Journal of Organometallic Chemistry** 849-850: 170-194.
- [DeFrancesco, 2016] DeFrancesco, H., J. Dudley and A. Coca (2016)**.** *"Boron chemistry: an overview"*.in Boron Reagents in Synthesis, ACS Publications**:** 1-25.
- [Desnoyers, 1972] Desnoyers, J. E. and G. Perron (1972). *"The viscosity of aqueous solutions of alkali and tetraalkylammonium halides at 25 C."* **Journal of Solution Chemistry** 1(3): 199-212.
- [Dhapte, 2015] Dhapte, V. and P. Mehta (2015). *"Advances in hydrotropic solutions: an updated review."* **St. Petersburg Polytechnical University Journal: Physics and Mathematics** 1(4): 424-435.
- [Dishon, 2009] Dishon, M., O. Zohar and U. Sivan (2009). *"From repulsion to attraction and back to repulsion: the effect of NaCl, KCl, and CsCl on the force between silica surfaces in aqueous solution."* **Langmuir** 25(5): 2831-2836.
- [Dluhy, 1988] Dluhy, R. A., N. A. Wright and P. R. Griffiths (1988). *"In situ measurement of the FT-IR spectra of phospholipid monolayers at the air/water interface."* **Applied spectroscopy** 42(1): 138-141.
- [Endo, 2001] Endo, Y., T. Iijima, Y. Yamakoshi, H. Fukasawa, C. Miyaura, M. Inada, A. Kubo and A. Itai (2001). *"Potent estrogen agonists based on carborane as a hydrophobic skeletal structure: a new medicinal application of boron clusters."* **Chemistry & Biology** 8(4): 341-355.
- [Errachid, 2007] Errachid, A., D. Caballero, E. Crespo, F. Bessueille, M. Pla-Roca, C. A. Mills, F. Teixidor and J. Samitier (2007). *"Electropolymerization of nano-dimensioned polypyrrole micro-ring arrays on gold substrates prepared using submerged micro-contact printing."* **Nanotechnology** 18(48): 485301.
- [Essa, 2007] Essa, H., E. Magner, J. Cooney and B. K. Hodnett (2007). *"Influence of pH and ionic strength on the adsorption, leaching and activity of myoglobin immobilized onto ordered mesoporous silicates."* **Journal of Molecular Catalysis B: Enzymatic** 49(1-4): 61-68.
- [Farràs, 2013] Farràs, P., C. Viñas and F. Teixidor (2013). *"Preferential chlorination vertices in cobaltabisdicarbollide anions. Substitution rate correlation with site charges computed by the two atoms natural population analysis method (2a-NPA)."* **Journal of Organometallic Chemistry** 747: 119-125.
- [Fernandez-Alvarez, 2017] Fernandez-Alvarez, R., V. Dordovic, M. Uchman and P. Matejicek (2017). *"Amphiphiles without head-and-tail design: nanostructures based on the self-assembly of anionic boron cluster compounds."* **Langmuir** 34(12): 3541-3554.
- [Flores, 2012] Flores, S. C., J. Kherb and P. S. Cremer (2012). *"Direct and reverse Hofmeister effects on interfacial water structure."* **The Journal of Physical Chemistry C** 116(27): 14408-14413.
- [Fuentes, 2018] Fuentes, I., T. García-Mendiola, S. Sato, M. Pita, H. Nakamura, E. Lorenzo, F. Teixidor, F. Marques and C. Viñas (2018). *"Metallacarboranes on the Road to Anticancer Therapies: Cellular Uptake, DNA Interaction, and Biological Evaluation of Cobaltabisdicarbollide [COSAN]−."* **Chemistry–A European Journal** 24(65): 17239-17254.

- [Gabel, 2015] Gabel, D. (2015). *"Boron clusters in medicinal chemistry: perspectives and problems."* **Pure and Applied Chemistry** 87(2): 173-179.
- [Gabel, 1987] Gabel, D., S. Foster and R. G. Fairchild (1987). *"The Monte Carlo simulation of the biological effect of the 10B (n, α) 7Li reaction in cells and tissue and its implication for boron neutron capture therapy."* **Radiation research** 111(1): 14-25.
- [Gabius, 2017]
- [Gan, 2004] Gan, X., T. Liu, J. Zhong, X. Liu and G. Li (2004). *"Effect of silver nanoparticles on the electron transfer reactivity and the catalytic activity of myoglobin."* **ChemBioChem** 5(12): 1686-1691.
- [Gassin, 2015] Gassin, P. M., L. Girard, G. Martin-Gassin, D. Brusselle, A. Jonchere, O. Diat, C. Vinas, F. Teixidor and P. Bauduin (2015). *"Surface Activity and Molecular Organization of Metallacarboranes at the Air-Water Interface Revealed by Nonlinear Optics."* **Langmuir** 31(8): 2297-2303.
- [Geng, 2011] Geng, J., M. Li, J. Ren, E. Wang and X. Qu (2011). *"Polyoxometalates as inhibitors of the aggregation of amyloid β peptides associated with Alzheimer's disease."* **Angewandte Chemie International Edition** 50(18): 4184-4188.
- [Gibb, 2019] Gibb, B. C. (2019). *"Hofmeister's curse."*
- [Giordano, 1997] Giordano, R., G. Maisano and J. Teixeira (1997). *"Sans studies of octyl-β-glucoside and glycine micellar solutions."* **Journal of Applied Crystallography** 30(5): 761-764.
- [Girard, 2019] Girard, L., B. Naskar, J.-F. Dufrêche, J. Lai, O. Diat and P. Bauduin (2019). *"A thermodynamic model of non-ionic surfactants' micellization in the presence of polyoxometalates."* **Journal of Molecular Liquids** 293: 111280.
- [Glatter, 2000] Glatter, O., G. Fritz, H. Lindner, J. Brunner-Popela, R. Mittelbach, R. Strey and S. U. Egelhaaf (2000). *"Nonionic micelles near the critical point: micellar growth and attractive interaction."* **Langmuir** 16(23): 8692-8701.
- [Goszczyński, 2017] Goszczyński, T. M., K. Fink, K. Kowalski, Z. J. Leśnikowski and J. Boratyński (2017). *"Interactions of boron clusters and their derivatives with serum albumin."* **Scientific reports** 7(1): 9800.
- [Greenwood, 1999] Greenwood, R. and K. Kendall (1999). *"Selection of suitable dispersants for aqueous suspensions of zirconia and titania powders using acoustophoresis."* **Journal of the European Ceramic Society** 19(4): 479-488.
- [Grimes, 2000] Grimes, R. N. (2000). *"Metallacarboranes in the new millennium."* **Coordination Chemistry Reviews** 200: 773-811.
- [Grimes, 2016] Grimes, R. N. (2016). *"Carboranes"*. in, Academic Press.
- [Gustavsson, 1975] Gustavsson, H. and B. Lindman (1975). *"Nuclear magnetic resonance studies of the interaction between alkali ions and micellar aggregates."* **Journal of the American Chemical Society** 97(14): 3923-3930.
- [Hanaor, 2012] Hanaor, D., M. Michelazzi, C. Leonelli and C. C. Sorrell (2012). *"The effects of carboxylic acids on the aqueous dispersion and electrophoretic deposition of ZrO2."* **Journal of the European Ceramic Society** 32(1): 235-244.
- [Hawthorne, 1998] Hawthorne, M. F. (1998). *"New horizons for therapy based on the boron neutron capture reaction."* **Molecular medicine today** 4(4): 174-181.
- [Hawthorne, 1968] Hawthorne, M. F., D. C. Young, T. D. Andrews, D. V. Howe, R. L. Pilling, A. D. Pitts, M. Reintjes, L. F. Warren Jr and P. A. Wegner (1968). *". pi.-Dicarbollyl derivatives of the transition metals. Metallocene analogs."* **Journal of the American Chemical Society** 90(4): 879-896.
- [Hawthorne, 1965] Hawthorne, M. F., D. C. Young and P. A. Wegner (1965). *"Carbametallic Boron Hydride Derivatives .I. Apparent Analogs of Ferrocene and Ferricinium Ion."* **Journal of the American Chemical Society** 87(8): 1818-1819.
- [He, 2000] He, L. Z., V. Garamus, B. Niemeyer, H. Helmholz and R. Willumeit (2000). *"Determination of micelle structure of octyl-β-glucoside in aqueous solution by small angel neutron scattering and geometric analysis."* **Journal of Molecular Liquids** 89(1-3): 239-249.

- [Heskins, 1968] Heskins, M. and J. E. Guillet (1968). *"Solution properties of poly (N-isopropylacrylamide)."* **Journal of Macromolecular Science—Chemistry** 2(8): 1441-1455.
- [Heyda, 2009] Heyda, J., J. Pokorná, L. Vrbka, R. Vácha, B. Jagoda-Cwiklik, J. Konvalinka, P. Jungwirth and J. Vondrášek (2009). *"Ion specific effects of sodium and potassium on the catalytic activity of HIV-1 protease."* **Physical Chemistry Chemical Physics** 11(35): 7599-7604.
- [Hill, 1990] Hill, C. L., M. S. Weeks and R. F. Schinazi (1990). *"Anti-HIV-1 activity, toxicity, and stability studies of representative structural families of polyoxometalates."* **Journal of medicinal chemistry** 33(10): 2767-2772.
- [Hinz, 1991] Hinz, H. J., H. Kuttenreich, R. Meyer, M. Renner, R. Fründ, R. Koynova, A. Boyanov and B. Tenchov (1991). *"Stereochemistry and size of sugar head groups determine structure and phase behavior of glycolipid membranes: densitometric, calorimetric, and X-ray studies."* **Biochemistry** 30(21): 5125-5138.
- [Hofmeister, 1888] Hofmeister, F. (1888). *"Zur lehre von der wirkung der salze."* **Archiv für experimentelle Pathologie und Pharmakologie** 25(1): 1-30.
- [Hohenschutz, 2020] Hohenschutz, M., I. Grillo, O. Diat and P. Bauduin (2020). *"How Nano-Ions Act Like Ionic Surfactants."* **Angewandte Chemie**.
- [Holland, 1992] Holland, P. M. and D. N. Rubingh (1992)**.** *"Mixed surfactant systems: an overview"*, ACS Publications.
- [Hoyo, 2016] Hoyo, J., E. Guaus and J. Torrent-Burgués (2016). *"Monogalactosyldiacylglycerol and digalactosyldiacylglycerol role, physical states, applications and biomimetic monolayer films."* **The European Physical Journal E** 39(3): 39.
- [Hua, 1982] Hua, X. Y. and M. J. Rosen (1982). *"Calculation of the coefficient in the Gibbs equation for the adsorption of ionic surfactants from aqueous binary mixtures with nonionic surfactants."* **Journal of Colloid and Interface Science** 87(2): 469-477.
- [Hunt, 1989] Hunt, R. D., M. L. Mitchell and R. A. Dluhy (1989). *"The interfacial structure of phospholipid monolayer films: an infrared reflectance study."* **Journal of molecular structure** 214: 93-109.
- [Israelachvili, 2011] Israelachvili, J. N. (2011). *"Intermolecular and surface forces"*. in, Academic press.
- [Israelachvili, 1976] Israelachvili, J. N., D. J. Mitchell and B. W. Ninham (1976). *"Theory of self-assembly of hydrocarbon amphiphiles into micelles and bilayers."* **Journal of the Chemical Society, Faraday Transactions 2: Molecular and Chemical Physics** 72: 1525-1568.
- [Jańczuk, 2019] Jańczuk, B. and A. Zdziennicka (2019). *"Critical micelle concentration, composition and thermodynamic properties of n-octyl-β-d-glucopyranoside and sodium dodecylsulfate mixed micelles."* **Journal of Molecular Liquids** 286: 110748.
- [Jarvis, 1968] Jarvis, N. L. and M. A. Scheiman (1968). *"Surface potentials of aqueous electrolyte solutions."* **The Journal of Physical Chemistry** 72(1): 74-78.
- [Jost, 1988] Jost, F., H. Leiter and M. J. Schwuger (1988). *"Synergisms in binary surfactant mixtures."* **Colloid and Polymer Science** 266(6): 554-561.
- [Judd, 2001] Judd, D. A., J. H. Nettles, N. Nevins, J. P. Snyder, D. C. Liotta, J. Tang, J. Ermolieff, R. F. Schinazi and C. L. Hill (2001). *"Polyoxometalate HIV-1 protease inhibitors. A new mode of protease inhibition."* **Journal of the American Chemical Society** 123(5): 886-897.
- [Jungwirth, 2000] Jungwirth, P. and D. J. Tobias (2000). *"Surface effects on aqueous ionic solvation: A molecular dynamics simulation study of NaCl at the air/water interface from infinite dilution to saturation."* **The Journal of Physical Chemistry B** 104(32): 7702-7706.
- [Karki, 2012] Karki, K., D. Gabel and D. Roccatano (2012). *"Structure and dynamics of dodecaborate clusters in water."* **Inorganic Chemistry** 51(9): 4894-4896.
- [Kobayashi, 2017] Kobayashi, D., H. Nakahara, O. Shibata, K. Unoura and H. Nabika (2017). *"Interplay of hydrophobic and electrostatic interactions between polyoxometalates and lipid molecules."* **The Journal of Physical Chemistry C** 121(23): 12895-12902.

- [Koelsch, 2004] Koelsch, P. and H. Motschmann (2004). *"An experimental route to Hofmeister."* **Current opinion in colloid & interface science** 9(1-2): 87-91.
- [Kohno, 1996] Kohno, J., T. Kawahata, T. Otake, M. Morimoto, H. Mori, N. Ueba, M. Nishio, A. Kinumaki, S. Komatsubara and K. Kawashima (1996). *"Boromycin, an anti-HIV antibiotic."* **Bioscience, biotechnology, and biochemistry** 60(6): 1036-1037.
- [Kožíšek, 2008] Kožíšek, M., P. Cígler, M. Lepšík, J. i. Fanfrlík, P. n. Řezáčová, J. i. Brynda, J. Pokorná, J. r. Plešek, B. r. Grüner and K. r. Grantz Šašková (2008). *"Inorganic polyhedral metallacarborane inhibitors of HIV protease: a new approach to overcoming antiviral resistance."* **Journal of medicinal chemistry** 51(15): 4839-4843.
- [Kronberg, 2003] Kronberg, B. and B. Lindman (2003). *"Surfactants and polymers in aqueous solution"*. in, John Wiley & Sons Ltd., Chichester.
- [Kumar, 2017] Kumar, A. and C. K. Dixit (2017)**.** *"Methods for characterization of nanoparticles"*.in Advances in Nanomedicine for the Delivery of Therapeutic Nucleic Acids, Elsevier**:** 43-58.
- [Kunitz, 1947] Kunitz, M. (1947). *"Crystalline soybean trypsin inhibitor II. General properties."* **Journal of General Physiology** 30(4): 291-310.
- [Kunz, 2010] Kunz, W. (2010). *"Specific ion effects"*. in, World Scientific.
- [Kunz, 2004] Kunz, W., J. Henle and B. W. Ninham (2004). *"'Zur Lehre von der Wirkung der Salze'(about the science of the effect of salts): Franz Hofmeister's historical papers."* **Current Opinion in Colloid & Interface Science** 9(1-2): 19-37.
- [Kuznetsov, 1997] Kuznetsov, I. B., P. S. Morozov and Y. G. Matushkin (1997). *"Prion proteins: evolution and preservation of secondary structure."* **FEBS letters** 412(3): 429-432.
- [Ładniak, 2019] Ładniak, A., M. Jurak and A. E. Wiącek (2019). *"Langmuir monolayer study of phospholipid DPPC on the titanium dioxide–chitosan–hyaluronic acid subphases."* **Adsorption** 25(3): 469-476.
- [Lainez, 2004] Lainez, A., P. del Burgo, E. Junquera and E. Aicart (2004). *"Mixed micelles formed by n-octyl-β-D-glucopyranoside and tetradecyltrimethylammonium bromide in aqueous media."* **Langmuir** 20(14): 5745-5752.
- [Lee, 2005] Lee, I. S., J. R. Long, S. B. Prusiner and J. G. Safar (2005). *"Selective precipitation of prions by polyoxometalate complexes."* **Journal of the American Chemical Society** 127(40): 13802-13803.
- [Leontidis, 2016] Leontidis, E. (2016). *"Chaotropic salts interacting with soft matter: beyond the lyotropic series."* **Current opinion in colloid & interface science** 23: 100-109.
- [Leontidis, 2017] Leontidis, E. (2017). *"Investigations of the Hofmeister series and other specific ion effects using lipid model systems."* **Advances in colloid and interface science** 243: 8-22.
- [Leontidis, 2009] Leontidis, E. and A. Aroti (2009). *"Liquid expanded monolayers of lipids as model systems to understand the anionic Hofmeister series: 2. Ion partitioning is mostly a matter of size."* **The Journal of Physical Chemistry B** 113(5): 1460-1467.
- [Leontidis, 2009] Leontidis, E., A. Aroti and L. Belloni (2009). *"Liquid expanded monolayers of lipids as model systems to understand the anionic Hofmeister series: 1. A tale of models."* **The Journal of Physical Chemistry B** 113(5): 1447-1459.
- [Leśnikowski, 2005] Leśnikowski, Z. J., E. Paradowska, A. B. Olejniczak, M. Studzińska, P. Seekamp, U. W. Schuessler, D. Gabel, R. F. Schinazi and J. Plešek (2005). *"Towards new boron carriers for boron neutron capture therapy: metallacarboranes and their nucleoside conjugates."* **Bioorganic & medicinal chemistry** 13(13): 4168-4175.
- [Lis, 1998] Lis, H. and N. Sharon (1998). *"Lectins: carbohydrate-specific proteins that mediate cellular recognition."* **Chemical reviews** 98(2): 637-674.
- [Loget, 2011] Loget, G., S. Chevance, C. Poriel, G. Simonneaux, C. Lagrost and J. Rault-Berthelot (2011). *"Direct Electron Transfer of Hemoglobin and Myoglobin at the Bare Glassy Carbon Electrode in an Aqueous BMI. BF4 Ionic-Liquid Mixture."* **ChemPhysChem** 12(2): 411-418.

- [López-León, 2008] López-León, T., M. J. Santander-Ortega, J. L. Ortega-Vinuesa and D. Bastos-González (2008). *"Hofmeister effects in colloidal systems: influence of the surface nature."* **The Journal of Physical Chemistry C** 112(41): 16060-16069.
- [Luo, 2006] Luo, G., S. Malkova, J. Yoon, D. G. Schultz, B. Lin, M. Meron, I. Benjamin, P. Vanýsek and M. L. Schlossman (2006). *"Ion distributions near a liquid-liquid interface."* **Science** 311(5758): 216-218.
- [Makhatadze, 1999]
- [Makhatadze, 1992] Makhatadze, G. I. and P. L. Privalov (1992). *"Protein interactions with urea and guanidinium chloride: a calorimetric study."* **Journal of molecular biology** 226(2): 491-505.
- [Malaspina, 2020] Malaspina, D. C., C. Vinas, F. Teixidor and J. Faraudo (2020). *"Atomistic Simulations of COSAN: Amphiphiles without a Head-and-Tail Design Display" Head and Tail" Surfactant Behavior."* **Angewandte Chemie (International ed. in English)** 59(8): 3088-3092.
- [Mańko, 2014] Mańko, D., A. Zdziennicka and B. Jańczuk (2014). *"Thermodynamic properties of adsorption and micellization of n-oktyl-β-d-glucopiranoside."* **Colloids and Surfaces B: Biointerfaces** 114: 170-176.
- [Marcus, 2009] Marcus, Y. (2009). *"Effect of ions on the structure of water: structure making and breaking."* **Chemical reviews** 109(3): 1346-1370.
- [Masalles, 2002] Masalles, C., J. Llop, C. Viñas and F. Teixidor (2002). *"Extraordinary Overoxidation Resistance Increase in Self-Doped Polypyrroles by Using Non-conventional Low Charge-Density Anions."* **Advanced Materials** 14(11): 826-829.
- [Matějíček, 2020] Matějíček, P. (2020). *"Erratic ions: self-assembly and coassembly of ions of nanometer size and of irregular structure."* **Current Opinion in Colloid & Interface Science** 45: 97-107.
- [Matějíček, 2006] Matějíček, P., P. Cígler, K. Procházka and V. Král (2006). *"Molecular assembly of metallacarboranes in water: light scattering and microscopy study."* **Langmuir** 22(2): 575-581.
- [Mátel, 1982] Mátel, Ľ., F. Macášek, P. Rajec, S. Heřmánek and J. Plešek (1982). *"B-Halogen derivatives of the bis (1, 2-dicarbollyl) cobalt (III) anion."* **Polyhedron** 1(6): 511-519.
- [McNaught, 1997] McNaught, A. D. and A. Wilkinson (1997). *"Compendium of chemical terminology"*. in, Blackwell Science Oxford.
- [Merhi, 2020] Merhi, T., A. Jonchère, L. Girard, O. Diat, M. Nuez, C. Viñas and P. Bauduin (2020). *"Highlights on the binding of cobalta-bis-(dicarbollide) with glucose units."* **Chemistry (Weinheim an der Bergstrasse, Germany)**.
- [Michler, 2015] Michler, D., N. Shahidzadeh, M. Westbroek, R. van Roij and D. Bonn (2015). *"Are antagonistic salts surfactants?"* **Langmuir** 31(3): 906-911.
- [Mitchell, 1988] Mitchell, M. L. and R. A. Dluhy (1988). *"In situ FT-IR investigation of phospholipid monolayer phase transitions at the air water interface."* **Journal of the American Chemical Society** 110(3): 712-718.
- [Mondal, 2015] Mondal, S., S. Das and S. Ghosh (2015). *"Interaction of myoglobin with cationic gemini surfactants in phosphate buffer at pH 7.4."* **Journal of Surfactants and Detergents** 18(3): 471-476.
- [Moreira, 2010] Moreira, L. and A. Firoozabadi (2010). *"Molecular thermodynamic modeling of specific ion effects on micellization of ionic surfactants."* **Langmuir** 26(19): 15177-15191.
- [Morris, 1968]Morris, D. F. C. (1968)**.** *"Ionic radii and enthalpies of hydration of ions"*.in Structure and bonding, Springer**:** 63-82.
- [Moussawi, 2017] Moussawi, M. A., M. Haouas, S. Floquet, W. E. Shepard, P. A. Abramov, M. N. Sokolov, V. P. Fedin, S. Cordier, A. Ponchel and E. Monflier (2017). *"Nonconventional three-component hierarchical host–guest assembly based on Mo-blue ring-shaped giant anion, γ-cyclodextrin, and Dawson-type polyoxometalate."* **Journal of the American Chemical Society** 139(41): 14376-14379.

- [Moussawi, 2017] Moussawi, M. A., N. Leclerc-Laronze, S. Floquet, P. A. Abramov, M. N. Sokolov, S. Cordier, A. Ponchel, E. Monflier, H. Bricout and D. Landy (2017). *"Polyoxometalate, cationic cluster, and γ-cyclodextrin: from primary interactions to supramolecular hybrid materials."* **Journal of the American Chemical Society** 139(36): 12793-12803.
- [Mrázová, 2008] Mrázová, B., M. Martínková, V. Martínek, E. Frei and M. Stiborová (2008). *"Optimalization of preparation of apocytochrome b5 utilizing apo-myoglobin."* **Interdisciplinary Toxicology** 1(2): 190-192.
- [Mukerjee, 1967] Mukerjee, P. (1967). *"The nature of the association equilibria and hydrophobic bonding in aqueous solutions of association colloids."* **Advances in Colloid and Interface Science** 1(3): 242-275.
- [Nabika, 2013] Nabika, H., Y. Inomata, E. Itoh and K. Unoura (2013). *"Activity of Keggin and Dawson polyoxometalates toward model cell membrane."* **RSC advances** 3(44): 21271-21274.
- [Naskar, 2015] Naskar, B., O. Diat, V. r. Nardello-Rataj and P. Bauduin (2015). *"Nanometer-size polyoxometalate anions adsorb strongly on neutral soft surfaces."* **The Journal of Physical Chemistry C** 119(36): 20985-20992.
- [Neuberg, 1916] Neuberg, C. (1916). *"Hydrotropic phenomena."* **Biochem. Z** 76(107): 107-176.
- [Nilsson, 1996] Nilsson, F., O. Söderman and I. Johansson (1996). *"Physical− chemical properties of the n-octyl β-d-glucoside/water system. A phase diagram, self-diffusion NMR, and SAXS study."* **Langmuir** 12(4): 902-908.
- [Ninham, 1983] Ninham, B. W., D. F. Evans and G. J. Wei (1983). *"The curious world of hydroxide surfactants. Spontaneous vesicles and anomalous micelles."* **The Journal of Physical Chemistry** 87(24): 5020-5025.
- [Norstrom, 2006] Norstrom, E. M. and J. A. Mastrianni (2006). *"The charge structure of helix 1 in the prion protein regulates conversion to pathogenic PrPSc."* **Journal of virology** 80(17): 8521-8529.
- [Oliveira, 2010] Oliveira, R. G., E. Schneck, B. E. Quinn, O. V. Konovalov, K. Brandenburg, T. Gutsmann, T. Gill, C. B. Hanna, D. A. Pink and M. Tanaka (2010). *"Crucial roles of charged saccharide moieties in survival of gram negative bacteria against protamine revealed by combination of grazing incidence x-ray structural characterizations and Monte Carlo simulations."* **Physical Review E** 81(4): 041901.
- [Onuki, 2016] Onuki, A., S. Yabunaka, T. Araki and R. Okamoto (2016). *"Structure formation due to antagonistic salts."* **Current Opinion in Colloid & Interface Science** 22: 59-64.
- [Ozdemir, 2011] Ozdemir, O., H. Du, S. I. Karakashev, A. V. Nguyen, M. S. Celik and J. D. Miller (2011). *"Understanding the role of ion interactions in soluble salt flotation with alkylammonium and alkylsulfate collectors."* **Advances in colloid and interface science** 163(1): 1-22.
- [Patel, 2009] Patel, T., G. Ghosh, V. Aswal and P. Bahadur (2009). *"Micellization of sodium dodecyl sulfate and polyoxyethylene dodecyl ethers in solution."* **Colloid and Polymer Science** 287(10): 1175-1181.
- [Patrickios, 1995] Patrickios, C. S. and E. N. Yamasaki (1995). *"Polypeptide amino acid composition and isoelectric point ii. comparison between experiment and theory."* **Analytical biochemistry** 231(1): 82-91.
- [Pearson, 1963] Pearson, R. G. (1963). *"Hard and soft acids and bases."* **Journal of the American Chemical society** 85(22): 3533-3539.
- [Pegram, 2008] Pegram, L. M. and M. T. Record Jr (2008). *"Thermodynamic origin of Hofmeister ion effects."* **The journal of physical chemistry B** 112(31): 9428-9436.
- [Pegram, 2007] Pegram, L. M. and M. T. Record (2007). *"Hofmeister salt effects on surface tension arise from partitioning of anions and cations between bulk water and the air− water interface."* **The journal of physical chemistry B** 111(19): 5411-5417.
- [Pope, 2003] Pope, M. T. (2003)**.** *"Introduction to polyoxometalate chemistry"*.in Polyoxometalate Molecular Science, Springer**:** 3-31.

- [Prejdová, 2004] Prejdová, J., M. Soucek and J. Konvalinka (2004). *"Determining and overcoming resistance to HIV protease inhibitors."* **Current Drug Targets-Infectious Disorders** 4(2): 137-152.
- [Prudent, 2008] Prudent, R., V. Moucadel, B. Laudet, C. Barette, L. Lafanechère, B. Hasenknopf, J. Li, S. Bareyt, E. Lacôte and S. Thorimbert (2008). *"Identification of polyoxometalates as nanomolar noncompetitive inhibitors of protein kinase CK2."* **Chemistry & biology** 15(7): 683-692.
- [Rahbari, 2009] Rahbari, R., T. Sheahan, V. Modes, P. Collier, C. Macfarlane and R. M. Badge (2009). *"A novel L1 retrotransposon marker for HeLa cell line identification."* **Biotechniques** 46(4): 277-284.
- [Rak, 2013] Rak, J., B. Dejlová, H. Lampová, R. Kaplánek, P. Matějíček, P. Cígler and V. Král (2013). *"On the solubility and lipophilicity of metallacarborane pharmacophores."* **Molecular pharmaceutics** 10(5): 1751-1759.
- [Rak, 2011] Rak, J., M. Jakubek, R. Kaplánek, P. Matějíček and V. Král (2011). *"Cobalt bis (dicarbollide) derivatives: Solubilization and self-assembly suppression."* **European journal of medicinal chemistry** 46(4): 1140-1146.
- [Regev, 1994] Regev, O., C. Kang and A. Khan (1994). *"Cryo-TEM and NMR studies of solution microstructures of double-tailed surfactant systems: didodecyldimethylammonium hydroxide, acetate, and sulfate."* **The Journal of Physical Chemistry** 98(26): 6619-6625.
- [Renoncourt, 2006] Renoncourt, A., P. Bauduin, E. Nicholl, D. Touraud, J. M. Verbavatz, M. Dubois, M. Drechsler and W. Kunz (2006). *"Spontaneous Vesicle Formation of an Industrial Single-Chain Surfactant at Acidic pH and at Room-Temperature."* **ChemPhysChem** 7(9): 1892-1896.
- [Retailleau, 1997] Retailleau, P., M. Ries-Kautt and A. Ducruix (1997). *"No salting-in of lysozyme chloride observed at low ionic strength over a large range of pH."* **Biophysical journal** 73(4): 2156.
- [Řezáčová, 2009] Řezáčová, P. n., J. Pokorná, J. i. Brynda, M. Kožíšek, P. Cígler, M. Lepšík, J. i. Fanfrlík, J. Rezác, K. r. Grantz Šašková and I. Sieglová (2009). *"Design of HIV protease inhibitors based on inorganic polyhedral metallacarboranes."* **Journal of medicinal chemistry** 52(22): 7132-7141.
- [Rhule, 1998] Rhule, J. T., C. L. Hill, D. A. Judd and R. F. Schinazi (1998). *"Polyoxometalates in medicine."* **Chemical Reviews** 98(1): 327-358.
- [Ries-Kautt, 1997] Ries-Kautt, M. and A. Ducruix (1997)**.** *"[3] Inferences drawn from physicochemical studies of crystallogenesis and precrystalline state"*.in Methods in enzymology, Elsevier. 276**:** 23-59.
- [Righetti, 1976] Righetti, P. G. and T. Caravaggio (1976). *"Isoelectric points and molecular weights of proteins: A table."* **Journal of Chromatography A** 127(1): 1-28.
- [Rokitskaya, 2017] Rokitskaya, T. I., I. D. Kosenko, I. B. Sivaev, Y. N. Antonenko and V. I. Bregadze (2017). *"Fast flip–flop of halogenated cobalt bis (dicarbollide) anion in a lipid bilayer membrane."* **Physical Chemistry Chemical Physics** 19(36): 25122-25128.
- [Rosen, 1982] Rosen, M. J. and X. Y. Hua (1982). *"Surface concentrations and molecular interactions in binary mixtures of surfactants."* **Journal of Colloid and Interface Science** 86(1): 164-172.
- [Ruiz, 2008] Ruiz, C. C. (2008). *"Sugar-based surfactants: fundamentals and applications"*. in, CRC Press.
- [Rydall, 1992] Rydall, J. R. and P. M. Macdonald (1992). *"Investigation of anion binding to neutral lipid membranes using deuterium NMR."* **Biochemistry** 31(4): 1092-1099.
- [Sachs, 2003] Sachs, J. N. and T. B. Woolf (2003). *"Understanding the Hofmeister effect in interactions between chaotropic anions and lipid bilayers: molecular dynamics simulations."* **Journal of the American Chemical Society** 125(29): 8742-8743.
- [Sadakane, 2013] Sadakane, K., M. Nagao, H. Endo and H. Seto (2013). *"Membrane formation by preferential solvation of ions in mixture of water, 3-methylpyridine, and sodium tetraphenylborate."* **The Journal of chemical physics** 139(23): 234905.

- [Sadakane, 2009] Sadakane, K., A. Onuki, K. Nishida, S. Koizumi and H. Seto (2009). *"Multilamellar structures induced by hydrophilic and hydrophobic ions added to a binary mixture of D 2 O and 3-methylpyridine."* **Physical review letters** 103(16): 167803.
- [Sadakane, 2018] Sadakane, K. and H. Seto (2018). *"Membrane formation in liquids by adding an antagonistic salt."* **Frontiers in Physics** 6: 26.
- [Scherer, 1953] Scherer, W. F., J. T. Syverton and G. O. Gey (1953). *"Studies on the propagation in vitro of poliomyelitis viruses: IV. Viral multiplication in a stable strain of human malignant epithelial cells (strain HeLa) derived from an epidermoid carcinoma of the cervix."* **The Journal of experimental medicine** 97(5): 695-710.
- [Schott, 1984] Schott, H. (1984). *"Lyotropic numbers of anions from cloud point changes of nonionic surfactants."* **Colloids and Surfaces** 11(1-2): 51-54.
- [Schulz, 1998] Schulz, J. and G. Warr (1998). *"Selective adsorption of metal cations onto AOT and dodecyl sulfate films at the air/solution interface."* **Journal of the Chemical Society, Faraday Transactions** 94(2): 253-257.
- [Schwierz, 2010] Schwierz, N., D. Horinek and R. R. Netz (2010). *"Reversed anionic Hofmeister series: the interplay of surface charge and surface polarity."* **Langmuir** 26(10): 7370-7379.
- [Shah, 2012] Shah, D. O. (2012). *"Improved oil recovery by surfactant and polymer flooding"*. in, Elsevier.
- [Sharon, 1993] Sharon, N. and H. Lis (1993). *"Carbohydrates in cell recognition."* **Scientific American** 268(1): 82-89.
- [Shinoda, 1962] Shinoda, K. and E. Hutchinson (1962). *"PSEUDO-PHASE SEPARATION MODEL FOR THERMODYNAMIC CALCULATIONS ON MICELLAR SOLUTIONS1."* **The Journal of Physical Chemistry** 66(4): 577-582.
- [Sivaev, 1999] Sivaev, I. B. and V. I. Bregadze (1999). *"Chemistry of cobalt bis (dicarbollides). A review."* **Collection of Czechoslovak Chemical Communications** 64(5): 783-805.
- [Song, 1998] Song, H. K. and S. W. Suh (1998). *"Kunitz-type soybean trypsin inhibitor revisited: refined structure of its complex with porcine trypsin reveals an insight into the interaction between a homologous inhibitor from Erythrina caffra and tissue-type plasminogen activator."* **Journal of molecular biology** 275(2): 347-363.
- [Stefaniu, 2019] Stefaniu, C., V. M. Latza, O. Gutowski, P. Fontaine, G. Brezesinski and E. Schneck (2019). *"Headgroup-ordered monolayers of uncharged glycolipids exhibit selective interactions with ions."* **The journal of physical chemistry letters** 10(8): 1684-1690.
- [Stoica, 2009] Stoica, A.-I., C. Viñas and F. Teixidor (2009). *"Cobaltabisdicarbollide anion receptor for enantiomer-selective membrane electrodes."* **Chemical Communications**(33): 4988-4990.
- [Stokes, 1948] Stokes, R. H. and R. A. Robinson (1948). *"Ionic hydration and activity in electrolyte solutions."* **Journal of the American Chemical Society** 70(5): 1870-1878.
- [Szejtli, 1998] Szejtli, J. (1998). *"Introduction and general overview of cyclodextrin chemistry."* **Chemical reviews** 98(5): 1743-1754.
- [Tarrés, 2015] Tarrés, M., E. Canetta, E. Paul, J. Forbes, K. Azzouni, C. Vinas, F. Teixidor and A. J. Harwood (2015). *"Biological interaction of living cells with COSAN-based synthetic vesicles."* **Scientific reports** 5: 7804.
- [Tarrés, 2014] Tarrés, M., E. Canetta, C. Vinas, F. Teixidor and A. J. Harwood (2014). *"Imaging in living cells using ν B–H Raman spectroscopy: monitoring COSAN uptake."* **Chemical Communications** 50(25): 3370-3372.
- [Thordarson, 2011] Thordarson, P. (2011). *"Determining association constants from titration experiments in supramolecular chemistry."* **Chemical Society Reviews** 40(3): 1305-1323.
- [Uchman, 2015] Uchman, M., V. Ďorďovič, Z. Tošner and P. Matějíček (2015). *"Classical Amphiphilic Behavior of Nonclassical Amphiphiles: A Comparison of Metallacarborane Self-Assembly with SDS Micellization."* **Angewandte Chemie International Edition** 54(47): 14113-14117.

- [Uchman, 2010] Uchman, M., P. Jurkiewicz, P. Cígler, B. r. Grüner, M. Hof, K. Procházka and P. Matějíček (2010). *"Interaction of fluorescently substituted metallacarboranes with cyclodextrins and phospholipid bilayers: fluorescence and light scattering study."* **Langmuir** 26(9): 6268-6275.
- [Ussing, 2013] Ussing, H. H., P. Kruhoffer, H. J. Thaysen and N. H. Thorn (2013). *"The Alkali Metal Ions in Biology: I. The Alkali Metal Ions in Isolated Systems and Tissues. II. The Alkali Metal Ions in the Organism"*. in, Springer Science & Business Media.
- [Vácha, 2010] Vácha, R., P. Jurkiewicz, M. Petrov, M. L. Berkowitz, R. A. Bockmann, J. Barucha-Kraszewska, M. Hof and P. Jungwirth (2010). *"Mechanism of interaction of monovalent ions with phosphatidylcholine lipid membranes."* **The Journal of Physical Chemistry B** 114(29): 9504-9509.
- [Verdiá-Báguena, 2014] Verdiá-Báguena, C., A. Alcaraz, V. M. Aguilella, A. M. Cioran, S. Tachikawa, H. Nakamura, F. Teixidor and C. Viñas (2014). *"Amphiphilic COSAN and I2-COSAN crossing synthetic lipid membranes: planar bilayers and liposomes."* **Chemical Communications** 50(51): 6700-6703.
- [Vlachy, 2008] Vlachy, N., M. Drechsler, J.-M. Verbavatz, D. Touraud and W. Kunz (2008). *"Role of the surfactant headgroup on the counterion specificity in the micelle-to-vesicle transition through salt addition."* **Journal of colloid and interface science** 319(2): 542-548.
- [Vlachy, 2009] Vlachy, N., B. Jagoda-Cwiklik, R. Vácha, D. Touraud, P. Jungwirth and W. Kunz (2009). *"Hofmeister series and specific interactions of charged headgroups with aqueous ions."* **Advances in colloid and interface science** 146(1-2): 42-47.
- [Volovetsky, 2017] Volovetsky, A. B., V. S. Sukhov, I. V. Balalaeva, V. V. Dudenkova, N. Y. Shilyagina, A. V. Feofanov, A. V. Efremenko, M. A. Grin, A. F. Mironov and I. B. Sivaev (2017). *"Pharmacokinetics of chlorin e6-cobalt bis (dicarbollide) conjugate in Balb/c mice with engrafted carcinoma."* **International journal of molecular sciences** 18(12): 2556.
- [Vrbka, 2006] Vrbka, L., P. Jungwirth, P. Bauduin, D. Touraud and W. Kunz (2006). *"Specific ion effects at protein surfaces: a molecular dynamics study of bovine pancreatic trypsin inhibitor and horseradish peroxidase in selected salt solutions."* **The journal of physical chemistry B** 110(13): 7036-7043.
- [Warneke, 2016] Warneke, J., C. Jenne, J. Bernarding, V. A. Azov and M. Plaumann (2016). *"Evidence for an intrinsic binding force between dodecaborate dianions and receptors with hydrophobic binding pockets."* **Chemical Communications** 52(37): 6300-6303.
- [Whitford, 2013] Whitford, D. (2013). *"Proteins: structure and function"*. in, John Wiley & Sons.
- [Wilkins, 1999] Wilkins, D. K., S. B. Grimshaw, V. Receveur, C. M. Dobson, J. A. Jones and L. J. Smith (1999). *"Hydrodynamic radii of native and denatured proteins measured by pulse field gradient NMR techniques."* **Biochemistry** 38(50): 16424-16431.
- [Wille, 2009] Wille, H., M. Shanmugam, M. Murugesu, J. Ollesch, G. Stubbs, J. R. Long, J. G. Safar and S. B. Prusiner (2009). *"Surface charge of polyoxometalates modulates polymerization of the scrapie prion protein."* **Proceedings of the National Academy of Sciences** 106(10): 3740-3745.
- [Winkler, 2017] Winkler, R., T. Buchecker, F. Hastreiter, D. Touraud and W. Kunz (2017). *"PPh 4 Cl in aqueous solution–the aggregation behavior of an antagonistic salt."* **Physical Chemistry Chemical Physics** 19(37): 25463-25470.
- [Wu, 2015] Wu, Y., R. Shi, Y.-L. Wu, J. M. Holcroft, Z. Liu, M. Frasconi, M. R. Wasielewski, H. Li and J. F. Stoddart (2015). *"Complexation of polyoxometalates with cyclodextrins."* **Journal of the American Chemical Society** 137(12): 4111-4118.
- [Yin, 2006] Yin, P. D., D. Das and H. Mitsuya (2006). *"Overcoming HIV drug resistance through rational drug design based on molecular, biochemical, and structural profiles of HIV resistance."* **Cellular and molecular life sciences** 63(15): 1706.
- [Zaulet, 2018] Zaulet, A., F. Teixidor, P. Bauduin, O. Diat, P. Hirva, A. Ofori and C. Vinas (2018). *"Deciphering the role of the cation in anionic cobaltabisdicarbollide clusters."* **Journal of Organometallic Chemistry** 865: 214-225.

- [Zhang, 1999] Zhang, R., P. A. Marone, P. Thiyagarajan and D. M. Tiede (1999). *"Structure and molecular fluctuations of N-alkyl-β-D-glucopyranoside micelles determined by X-ray and neutron scattering."* **Langmuir** 15(22): 7510-7519.
- [Zhang, 2004] Zhang, R., L. Zhang and P. Somasundaran (2004). *"Study of mixtures of n-dodecyl-β-d-maltoside with anionic, cationic, and nonionic surfactant in aqueous solutions using surface tension and fluorescence techniques."* **Journal of colloid and interface science** 278(2): 453-460.
- [Zhang, 2009] Zhang, Y. and P. S. Cremer (2009). *"The inverse and direct Hofmeister series for lysozyme."* **Proceedings of the National Academy of Sciences** 106(36): 15249-15253.